The University of Maine
DigitalCommons@UMaine

Electronic Theses and Dissertations | Fogler Library

Fall 12-15-2023

The Development of an Advanced Biorefinery to Produce Cellulosic Sugars and Bionanomaterials

Carlaile Fernanda de Oliveira Nogueira
University of Maine, carlaile.nogueira@maine.edu

Follow this and additional works at: https://digitalcommons.library.umaine.edu/etd

 Part of the Biochemical and Biomolecular Engineering Commons, Catalysis and Reaction Engineering Commons, Nanoscience and Nanotechnology Commons, and the Polymer Science Commons

Recommended Citation

de Oliveira Nogueira, Carlaile Fernanda, "The Development of an Advanced Biorefinery to Produce Cellulosic Sugars and Bionanomaterials" (2023). *Electronic Theses and Dissertations*. 3901.
https://digitalcommons.library.umaine.edu/etd/3901

This Open-Access Dissertation is brought to you for free and open access by DigitalCommons@UMaine. It has been accepted for inclusion in Electronic Theses and Dissertations by an authorized administrator of DigitalCommons@UMaine. For more information, please contact um.library.technical.services@maine.edu.

THE DEVELOPMENT OF AN ADVANCED BIOREFINERY TO PRODUCE CELLULOSIC SUGARS AND BIONANOMATERIALS

By

Carlaile Fernanda de Oliveira Nogueira

B.S. University of São Paulo, Lorena, Brazil, 2014

M.Sc. University of São Paulo, Lorena, Brazil, 2017

A DISSERTATION

Submitted in Partial Fulfillment of the

Requirements for the joint doctorade degree of

Doctor of Philosophy

(Chemical Engineering) from University of Maine (UM)

Doctor in Science

(Industrial Biotechnology) from University of São Paulo (USP)

The Graduate School

The University of Maine

December 2023

Advisory Committee:

Adriaan R. P. van Heiningen, Professor of Chemical Engineering, co-Advisor

Valdeir Arantes, Professor of Industrial Biotechnology, University of São Paulo, co-Advisor

Douglas W. Bousfield, Professor of Chemical Engineering

M. Clayton Wheeler, Professor of Chemical Engineering

Mehdi Tajvidi, Associate Professor of Renewable Nanomaterials

© 2023 Carlaile Fernanda de Oliveira Nogueira

All Rights Reserved

THE DEVELOPMENT OF AN ADVANCED BIOREFINERY TO PRODUCE CELLULOSIC SUGARS AND BIONANOMATERIALS

By Carlaile Fernanda de Oliveira Nogueira

Dissertation co-Advisors: Adriaan R. P. van Heiningen and Valdeir Arantes

An Abstract of the Dissertation Presented
in Partial Fulfillment of the Requirements for the joint doctorade
Degree of Doctor of Philosophy
(Chemical Engineering) from University of Maine (UM)
Degree of Doctor in Science
(Industrial Biotechnology) from University of São Paulo (USP)
December 2023

Market trends show growing interest in cellulose nanomaterials due to their low environmental impact. However, current nanocellulose isolation technologies face technoeconomic and life cycle limitations. Previous research has shown that enzymatic treatments effectively reduce the energy input for mechanical nanocellulose isolation. Simultaneously, there is potential to improve the viability of cellulosic ethanol facilities by coproducing nanocelluloses as high-value product obtained from agricultural feedstock. Here, our goal was to study the mass balance of enzymatic-mechanical processes that coproduces cellulosic sugars and nanocelluloses, evaluating the technical feasibility of converting lignified and non-lignified materials.

First, we have determined a feasible 50:50 mass ratio to obtain nanocelluloses and sugars using efficient-saccharification enzyme cocktails. This ratio, derived from breakeven point in the enzyme cost equation, was set as target for converting carbohydrates.

We investigated the coproduction of nanocelluloses (CNC and CNF) and high-titer sugars from hardwood bleached kraft pulp (HBKP), varying cellulose conversion. The integration was technically feasible and required low energy consumption. Total sugars concentration was 61–165 $g.L^{-1}$. Optimizing CNC yield via response surface yielded in 4.4–

8.7 g/100g of HBKP. CTec2 treatment significantly reduced the energy input for CNF isolation with energy savings up to 80% when compared to ultra-refining HBPK without pretreatment (25 $kWh.kg^{-1}$).

A new process method was studied to pretretreat sugarcane bagasse (SCB) and sugarcane straw (SCS), obtain sodium acetate and sugars, and isolate lignin-containing nanocelluloses (LCNC and LCNF). The pretreatment involved a modified version of the Deacetylation and Mechanical Refining (DMR) process, that was considered versatile and promoted full valorization of the biomasses. The pretreated materials had high fines level (83.6 – 87.9%) after Cellic CTec3/HTec3 treatment, hence significantly low energy input was required during ultra-refining. Total sugars concentration was 37–48 $g.L^{-1}$ for SCB and 31.3 $g.L^{-1}$ for SCS. LCNC yield was 5–7 g/100g of SCB and 6 g/100g of SCS. LCNF yield was 67–72 g/100g of SCB and 72 g/100g of SCS.

The isolated lignin-containing nanocelluloses showed promising surface chemistry both as suspensions and films. LCNFs had high hydrophobicity (94º to 102º), low wettability (up to 810s), and good thermostability (T_{max} 334–337 ºC).

DEDICATION

In honor to my beloved parents, grandparents, and ancestors, who gave me life and taught me the importance of seeking knowledge to materialize a better future for myself and coming generations. I am truly grateful for having the opportunity to be the first in our family to pursue doctorate studies.

I deeply appreciate all the love and support from my family, Luís Irajá Jr., Maria do Carmo, and Luís Irajá Neto. You are the reason I can find enough courage and strengh.

ACKNOWLEDGEMENTS

I would like to thank my advisors Prof. Dr. Valdeir Arantes, Prof. Dr. Marina Dias, and Prof. Dr. Adriaan van Heiningen for being my mentors during my PhD journey. My research and all the experiences I have lived during the PhD would not be as rich without your constant support. Especially, I thank you to provide me access to the best infra-structure for my project and mentorship to my personal development, improving critical thinking, and strategy for performing my research. I will always be appreciative for the teachings, feedback, attention, and presence at all times it was needed. I take to the heart the opportunity to make my PhD project to happen as close as I could envisioned.

For financial support, I would like to thank…

The Coordenação de Aperfeiçoamento de Pessoal de Nível Superior (CAPES) for the financial support with the doctoral scholarship grant in Brazil (CAPES/DS) and for the financial support with the Sandwich doctoral scholarship (CAPES/PRINT) – Finance code 001. I extend my gratitude to all Brazilian taxpayers that are the true sponsors of the financial support I was granted.

The Programa de Pos-graduação em Biotecnologia Industrial (PPGBI, Brazil) at EEL-USP for financial support through CAPES-PROAP aid for fieldwork at LNNano (CNPEM, Campinas-SP, Brazil) and Anton Parr Brazil. I extend all my gratitude to the PPGBI professors and all EEL-staff. The PPGBI professors taught me for most of my academic journey from who I learn the important lesson “to learn how to learn”. In special, I would like to thank Prof. Dr. Julio Santos and Andre Silva for constant support during the Sandwich doctorate.

To Prof. Adriaan van Heiningen and the Department of Chemical Engineering, I profoundly appreciate the opportunity of being a student of this Department and of receiving financial support with the Graduate Research assistantship (J. Larcom Ober Fund chair). I

extend my gratitude to Angela Hildreth and Cathy Dunn for being attentive with my needs as a graduate student (endless paperwork all done!) and Amos Cline for lab support.

For support with materials, I would like to thank…

Fibria/Suzano (Brazil) for providing beached Kraft Pulp.

Zilor (Quata-SP, Brazil) for providing sugarcane bagasse, especially to Larissa Voleck Lopes for making the donation arrangements and being the contact point. I thank EEL-USP to the support with transportation and shipping costs to bring sugarcane bagasse to UMaine (USA).

Prof. Dr. Brenda Tubana (Louisiana State University-LSU, Louisiana, USA) for providing sugarcane bagasse, especially to Barbara Ferreira for making the donation arrangements and being the contact point. I thank the Ober Fund for the support with shipping costs to bring sugarcane bagasse from LSU to UMaine.

American Process and GranBio for providing sugarcane straw.

Novozymes (Denmark) for providing enzyme cocktails.

Undoubtedly, my PhD project would not be possible without strong collaboration with all the amazing people and professionals that I had the chance to work with. For that, I thank…

The NanoBiotech for the material and equipment essential to perform my research. Special thanks to my very good friends at the laboratory Barbara Pereira, Braz Marotti, Gabriela Berto, Isabella Dias, Kelly Benini, Paulo Henrique Pereira, and Willian Marcondes for support and friendship during all the times. You were my family during my PhD years.

The Ober Laboratory and the Process Development Laboratory, for the material and equipment essential to perform my research. Special thanks to Azadeh Pahlevanzadeh for the support, friendship, and for always being welcoming. I will always appreciate our lunches outside during the Fall of 2019.

The National Nanotechnology Laboratory (LNNano), CNPEM, Brazil, for the support with multi-user equipment in conducting Atomic Force Microscopy (AFM) analysis, image processing, and data processing. Special thanks to Carlos Costa and Cleyton Biffe for their constant support to the external user, attention, willingness, and professionalism during the entire analysis scheduling and sample preparation.

The Forest Bioproducts Research Institute (FBRI) and Technology Research Center (TRC) for allowing the use of HPLC and many other multi-user equipment essential to perform my research. I thank Ravi Patil, Laurel Grosjean, Amy Luce, Indira Silwal, Sampath Karunarathne and Sampath Gunukula for support and friendship during all my time at UMaine. Special thanks to Amy Luce for always accommodate my research needs before and during the COVID pandemic.

The Process Development Center (PDC) for the support with multi-user equipment, trainings, and allowing the use of PFI mill, Supermass collider, and Morfi. I thank Seongkyung Park, Nayereh Dadoo, and Haixuan Zou for support during all my time at UMaine, and specially to Colleen Walker for always accommodate my research needs even during the COVID pandemic.

The Composite Center (UMaine, USA) for granting access in the Nano laboratory, providing materials, and support with equipment and personal to conduct Differential scanning calorimetry (DSC) analysis. Special thanks to Andrew Foster for support with analysis scheduling and training during the COVID pandemic.

The Electron Microscopy Laboratory (UMaine, USA) for the support with multi-user equipment in conducting Scanning Electron Microscopy (SEM) analysis. Special thanks to Emma Perry for her attention, willingness, and professionalism. I also extend my appreciation to the CORE Facility staff at UMaine for accommodating my research needs during the COVID pandemic and for the CORE Voucher financial support to complete the SEM analysis.

Anton Parr Brazil for the rheometric analysis. Special thanks to Kiria Serranegra for analysis support.

Prof. Dr. André Ferraz (PPGBI, EEL-USP, Brazil) for allowing access in his laboratory and providing support with material, equipment, and personal to conduct Optical Microscopy analysis. Special thanks to José Moreira, Angela Machado, and Uirajá Ruschoni for constant support and friendship.

Prof. Dr. Carl Tripp (UMaine, USA) for allowing access in his laboratory and providing support with material, equipment, and personal to conduct Zeta potential analysis during the COVID pandemic. I thank all his students for being welcoming, specially to Sabrina Sultana and Rihab Masmoudi for support.

Prof. Dr. Mehdi Tajvidi (UMaine, USA) for allowing access in his laboratory and providing support with material, equipment, and personal to conduct Thermogravimetry analysis, Contact Angle analysis, FTIR, and Freeze dryer during COVID pandemic. I thank all the students at the Laboratory of Renewable Nanomaterials for being welcoming, specially to Wenjing Sun and Rakibul Hossain for support and friendship.

To UMaine, especially to OIP, and all the student organization, especially to ISA.

TABLE OF CONTENTS

LIST OF TABLES

LIST OF FIGURES

PLANNED CONTRIBUTIONS

Paper I

Arantes, V, Dias, IKR, Berto, GL, Pereira, B, Marotti, BS, Nogueira, CFO. The current status of the enzyme-mediated isolation and functionalization of nanocelluloses: production, properties, technoeconomics, and opportunities. Cellulose (2020) 27:10571–10630. https://doi.org/10.1007/s10570-020-03332-1

Paper II

Provisional title: "*Process development for the coproduction of CNC and high titer of sugars from bleached Kraft pulp through a combined enzymatic-mechanical approach*"

Paper III

Provisional title: "*Feasibility analysis of the coproduction of CNC, CNF, and high titers of sugars from bleached kraft pulp using an enzymatic-mechanical approach and characterization of its products*"

Paper IV

Provisional title: "*A new process development for the production of lignin-containing nanocelluloses, sodium acetate, and cellulosic sugars from sugarcane bagasse and straw*"

Other contributions

Nogueira, C. F. O.; van Heiningen, A.R.P.; Arantes, V. The current status of the enzyme-mediated isolation and functionalization of nanocelluloses: production, properties, technoeconomics, and opportunities. In: 3rd Cellulose Nanomaterials Researchers Forum, August 25-26, 2021, Orono, Maine, USA. (poster)

Nogueira, C. F. O.; Arantes, V. Optimization of cellulose nanocrystals recovery after enzymatic hydrolysis. In: 2019 TAPPI NANO - International Conference on Nanotechnology for Renewable Materials, 2019, Chiba, Japan. (poster)

Nogueira, C.F.O.; Dias, M; Arantes, V. A preliminary economic assessment of bionanomaterials and high concentration sugar production In: 41st Symposium on Biotechnology for Fuels and Chemicals, 2019, Seattle, Washington, USA. Access: https://sim.confex.com/sim/41st/meetingapp.cgi/Paper/38757 (poster and fast track oral presentation)

Nogueira, C.F.O.; Dias, M; Arantes, V. A preliminary assessment of integration of bionanomaterials and high concentration sugar In: 3rd Workshop of Nanocellulose, 2019, Campinas, Sao Paulo, Brazil. Access: http://pages.cnpem.br/nanocell/wp-content/uploads/sites/109/2019/07/3rd-Nanocellulose_Abstract-book_v3.pdf (poster)

CHAPTER 1 INTRODUCTION

1.1 Research motivation

The sugarcane biorefinery and the pulp and paper industries are some of the largest lignocellulosic biorefineries worldwide. Because they are based on commodities, they use robust technologies aiming for a zero-waste goal to follow a circular bioeconomy. However, there is great potential for diversifying their product portfolio by improving the valorization of their side streams. The lack of cost-effective technologies to produce market competitive products from their side streams has led these industries to use this feedstock mostly for energy cogeneration and hence meet the internal demands for heat and power, selling electricity surplus to the power grid.

The abundant production of side streams in the sugarcane biorefinery motivates us to research new processes for their valorization while presenting alternatives to address pressing global problems, such as climate change and persistent pollution by plastics. Examples of abundant side streams within sugarcane biorefinery are biomass surplus (*e.g.*, sugarcane bagasse, straw, and tips), and industrial bio-residues (*i.e.*, fractions underutilized in the current cellulosic sugar production, such as lignin and the cellulosic solid residue (CSR) recovered after enzymatic hydrolysis).

The pulp and paper industries could serve as a model on how the sugarcane biorefineries could benefit from stream valorization and product diversification. The pulp and paper industries have been facing a market shift from its traditional fiber-based products to a new generation of forest products driven by innovation to ensure profit. Nanocellulose (as an additional fiber crop) is a potential option to offset the strong trends of decline in their traditional markets (*e.g.*, graphic and printing papers).

Nanocelluloses are biobased, renewable, non-toxic, and recyclable bionanomaterials that can be isolated from abundant plant biomass. The market interest in nanocelluloses has

emerged because nanocelluloses have the potential to combine properties, performance, sustainability, and economic return. This is demonstrated by their high compound annual growth rate (CARG), forecasted to be 23.50% period 2023-2032 (Global Market Insights, 2023), which indicates the expectation of nanocelluloses to break into new value chains and grow the market size and market share.

1.2 Research questions

Numerous raw materials and pathways have been explored for nanocellulose isolation, yet a comprehensive feasibility analysis is lacking. Thus, the question whether the isolation of nanocelluloses from non-wood pulp is more economically advantageous compared to wood-pulp is still pending to be answered. We attempt to contribute to the field by advancing the knowledge of enzyme-assisted mechanical treatment to isolate nanocelluloses from non-wood lignified pulp and non-lignified wood-pulp.

One alternative route to isolate nanocelluloses from non-wood pulp in a biorefinery concept is to base the study on the production of cellulosic ethanol and incorporate the simultaneous production of nanocellulose. However, an optimum ratio between cellulosic sugars and nanocellulose production remains to be determined. We attempted to answer this question by studying the equation of enzyme cost proposed by Lynd *et al.* (2017) and Stephen *et al.* (2012), for which we proposed an adjustment that shows a feasible mass ratio for coproducts produced via enzymatic treatment (Chapter 5).

The use of enzymatic treatments for nanocellulose isolation is a versatile approach to co-produce cellulose nanofibrils (CNF), cellulose nanocrystals (CNC), and cellulosic sugars although its feasibility as a stand-alone process has not been much explored. Additionally, the enzyme cocktails commercially available target full saccharification of the lignocellulosic material into sugars, which may not be optimal for nanocellulose isolation, hence necessitating further study. We attempt to address this question first by evaluating different degrees of

cellulose conversion by varying the enzyme loading in the enzymatic hydrolysis to co-produce cellulosic sugars, cellulose nanofibrils (CNF), and cellulose nanocrystals (CNC) (Chapter 6 and 7) and then study the mass balance.

Lastly, the state of the art in nanocellulose isolation suggests that the choice of raw material and pretreatment impact the nanocellulose yield and properties. Thus, it is essential to analyze these parameters to understand the technical feasibility to produce nanocelluloses within a biorefinery. In Chapter 8, we proposed and discussed a new process with focus on cellulose nanomaterials based on the well-studied Deacetylation and Mechanical Refining (DMR) process developed by the National Renewable Energy Laboratory (NREL). The production of nanocelluloses using the DMR process to obtain nanomaterials and cellulosic sugars has not appeared in the literature sofar. Additionally, we discussed the properties of lignin-containing cellulose nanocrystals (LCNC) and lignin-containing cellulose nanofibrils (LCNF) obtained thereby in Chapter 9.

1.3 Research goal

Our research goal is to study the enzyme-mediated process to co-produce nanocelluloses and cellulose sugars using the biorefinery concept. For that, we aim to study the coproduction of cellulosic sugars, sodium acetate, and lignin-containing nanocelluloses (LCNC and LCNF) from non-wood lignified feedstock, sugarcane bagasse (SCB) and sugarcane straw (SCS), based on the most currently feasible process to produce cellulose sugars, the Deacetylation and Mechanical Refining (DMR). Our reference will be the coproduction of cellulosic sugars and nanocelluloses (CNC and CNF) based on Hardwood Bleached Kraft pulp (HBKP) that is the feedstock currently used to isolate CNF. The expected outcome was to establish the overall mass balance of each sub-process and investigate possible bottlenecks by analyzing the valorization of raw material.

CHAPTER 2 LITERATURE REVIEW[1]

2.1 Availability of sugarcane bagasse and straw and their relevance

Sugarcane, maize, wheat, and rice are the four crops that account for half of the global primary crop production according to the Food and Agriculture Organization (FAO). Historical data gathered by FAOSTAT between 2000 – 2018 shows that sugarcane is the main crop produced worldwide, representing 20% of world crop production during the period with a total of 1.6 billion tonnes (Faostat, 2020). The same report shows that South America is the leading region in the production of sugarcane (54% of the world total crop production), pointing Brazil as one of the main sugarcane producers (40% the world total crop production), and China and the United States ranking in the 3rd and 11th positions, respectively. Regarding world production of raw sugar, the major producers are Brazil (22% world share with a total of 40 million tonnes per year), India, Thailand, China, and the US (around 29 million tonnes per year). The Brazilian sugar-energy sector based solely on sugarcane contributes to 2% of Brazilian's gross domestic product (GDP) and generates an annual value of US$ 100 billion Ministério de Minas e Energia (MME) (2016); Carpio and Souza, 2019). The ethanol industry contributed with US$ 34.7 billion to the U.S.'s GDP while the total economic impact of the sugar industry on the US economy exceeds $19 billion dollars based on sugarcane and sugar beets for sugar production and corn for ethanol production. These results are obtained only by using first generation (1G) technology of sugar and ethanol production.

[1] *Part of this chapter was published on the Review paper:*
Arantes, V, Dias, IKR, Berto, GL, Pereira, B, Marotti, BS, Nogueira, CFO. The current status of the enzyme-mediated isolation and functionalization of nanocelluloses: production, properties, technoeconomics, and opportunities. Cellulose (2020) 27:10571–10630. https://doi.org/10.1007/s10570-020-03332-1

The Brazilian sugar-energy sector relies on the production of sugar, ethanol, and bioenergy. However, there is still biomass available to manufacture products. The current optimized cogeneration systems, with turbines up to 75 – 85% efficiency, require smaller amounts of bagasse to meet the energy self-sufficiency for 1G ethanol production (Coelho *et al.*, 2006;Walter *et al.*, 2015;Khatiwada *et al.*, 2016). Brazilian sugarcane producers report that 90% of the sugarcane bagasse would be enough to meet the mill's internal demand for electricity, leaving around 10% available to manufacture value added products (Nova Cana, 2014) while around 50% of straw (leaves and tops removed during harvest and before crushing) stay in the fields for fertilization (Souza *et al.*, 2020). The biomass production for each harvest is approximately 15.0% of sugars (dry), 13.5% of bagasse, 14.0% of tops and leaves (Negrão *et al.*, 2021). Taking the Brazilian biggest sugar-ethanol biorefinery Raízen as a case of study, which crushes 73 million ton of sugarcane per year (Raizen, 2019), and considering the biomass production per harvest, it would result in approximately 1 million tonnes of bagasse (dry) surplus and approximately 2.5 million tonnes of baled sugarcane straw per year. Thus, large quantities of bagasse and straw would be available to use (in part or totally) to produce value added products and greater economic return (*e.g.*, nanocelluloses). However, the availability of sugarcane bagasse or straw solely is not enough to guarantee the development of new technologies in this sector. It is essential to understand the lignocellulosic material and demonstrate how to efficiently fractionate and transform its fractions into products. Thus, a combination of process and market development is essential to unlock the potential of new bioproducts.

2.2 Lignocellulosic material composition and ultrastructure

Lignocellulosic material refers to the fraction of plant that is responsible to provide structural support for growth and protection against degradation. The main components of lignocellulosic materials are about 35-50% of cellulose, 15-30% of hemicellulose, and 15-30%

of lignin. The minor components are proteins, lipids, pectin, soluble sugars, and minerals (Fengel, 1970, 1969).

The ultrastructure model for lignocellulosic material is typically discussed based on wood cell walls (Fengel, 1970, 1969; Meier, 1962; Heyn, 1969). The plant cell wall is composed of a middle lamella (ML) and two cell walls, called primary and secondary walls. The middle lamella is the outer structure of plant cell walls. It is composed of lignin (at high concentration), hemicelluloses, and pectins, which promotes rigidity and protection against degradation. The primary cell wall is a thin layer composed by an association of cellulose, hemicellulose, pectin, and phenolic fractions, which enables strength and resiliency during early stages of growth. The secondary wall is composed by three layers (S1, S2, and S3) and contains the major fraction of cellulose embedded in hemicellulose and lignin (Fengel, 1970). Cellulose is found in both primary and secondary walls of the plant cell wall, being the main component of the S2 layer in the secondary wall. Cellulose forms different fibril patterns in each layer of the secondary wall that satisfies the requirement for high tensile and compressive strength in the plant cell wall structure. The ultrastructure of the plant cell wall is illustrated on Figure 1.

The distribution of the main components of the lignocellulose matrix varies along the different layers of the plant cell wall as well as the contents of each component, which will depend on the plant species, tissue, weather, geographic location, age, among other factors (Alwani *et al.*, 2014; Fengel, 1969). Nevertheless, their natural construction follows a rationale in which one component provides tensile strength embedded in a matrix that confers resistance to compression (Fengel and Wegener, 1983). Table 1 provides a summary of the average composition from the cell wall main components, highlighting the differences between grasses and dicotyledons (*e.g.*, hardwood). An important difference between grasses and wood species are related to the composition and distribution of the components of the lignocellulosic matrix

(pectins, hemicelluloses, and lignin) in which cellulose is embedded (Carpita and Gibeaut, 1993; Smith and Harris, 1999).

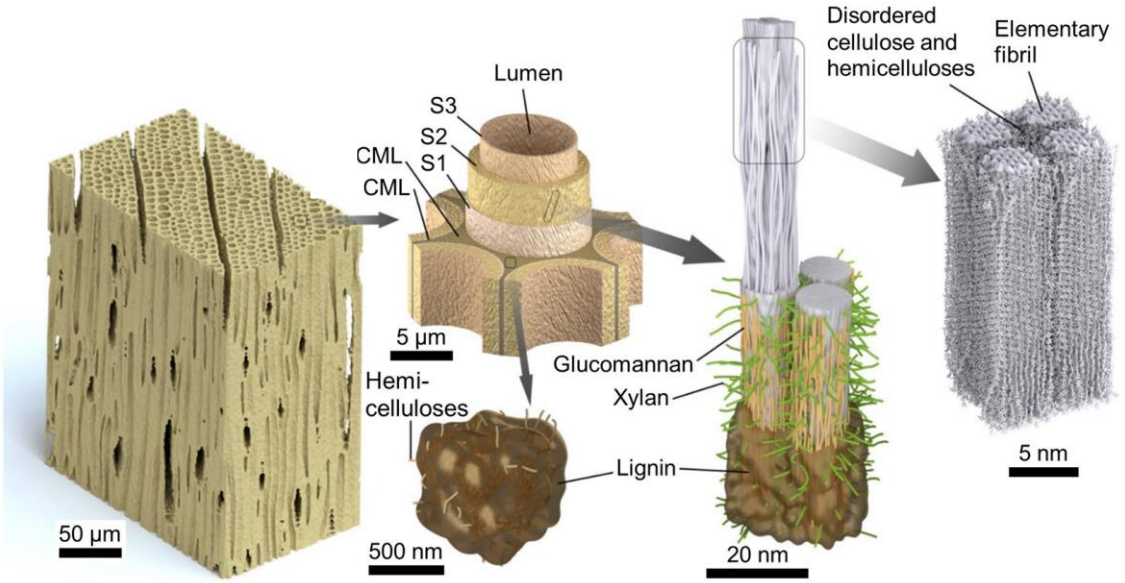

ML: middle lamella, S1, S2, and S3: three layers of secondary wall

Fig. 1. Illustration of softwood plant cell wall with a breakdown view of its layers, including the lignocellulose main components (cellulose, hemicellulose, and lignin), highlighting the cellulose structural hierarchy from fiber to elementary fibril (Adapted from Jakes *et al.*, 2020)

Table 1. Occurrence of lignocellulose main components in primary and secondary walls according to the type of biomass (grass and dicotyledon) (Scheller and Ulvskov, 2010)

Components	**Primary cell wall**		**Secondary cell wall**	
	Grass	**Dicot**	**Grass**	**Dicot**
Cellulose	20 – 30	15 – 30	35 – 45	45 – 50
Hemicellulose				
Xylan	20 – 40	5	40 – 50	20 – 30
Mixed linkage glucans (MLG)	10 – 30	Absent	Minor	Absent
Xyloglucan	1 – 5	20 – 25	Minor	Minor
Mannans and glucomannans	Minor	5 – 10	Minor	3 – 5
Pectins	5	20 – 35	0.1	0.1
Lignin	Minor	Minor	20	7 –10
Ferulic and *p*-coumaric acids	1 – 5	Minor	0.5 – 1.5	Minor
Silica	-	-	5 – 15	Variable

-: not available; Dicot: Dicotyledon

2.2.1 Cellulose

The main structural polysaccharide of lignocellulosic matrix is cellulose, which is industrially known as fibers. Non-wood fiber from sugarcane bagasse and straw are an alternate source for hardwood fibers, both presenting short fibers (Abd El-Sayed *et al.*, 2020). Sugarcane bagasse and straw fibers typically measure 1 – 2 mm in length and have a diameter of 10 – 20 μm (Ferdous *et al.*, 2021).

Cellulose is a linear homopolymer consisting of repeating units of cellobiose, a disaccharide formed by anhydroglucose residues linked by β-1,4 glycosidic bonds. The hydroxyl (OH) group of glucose's carbon-1 (C1) is in the form of a hemiacetal which has a reducing character and is responsible for cellulose chain growth and has significant chemical reactivity. The cellulose chain formation occurs by multiple repeating units of cellobiose releasing a water molecule (Fengel and Wegener, 1983). At the end of the cellulose chain, there is a OH group that is linked to C1, referred as "reducing end", while, at the opposite end of the chain, there is a OH group is linked to C4, referred as a "non-reducing end"(Miller, 1959). Additionally, the OH groups provide reactivity to the cellulose surface. The inter and intramolecular hydrogen bonds play an important role for the formation of the cellulose crystalline microstructure. Intramolecular hydrogen bonds lead to stiffening of the chain while intermolecular hydrogen bond results in the aggregation of several chains (Fengel, 1971). The aggregation of microfibrils eliminates the surface interaction with the environment and hence reduce the accessibility to hydrogen bonding sites. The aggregations and consequently the reduction of water bound to the fibril causes a reduction in the specific surface area (SSA). Experiments on fiber saturation shows that, in non-aggregate state, a microfibril, the microfibril bundle, and fiber present SSA equal to 850 – 870 m^2/g, 520 –630 and 470 m^2/g, respectively (Paajanen *et al.*, 2019).

The basic unit of the hierarchical structure of cellulose is formed by an aggregate of linear chains, which is called microfibril or elementary fibril. The literature suggests that the

vegetal microfibril is formed by 18-, 24-, or 36- cellulose chains, which are models based on the configuration of the rosette (protein complexes embedded in the plasma membrane that are responsible for the synthesis of microfibrils) (Cosgrove, 2014; Paajanen *et al.*, 2019). A bundle of microfibrils (typically modelled as four microfibrils) is called macrofibril or fibril, and a bundle of macrofibrils in a network forms the fibers (Fengel, 1970, 1969; Paajanen *et al.*, 2019). The vegetal microfibril has diameter of approximately 3.5 nm, the macrofibril has the diameter found in multiples of 3.5 nm, and a fiber can be found with lengths of 1 to 3 mm and widths of 10 to 50 μm depending on the cellulose origin (Fengel, 1970, 1969; Meier, 1962; Heyn, 1969; Paajanen *et al.*, 2019) as illustrated on Figure 2. The hemicelluloses are found to aggregate in the longitudinal direction being able to interact with the microfibrils (Fengel, 1970, 1969) and the macrofibrils are embedded in the lignin–Carbohydrate Complex (LCC) (Buranov and Mazza, 2008a; Tarasov *et al.*, 2018).

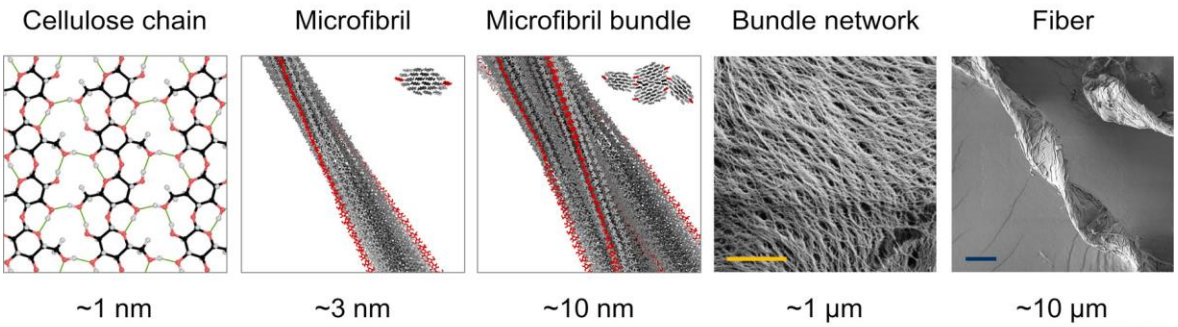

Fig. 2. Hierarchical structure of cellulose, highlighting the scale which defines the typical size referred for a cellulose chain, elementary fibril, microfibril, and fiber. (Paajanen *et al.* 2019).

The microfibrils are so tightly bound that even enzymes or molecules of low molecular weight have difficulty to access. However, there are still regions between the microfibrils that are not so tightly bound which causes a lattice defect in its microcrystalline structure, hence known as non-crystalline, semi-crystalline, or amorphous regions (Heyn, 1969). Due to the less rigid arrangement, the non-crystalline regions appear to promote flexibility to the plant cell wall while the crystalline regions promote stiffness (more rigid arrangement) (Fengel, 1971).

The slightly disorganization in the crystalline arrangement is enough to turn these regions accessible for chemical or biological attack, which explains the fact that non-crystalline regions are hydrolyzed more easily compared to crystalline regions (Fengel, 1970; Arantes and Saddler, 2010). The difficulty to fully hydrolyze cellulose is named cellulose recalcitrance (Arantes and Saddler, 2011; Himmel *et al.* 2007; Mansfield *et al.*, 1999).

2.2.2 Hemicellulose

The hemicelluloses, also termed as polyoses or cross-linking glycans, are a heterogeneous group of polysaccharides that constitutes the second major carbohydrate portion present in lignocellulose ultrastructure. The hemicelluloses are known to have its backbone constituted solely by xylose (xylan) or mannose (mannan), and glucose (mixed linkage glucans, MLG) or a combination of these monomers in disaccharides, such as xyloglucan and glucomannan. The hemicellulose backbone is linked by β-1,4 glycosidic bonds and can contain various pendant groups, such as acetyl, derived from hexoses (mannose, glucose, and galactose), derived from pentoses (xylose and arabinose), uronic acids (glucuronic, galacturonic, and methyl galacturonic acid), and derived from deoxyhexoses (rhamnose and fucose) (Scheller and Ulvskov, 2010).

Hemicellulose can be found in both primary and secondary cell walls, and their occurrence and type vary according to the type of biomass (Scheller and Ulvskov, 2010). The main polyoses in grasses are glucuronoarabinoxylans (GAX), mixed linkage glucans (MLG), and xyloglucan (Carpita, 1996; Smith and Harris, 1999; Vogel, 2008).

The typical amounts of each hemicellulose type in grasses and hardwood are shown on Table 1. GAX is a common type of grasses xylan that contains glucuronic acid and arabinosyl residues. GAX presents no clear pattern of substitution, thus they are often referred as GAX with high or low degree of substitution. GAX are also acetylated in various degrees (Carpita, 1996; Scheller and Ulvskov, 2010; Smith and Harris, 1999). MLGs are unique to grasses cell

walls of the family Poaceae, in which Sugarcane is a member. The MLG are the second most occurring polyoses in these types of grasses, playing an important role for the primary cell wall resiliency. MLG are constituted by glucose residues linked by β-1,3- and β-1,4-linkages, which make them known as β-glucans (Vogel, 2008). Xyloglucan is a minor type of polyoses in the grasses, mainly located in the primary cell wall. Xyloglucan is often found making interaction with cellulose microfibrils. Xyloglucan can be branched with arabinose and galactose residues (Scheller and Ulvskov, 2010).

The main role of hemicelluloses is to maintain the order of the lignocellulose matrix by forming interactions with cellulose (cellulose-hemicellulose) and lignin-Carbohydrate Complexes (LCC). The cellulose-hemicellulose interactions through hydrogen bonding enables, flexibility (tensile strength) to the cell wall and hemicellulose's diversity of pendant groups provides polarity and electrostatic repelling forces that prevent microfibrils aggregation (Reis and Vian, 2004). Conversely, the LCC occurs by actual linkages involving hemicellulose pendant groups with lignin. In grasses, GAX renders a role in both polysaccharide-polysaccharide and polysaccharide-lignin interactions. GAX with fewer substitution presents more interaction with cellulose whereas GAX with high substitution interacts more with lignin at various positions by ester- and ether-linkages and unbound hydroxycinnamic acids. (Vogel, 2008).

2.2.3 Lignin

Lignin is one of the three major components in the plant cell wall. The presence of lignin imparts mechanical and biological properties to lignocellulosic materials, such as rigidity, hydrophobicity, and protection against degradation (Hatfield and Vermerris, 2001). From a biorefinery point of view, lignin is the primary component associated with the recalcitrance of lignocellulosic materials due its complex phenolic composition, and different types of linkages within the lignin structure and with polysaccharides in the LCC (lignin-

Carbohydrate Complexes). Lignin hinders the accessibility to the polysaccharides especially by surface deposition (Li *et al.*, 2016).

Lignin is a macromolecule formed by oxidative coupling of hydroxycinnamic alcohols, phenylpropane precursors known as lignin units that are typically inter-linked by β-O-4′, β-5′, α-O-4′, 4-O-5′, β-β′ linkages and less commonly by β-1′, and 5-5′ linkages (Hatfield and Vermerris, 2001; Li *et al.*, 2016). The hydroxycinnamic alcohols are *p*-coumaryl alcohol (H unit: *p*-hydroxyphenyl), coniferyl alcohol (G unit: guaiacyl), and synapyl alcohol (S unit: syringyl). The difference between the three lignin units is the degree of methoxylation of the phenol ring, with the H, G, and S units containing respectively none, one, and two methoxyl substitutions. The amount of each lignin unit forming the macromolecule varies according to plant tissue and species. Softwood lignin is mainly constituted of G-units and hardwood lignin of G and S units. Lignin in grasses have the most varied composition, containing the three types of lignin units in the following average percentages: 4 – 15% of H-unit, 35 – 49% of G- unit, and 40 – 61% of S-unit (Vogel, 2008). Del Río *et al.* (2015) extensively studied the chemical structure of lignin in sugarcane bagasse and straw. They determined that the molar composition of core lignin (H:G:S) and S/G ration are: 2:38:60 and 4:68:28, and 1.6 and 0.4, respectively for bagasse and straw. Del Rio *et al.* (2015) shows that lignin from sugarcane bagasse and straw contain mostly β-O-4’ linkages, 80% and 75% respectively, and sugarcane straw lignin contains a higher amount of condensed lignin components (15% phenylcoumaran with β-5’ linkages and 3% of dibenzodioxocins with 5-5’ linkages). A high proportion of β-O-4’ ether linkages are characteristic of linear lignin structures, which would be easier to depolymerize and remove than highly branched and more condensed types of lignin (Grabber, 2005). Ferulate and *p*-coumarate are *p*-hydroxycinnamates compounds so-called non-core lignin (NCL) mostly found esterified with arabinoxylan (GAX). Ferulate and *p*-coumarate are the main components

connecting hemicellulose and lignin within the lignin-Carbohydrate Complexes (LCC) (Buranov and Mazza, 2008a).

Due to the complexity of lignin, any choice of pretreatment to open the cell wall ultrastructure and remove lignin affects both the chemical and physical properties of the recovered lignin as well as that remaining in the lignocellulosic residue. Li *et al.* (2016) identified desirable lignin characteristics to reduce recalcitrance and increase lignin hydrophilicity (*e.g.*, H units, esterified monomers, sulfonation, and aliphatic hydroxyls); however, they highlighted that the complexities of the remaining substrate after the pretreatment need to be considered for a subsequent treatment step, such as lignin redeposition, unproductive binding of enzymes in case of enzymatic hydrolysis, and accumulation of lignin fragments that are toxic for yeasts in case of subsequent fermentation of the sugar stream.

2.2.4 Acetyl residues

The content of acetyl depends on the plant species, *i.e.*, 2.5 – 3.7% sugarcane bagasse, 1.4 – 1.7% sugarcane straw, 3.2% eucalyptus globulus (Carvalho *et al.*, 2015; Lima *et al.*, 2018). The largest amount of acetyl residues is found in the secondary cell walls since it constitutes the bulk of biomass. Acetylation naturally occurs in hemicellulose, pectins, and lignin. Hemicellulose acetylation occurs at various degrees and at a greater amount compared to other lignocellulosic components. Acetyl groups of xylans, mannas, and pectin are attached to xylose residues at the position O-3 of and to O-2 to a lesser extent. Acetylation of xyloglucan occurs on the galactose residues, mostly at the position on O-6 (Scheller and Ulvskov, 2010). Naturally acetylated lignin (acetyl group in the gamma-carbon of the aliphatic sidechain) occurs in the S- and G-units. The degree of acetylation (DA) in lignin can be variable according to plant species. The occurrence of acetylation in the S- and G-units is 0.8% and 1.5% for sugarcane bagasse and 1.8% and 0.8% in sugarcane straw, respectively (del Rio *et al.*, 2015).

2.2.5 Ash

Inorganic components of agricultural biomass can be classified as intrinsic and extrinsic depending on the origin. The main source of ash is external (*i.e.*, as a co-harvested contaminant). Usually, the amount of ash is around 10%, however average amounts of ash can be found for sugarcane bagasse and straw of 1 – 6.5% and 4 – 29%, respectively (Negrão *et al.*, 2021). Extrinsic inorganic elements generally comprise soil (fine and coarse particles) and debris from mechanized harvest, which consists of silica. Common intrinsic inorganic elements that can be found in dry sugarcane leaves are N (3.3 g/kg), Ca (3.7 g/kg), K (2.0 g/kg), Cl (1.9 g/kg), Mg (1.1 g/kg), and other elements present at amounts lesser than 1 g/kg (Negrão *et al.*, 2021).

2.3 Current challenges for cellulosic sugars and ethanol production

Second generation (2G) technology of sugars and ethanol production (cellulosic sugar and ethanol) is a very promising alternative to further increase the ethanol production. However, stand-alone production of cellulosic sugars and ethanol is experiencing technoeconomic challenges because working with most lignocellulosic materials is more challenging than with starchy materials (Stephen *et al.*, 2012). Studies over more than ten years investigated different strategies to deconstruct lignocellulosic materials to produce cellulosic sugars, and ferment it to produce ethanol in a manner that is technically feasible and competitive with the ethanol production from sugarcane and corn (Davis *et al.*, 2018; Humbird *et al.*, 2011; Kazi *et al.*, 2010; Nguyen *et al.*, 1996). Even though significant progress has been made by reducing the minimum product selling price (MPSP), current ethanol 2G MPSP ranges from US$2.24 to US$2.54/gal (US$2.49/gallon of gasoline equivalent) (Davis *et al.*, 2021). Hence, the world has witnessed the shutdown and/or bankruptcy of several commercial cellulosic ethanol facilities.

There were eight first-of-a-kind facilities that started up since around 2014 aiming to process low-cost agricultural feedstock to produce cellulosic ethanol: Abengoa (USA), Beta Renewables (ITA), DuPont (USA), GranBio (former GraalBio - BRA), Henan Tianguan Group (CHN), Longlive (CHN), POET-DSM (USA), and Raizen Energy (BRA) (Padella *et al.*, 2019). Padella *et al.* (2019) discussed the status of these facilities that went through phases of being operational and then idle, followed by having the facilities being sold or changing business strategies. According to European Technology and Innovation Platform (ETIP) Bioenergy (2020) and International Energy Agency (IEA) Task 39 (2020), there are five facilities confirmed to be operational in 2021 and producing cellulosic ethanol at commercial level. Table 2 summarize information about these facilities.

Table 2. Ethanol 2G facilities operational in 2021, highlighting the country, technology readiness levels (TRLs), production capacity of cellulosic ethanol, raw material, products, technology, and whether it is co-located or stand-alone (ETIP Bioenergy, 2020; IEA Task 39, 2020).

Company (Country)	TRL	Production capacity	Raw material	Products	Technology	Integration
Borregaard (NOR)	9	15,800 t/y	Spruce wood	Technical lignin, Cellulosic sugars, and MFC	Sulfite pulping	SA
AustroCel Hallein (AUT)	8	30,000 t/y	Spruce wood	Textile pulp and Cellulosic sugars	Sulfite pulping	SA
GranBio (BRA)	8	35.9 m^3/y	Sugarcane bagasse and straw	Cellulosic sugars, Energy (consider nanocellulose production)	PROESA©	SA
Raízen Energy (BRA)	8	60,000 m^3/y	Sugarcrop residues	Raw sugars, Ethanol 1G and 2G, Energy, and Biogas	Raízen - Iogen©	CL
RISE Research Institute (SWE)	8	160 t/y	wood and non-wood (agriculture residues and wastes)	Cellulosic sugars, Lignin, Biogas (consider nanocellulose production)	CelluAPP©	-

MFC: Microfibrillated cellulose, SA: stand-alone, CL: co-located, -: not available

Facilities using acid hydrolysis technologies had more obstacles during the pretreatment and downstream steps. Combined with the high content of inorganics in the agricultural raw

materials, there were erosive-corrosive effect in the designed equipment, precipitation of condensed lignin (generally referred as “sticky lignin”), and carbohydrates degradation (*i.e.*, sugar dehydrations compounds, such as furfural and hydroxymethylfurfural) (Galbe and Wallberg, 2019). Downstream challenges were the inefficiency to recover and recycle the sulfuric acid (H_2SO_4) as well as to detoxify the spent liquor to ferment the sugar stream (Kazi *et al.*, 2010; Taherzadeh and Karimi, 2008). Feedstock handling at high pressures and feeding the reactor were also reported as a challenge (Galbe and Wallberg, 2019).

The acetyl groups are easily extractable from lignocellulosic material. Most pretreatments employed for cellulosic sugar production remove acetyl groups, and their sugar hydrolysates contain acetic acid in the range of 0.4 - 0.6% (v/v) and concentration up to 11 $g.L^{-1}$ (Vanmarcke *et al.*, 2021). The accumulation of acetic acid in the sugar stream causes pH to drop, reducing the fermentation efficiency and yeasts viability. Acetic acid has an inhibitor effect at levels around 3 $g.L^{-1}$ and present a combined inhibitor effect with other compounds formed by carbohydrates dehydration or lignin fractions considered toxic for current ethanol 2G fermenting yeasts (Vanmarcke *et al.*, 2021). Most alternatives to detoxify the sugar hydrolysates incur higher costs to prepare the sugar stream prior to fermentation which affects the minimum sugar selling price (MSSP). More economical detoxication alternatives are still being studied (Travália and Soares Forte, 2020). Other process hurdles have been more extensively discussed elsewhere (Lynd *et al.*, 2017;Padella *et al.*, 2019). Additionally, microeconomic and macroeconomic effects, such as respectively the necessity of government subsidies and changes in the price of oil, play an important role for the commercial success of these new bioindustries as well as the low return on investments (Galbe and Wallberg, 2019).

2.3.1 Deacetylation and Mechanical Refining (DMR)

Chen and co-workers have been investigating the combined process of mild alkaline treatment followed by mechanical refining, referred as Deacetylation and Mechanical Refining

(DMR) (Chen *et al.*, 2014; X. Chen *et al.*, 2015; Xiaowen Chen *et al.*, 2012b; Davis *et al.*, 2021). Their initial work in 2011 obtained an overall digestibility (glucan and xylan conversion) of the pretreated corn stover greater than 80% by combining deacetylation treatment with concentrated acid hydrolysis whereas solely acid hydrolysis would not lead to an overall digestibility higher than 70%. The deacetylation treatment (5%wt NaOH loading on corn stover) at temperature range of 60ºC – 80ºC removed 73 – 80% of acetyl groups, 12 – 23% of lignin, 2.9 – 4.7% of xylan, and 0.8 – 1.9% of glucan. Interestingly, low-solids enzymatic hydrolysis of unwashed solids of deacetylation pretreatment at 60ºC led to a higher glucan and xylan conversion (about 60% and 35%, respectively) comparatively to washed solids (about 43% and 23%, respectively) (Chen *et al.*, 2011). Chen and collaborators investigated the fermentability of the sugar stream produced after the combined deacetylation-acid treatment for different corn stover hybrids. They confirmed the deacetylation step was effective to reduce the formation of furfural during the acid hydrolysis stage. Furfural and acetic acid concentration at sugar stream after enzymatic hydrolysis were < 0.15 $g.L^{-1}$ and < 1 $g.L^{-1}$, which was not detrimental to the yeast growth or to the fermentation efficiency (Xiaowen Chen *et al.*, 2012a). Later, they concluded that coupling a concentrated acid pretreatment at high temperatures would not be economically viable due to expensive reactors and steam required, resulting in higher CAPEX and OPEX (Tao *et al.*, 2011). Hence, they investigated the feasibility of the combined process deacetylation-dilute acid hydrolysis together with a mechanical refining step (PFI milling) (Xiaowen Chen *et al.*, 2012b). The greatest benefit of coupling either deacetylation treatment and/or mechanical refining was to prevent the loss of xylan, which increased the amount of xylose recovered after the enzymatic hydrolysis, leading to higher ethanol titer in the fermentation. The synergistic effect of the combined pretreatment resulted in glucan and xylan conversions both up to 90% even for different corn stove hybrids. High-solids enzymatic hydrolysis of washed and unwashed solids obtained from the combined

process led to glucan conversion up to 90% and 85%, respectively. The combined process produced glucose and xylose concentrations in the range of 120 – 140 $g.L^{-1}$ and 50 – 70 $g.L^{-1}$, respectively, and ethanol titer up to 70 $g.L^{-1}$ (Xiaowen Chen *et al.*, 2012b). In 2014, Chen and coworkers proposed the combined deacetylation and mechanical refining (DMR) as the newest process alternative that can effectively fractionate herbaceous biomass to obtain high digestibility into sugars (90% of carbohydrates conversion, accounting monomeric and oligomeric sugars), removal of about 30% of lignin, removal 80% of acetyl groups with reduced formation of inhibitor compounds, reduced loss of hemicelluloses up to 10%, and higher ethanol titers (around 86 $g.L^{-1}$) (Chen *et al.*, 2014; X. Chen *et al.*, 2015). Technoeconomic assessment suggest that DMR process can achieve competitive minimum sugar selling price (MSSP) and minimum ethanol selling price (MESP) of $349/ton and $2.12/gallon of ethanol, respectively (X. Chen *et al.*, 2015; Davis *et al.*, 2018). The economics of the DMR process relies on efficient mechanical refining to ensure reduced enzyme loading can be used with high-solids enzymatic hydrolysis (Chen *et al.*, 2015). With a single disk-refiner and an energy consumption of 212 kWh/ton, the most efficient enzyme hydrolysis conditions was 20% solids with enzyme loadings of 20 $mg.g^{-1}$ of cellulose (4:1 ratio of Cellic CTec3:HTec3), reaching a glucan and xylan conversion of 82% and 77%, respectively (Chen *et al.*, 2014). Using a double refining step (Disk refiner and Szego milling) and same energy consumption, more economical conditions were obtained during the enzymatic hydrolysis: up to 25% solids with enzyme loadings of 10 $mg.g^{-1}$ of cellulose (4:1 ratio of Cellic CTec3:HTec3), reaching glucan and xylan conversion both up to 80% (monomeric and oligomeric sugars) (Chen *et al.*, 2015).

Davis *et al.* (2018) modeled a corn stover biorefinery that fractionates 2,205 ton (dry) per day to convert biomass into biofuels using the DMR process with MPSP of $2.50/GGE (gasoline gallon equivalent). They assessed a more severe deacetylation treatment (7%wt NaOH loading on corn stover at 90ºC for 1.5h), aiming to recover a higher amount of lignin

(47% of lignin solubilization) and convert it into products (*i.e.*, adipic acid and 2,3-butanediol). Because lignin is not destined to produce heat and power, it is necessary to import electricity (44 – 42 MW) from which pretreatment and enzymatic hydrolysis require 26 – 31% and 25%, respectively (Davis *et al.*, 2018). A five-times recirculation method is proposed as an alternative to concentrate the deacetylation spent liquor, reduce the solid to liquid ratio from 1:20 to 1:6.5, and obtain sodium, acetate, and lignin concentrations of 12 $g.L^{-1}$, ~15 $g.L^{-1}$, and 20 $g.L^{-1}$, respectively (X. Chen *et al.*, 2018). The method proposed to recover NaOH is the neutralization with sulfuric acid and production of sodium sulfate salt, which can be sold for $0.0706/lb (Davis *et al.*, 2018). However, the market price for NaOH and acetic acid are $588-738/ton and $350-650/ton, respectively for historical period of 2013-2017 (ICIS, 2018).

More efficient alternatives to recover NaOH and sodium acetate from the deacetylation spent liquor is the use of membrane electrodialysis (*i.e.*, BPMED) and microbial electrochemical technology (MET). These separation process use electrical potential difference to selectively recover chemicals (Jiang *et al.*, 2022; Patil *et al.*, 2017, 2015). Jian and coworkers showed the recovery of 82% of NaOH and production of H_2, which is an efficient and innovative alternative to produce energy from biomass (Jian *et al.* 2022).

2.3.1.1 Effect of deacetylation in the lignocellulosic ultrastructure

External and internal structure changes in the lignocellulosic ultrastructure modifies the interaction between the cell wall components and the environment by affecting the cell wall porosity and specific surface area (SSA) that leads to fiber swelling and enhanced carbohydrate accessibility (Hartman, 1985). These changes can be accomplished by mechanical and/or (bio)chemical treatments (Galbe and Wallberg, 2019). External structure changes occur with the removal of outer walls (primary and S1) of the lignocellulosic ultrastructure and its components (lignin and pectin) through external fibrillation and exposure of the secondary cell wall (S2), which enhances the access to the carbohydrates and contributes to fiber swelling

(Fengel and Wegener, 1983; Hartman, 1985). With this, hydrophobic interactions of lignin that are on the most outer surface are replaced by the hydrophilic interactions of hemicelluloses (Hartman, 1985). Internal structure changes occur in the varied bonds in the lignocellulose ultrastructure. The alkaline reaction mechanisms consist of the attack on ester and ether bonds, which breakdown the LCC (lignin-Carbohydrate Complexes) and lignin alkaline-labile bonds, turning lignin more hydrophilic and less condensed (Buranov and Mazza, 2008a; Fengel and Wegener, 1983; Li *et al.*, 2016; Tarasov *et al.*, 2018). The solubilization of lignin collapses the cell wall ultrastructure by reducing the hindrance barrier that recovers the carbohydrates and ultimately exposing the fibers, which increases the cellulose surface area (Fengel and Wegener, 1983; Li *et al.*, 2016). The extent of hemicellulose removal and lignin solubilization depends on the conditions of alkaline reaction. Traditional Kraft processes have yield of 40 – 65% and remove approximately 30% of xylan (X. Chen *et al.*, 2018; Fengel and Wegener, 1983).

Lima and collaborators studied the effect of deacetylation in the cell wall ultrastructure of SCB and SCS using NaOH loading on biomass of 1.2 – 8.4% for different temperatures (55, 70 and 85 °C) and periods (1, 3 and 5 h) (Lima *et al.*, 2018). They showed that deacetylation reactions increase the nanopores size of SCB in the range of 10 – 200 nm, which is greater than obtained with hydrothermal pretreatments. The increased nanopores are obtained after an overall solubilization threshold is met (around 10% and 20% for SCB and SCS, respectively). Additionally, they studied moisture sorption isotherms and suggested the deacetylation treatment increase the hydration of the cell wall structure, which occur because the water-accessible surface turned more hydrophilic and water uptake was favored by increased nanopores. They also showed that the extend of internal changes caused by deacetylation in the SCB's and SCS's ultrastructure. The transmission electron microscopy (TEM) micrographs of the deacetylated SCB shows the swelling effect for mild (4.8% NaOH loading on biomass, 70^{o}C for 3h) and severe deacetylation conditions tested (8.4% NaOH loading on biomass, 55^{o}C

for 1h), highlighting a delamination effect (Figure 3). This effect is evidence that a mild alkaline treatment as deacetylation can promote the relaxation of hydrogen bonds and increase fiber surface area (Lima *et al.*, 2018), which facilitates posterior steps of mechanical refining and improve access of enzymes for an increased carbohydrate digestibility (Chen *et al.*, 2015; Leu and Zhu, 2013).

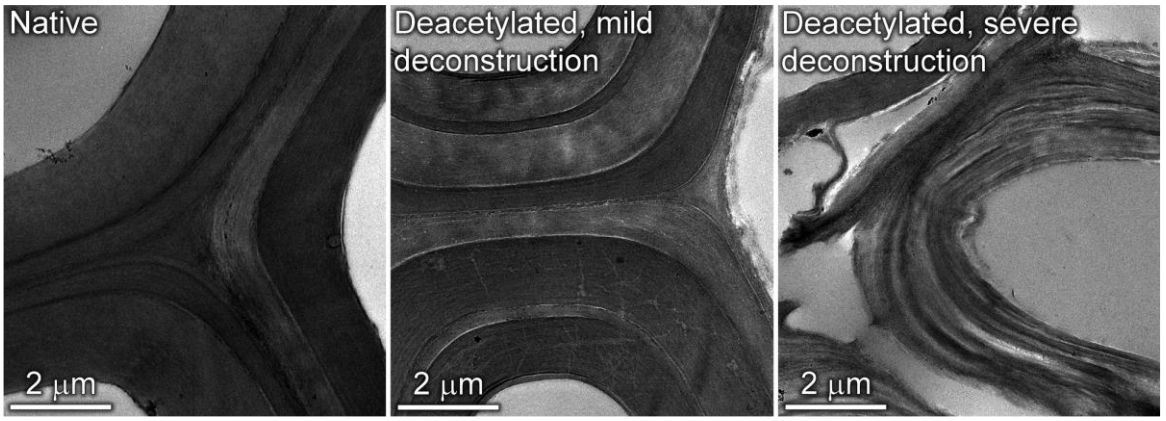

Fig. 3. Transmission electron microscopy (TEM) micrographs of native SCB and deacetylated SCB recovered after mild and severe deconstructions (Lima *et al.*, 2018).

Regarding the effect of deacetylation in terms of removal of main components, Lima and coworkers showed that acetyl groups can be fully recovered with solubilization of SCB and SCS of about 15% and 25%, respectively (Lima *et al.*, 2018). They showed that SCS xylan is more susceptible to the deacetylation treatment than SCB xylan (removal of 22% and 3%, respectively) (Lima *et al.*, 2018). Liu and collaborators studied the kinetics of hemicellulose dissolution and degradation during mild alkaline pretreatments of SCB and suggested that there is a fraction of hemicelluloses that is easily extractable from SCB in the initial stages of the treatment (dissolution rates 34.68%, 50.60%, and 60.28% at 50^{o}C, 70^{o}C, and 90^{o}C, respectively); A second hemicellulose fraction is more recalcitrant and requires longer time and/or higher temperature to be extracted. Thus, deacetylation conditions are less likely to produce carbohydrate degradation (degradation rates 2.72%, 4.28%, and 5.48% at 50^{o}C, 70^{o}C, and 90^{o}C, respectively) (Liu *et al.*, 2014). Regarding the effect of deacetylation on cellulose,

Lima and coworkers suggested that mild alkaline conditions do not promote a significant change in cellulose native crystalline organization for SCB and SCS because they did not observe significative cellulose co-crystallization (Lima *et al.* 2018).

2.3.1.2 Effect of mechanical refining in the lignocellulosic ultrastructure

The mechanical refining aims to reduce the particle size and increase the cellulose surface area by fiber cutting or shortening (comminution) and external and internal fibrillation that produces shorter fibers and delaminates fiber into fibrils (Hartman, 1985; Kortschot, 1997; Leu and Zhu, 2013). A scheme of refining effect in a long fiber is shown on Figure 4.

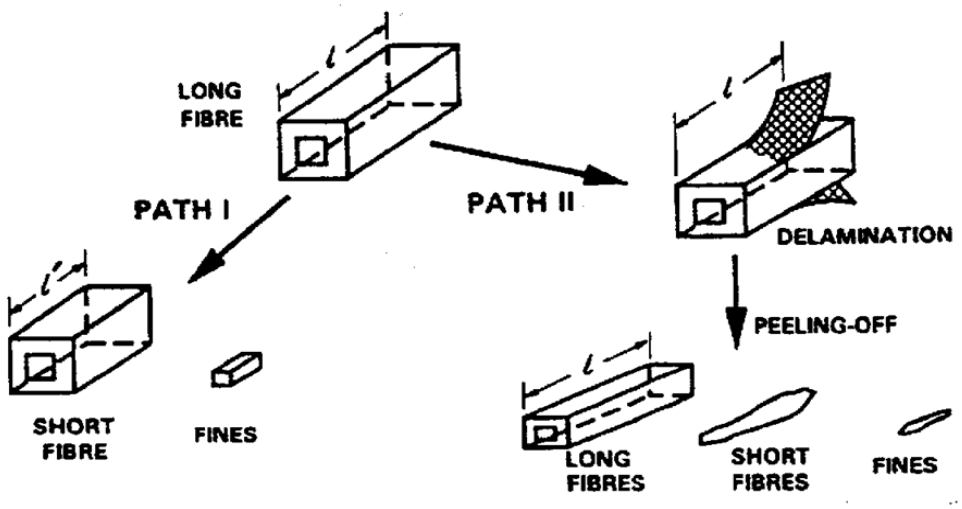

Fig. 4. Scheme of refining effect in a long fiber, highlighting the delamination effect, and production of short fiber and fines (Kortschot, 1997).

Fiber cutting results in shorter fibers with higher uniformity and fines (fragments in the 200 μm scale). External fibrillation (Figure 4, path I) removes the primary wall and produces an effect of pulling out fibrils from the outer fiber surface, which produce hair-like morphology (Hartman, 1985; Wang *et al.*, 2012). External fibrillation also causes the fibrils to break off, forming fines (Hartman, 1985). The shearing effects during mechanical treatment are especially responsible for the external fibrillation, which increases the surface area and hence fiber-fiber interaction (Chen *et al.*, 2013). This effect is widely employed prior a pretreatment to increase access to cell wall pores and improve mass transfer. It can also be employed subsequently after

a pretreatment aiming to enhance the cell wall deconstruction promoted by the pretreatment (Leu and Zhu, 2013). A more extensive cell wall deconstruction until fibril isolation is possible when external and internal fibrillation are present (Figure 4, path II). The internal fibrillation consists of the break of hydrogen bonds intra-fiber and replace with water molecules (Hartman, 1985). This phenomenon is referred as delamination, and it marks the individualization of fibrils (Wang *et al.* 2012). The delamination is especially promoted by compression forces and causes physical changes in the cell wall, which promotes a reduction in the crystallinity index (CI) and improves the cellulose accessibility (Hoeger *et al.*, 2013; Leu and Zhu, 2013).

Hoeger and coworkers studied the effect of internal and external fibrillation on different properties of lignified and non-lignified materials by using different periods of ultra-refining treatments and investigated their impact on cellulose conversion by subjecting the fibrillated materials to enzymatic hydrolysis with Cellic CTec2 for 48 (Hoeger *et al.*, 2013). They observed an overall reduction on the CI by about 15-25% after ultra-refining treatments and identifies that the CI reduction behaves differently for lignified and non-lignified materials. For bleached softwood kraft pulp (BSKP), the CI reduction occurs in the early stage of ultra-refining (first 2h) and, for ground softwood pulp (GSP), it would occur at an extended ultra-refining period (after 4h) due to a more preserved cell wall structure. Regarding the effect on cellulose digestibility, they observed a 5-fold improvement on cellulose conversion of GSP with external fibrillation (15 min of fibrillation resulted on cellulose conversion to improve from 6% to 30% using enzyme loading of 10 $FPU.g^{-1}$ of glucan) and a 10-fold cellulose conversion improvement (up to 60% cellulose conversion) with an extended ultra-refining period for 6h that caused external and internal fibrillation (Hoeger *et al.*, 2013). They indicated that external and internal fibrillation could reduce the enzyme loading by varying the ultra-refining time and suggested that the impact on cellulose conversion would vary for lignified and non-lignified materials due to limitation on enzymatic hydrolysis, such as unproductive

binding and limited pores availability. A reduction on the enzyme loading of 50% (from 10 to 5 FPU.g^{-1} of glucan) was obtained as a result of 6h-fibrillation of GSP, reaching cellulose conversion of 60%, whereas only 2 FPU.g^{-1} of glucan and 1h-fibrillation was necessary to obtain same cellulose conversion for BSKP (Hoeger *et al.* 2013).

2.4 Nanocelluloses and their current methods of production

The International Organization for Standardization (ISO/TC 229) defines nanocelluloses as a nanostructured material of which one or more dimensions are equal or smaller than 100 nm (International Organization for Standardization, 2005). Moreover, there is an on-going effort to establish internationally the nomenclature, terminology, methodologies, environmental health and human safety management for the use and testing of nanocelluloses (Halappanavar *et al.*, 2021; Moon *et al.*, 2023). The general method to isolate nanocelluloses from lignocellulosic materials consists of three main steps. The first two steps are intended to prepare the lignocellulosic material to produce a cellulose-rich pulp: 1) disruption of the lignocellulosic macrostructure by increasing porosity and accessibility to the polysaccharides, 2) extraction of cellulose by removing the hemicellulose and lignin, and 3) isolation of nanocelluloses (García *et al.*, 2017; Reid *et al.*, 2017). The choice of process for nanocellulose isolation can affect the nanocelluloses' morphology, particle dimensions, surface charges, behavior in solution, thermostability, and mechanical properties (García *et al.*, 2017). Regarding nanocelluloses' morphology, there are two main morphology types of nanocellulose that can be obtained according to the isolation process: cellulose nanocrystals (CNC) and cellulose nanofibrils (CNF), as shown on Figure 5.

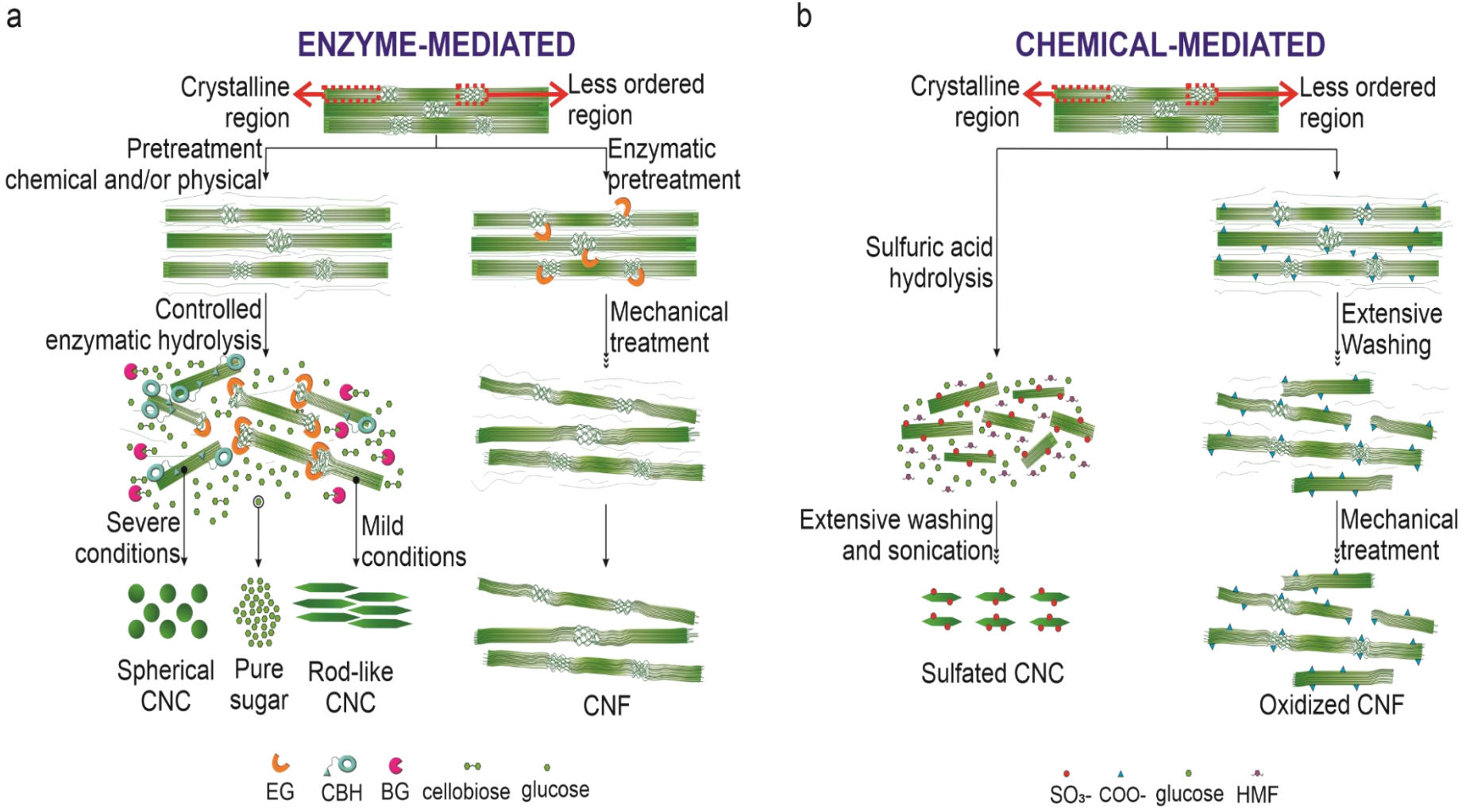

Fig. 5. Main steps to isolate cellulose nanocrystals (CNC) and cellulose nanofibrils (CNF) according to the method employed: a) enzyme-mediated and b) chemical-mediated. EG: Endoglucanase, CBH: cellobiohydrolase, BG: β-glucosidase, HMF: hydroximethylfurfural (Arantes *et al.*, 2020).

2.4.1 Cellulose nanocrystal (CNC)

Cellulose nanocrystal (CNC) is a crystalline nanomaterial with highly homogeneous morphology identified by transmission electron microscopy (TEM) micrography or atomic force microscopy (AFM) topography as rod-like or spherical shape, depending on the raw material and the treatments employed (Arantes *et al.*, 2020; X. Q. Chen *et al.*, 2019; de Oliveira Júnior *et al.*, 2022; Ji *et al.*, 2019; Tong *et al.*, 2020).

Concentrated acid hydrolysis is the preferred method to isolate CNC at large scale (Miller, 2019), resulting in the widely known CNC model. The acid hydrolysis reaction employed for CNC isolation consists of controlled conditions to promote the attack of hydronium ions preferably in the less structured regions of the cellulose, which isolate the crystalline regions, followed by esterification of the hydroxyl groups that result in a sulfated CNC (Figure 5b). The advantages of concentrated acid hydrolysis are the reproducibility of the method and characteristics of acid-CNC, low cost of sulfuric acid as the preferred reagent (US$ 90/t according to De Assis *et al.* 2017a), and high yield obtained (*i.e.*, yields are 30–50% and up to 70% for a narrow reaction condition according to Chen *et al.* (2015).

The typical characteristics of acid-CNC are: diameter of 4 –20 nm, length of 50 – 350 nm, high aspect ratio (length to diameter ratio, L/D ratio of 50), high crystallinity (>80%), good colloid stability in water obtained by zeta potential (-34 to -42 mV), sulfur content of 0.15 to 1.1 g/100g of CNC, and good thermal stability (maximum temperature of degradation of 275 – 300 ^{o}C) (García *et al.*, 2017; Reid *et al.*, 2017; Delepierre *et al.*, 2021; Moon *et al.*, 2023). A summary of characteristics and properties of commercial CNCs are shown on Table 3.

An economic drawback of the concentrated acid hydrolysis to isolate CNCs is the necessity of acid-resistant equipment, pipelines, and robust reactor, which incurs in a high CAPEX in the range of US$ 95 - 224 M (Table 4). The use of concentrated sulfuric acid negatively affects operational expenses (OPEX) due to depreciation expenses, requirement of

acid makeup, and challenges to recover and recycle the sulfuric acid at reasonable prices as well as to recover the solubilized sugars from the spent liquor (de Assis *et al.*, 2017a). Thus far, the simplest and most viable solution to recycle sulfuric acid is the neutralization using lime, which generates large quantities of gypsum ($CaSO_4$) (de Assis *et al.*, 2017a; Leistritz *et al.*, 2006). The disposal of gypsum and the high demand for pure water (reverse osmosis) during dialysis or ultrafiltration stages not only have a negative impact on environmental indices but also generates high effluent treatment costs (Leão *et al.*, 2017; Rosales-Calderon *et al.*, 2021).

De Assis *et al.* (2017a) assessed the acid hydrolysis with concentrated sulfuric acid to isolate CNC from dissolving pulp and estimated the CNC's MPSP is 4.4 – 7.2 US$/kg, considering a CNC yield of 50% and an internal rate of return (IRR) of 16% (Table 4). They concluded that initiatives to increase the CNC yield and lower the cost of raw material, combined with actions to save CAPEX are essential to achieve a reduction of the CNC's MPSP.

Rosales-Calderon *et al.* (2021) assessed the acid hydrolysis with concentrated sulfuric acid to isolate CNC from BHKP, which has a smaller content of cellulose and lower average prices comparatively to dissolving pulp. They suggested that the amount of acid required changes according to the cellulose source and hence the recovery and recycle of acid become more important for the economics when starting from raw materials with smaller content of cellulose.

Moreover, the use of starting material other than pulp would require a step of raw material preparation that impact the CNC yields and process economics. We estimated that acid-CNC yields could be in the range of 9.5 – 31.5 (g/100g) based on untreated lignocellulosic material, considering the average composition of cellulose in lignocellulosic materials of 35 – 50%, cellulose extraction using alkaline and bleaching steps (about 90% of cellulose recovery), and an acid hydrolysis yield of 30 – 70% on pulp basis.

Table 3. Summary of raw material, process of isolation, characteristics, and properties from commercially available CNCs (Nelson and Retsina, 2014; Reid *et al.*, 2016; Delepierre *et al.*, 2021).

Company	**Trade name / Capacity (kg/day)**	**Cellulose source**	**Process of isolation**	**Diameter (nm)**	**Length (nm)**	**Aspect ratio (L/D)**	**CI (%)**	**Zeta potential (mV)**	**Sulfur content (g/100g CNC)**	**T*max* (ºC)**	**Viscosity (cP)**
CelluForce	CelluForce NCC® / 300	BKP	Sulfuric acid 64%	6±2	183±88	31	89.9	-38	0.8	275-300	-
Alberta Innovates – AITF	- / 20	Cotton	Sulfuric acid 63,5%, 45 ºC, 120 min	8±2	134±56	17	91.2	−42 ± 1 (cotton) −34 ± 1 (dissolving pulp)	0.75	275-300	-
Forest Products Laboratory - FPL	- /10	Dissolving pulp	Sulfuric acid 64%, 45 ºC, 60 min	7±2	134±52	19	53.9 (CNC I) 46.1 (CNC II)	-46	1.1	275-300	-
American Process - API	BioPlus Crystals® / 130	Variety of sources	AVAP® (SEW)	4 - 5	50 - 500	10 – 125	93	-	-	-	-
NORAM-AITF	- / -	Wood pulp	Sulfuric acid	5±1	160±30	40±10	82	−34 ± 2	0.31	300	3.5
Melodea	- / 100	HBKP, NBKP, and agricultural residues	Sulfuric acid	4±1	210±60	70±30	79	−31 ± 1	0.15	300	650
Anomera	DextraCel™ / -	SWP	Dilute hydrogen peroxide oxidation	5±2	150±30	30±10	80	−21 ± 1	0.16	300-350	1.6
Blue Goose Biorefineries - BGB	BGB Ultra™ / 10	Dissolving pulp	Oxidation catalyzed by transition metal	5±2	210±50	40±20	93	−28 ± 2	0.15	300-350	25

HBKP: Hardwood Bleached Kraft pulp, NBKP: Northern Bleached Kraft pulp, BKP: Bleached Kraft pulp, SWP: Softwood pulp, SEW: SO_2-Ethanol-Water treatment, CI: crystallinity index T*max*: temperature of maximum degradation.

Table 4. Summary of technoeconomic aspects of CNC isolation (Adapted from Arantes *et al.*, 2020).

Author	CNC MPSP (US$/kg)	CAPEX (US$ M)	OPEX (US$ M per year)	Production cost (US$/t of NC)	Productivity (t/year)	Ethanol (L/t)	Isolation Method	Yield (starting material basis)	Raw material	Feedstock (t/year)	Pretreatment
Leistritz *et al.* (2006)	1.87 [C*]	185	92.4	1,254	1,050	228.8	AH by MBI international	6%, 45.50% (CSR)	Wheat straw	900,000	AFEX + EH
Albarelli *et al.* (2016)	2.21 [F*]	-	-	-	100	70.71	AH (64% H_2SO_4, 45 °C, 30 min)	3.36%	SCB	2,976	SO_2 explosion + EH
	2.21 [F*]	-	-	-	100	77.32	AH (64% H_2SO_4, 45 °C, 30 min)	2.62%	SCB	3,822	Supercritical CO_2 explosion + EH
	2.21 [F*]	-	-	-	100	85.28	AH (64% H_2SO_4, 45 °C, 30 min)	1.71%	SCB	5,861	OS + EH
	2.21 [F*]	-	-	-	100	97.79	AH (64% H_2SO_4, 45 °C, 30 min)	0.29%	SCB	34,661	Supercritical CO_2-OS + EH
Savignon and Gonçalves (2016)	400 – 1,000 [F*]	83.8	107.9 – 178.3	525,832 – 868,800	205.3	(1.8 % sugars)	EH (Filson *et al.* 2009)	20 – 40%	Recycled pulp	513.3 - 1,026.5	None

(To be continued)

Table 4 (conclusion)

Author	CNC MPSP (US$/kg)	CAPEX (US$ M)	OPEX (US$ M per year)	Production cost (US$/t of NC)	Productivity (t/year)	Ethanol (L/t)	Isolation Method	Yield (starting material basis)	Raw material	Feedstock (t/year)	Pretreatment
de Assis *et al.* (2017a)	4.4 – 7.2 C*	95 – 188	181.6 – 221	3,632 – 4,420	50	(3 % sugars)	AH (64% H_2SO_4, 45 ºC, 60 min)	50%	Dissolution pulp	100.5	None
Junyuan (2017)	22.2* F*	-	12.9*	12.9*	1,000	-	AH (63% H_2SO_4, 45 ºC, 45 min)	31.30%	MCC AaltoCell	3,195	None
	22.2* F*	-	10.9*	10.9*	1,000	-	AH (63% H_2SO_4, 65 ºC, 20 min)	30%	MCC AaltoCell	3,320	None
Rosales-Calderon *et al.* (2021)	10.03 C*	223.6	231.4	7,779	29,750	(glucose yield 28%, xylose yield 92%)	AH (62%, 50 ºC, 75 min)	68%	HBKP	43,750	None
	65.74 C*	86.8	125.2	49,318	2,538	Sugars 125 g/L (glucose yield 56%, xylose yield 92%)	EH (Pereira and Arantes, 2020)	5.8%	HBKP	43,750	None
Wang *et al.* (2021)	-	-	-	-	-	glucose yield 42.1%, xylose yield 13.02%, Ethanol 22 $g.L^{-1}$	AH (64% H_2SO_4, 45 ºC, 60 min)	8.9 ± 0.8	HBKP		EH (15 FPU/g of NS 51129, 50ºC, 8h)

- : not reported; CNC: cellulose nanocrystal; CNF: cellulose nanofibrils; MFC: microfibrillated cellulose; NC: Nanocellulose; MPSP: Minimum product selling price; CAPEX: capital expenditure; OPEX: operational expenditure; C*: MPSP calculated; F*: MPSP assumption (fixed for the analysis); AH: Acid hydrolysis; EH: Enzymatic hydrolysis; AFEX: Ammonia fiber explosion; OS: Organosolv; MCC: Microcrystalline cellulose; CSR: cellulosic solid residue; HBKP: Hardwood Bleached Kraft Pulp; *Currency conversion: 1€ = 1.11 US$ (Dec, 2019

2.4.2 Cellulose nanofibrils (CNF)

Cellulose nanofibrils (CNF) is the product generated by the complete release of fibrils from the cellulose microstructure resultant by breaking the interaction forces between the elementary fibrils through mechanical treatment (high rates of compression, friction, and shear) (Iwamoto *et al.*, 2007) or chemical treatment (overcharging non-crystalline domains) (Tejado *et al.*, 2012). The typical characteristic of CNFs is long non-branched fibrils that can be observed as individualized or entangled fibrils by microscopy techniques such as TEM, AFM, and scanning electron microscopy coupled with TEM detector (SEM/STEM). The CNF microstructure comprises both crystalline and less ordered regions of cellulose (Moon *et al.*, 2023). The CNF average size has a diameter in the range of 3 - 100 nm and length in the micrometric scale, resulting in a high aspect ratio (L/D ratio > 10) and hence high specific surface area (SSA), although smaller SSA and degree of crystallinity (40 – 50 %) when compared to CNCs (Berto and Arantes, 2019; Iwamoto *et al.*, 2007; Moon *et al.*, 2023).

There are several methodologies and equipment useful to produce CNFs, which may or may not be proceeded by a pretreatment step to reduce clogging and decrease energy demand. The three equipment commonly employed in the preparation of CNFs, that is the homogenizer, microfluidizer, and disc ultra-refiner (Spence *et al.* 2011). The type of equipment and operating conditions (*e.g.*, solids loading, number of passes, flow rate, pressure requirements, and disc's material) are factors that affect the energy consumption, the scalability potential, and other aspects related to downtime, maintenance, and depreciation expenses (de Assis *et al.*, 2017b; Spence *et al.*, 2011). New methods and equipment for CNF isolation were reviewed by Arantes *et al.* (2020), including extrusion and ball milling.

The homogenizer and microfluidizer are operated at high pressure and low solids loading (0.2 to 3% dry matter) (Arantes *et al.* 2020). They are operated by forcing the pulp suspension against slits of micro size that generates shear forces and cavitation that cause fiber

fibrillation. The main drawback of using high pressure systems to isolate CNF are the clogging and energy demand due to the several numbers of passes, which requires pretreatments to reduce operational problems and energy consumption (Henriksson *et al.*, 2007; Hu *et al.*, 2015; Nechyporchuk *et al.*, 2016; Siddiqui *et al.*, 2010; Spence *et al.*, 2011). On the other hand, the ultra-refiner presents fewer operation problems and downtime with fiber encrustations when compared to other methods, which allows the use of higher solids contents up to 2 – 4.5% without pretreatment (Arantes *et al.* 2020). The maximum consistency reported for disc ultra-refiners is 5 – 10% employed for different materials (*e.g.*, wood pulps, chitosan, tunicin cellulose, and collagen) (Taniguchi and Okamura, 1998).

The disc ultra-refiner (also referred as wet refiner, wet grinder, micro-grinder, ultra-grinder, or grinder with stone disk) is operated similarly to common refiners in the pulp and paper industry. In the ultra-refining method, the pulp suspension is subjected to defibrillation due to the compression, shear, and friction forces when fibers pass a rotating and a static disc with working gap that can be adjusted with a clearance typically equal or smaller than -100 μm. The pulp suspension is fed by gravity and subjected to centrifugal force into the clearance between the two stones discs. One ultra-refining cycle consists of complete pass of the suspension and its recovery in the outlet for a subsequent feed that allows a continuous operation (Hu *et al.*, 2015; Wang *et al.*, 2012). Figure 5 shows an illustration of the most known disc ultra-refiner, the SuperMassColloider from Masuko Sangyo Co. Ltd. (Japan), and its scheme of operation. For most Supermasscolloider models that does not operate with the weight of the top disk, the energy consumption is proportional to the refining time, and the energy demand is almost exclusively originating from the force required to defibrillate the material according to the gap clearance (Hoeger *et al.*, 2013; Hu *et al.*, 2015; Liu *et al.*, 2018). For standard refiners, the gross energy (including no-load (idle) and disc's motion) is relevant not only the net refining energy as occurs for Supermasscolloider models where the disc's

motion is not representative (Hu *et al.* 2015; Liu *et al.* 2018). Lindström, (2017) attributes the energy required for cellulose delamination to the cell wall cohesion and presence of charges, such as carboxyl groups present in xylan (Liu *et al.* 2018) or groups inserted during pretreatments (Tejado *et al.* 2012).

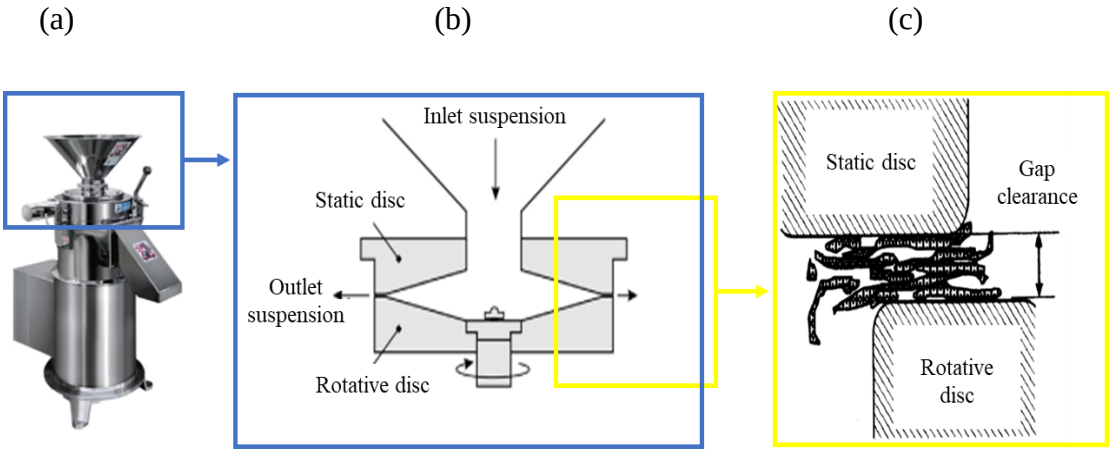

Fig. 5. (a) Illustration of SuperMass Colloider, (b) scheme of operation, (c) highlight of gap clearance and showing fibers between the static and rotative stones. Source: Adapted from Nechyporchuk *et al.* (2016) and Roux and Mayade (1999).

Ultra-refining leads to an increase in specific surface area (SSA) and fine content with reduction of fiber length (Roux and Mayade, 1999). Because the effects of mechanical operation occur randomly over several cycles, a mixture of micro- and nanoscale particles with high polydispersity is generated, depending on the extent of fibrillation. The extended fibrillation can reach higher diameter uniformity; however, it generally results in fiber cutting effect that is negative for CNF properties (Berto and Arantes, 2019; Kelly *et al.*, 2021; Malucelli *et al.*, 2018; Nakagaito and Yano, 2004). Currently, a mixture of cellulose nanofibrils and cellulose microfibers (CMNF) is referred as nanocelluloses, and the term is used interchangeably with the term CNF (Moon *et al.* 2023).

2.5 Integrated production of nanocelluloses via enzyme-mediated process

2.5.1 Enzymatic hydrolysis

Enzymatic hydrolysis of lignocellulosic carbohydrates is a process catalyzed by enzyme cocktails constituted by carbohydrate active enzymes (CAZymes) able to breakdown or modify the structural polysaccharides of lignocellulosic materials, according to the enzyme's tridimensional structure and the sequence of amino acids in their catalytic domain (Henrissat, 1991; Henrissat and Davies, 1997); Levasseur *et al.*, 2013). Enzyme cocktails can contain a single-component (mono-enzyme) or pool of enzymes that act on specific links of polysaccharides and/or oligomers substrates. Single-component cocktail cannot completely depolymerize the structural polysaccharides from biomass. Current commercial enzyme cocktails for biomass conversion (*i.e.*, Cellic CTec series from Novozymes) are constituted by a pool of enzymes that act collaboratively and synergically and target a high-carbohydrate conversion. These high-carbohydrate conversion enzyme cocktails can be used in high-solids enzymatic hydrolysis with minimal inhibition by the end-product (glucose, cellobiose, and xylose) and minimal deactivation (high thermostability) (Modenbach and Nokes, 2013; Teter, 2012).

Figure 6 illustrate the diverse type of CAZymes families and the need for collaborative hydrolytic and oxidative action (glycoside hydrolase (GH) and auxiliary enzymes (AA), respectively) for the complete depolymerization of cellulose (Arantes and Saddler, 2010; Bissaro *et al.*, 2016; Dimarogona *et al.*, 2012; Horn *et al.*, 2012). In deep discussion of the CAZymes families and mode of actions for cellulose depolymerization was presented by Payne *et al.* (2015). A detailed discussion of the effect of CAZymes families at the fiber level was presented by Arantes *et al.* (2020). The complete depolymerization of hemicellulose requires different families of CAZymes due to its varied composition and types of links constituting the hemicelluloses (Glass *et al.*, 2013; Payne *et al.*, 2015).

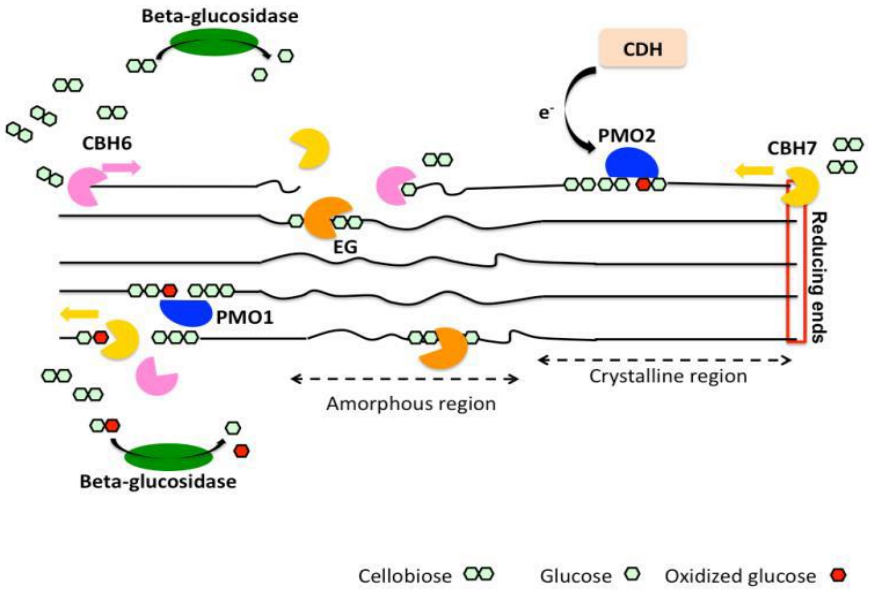

EG: endoglucanases (GH5 to GH9, GH12, GH45), CDH: cellobiose dehydrogenases (auxiliary enzymes AA3 and AA8), PMO or LPMO: Lytic polysaccharide monooxygenases 1 and 2 (auxiliary enzymes AA9)

Fig. 6. Illustration of the cellulose depolymerization model during enzymatic hydrolysis by a complete saccharification enzyme cocktail, highlighting the main hydrolytic and oxidative enzymes involved in the full depolymerization of cellulose (Dimarogona *et al.*, 2012).

The enzymatic route is the most economically feasible to produce sugars at high titers with high profitability (Kazi *et al.* 2010) and free of inhibitors (Himmel *et al.* 2007). However, a complete carbohydrate conversion into fermentable sugars is not economically advantageous to produce cellulosic ethanol (Dias *et al.*, 2013). Dias and collaborators assessed different conditions for pretreatment and enzymatic hydrolysis and demonstrated that a higher production of 1G/2G ethanol can be obtained using intermediate conditions of solids consistency and sugar conversion (15% and 60%, respectively) for better economic feasibility. The extended carbohydrate conversions (higher than 80%) incurs in higher costs for the enzymatic hydrolysis step due to longer residence time required (72h or more), reduced gains in sugar conversion levels at longer reaction times, increased demand for heat to maintain the temperature of the bioprocess, and need for liquor concentration in case of obtaining low sugar concentration (Modenbach and Nokes, 2013; Newman *et al.*, 2013). Suitable ranges of enzymatic hydrolysis conditions to obtain high titers of sugar (>100 g/L) for industrial

operation are established in the literature, which are enzyme loading < 30 mg/g, high solids loading (>15%), and time up to 48 h (Dias *et al.*, 2013; Humbird *et al.*, 2010; Modenbach and Nokes, 2013; Newman *et al.*, 2013; Stephen *et al.*, 2012) The National Renewable Energy Laboratory (NREL) targets cellulose and xylan conversion both at 90% and arabinan conversion at 85% using total enzyme loading at 10 mg enzyme protein/g of cellulose although their latest technology uses an enzyme loading of 12 mg/g on DMR substrates (Davis *et al.*, 2018).

It is noteworthy to mention that the isolation of nanocelluloses from the remaining residue of enzymatic hydrolysis, also referred as cellulosic solid residue (CSR), is more advantageous than the current practice of burning it together with lignin (Leistritz *et al.* 2006, 2009; Albarelli *et al.* 2016). The lignin and CSR recovered often contains too much moisture to be burnt (Davis *et al.*, 2018) and they do not have the same heating value (hemicellulose 17.7 $MJ.kg^{-1}$, cellulose 17.3 $MJ.kg^{-1}$, SCB lignin 26.9 $MJ.kg^{-1}$, dry bagasse 19.1 $MJ.kg^{-1}$) (Dias, 2011). Kazi *et al.* (2010) assessed different scenarios of pioneer plants for cellulosic ethanol production, including four types of pretreatments and three downstream methods, and concluded that is not economically advantageous to burn plant by-products to meet the demand for heat and power. They suggested that obtaining steam and electricity from other sources (*i.e.*, the combustion of natural gas) would be more economic favorable due to the high cost of installation of a fluidized bed combustor (around US$ 50M, Davis *et al.*, 2018) comparatively to the cost of an installed natural gas boiler (US$ 3 M, Kazi *et al.* 2010). Additionally, the heating value of natural gas is significatively higher (42-55 $MJ.kg^{-1}$, The Engineering ToolBox, 2003).

Enzymatic hydrolysis can be employed to isolate CNC and/or CNF, together with sugars or not (Arantes *et al.*, 2020). There are two process strategies via enzyme-mediated treatment to integrate the production of nanocellulose and sugars. First strategy uses enzymatic

hydrolysis as a pretreatment to promote mild cellulose disruption (cellulose swelling), which may or may not recover considerable quantity of sugars to be recovered as a valuable stream. Examples of enzyme-mediated process as a pretreatment consists of its use prior to refining step to reduce energy consumption in the fibrillation process when isolating CNF (Berto *et al.*, 2021; Henriksson *et al.*, 2007; Xiuyu Liu *et al.*, 2019) or prior to acid hydrolysis to maximize the valorization of the raw material and reduce the amount of sulfuric acid when isolating CNC (Beltramino *et al.*, 2015; Beyene *et al.*, 2017; Dai *et al.*, 2018; J. Wang *et al.*, 2021a). The second process strategy employs a more severe enzymatic treatment that produces sugars at high titers together with CNC and/or CNF (Beyene *et al.*, 2017; Bondancia *et al.*, 2017; Camargo *et al.*, 2016; Pereira *et al.*, 2021; Pereira and Arantes, 2020; Song *et al.*, 2014; J. Wang *et al.*, 2021a; Zhu *et al.*, 2011). Based on the latter references, it is possible to propose an integrated route to produce nanocellulose and sugars for integral valorization of the raw material.

2.5.2 Feasibility of enzyme-mediated isolation of CNC

CNC isolated by enzymatic hydrolysis (enzymatic-CNC) possesses final properties highly dependent on the type of enzyme, hydrolysis conditions, and composition of the cellulose source. Table 5 shows a summary of enzymatic-CNC properties obtained solely by enzymatic hydrolysis treatment. Typically, but not necessarily, enzymatic hydrolysis maintains the cellulose surface intact (when using hydrolytic enzymes), which produces enzymatic-CNC with lower colloidal stability (high tendency to aggregate) and higher thermostability comparatively to acid-CNC. Other characteristic of the enzyme-mediated isolation is the ability to tailor CNC shapes (rod-like or spherical) (Figure 5). Enzymatic-CNCs can be very uniform in size with high aspect ratio depending on the reaction conditions (X.-Q. Chen *et al.*, 2019, 2018; de Oliveira Júnior *et al.*, 2022; Kafle *et al.*, 2015)

Table 5. Enzymatic hydrolysis conditions to isolate CNC and its properties in terms of size, crystallinity index, thermostability and zeta potential (Adapted from Arantes *et al.*, 2020).

Morphology	Size		CI (%)	Thermostability (◦C)		Zeta Potencial (mV)	Yield (%)	Sugars (g/L)	EH conditions	Raw material	Reference
	Length (nm)	Diameter (nm)		T_{onset}	T_{max}						
Rod-like	100–1,800	30–80	Decreased	-	-	−31.37	3.4–38	-	Celluclast 1.5l FG (84EGU/200mg) at 50-60◦C for 60 min	Recycled pulp	Filson *et al.* (2009)
Rod-like	120.27 ± 36.25	40.74 ± 7.59	88.26 to 78.39	-	-	−14.6	< 22	-	Microbial hydrolysis at 25-30◦C up to 5 days	Microcrystalline cellulose (MCC)	Satyamurthy *et al.* (2011)
Rod-like	70–280	10–40	-	-	-	-	20	-	*T. reesei* cellulase (10 - 19 FPU/g) at 45-50◦C up to 72h	Cotton fibers pretreated with DMSO	Chen *et al.* (2012)
Spherical	-	20	78.1	-	-	-	30–35	-	*T. reesei* cellulase (10 - 19 FPU/g) at 45-50◦C up to 72h	Cotton fibers pretreated with NaOH (20%)	
Spherical	-	6	didn't change	-	-	-	20–25	-	*T. viride G* cellulase (10 - 19 FPU/g) at 45-50◦C up to 72h	Cotton fibers pretreated with ultrassound	
-	-	-	-	-	-	-	10–15	-	*T. viride G* cellulase (10 - 19 FPU/g) at 45-50◦C up to 72h	Cotton fibers	
Rod-like	286	24	80.2 to 72.0	-	-	−11.4	18	-	*T. reesei* cellulases	Bamboo fibers	Zhang *et al.*, (2012)
Spherical	-	40-90	80.46 to 78.98	250	350	-	< 20	-	Cellusoft L (0.5 - 2.5%) at 50◦C up to 192 h	Cotton fibers	Meyabadi *et al.* (2014)
Rod-like	500–1,200	4–12	72.76 to 81.02	-	-	-	-	2–8	EG and BG blend at 85◦C up to 72 h or Optimash at 45◦C up to 72h	MFC Celish ® KY	Teixeira *et al.* (2015)
Rod-like	500–1,000	4–6	58.42 to 65.94	-	-	-	-	0.5–1	EG and BG blend at 85◦C up to 72 h or Optimash at 45◦C up to 72h	Eucalyptus bleached pulp ultragrinded	

(To be continued)

Table 5 (continued)

Morphology	Size		CI (%)	Thermostability (◦C)		Zeta Potencial (mV)	Yield (%)	Sugars (g/L)	EH conditions	Raw material	Reference
	Length (nm)	Diameter (nm)		T_{onset}	T_{max}						
Rod-like	500–1,500	4–10	59.33 to 68.48	-	-	-	-	2–3	EG and BG blend at 85◦C up to 72 h or Optimash at 45◦C up to 72h	Unbleached Kraft softwood pulp ultragrinded	Teixeira *et al.* (2015)
Rod-like	250–1,000	4–8	59.60 to 61.59	-	-	-	-	0.5–1	EG and BG blend at 85◦C up to 72 h or Optimash at 45◦C up to 72h	Sugarcane bagasse ultragrinded	
Rod-like	100–400	15–80	54.21 to 57.80	-	284 - 312	-	< 23.98	-	EG (84 EGU) at 50◦C up to 36 h with sonication treatment	Old corrugated container (OCC) treated with NaOH and Phosphoric acid	Tang *et al.* (2015)
Rod-like	200–500	5–10	60.37 to 83.41	310	360	-	12.14 - 17.58	-	Celluclast 1.5 L at 50◦C up to 120h	Microcrystalline cellulose (MCC)	Cui *et al.* (2016)
Rod-like	100–200	5–10	60.37 to 87.46	300	360	-	14.81 - 19.34	-	Celluclast 1.5 L at 50◦C up to 120h with post ultrasound for 30 min	Microcrystalline cellulose (MCC)	
Rod-like	40–50	5–8	60.37 to 82.26	250	350	-	15.76 - 22.57	-	Celluclast 1.5 L at 50◦C up to 120h with post ultrasound for 60 min	Microcrystalline cellulose (MCC)	
Rod-like	216 ± 86	15 ± 6	72 - 83	-	325	-	-	44.8–125.4	Cellic Ctec3 (5-17 mg/g), 8-22% DM at 50◦C up to 144h	Bleached Kraft eucalyptus pulp	Bondancia *et al.* (2017)
Spherical	-	-	-	-	-	-	20.17	reducing sugars 17.09%	Cellulase 200U/mL at 50◦C up to 5h	Bleached Kraft eucalyptus pulp PFI refined and glycerin treatment	Chen *et al.* (2018)

(To be continued)

Table 5 (conclusion)

Morphology	Size		CI (%)	Thermostability (◦C)		Zeta Potencial (mV)	Yield (%)	Sugars (g/L)	EH conditions	Raw material	Reference
	Length (nm)	Diameter (nm)		T_{onset}	T_{max}						
Spherical	-	30	-	-	-	-	12	reducing sugars 6%	Cellulase and xylanase (*T. viride* G) blend 20U/ml, 5% DM at 50◦C up to 5h	Bleached Kraft eucalyptus pulp PFI refined and glycerin treatment	Chen *et al.* (2018)
Rod-like	286.7–629.8	4.8–17.8	69.5 to 73.7	309.7–313.8	342.9–342.1	−25	9-11	65 (48h), 85 (96h)	Cellic Ctec3 (10 mg/g), 10% DM at 50◦C up to 96h	Sugarcane bagasse treated with NaOH (10%) and bleached (2.5% lignin)	de Aguiar *et al.* (2020)
Rod-like	395.5–507.7	5.3–20	66.7 to 70.4	315.2–313.4	349.8–347.2	−25	8-12	65 (48h), 75 (96h)	Cellic Ctec3 (10 mg/g), 10% DM at 50◦C up to 96h	Sugarcane straw treated with NaOH (10%) and bleached (1.5% lignin)	
Spherical	-	2.48–60.77	52.99	-	-	-	-	10 – 12	Commercial cocktail (7.5 FPU/g), 5% DM at 55◦C up to 96h	Sugarcane bagasse treated with NaOH (4%) (9.92% lignin)	de Oliveira Júnior *et al.* (2022)
Rod-like	-	2-20	94.1	284	360	-	5.8	125	Cellic Ctec2 (12.5 mg/g), 17.5% DM at 50◦C up to 72h	Bleached Kraft eucalyptus pulp	Pereira and Arantes (2020)
Rod-like	-	12-30	96.5	294	363	-	7.4	126	Cellic Ctec2 (12.5 mg/g), 17.5% DM at 50◦C up to 72h	Sugarcane bagasse treated with NaOH (1%) and bleached (9.9% lignin)	
Rod-like	851.1–1,576.6	16.6–32.8	85 to 87.9	210–262	337–356	−32	15–20	-	EG (5 mg/g), 1%DM at 50◦C up to 48h with sonication	Whatman filter paper	Alonso-Lerma *et al.* (2020)

- : not reported; CI: crystallinity index; EH: enzymatic hydrolysis, EG: endoglucanase, T*onset*: initial temperature of degradation; T*max*: temperature of maximum degradation

From the point of view of a biorefinery approach, the use of enzymatic hydrolysis represents an important economic and sustainability improvement over concentrated sulfuric acid hydrolysis to isolate CNCs. Enzymatic hydrolysis is highly specific and environment friendly process. It does not generate carbohydrate degradation products nor requires the use of neutralizing chemicals, thus eliminating expensive downstream steps, extensive demand for pure water, and acid recycle (Rosales-Calderon *et al.*, 2021). Additionally, the enzymatic route employs mild reactions (typically, at 50^{o}C) and requires less robust equipment, thereby a smaller CAPEX than acid hydrolysis (Savignon and Gonçalves 2016; Rosales-Calderon *et al.*, 2021).

Most studies employing enzymatic treatment for carbohydrates conversion were developed to fully depolymerize biomass polysaccharides, hence a learning curve is necessary to assess and develop suitable enzyme cocktails for CNC isolation. Initial studies on enzyme-mediated treatments to isolate CNC have focused on understanding how to benefit from different enzyme types and their mode of actions to develop new cocktails or to validate existent cocktails to isolate CNC (Alonso-Lerma *et al.*, 2020; Anderson *et al.*, 2014; De Aguiar *et al.*, 2020; Siqueira *et al.*, 2019; Xu *et al.*, 2013; Yarbrough *et al.*, 2017). Other important studies were dedicated to understanding the influence of the composition of the cellulose source on enzyme-mediated isolation of CNC cite what is the influence found (Kafle *et al.*, 2015; Penttilä *et al.*, 2013). However, just a few studies have reported on the yield of enzymatic-CNC or discussed the process feasibility (Bondancia *et al.*, 2017; Xiaoquan Chen *et al.*, 2012; X. Q. Chen *et al.*, 2018; de Aguiar *et al.*, 2020; Meyabadi and Dadashian, 2012; Pereira and Arantes, 2020). Thus far, the yield achieved by enzymatic production of CNC is low and ranges between 2.5 - 38%, in which CNC is primarily obtained from cellulose-rich material (Table 5). The study by Filson *et al.* (2009) was the only to achieve yields as high as 38% (pulp basis) by introducing enzymatic hydrolysis with a microwave heating post treatment. Further studies are

necessary to optimize the enzymatic hydrolysis conditions (enzyme loading, solids consistency, and reaction time) to isolate CNCs and achieve higher CNC yields.

To the best of our knowledge, there are only two technoeconomic assessments of enzyme-mediated CNC isolation. Savignon and Gonçalves (2016) conducted the first early-evaluation study of enzymatic CNC production based on the results reported by Filson *et al.* (2009). They assessed both CAPEX and OPEX lower than the ones estimated for acid technology, producing 205.5 t/year of enzymatic-CNC from recycled pulp (Table 4). They showed the correlation of the internal rate of return (IRR) and enzyme price is inversely proportional and the correlation between IRR to CNC yield is directly proportional, revealing the importance of investigating and optimizing the reaction conditions of enzymatic hydrolysis and CNC yield. The technoeconomic assessment obtained by Rosales-Calderon *et al.* (2021) corroborates to the necessity to optimize the enzyme cocktails and enzymatic hydrolysis conditions to improve the CNC yield and reduce the use of pure water. They demonstrate that a considerable amount of cellulose-rich material is left as CSR is feasible to produce value-added products although there are opportunities to improve the viability. An important highlight of their study was the coproduction of nanocelluloses and high titer of sugars (greater than 100 $g.L^{-1}$).

Other preliminary technoeconomic assessments use part of the CSR to isolate nanocelluloses, however these studies do not truly rely on enzymatic technologies to isolate nanocelluloses but to obtain cellulosic sugars and produce cellulosic ethanol. Albarelli *et al.* (2016) assessed different types of pretreatments to produce cellulosic ethanol via enzymatic hydrolysis and CNC via the acid treatment route. They suggested that pretreatments able to minimize carbohydrate depolymerization were preferred for CNC production, and the opposite is expected when higher ethanol yields are desirable. Albarelli and coworkers highlight that the suitable choice of process conditions will depend on the biorefinery goal (commodities or

specialties). A noteworthy discussion on technical aspects, such as energy and water consumption, is available for each pretreatment assessed (Albarelli *et al.* 2016). Leistritz *et al.* (2006), in a prospective study, evaluated the utilization of 1% cellulosic solid residue (CSR) using an alternative technology developed by Michigan Biotechnology Incorporate (MBI) International, that co-produces cellulosic ethanol and CNC via acid hydrolysis (Table 4). Their results indicate an extraordinary potential of economic return by using CSR to isolate CNC (CNC-only scenario IRR 40%), whereas the ethanol-only and coproduction scenarios result in an IRR of 7.06% and 7.33%, respectively. The significative IRR was obtained using a co-located infrastructure with readily available side-streams. However, they do not consider the cost of raw material, energy consumption, and effluent treatment expenses to estimate the CNC MPSP. In a more detailed scenario, the CSR should cost at least the same price as the electricity that it can produce. Despite that, they obtained a CNC MPSP of US$ 1.87/kg, which is somehow similar to the CNC MSPS estimated by De Assis *et al.* (2017a) for a stand-alone scenario (US$/kg 4.4 – 7.2 for IRR 16%) (Table 4).

2.5.3 Feasibility of enzyme-mediated isolation of CNF

The isolation of CNF has been demonstrated through either stand-alone or integrated plants with synergy to pulp and paper industry (Arantes *et al.*, 2020; Chauve and Bras, 2014; Miller, 2019; The Process Development Center (PDC), 2022). The most efficient pretreatments to reduce energy consumption and improve the final properties of CNFs are the enzyme-mediated (Arantes *et al.*, 2020) and chemical oxidative treatments, such as TEMPO-mediated (Klemm *et al.*, 2018; Xie *et al.*, 2018). Enzyme-mediated isolation of CNF (enzymatic-CNF), especially using hydrolytic enzymes, and TEMPO-mediated isolation of CNF (TEMPO-CNF) have different morphologies (aspect ratio) and surface charges (intact and carboxylated, respectively) which result in different properties for CNF. Therefore, it is suggested that these

types of CNFs would occupy different markets (Chauve and Bras, 2014; Delgado-Aguilar *et al.*, 2015; Klemm *et al.*, 2018).

There are two models of cellulose depolymerization more extensively investigated as pretreatments to isolate CNF, that is the action by endoglucanases exploring a mild cellulose depolymerization and complex enzyme cocktail that promotes a drastic cellulose depolymerization and can co-produce sugars (Arantes *et al.* 2020).

The treatment with single-component cocktails of endoglucanases (*e.g.*, commercial cocktails FiberCare and Novozym 476 from Novozymes) aim to reduce energy consumption during mechanical fibrillation and obtain high CNF yield without co-produce significative amounts of sugars (Berto *et al.*, 2021; Xiuyu Liu *et al.*, 2019; Wang *et al.*, 2015). Endoglucanases target less ordered regions of cellulose and promotes changes in the fiber morphology by fiber fragmentation, also referred as cutting effect. The cutting effect promotes external fibrillation and fiber swelling, which further facilitates mechanical fibrillation and fibril isolation into CNF (Wang *et al.* 2015; Liu *et al.* 2019). Although the conditions of enzymatic hydrolysis with endoglucanases have been diverse, most studies concluded that a lower endoglucanase loading (0.1 - 10 $mg.g^{-1}$) is effective to provide energy savings from 20 – 60% relative to mechanical fibrillation without pretreatment (Berto *et al.*, 2021; de Amorim dos Santos *et al.*, 2023; Xiuyu Liu *et al.*, 2019; Wang *et al.*, 2015), even for periods of enzymatic hydrolysis as low as 1h (Berto *et al.* 2021). This is because fiber fragmentation can be intensified with an increased endoglucanase loading but the endoglucanases action can vary according to its family, and it can plateau due to substrate saturation, specific catalytic activity, and composition of commercial cocktails (single- component or preparation of enzymes with collaborative action) (Wang *et al.* 2015; Nagl *et al* 2021). Thus, the enzyme loading is not necessarily proportional to the reduction of fiber width and length, nor to energy savings during mechanical treatment (Henríquez-Gallegos *et al.*, 2021; Xiuyu Liu *et al.*, 2019; Nagl *et al.*,

2021; Wang *et al.*, 2015). Nagl and coworkers showed that the endoglucanase causing the lowest release of sugars provided the highest degree of refining (°SR) (Nagl *et al* 2021). Enzymatic-CNF obtained with FiberCare pretreatments have diameter ranges of 5 – 11 nm and length ranges of 5 - 40 µm (Zhou *et al.*, 2019). The treatment with FiberCare is known to produce drastic fiber changes even at low enzyme loadings (0.1 $mg.g^{-1}$) (DP 1,160 to 640). It can reduce the DP by approximately 50% (DP 1,160 to 542) with enzyme loading of 1 $mg.g^{-1}$ without producing considerable amounts of sugar. An increase of FiberCare enzyme loading up to 10 $mg.g^{-1}$ result in a pulp yield of about 95% and DP of about 440 (Wang *et al.* 2015). Other characteristics are also dependent on reaction conditions, endoglucanase type and loading, and intensity of mechanical fibrillation, such as crystallinity index ranges of 50 - 84% (Iwamoto *et al.*, 2007; Nechyporchuk *et al.* 2015; Liu *et al.* 2019; Berto *et al.* 2021) and transmittance can vary 25 - 90%, in which high transmittance is obtained by applying a dispersion post-treatment (Wang *et al.* 2015; Liu *et al.* 2019; Henríquez-Gallegos *et al.* 2021). The colloid stability in water obtained by zeta potential for enzymatic-CNF is approximately -30 to - 20 mV (Espinosa *et al.*, 2017; Pereira *et al.*, 2021) and thermal stability is similar to the cellulose (Onset decomposition temperature of 230 ^{o}C) (Berto *et al.*, 2021).

The coproduction of enzymatic-CNF and sugars can be obtained by a mixture of cellulases (endoglucanases and cellobiohydrolates, such as Celluclast 1.5 and Cellic CTec) and xylanases (*e.g.*, Genencor multifect B and HTec), or a high saccharification cocktail that consists of multienzymes from different CAZyme families, that is a combination of cellulases, β-glucosidades, xylanases, and accessory enzymes (*e.g.*, Cellic CTec and HTec series 2 and 3 from Novozymes). Enzyme cocktails composed by a pool of enzymes are generally used at higher enzyme loading (10 - 30 $mg.g^{-1}$) and reaction times (> 48h) (Arantes *et al.* 2020). These pretreatments isolate enzyme-CNF energy savings of about 50%, compared to CNF isolation without pretreatment, and can recover sugar at concentration up to 100 $g.L^{-1}$ with carbohydrate

conversion of up to 44% (Pereira *et al.*, 2021). The coproduction of sugars by high saccharification enzymatic cocktails incurs in a reduction of CNF yield compared to mild enzymatic or no pretreatment, however it can isolate CNFs with great diameter uniformity and high wet-SSA (Pereira *et al.*, 2021). The process integration is proposed by recovering the cellulosic solid residue (CSR) to isolate CNF and/or CNC. Some authors showed that nanocelluloses obtained after intensive enzymatic hydrolysis treatment (*e.g.*, high enzyme loading and/or longer hydrolysis period) have CNC-like morphology, that is reduced length and high crystallinity (Bondancia *et al.*, 2017; de Campos *et al.*, 2013; Qing *et al.*, 2013; Siqueira *et al.*, 2010; Song *et al.*, 2014; Zhu *et al.*, 2011), which often result in high tensile resistance but lowered tear strength when tested for mechanical properties for paper additives.

Applied research and development in the pulp and paper industry has led to diverse patents using enzyme-mediated processes to isolate CNF (Arantes *et al.* 2020). The common aspect explored by these emerging technologies was the use of enzymatic treatment to lower energy consumption and increase the solids consistency during the defibrillation step to produce high-solids CNF suspensions, which aims to solve problems with dewatering due to production of nanocelluloses at low solids and lower costs with transportation. Stora Enso OYJ is an assignee of a technology that describes the use of concomitant enzymatic pretreatment and refining steps to produce one-pot MFC, coupling a series of refiners (Heiskanen *et al.*, 2012). Heiskanen and collaborators claim to operate with high solids loading at solid consistency of 20-35%. Their patent claims their technology would be useful for operation with up to 45% dry matter. VTT is an assignee of a technology that proposes the use of enzymatic treatment and extruders to isolate CNF. They claim their technology operates at solid consistencies of 15 - 40% and their patent protects their technology to operate with up to 60% dry matter (Hiltunen *et al.*, 2015).

The reaction with 2,2,6,6-Tetramethylpiperidine-1-oxyl radical (TEMPO) is often cited as the pretreatment which requires the least energy (*i.e.*, 0.125 - 0.936 kWh/kg in homogenizer) and produces CNF with exceptional interface properties (Serra *et al.*, 2017). However, the high cost of the chemicals used for TEMPO pretreatment offsets the benefits of energy savings (reagents cost ranges 44-141 €/kg of CNF (Delgado-Aguilar *et al.*, 2015), with TEMPO costing 180 $/kg and NaBr 5 $/kg reported by Xu *et al.* (2022)). Hence, the necessity to recover and recycle the chemicals hinders an economically feasible upscaling of TEMPO-CNF (Klemm *et al.* 2018; Delgado-Aguiar *et al.* 2016; Serra *et al.* 2017; Xu *et al.* 2022). Authors that investigated the effect of reducing the amount of TEMPO to isolate oxidized-CNF highlight that the reduction of carboxyl content incur in the loss of properties (*e.g.*, optical transmittance, water retention, and SSA), increase of energy consumption during mechanical fibrillation, and increase of reaction time (1- 5h) (Serra *et al.* 2017). Serra and coworkers concluded that a reduction of 80% on TEMPO reagent is possible without a reduction on cationic demand, which would incur in an overall reduction of 21% in the cost to isolate TEMPO-CNF. However, it would still not make TEMPO-CNF cost-competitive with traditional polymers (Serra *et al.* 2017). A recent study has a detailed investigation regarding the impact of reducing the reagents necessary for TEMPO pretreatment (NaClO, TEMPO, and NaBr). Traditional pretreatment conditions are reagents loading of 372:16:103 $mg.g^{-1}$ cellulose (NaClO:TEMPO:NaBr) for 2h at room temperature (25^{o}C) in alkaline medium (pH 10) to obtain a pulp yield of 57% (Xu *et al* 2022). Xu and coworkers reported a relationship between the cationic demand, reaction time, and pulp yield with TEMPO treatment. They showed the pulp yield can vary depending on the desired cationic demand, that is 57 – 90% and 750 – 2500 $\mu Eq.g^{-1}$, respectively. A pulp yield of 79% could be obtained by reducing the reagents loading for a reaction period of 50 min while maintaining desirable TEMPO-CNF properties (Xu *et al.* 2022), however the possibility to recovery the remainder oxidized compounds as value added products is not discussed.

Current market price of mechanical-based CNF without pretreatment is US$167/kg (mixture CNF and CMF, also referred as CMNF) and US$ 222/kg (high-fines CNF) using disc refiner technology (FibreFiner© GLV). TEMPO-CNF is sold by US$ 3,750/kg based on same mechanical technology (The Process Development Center (PDC), 2022). TEMPO-CNF properties can vary according to the carboxyl content and the oxidation system of reagents (Isogai *et al.*, 2011). TEMPO-CNF with typical carboxyl content of 1.0 - 1.75 mmol.g^{-1} results in diameters of 4 -14 nm and length of < 2–3 mm, excellent colloid stability in water obtained by zeta potential (-70 to -85 mV), transmittance of 70 – 80%, initial contact angle of 47^{o}, degree of polymerization (DP) of around 40 – 300, high crystallinity index of 84%, fines content 63.5%, and reduced thermal stability (T*onset* of 200 ^{o}C and T*max* at 250 ^{o}C) (Isogai *et al.*, 2011; Nechyporchuk *et al.*, 2014).

To the best of our knowledge, there are only two technoeconomic assessments of CNF production. A summary of technoeconomic aspects of CNF isolation is shown on Table 6, which highlights promising results for the enzyme-mediate pretreatments. De Assis *et al.* (2017b) assessed the production of cellulose micro- and nanofibrils (CMNF) at 50 t per day from NBSK pulp using a standard disc refiner. They estimated an operational cost in the range of US$1,493 – 1,899/t for refining without pretreatment at pilot plant UMaine-FPL and a CMNF MPSP in the range of 1.8 – 2.5 US$/kg at IRR 16%.

Ålander *et al.* (2017) conducted a preliminary analysis of microfibrillated cellulose (MFC) production at the RISE Bioeconomy (Innventia) pilot plant that employs a technology developed by Ankerfors *et al.* (2009), consisting of an enzymatic pretreatment followed by a defibrillation step using homogenizer. The results indicated an energy consumption as low as 1.8-1.9 kWh/kg at an operational cost of 90 €/t, producing a mixture MFC at an estimated price of 794 €/t evaluated for paper reinforcement (Ankerfors *et al.*, 2009; Ålander *et al.*, 2017).

Table 6. Summary of technoeconomic aspects of CNF isolation (Adapted from Arantes *et al.*, 2020)

Author	CNF MPSP (US$/kg)	CAPEX (US$ M)	OPEX (US$ M per year)	Production cost (US$/t of CNF)	CNF volume (t/year)	Ethanol (g/L)	Pretreatment	Isolation method	Yield (starting material basis)	Raw material	Feedstock processing (t/year)
De Assis *et al.* (2017b)	1.89 – 2.44 C*	18.5 – 37.7	25.4 – 32.3	1,493 – 1,899	CMNF (17,000)	-	-	Disc refining	100%	NBSK	17,000
Delgado-Aguilar *et al.* (2015)	-	-	-	228,363.4*	CNF	-	PFI beating 4,000 + TEMPO-mediated oxidation alkaline	Homogenizer	> 95% Degree of fibrillation	HBKP	-
	-	-	-	194,684.1*	CNF	-	PFI beating 4,000 + TEMPO-mediated oxidation neutral	Homogenizer	> 95% Degree of fibrillation	HBKP	-
	-	-	-	8,135.6*	CNF	-	AH (15% H_2SO_4 for 10h at 60 °C)	Homogenizer	72% Degree of fibrillation	HBKP	-
	-	-	-	15,158.3*	CNF	-	PFI beating 4,000 + EH (Novozym 476)	Homogenizer	69% Degree of fibrillation	HBKP	-
	-	-	-	2,494.4*	CNF	-	PFI beating 20,000	Homogenizer	21% Degree of fibrillation	HBKP	-
Spence *et al.* (2011)	-	-	-	745 – 1,960	MFC	-	Beating	Disc ultra-refiner/ Microfluidizer/ Homogenizer	-	HBKP	-
	-	-	-	445 – 1,660	MFC	-	Beating	Disc ultra-refiner/ Microfluidizer/ Homogenizer	-	UBHW	-
	-	-	-	195	MFC	-	-	Disc ultra-refiner	-	Recycled fiber	-
	-	-	-	115	MFC	-	-	Disc ultra-refiner	-	Sludge	-
Kangas and Pere (2016)	-	-	-	244.2* (chemicals + energy)	CNF	(80% cellobiose)	Pretreatment to reduce lignin content < 10% + EH (*T. reesei*)	Homogenizer	≥ 90% (CSR)	Wood and non-wood pulps, recycled fibres, agro-based residues	-

(To be continued)

Table 6 (conclusion)

Author	CNF MPSP (US$/kg)	CAPEX (US$ M)	OPEX (US$ M per year)	Production cost (US$/t of CNF)	CNF volume (t/year)	Ethanol (g/L)	Pretreatment	Isolation method	Yield (starting material basis)	Raw material	Feedstock processing (t/year)
Espinosa *et al.* (2016)	-	-	-	15,218.1* (enzyme, chemicals, and energy)	CNF	-	EH (consistency 5%wt, endoglucanases loading 0.83% for 3h at 50ºC)	Homogenizer 300 bar, 4 passes (Henriksson *et al.*, 2007)	-	HBKP	-
	-	-	-	3,452.1*	CNF	-	PFI Beating 20,000	Homogenizer 300 bar, 4 passes (Henriksson *et al.*, 2007)	-	HBKP	-
Ankerfors *et al.* (2009), Ålander *et al.* (2017)	0.881*	-	-	99.9*	MFC	-	EH (FiberCare)	Homogenizer (consistency 2.3%wt at 1,500 bar)/ Refiner	-	HBKP and SBP sulphite pulp	-
Pereira *et al.* (2021)	-	-	-	-	CNF	67.1	SE, alkaline treated & bleached, and EH (Cellic CTec 2)	Disc ultra-refiner	26.14% (SCB basis)	SCB	-

- : None or not reported; CNC: cellulose nanocrystal; CNF: cellulose nanofibril; MFC: microfibrillated cellulose; NC: Nanocellulose; MPSP: Minimum product selling price; CAPEX: capital expenditure; OPEX: operational expenditure; C*: MPSP calculated; F**: MPSP fixed for analysis (assumption); AH: Acid hydrolysis; EH: Enzymatic hydrolysis; SE: Steam Explosion; MCC: Microcrystalline cellulose; CSR: cellulosic solid residue; HBP: Hardwood Bleached Pulp; HBKP: Hardwood Bleached Kraft pulp; UBHW: Unbleached Bleached Hardwood pulp; NBSK: Northern Bleached Softwood; Kraft pulp; SBP: Softwood Bleached Pulp; SCB: Sugarcane bagasse.
*Currency conversion: 1€ = 1.11 US$ (Dec, 2019)

Kangas and Pere (2016) reported a two-step production of CNF HefCel (VTT) using enzymatic pretreatment and subsequent defibrillation at high solids loading. They estimated the chemical and energy costs at €110/t CNF and energy consumption as low as 0.600 kWh/kg although their methodology of assessment was not disclosed. Their recent work employed a simultaneous enzyme-mechanical treatment with a commercial enzyme cocktail (EcoPulp Energy), containing CBH and EG, and operated a two-shaft sigma mixer at solids consistency of 25 % with enzyme loading of 6 $mg.g^{-1}$ for 8h at 70 °C to isolate CNF HefCel with 87% yield (Pere *et al.*, 2020).

2.5.4 Lignin-containing CNC and CNF (LCNC and LCNF)

Conventionally, lignin removal from lignocellulose materials has been considered a necessary step in the preparation of nanocelluloses (García *et al.*, 2017; Hubbe *et al.*, 2008). However, remaining fractions of polysaccharides and lignin may improve nanocelluloses properties, such as higher colloidal stability and higher hydrophobicity.

Conventional CNC and CNF are routinely targeted for chemical modification to improve the compatibilization with other polymers. However, due to CNCs' inherent hydrophilicity, incorporating them into hydrophobic environments is challenging and frequently involves functionalization (Arantes *et al* 2020). The hydrophilicity leads to high water adsorption, which may have a negative impact on the performance of some materials and alter their properties.

Recent studies have investigated lignin-containing nanocelluloses that were either blended from streams containing pure lignin or lignocellulose streams (Wei *et al.*, 2018), or directly tailored and isolated from lignocellulose feedstocks (Xuran Liu *et al.*, 2019; Trifol *et al.*, 2021; Xu *et al.*, 2021). The percentage composition of cellulose and lignin can vary depending on the specific source of lignocellulosic biomass and the extraction process. There is no system of classification available for lignin-containing nanocelluloses thus far. To be

considered as lignin-containing nanocellulose, the material typically contains a significant amount of cellulose with a portion of lignin. The percentage may vary depending on the desired properties and applications of the nanocellulose material. Some authors claim that a higher lignin content may confer enhanced mechanical strength and hydrophobicity, reduce energy consumption during fibrillation (Diop *et al.*, 2017) and may facilitate water drainage. Although there is no specific threshold for the percentage composition of a lignin-containing nanocellulose, a typical cellulose and lignin composition found in the literature is: cellulose content of approximately 50% to 90% or more, and a lignin content of 1% to 50% (Trifol *et al.*, 2021; Wei *et al.*, 2018), typically equal or less 20% (Bian *et al.*, 2019; Copenhaver *et al.*, 2021; Xuran Liu *et al.*, 2019)

To the best of our knowledge, there is no published technoeconomic assessment available of LCNC or LCNF isolation from pretreated agricultural pulp. Further studies are still needed to understand the impact of pretreatment of the agricultural raw material on the ability to extract cellulose in a co-localized infrastructure, or the use of other industrial lignocellulosic residues.

2.6 Problem summary

There is a growing demand for renewable and sustainable products and to circumvent current problems with plastic pollution. Sugarcane bagasse and straw are abundant lignocellulosic materials that can be used as low-cost feedstock to obtain bioproducts and biofuels. However, new solutions of process development are needed to focus on obtaining bioproducts rather than biofuels to improve the viability through low- and high-value products.

The recalcitrance of the lignocellulosic material is a concept that refers to the difficulty of fully fractionating and efficiently recovering its main components for economic utilization. From a chemistry point of view, the recalcitrance is determined by the plant cell wall ultrastructure, which refers to the complex association of the plant cell wall components and

their arrangement. From a biorefinery point of view, the current goal for the pretreatment is to recover the lignocellulosic fractions as value-added products, maximize the overall yield, and reduce the energy requirement as low as possible (Galbe and Wallberg, 2019). Moreover, the parameters that envolves sustainability, such as the recycleability of chemicals and process alternatives to minimize the demand for resources (especially, water and energy) are essential considerations for the feasibility.

The enzymatic technology has been suggested in the literature as the most profitable option to obtain sugar streams at high titers (Kazi *et al.* 2010). Additionally, the enzyme-mediated treatment reduces the energy consumption required to isolate nanocelluloses using the mechanical route (Henriksson *et al.*, 2007; Pääkko *et al.*, 2007a; Wang *et al.*, 2015; Xiuyu Liu *et al.*, 2019; Berto *et al.*, 2021). Ultimately, the opportunity to co-produce nanocelluloses together with cellulosic ethanol using the cellulosic solid residue (CSR) would be synergetic to increase valorization of the lignocellulosic main fractions. For that, the cellulosic sugars stream is recovered after the enzymatic hydrolysis and the CSR is used to isolate cellulose nanomaterials by mechanical methods (Camargo *et al.*, 2016; de Campos *et al.*, 2013; Feng *et al.*, 2018; Lam *et al.*, 2017; Pereira and Arantes, 2020; Saelee *et al.*, 2016).

Despite the potential of nanocelluloses as a value-added product, there is still limited information available regarding the feasibility of the coproduction of cellulose nanomaterials and cellulosic sugars/ethanol (Albarelli *et al.*, 2016; Leistritz *et al.*, 2006; Pereira *et al.*, 2021; Rosales-Calderon *et al.*, 2021), or how to transition from a biorefinery based on biofuels to bionanomaterials, especially when the biorefineries employ enzyme-mediated processes. Thus, a detailed mass balance study is necessary to assess the coproduction of sugars and cellulose nanomaterials from lignified and non-lignified biomass using enzyme-mediated processes. Furthermore, a discussion on how raw materials and process choices impact the properties of lignin-containing nanocelluloses, particularly when derived directly from non-wood biomass,

remains essential. Additionally, exploring how native-like lignin can impart unique properties to cellulose nanomaterials is still necessary.

CHAPTER 3 OBJECTIVES

3.1 Objectives

To investigate the combined enzymatic-mechanical approach to co-produce lignin-containing cellulose nanocrystal (LCNC), lignin-containing cellulose nanofiber (CNF), and cellulosic sugars from sugarcane bagasse (SCB) and straw (SCS). The Hardwood Bleached Kraft pulp (HBKP) will be used as a reference feedstock to co-produce nanocelluloses (CNC and CNF) and cellulosic sugars.

Specifically, the goals were:

1- To determine the mass balance to co-produce nanocelluloses (CNC and CNF) and cellulosic sugars from HBKP and characterize the nanocelluloses in terms of diameter size;

2- To determine the mass balance to co-produce lignin-containing nanocelluloses (LCNC and LCNF) from SCB and characterize the nanocelluloses in terms of diameter size;

3- To determine the mass balance to co-produce lignin-containing nanocelluloses (LCNC and LCNF) from SCS and characterize the nanocelluloses in terms of diameter size;

4- To determine the chemical composition of the lignin-containing nanocelluloses (LCNC and LCNF) and their propertied in solution and as films.

CHAPTER 4 MATERIALS AND METHODS

4.1 Materials

Eucalyptus bleached kraft pulp, referred as HBKP, kindly donated by Suzano (Jacareí-SP, Brazil). Northern bleached softwood Kraft (NBSK) pulp was obtained as baled market pulp and unbleached softwood Kraft (UBK) pulp was obtained as a board grade unbleached kraft pulp. NBSK and UBK were supplied by the Process Development Center (PDC) at the University of Maine (Orono, ME, USA). The chemical composition of HBKP was 78.6%(w/w) of cellulose, 14.6%(w/w) of xylan and 2.7% (w/w) of lignin determined by Pereira and Arantes (2020). The chemical composition of NBSK pulp was 76.19%(w/w) of cellulose, 17.41%(w/w) of xylan, and negligible amount of total lignin according to Copenhaver *et al.* (2021). UBK had 10 – 15% residual lignin (kappa number 70–100) according to Tayeb *et al.* (2020). UBK chemical composition was 66.9%(w/w) of cellulose, 5.74%(w/w) of xylan, and 13.3% (w/w) of lignin according to Imani *et al.* (2019).

Sugarcane bagasse, referred as SCB, kindly donated by Usina Quatá (Zillor, Quatá, SP, Brazil), and Sugarcane straw, referred as SCS, kindly donated by American Process (Thomaston, GA, USA) harvested by Granbio. SCB and SCS were air dried to final moisture content of 5 – 6% and kept in polyethylene bags.

Commercial enzyme cocktails Cellic CTec2 (VCS00002, lot #SLBS6227, protein concentration 200 mg/mL determined by Pereira and Arantes 2020 following a modified Mok *et al.* (2015) protocol), cellulase Cellic CTec3 equivalent (NS 22257, protein concentration 194 ± 7 mg/mL, 176 ± 5 FPU/g, 520 U/g CMCase), xylanase HTec3 equivalent (NS 22244, protein concentration 102 ± 7 mg/mL, 10.81 ± 0.06 FPU/g, 318 U/g CMCase) were kindly donated by Novozymes (Denmark). Protein concentration was determined according to Mok *et al.* (2015) using a reaction volume 10 times larger. All enzymatic activities were measured using the methods reported by Ghose,1987).

Filtered tap water from the University of Maine was used as provided. Tap water from Lorena School of Engineering water well was autoclaved (121 ^{o}C, 1.5 atm, 15 min) and analyzed for total hardness 23.415 mg/L determined by standard method SM 2340 C, conductivity of 172.1 µS/cm (23^{o}C), total solids of 102 mg/L determined by standard method SM 2540 A, B, C, D, E, G, cations composition of [Na^{+}] 0.67 mM, [Ca^{+2}] 0.19 mM, [K^{+}] 0.06 mM, [Mg^{+2}] 0.04 mM determined by standard method EPA 6010C, and anions composition of [Cl^{-}] 0.12 mM determined by standard method SM 4500-Cl-B (Laboratório Ampro Análises Industriais, Lorena, SP, Brazil).

4.2 Methods

The methods session is divided into two parts – fractionation methods and analytical methods. The fractionation methodology describes the proposed process to coproduce fermentable sugars, CNC, and CNF, two designs of experiments and statistical analysis as well as the yield calculation. The analytical methodology describes the characterization employed for the solid and liquid fractions recovered after each treatment.

4.2.1 Fractionation methods

The proposed process to coproduce acetic acid, fermentable sugars (glucose and hemicellulose hydrolysate), CNC, and CNF is summarized in Figure 7. It shows the main fractionations studied to obtain the recalcitrant cellulosic solid residue (CSR) after enzymatic treatment. The CSR is further used to isolate CNC and CNF.

The entire process was perfomed with SCB and SCS (Figure 7, part #1 and 2). The HBKP was used to study the coproduction of fermentable sugars, CNC, and CNF and investigate optimization alternatives (Figure 7, part#1). NBSK pulp and UBK pulp were solely used during the ultra-refining step for a comparative study with SCB and SCS.

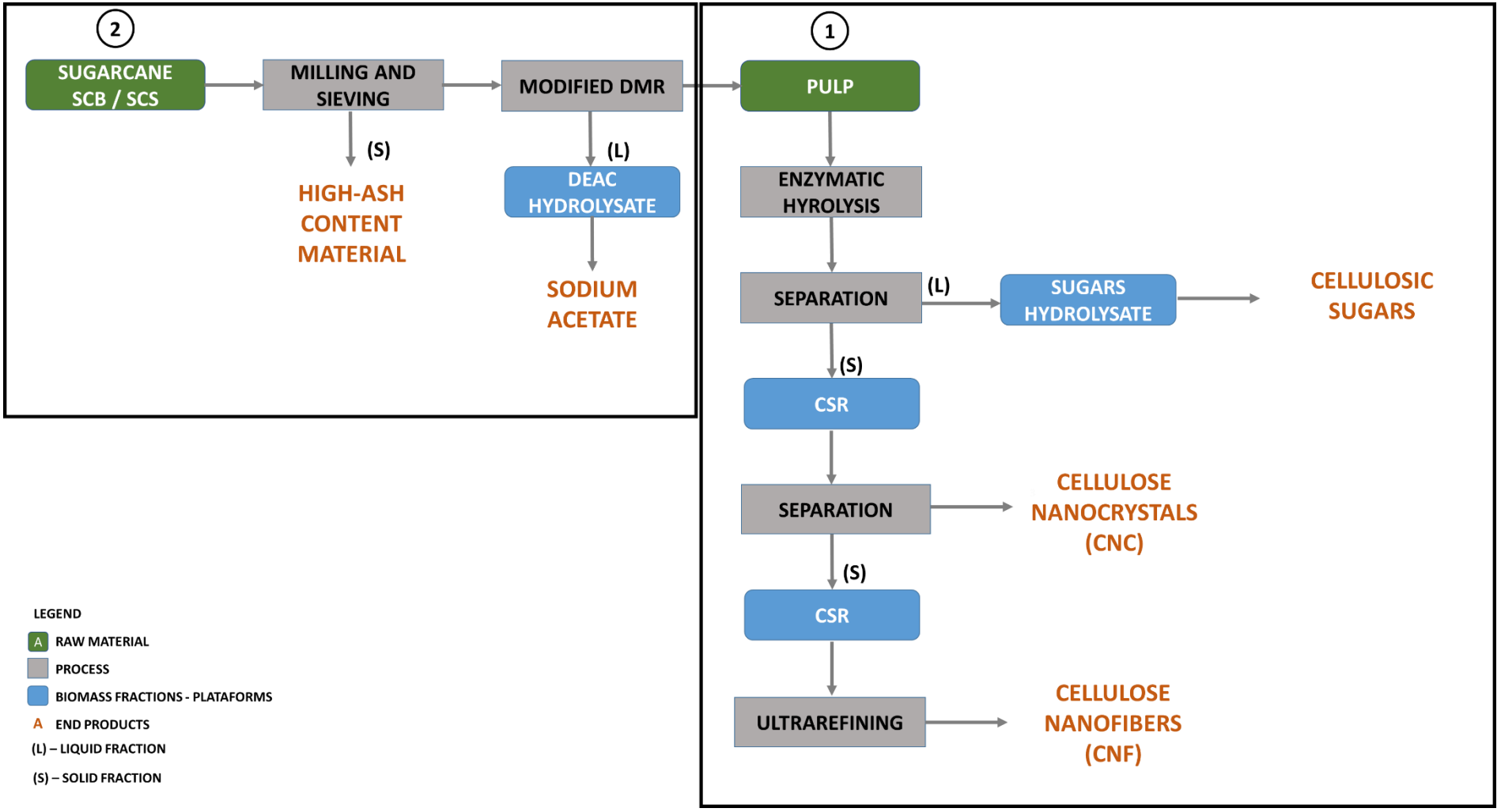

Fig. 7. Scheme of the proposed process to coproduce fermentable sugars, CNC, and CNF. Numbers 1 and 2 indicate the order for developing the experimental study. SCB: Sugarcane bagasse, SCS: Sugarcane straw, DMR: Deacetylation and Mechanical refining, DEAC: Deacetylation, CSR: cellulosic solid residue.

4.2.1.1 Milling and sieving

SCB and SCS were size reduced using a hammer mill (Munson Mill Machinery Co, USA) and the fraction passing a 5-mm screen was used. The Munson mill was coupled to a dust collector (Craftsman Professional). 3 g/100g of starting SCS, which were used to further treatments. The milled SCB was screened using a vibrating sieve of 100-mesh (opening 150 μm) and the SCS was screened using a vibrating sieve of 30-mesh (opening 595 μm) on a mechanical shaker (Humboldt) for 15 min.

The retained portions were 94.6 ± 0.5 g/100g of starting SCB and 49 ± 3 g/100g of starting SCS, which were used to further treatments. The retained portion of each material is referred to as SCB and SCS milled and sieved.

The portion that passed the sieve as well as the dust collected were discarded. For mass balance purpose, the ash composition was determined for SCB and SCS before and after sieving as well as for the discarded sieved portion.

4.2.1.2 Modified Deacetylation and Mechanical refining (DMR)

The modified Deacetylation and Mechanical refining (DMR) technology refers to a two-step treatment pursued by NREL consisting of a mild alkaline treatment and mechanical refining, in which the goal is to remove a maximum of acetic acid, preserve the carbohydrates while promoting a low removal of lignin. The deacetylation of xylan leads to improved accessibility of the lignocellulosic material, and therefore likely to improved enzymatic hydrolysis (Inalbon *et al.*, 2013).

In the present study, alkaline treatments were conducted at least duplicates with 12 g o.d. of biomass (SCB and SCS). Reactions were conducted in PE/PET bags (Kapak pouches 502, thickness 4½") sealed with heat after loaded with biomass at solid-liquid ratios of 1:4, 1:6, or 1:8 (g/mL) and NaOH loading on biomass of 4%(w/w), 6%(w/w), or 8%(w/w) using a solution of NaOH 5%(w/w) without prior impregnation. Reactions were conducted in a water

bath with temperature controller (Solo 4848 Automation Direct) at temperature of 50.0ºC or 80.0ºC for 90 min. Control reactions were conducted with deionized water. Kneading of the bags was performed every 15 min. At the end of the residence time, the reaction bags were cooled for 10 min in cold tap water. The treated material was transferred to a 100-mesh nylon bag (FSI-Pall Corporation) and filter pressed to recover the liquor, referred as DEAC SCB and DEAC SCS. The solid fractions were washed three times in a ratio of deacetylated material:deionized water of 1:10 (total water usage of 30 L/kg of treated material) and filter pressed between the washing steps. The final pH of the liquors was recorded. Both solid and liquid fractions were submitted to gravimetric analysis for yield calculation and ash determination. The chemical composition was determined for solid fraction.

For more relevant results, the deacetylation reactions were scaled up to 50 g o.d. of biomass (SCB and SCS) and conducted in duplicates. The alkaline treatment was solid-liquid ratio 1:4, NaOH loading on biomass of 4%(w/w) and 6%(w/w) for SCB and NaOH loading on biomass of 4%(w/w) for SCS. Reactions were conducted at 50.0ºC for 90 min. At the end of the treatment, the solids were washed with deionized water three times at a solid:liquid ratio of 1:10 and 1:12, respectively for DEAC SCB and DEAC SCS, followed by manual squeezing the material inside the 100-mesh nylon bag (FSI-Pall Corporation). The total water usage summed 30 L/kg DEAC SCB and 52L/kg of DEAC SCS. The liquors were recovered, and the final pH was recorded. The final moisture content of the pretreated materials was approximately 20%. The reaction duplicates were mixedtogether, and the pretreated materials were kept in ziplock bags and stored at 4ºC. Both solid and liquid fractions were submitted to gravimetric analysis for yield calculation, ash determination, and chemical composition determination.

The DEAC SCB4, DEAC SCB6, and DEAC SCS4 were refined using a PFI mill (model 88036, Noram, Quebec CA) following test method TAPPI/ANSI T 248 sp-21 (TAPPI/ANSI,

2021). The beating consistency was 20% solids (30 g o.d.) at 6,000rev with the beating gap set to 0.2 mm. No prior disintegration was performed.

4.2.1.3 Enzymatic hydrolysis of DEAC SCB and DEAC SCS

The enzymatic hydrolysis assays were conducted at microscale to explore the digestibility effect of the previous treatments (alkaline treatment plus PFI refining) comparatively with solely alkaline treatment using different enzymatic loadings and different ratios of enzyme cocktails Cellic CTec3:HTec3. The microscale enzymatic treatments were conducted in duplicate using 5-mL microcentrifuge tubes, total reaction mixture of 4 ml with 2%(w/v) solids loading and enzyme solution prepared in 50 mM sodium acetate buffer (pH 4.8) and 0.01%(w/w) sodium azide. The enzyme loading were varied (2.3 – 12.5 $mg.g^{-1}$ o.d. of biomass) and enzyme cocktail ratios were studied as shown in Table 7. Tubes were incubated in a shaking incubator (model I 24, New Brunswick Scientific) at 50ºC and 200 rpm for up to 72 h. Reactions were stopped by immersion in boiling water for 15 min. The sugars hydrolysates were collected by centrifugation at 1,252×*g* (4,000 rpm) for 30 min at room temperature using Fisher Scientific accuSpin 400 centrifuge (Swinging Bucket Rotor #5197). The content of glucose, xylose, and arabinose released during enzymatic treatment was analyzed by high performance liquid chromatography (HPLC).

The enzymatic hydrolysis at larger scale were carried out using 1-L Nalgene polypropylene centrifuge tubes with a total reaction mass of 100-g containing 15%(w/w) solids loading using enzyme loadings of 15 mg per gram of dry material, Cellic CTec3:HTec3 ratio of 1:2, prepared in 50 mM sodium citrate buffer (pH 4.8) and 0.01%(w/w) sodium azide. Reactions were conducted at least in duplicates. Tubes were incubated in an oven at 50ºC containing a compact roller system (Wheaton small bench-top apparatus, DWK Life Sciences) set up to rotate at 3.8 rpm for 72h. Reactions were stopped, and the sugars hydrolysates were collected by centrifugation at 10,540×*g* for 20 min at 25 °C using Sorvall centrifuge (rotor

SCL-4000). The content of glucose, xylose, arabinose, and acetic acid released during enzymatic treatment was analyzed by HPLC. The cellulosic solid residues (CSR) were suspended in tap water to a final volume of 500 mL to proceed with CNC isolation.

Table 7. Combination of enzyme loading and reaction time for enzymatic hydrolysis

Enzymatic loading (mg/g)	on cellulose	5	15	15	15	21	25	25
	on SCB	2.5	7.5	7.5	7.5	10.5	12.5	12.5
	on SCS	2.3	6.9	6.9	6.9	9.7	11.5	11.5
Enzyme cocktails ratio	CTec3:HTec3	1:0	1:2	2:1	14:1	20:1	1:4	4:1
Time tested (h)		24, 48, 72	24, 48, 72	48	48	48	24, 48, 72	48

4.2.1.4 Enzymatic hydrolysis of HBKP

A series of enzymatic hydrolysis assays were conducted to study the effect of the severity of enzymatic hydrolysis (SEH), which consisted of varying the enzymatic loading and time of reaction, in recovering CNC and CNF from CSR (Figure 7, part#1). Reactions were conducted in duplicates in a rotary incubator (model HB-3D, Techne®, Hybrigene) with a total reaction mass of 800 g containing 17.5%(w/w) solids loading of eucalyptus bleached kraft pulp (HBKP) using an enzyme solution of Cellic CTec2 (protein loading 10 – 20 $mg.g^{-1}$ pulp) prepared in 50 mM sodium acetate buffer (pH 4.8) and 0.01%(w/w) sodium azide. The reactions were incubated at 50°C for up to 72 h with rotation of 20 rpm. Reactions were stopped by immersion in boiling water for 30 min. The conditions for enzyme assay were tested as shown in the Table 8.

The mixtures were vacuum filtered (Whatman® nº 1 Filter paper, porous size 11 μm) to recover the liquid fraction and separate the cellulosic solid residue (CSR). The CSR was washed three times with 500 mL deionized water (total 1.5 L) while being vacuum filtered to lower sugar and ions concentration. The third stage of washing resulted in a final spent wash

liquor conductivity equal or below 250 µS.cm^{-1}. The CSR was used in the design of experiments to isolate CNC and CNF.

Table 8. Combination of enzyme loading and reaction time for different enzymatic hydrolysis conditions

SEH	EH-5-30	EH-5-72	EH-10-30	EH-10-72	EH-20-30	EH-20-72	EH-30-30	EH-30-72
Enzymatic loading on pulp (mg/g)	5	5	10	10	20	20	30	30
Time (h)	30	72	30	72	30	72	30	72

EH-E-T was used to refer to each enzymatic loading (E) and time (T) tested.

4.2.1.5 Isolation of CNC by centrifugation

The isolation of CNC from CSR consisted of a series of centrifugation steps. The turbid top layer was cumulatively collected until turbidity was not observed after a centrifugation (end of separation). Both CNC suspension and remaining CSR were submitted to gravimetry analysis to calculate the yield of CNC isolation.

For the experiments with HBKP, the centrifugation equipment and operation conditions are explained on the item 6.2.1.6. To isolate CNC To isolate LCNC from pretreated SCB and SCS the suspensions were centrifuged at 750×g for 15 min at 25 °C using Sorvall centrifuge (rotor SCL-4000). No ultrasonication was performed. CNC samples were kept in solution or dried according to the subsequent analysis. The CNC suspensions were concentrated by oven dry and used to produce films at 0.1% solids by casting at 50°C overnight or lyophilized.

4.2.1.6 Isolation of CNC using Design of Experiment (DoE)

The design of experiment was applied in a two-part study to understand how the cellulose conversion by enzymatic hydrolysis affects the isolation of CNC, the recovery of CNC by centrifugation from CSR, and the energy consumption to ultra-refine the remaining CSR. The two-step study consisted of a 12-experiment Plackett-Burman (PB) design to screen

the centrifugation operation parameters and a full factorial design (central composite rotational design - CCRD) for two parameters (5 levels) chosen from PB design of experiment. The experimental matrixes and statistical analysis were generated by Minitab software v.18 (Minitab Inc., State College, PA, USA). Statistical analysis included tests for normal distribution and randomness using a confidence interval of 95% ($p = 0.05$) to select the most important variables with a confidence interval of 90% ($p = 0.1$).

The isolation of CNC from the CSR was carried out by centrifugation using a Rotanda centrifuge (model 460R, Hettich Zentrifugen) with swing-out rotor (model 5647). Acceleration and deacceleration ramp were set to level 9 with at least 5 min until rotation stop. The centrifugation conditions as well as the amount of material were set according to the experimental matrixes.

The PB design of experiment consisted of 12 experiments, without duplicates, using 8 “real” factors (Factors A, B, C, D, E, F, G e H) and 3 additional factors without an assigned parameter (dummy factors). The centrifugation parameters assigned to each factor, in two levels, are shown on Table 9. The complete experimental matrix is shown on the Appendix A. Twelve experiments resulted in 12 CNC suspensions for which 15 responses were investigated (Number of centrifugation steps (C #), volume of suspension recovered (mL), CNC o.d. weight (g), CNC yield (%), Remaining CSR o.d. weight (g), CSR (%), W/C ratio (g/#C), Span, Uniformity, wet-SSA (m^2/kg), D [3,2] (μm), D [4,3] (μm), D10 (μm), D50 (μm), D90 (μm)) and are shown on Appendix A.

The Central Composite Design (CCD) was performed based on the results obtained with 12-experiments PB design, using the cellulose conversion (factor A) and rotation (factor E) as variables. Other variables tested with PB design were set as following with the goal to minimize resources (material, water, or energy): factor B low level, factor C low level, factor D low level, factor F low level, factor G high level, factor H low level. A full factorial

experiment 2^2 with 3 central points and triplicate of each point was conducted, using a wider range for cellulose conversion and rotation than used in the PB design. The experimental matrix is shown on Appendix B. The model had a statistically significant curvature, therefore axial points were added to the full factorial experiment ($\alpha = \sqrt{2}$). Table 10 shows variables and the levels used to build a response surface model.

Table 9. Factors, variables, and levels used for the 12-experiment Plackett-Burman (PB) design.

Factor	Variable	Level	
		-1 (low)	+1 (high)
A	Cellulose conversion	28 % (EH–10–30)	38 % (EH–10–72)
B	CSR (g)	2.5	5.0
C	Water volume (mL)	20	100
D	Water type	Tap water	Reverse Osmosis
E	Rotation (×*g*)	500	2,838
F	Time (min)	10	30
G	Temperature (ºC)	4	25
H	Tube capacity	Falcon (50 mL)	Centrifuge tube (500 mL)
I	No variable assigned*	-	-
J	No variable assigned*	-	-
K	No variable assigned*	-	-

* Factors with no defined variable are used to estimate the experimental error.

Table 10. Central Composite Rotational Design with 2 variables and 5 levels

Factor	Variable	Level				
		-1.41	-1	0	+1	+1.41
A	Cellulose conversion	18 % EH–5–30	28 % EH–10–30	50 % EH–20–30	63 % EH–20–72	79 % EH–30–72
B	Rotation (×*g*)	398	500	750	1,000	1,103

The full factorial design was performed in 33 experiments to determine the normal distribution and 25 experiments were used in the regression analysis to build the response surface model. The regression model explains the CNC yield (CSR basis) by using a quadratic relationship between cellulose conversion and rotational speed with effects non-coded. The model parameters, S, R^2, adjusted R^2, and predicted R^2, were analyzed together with the *p-value* to determine the most important terms and interaction terms to describe the CNC yield. The parameter A*B was removed from the model because its removal did not affect the prediction capability, whereas the term B and the quadratic parameter A*A were kept in the model because they provided an improved prediction (*i.e.*, presented higher R^2 and predicted R^2) even though they were not considered statistically significant by solely analyzing the *p-value*.

Eight experiments were conducted to validate the prediction capability of the response surface model using different degrees of cellulose conversion obtained by a combination of enzymes loading (5, 10, 20, 30 $mg.g^{-1}$) and reaction time (30 h and 72 h), which were chosen based on common values reported in the literature. The conditions EH-30-30, EH-5-72, and EH-10-72 were not used to build the model, only to validate. The rotation speed was set at 750×*g*. The prediction error of the model varied 1 – 56 %.

4.2.1.7 Ultra-refining of CSR after enzymatic treatment

After CNC isolation by centrifugation, the remaining CSR was suspended in filtered water to produce suspensions containing 1.5% solids (total volume for HBKP-CSR, SCB-CSR and SCS-CSR was 1 L, 1.5L, and 1.5L). The suspensions were manually fed to a disc ultra-refiner Supermasscolloider (Masuko Sangyo, Japan) to isolate CNF. The summary of the ultra-refining model and operation conditions are shown on Table 11. One pass refers to the circulation of the complete volume. The Supermasscolloider had the upper disc attached or not according to the model used and the bottom disc rotating at 1,600 rpm with disc gap set manually. The process had the energy monitored by an energy meter, and number of cycles and

total time recorded. Aliquots of the suspensions were collected during the fibrillation procedure and submitted to particle size analysis. The overall mass recovery was considered to be 100% because the only possible loss was related to handling and recovery of the mass from the equipment.

Table 11. Summary of the disc ultra-refiner Supermasscolloider and operation conditions

Model	Upper disc	Disc gap	Cooling	Aliquot size (mL)	Total passes #	Energy monitor	Material processed
MKCA6-2 J, disc model MKGA10-80	Attached to the feed	Maintained at -100 µm	Yes	1	25	ForLong DRT-341D	Eight CSR suspensions from HBKP
MKCA6-2, motor 208 U 1.5 kW	Non-attached to the feed	Started at -100 µm and closed until up to -260 µm to maintain 60% laod	No	15	20	Load meter model DM-100, LCT	NBSK, UBK, DEAC SCB4 PFI-EH, DEAC SCB6 PFI-EH, DEAC SCS4 PFI-EH

CNF suspensions were concentrated by oven dry up to 3% solids as needed and samples were used to produce films by casting in oven at 50°C overnight or lyophilized.

4.2.2 Analytical methods

4.2.2.1 Yield calculation

The solid yield was determined by gravimetry (constant weight at 105 ^{o}C), which requires the quantification of each sample (dry weight) before and after treatments in triplicate. The yield calculation is a percentage ratio that was determined by the difference between the initial and final weight after each treatment by its initial weight. Solids content in treated materials were calculated based on 0.5 – 1 g of material placed in the oven at 105 ^{o}C or by infrared moisture analyzer. For sodium acetate, aliquots of 2 mL of the alkaline liquors were analyzed. For CNF suspensions (< 1.5 % solids), aliquots of 0.5 – 1 g were collected for the

solids yield analysis. For CNC suspensions (< 0.5 % solids), aliquots of 15-20 mL were collected for the solids yield analysis.

To determine the CNC yield (CSR basis), it was used according to Pereira and Arantes (2019):

$$CNC\ yield\ (CSR\ basis) = \frac{CNC\ o.d.weight * Total\ volume\ recovered}{CSR\ o.d.weight * Volume\ for\ gravimetry\ analysis}\ x\ 100\% \quad \text{(Eq. 1)}$$

To determine the CNC yield (pulp basis), it was used according to Beyene *et al.* (2017):

$$CNC\ yield\ \ (pulp\ basis) = CNC\ yield\ percentage\ (CSR\ basis) * CSR\ o.d.weigh\ /100 \quad \text{(Eq. 2)}$$

4.2.2.2 Chemical composition of solid and liquid fractions

The chemical characterization of solid materials was carried out according to the following National Renewable Energy Laboratory (NREL, USA) analytical protocols: NREL/TP-510-42622 for ash (A. Sluiter *et al.*, 2008a), using samples of 0.500 – 1.000 g o.d. at least 5 times for each material.; NREL/TP-184 510-42619 for extractives (A Sluiter *et al.*, 2008), using samples of 1.000 g o.d. in triplicates, and NREL/TP-510-42618 for monomeric sugars and lignin in biomass samples (Sluiter *et al.*, 2012), using 0.300 g o.d. in triplicates. The chemical characterization of liquid fractions was carried out according to NREL/TP-510-42623 (A. Sluiter *et al.*, 2008b), using liquid samples containing approximately 0.3% solids.

The monomeric sugars, acetic acid, and acid-soluble lignin resultant from biomass treatment using a two-step acid hydrolysis (1st step H_2SO_4 72%(w/w) for 1h at 30 °C, 2nd step H_2SO_4 4%(w/w) for 1h at 121°C) were recovered by filtration (glass microfiber filter Whatman grade 934-AH) to separate from acid-insoluble lignin and were subsequently filtrated with PTFE filters pore size 0.45 μm. The monomeric sugars and acetic acid recovered after enzymatic hydrolysis were filtrated using Nylon filters pore size 0.45 μm. Glucose, xylose, arabinose, and acetic acid were determined by High Performance Liquid Chromatography (Shimadzu Corporation), using the column Aminex HPX-87H (Bio-rad) at 45°C and refractive index detector (Shimadzu RID-10A) cell at 40°C. Samples were eluted with 5 mmol.L^{-1} sulfuric

acid at 0.6 mL.min^{-1}. The concentration obtained from standard curves for glucose, xylose, arabinosyl, and acetyl were estimated using software Shimadzu EZStart Lab Solutions v.5.101. To calculate the polysaccharide and acetic acid yields, correction factors of 0.9, 0.88, 0.88, and 0.72 were used respectively for glucan, xylan, arabinan, and acetic acid. Post-hydrolysis was not conducted.

The acid-insoluble lignin was determined by gravimetry. The acid-soluble lignin was determined by measuring the absorbance of aliquots of 1 mL diluted 10-20x and using the molar absorptivity constant of 105 L.g^{-1}cm^{-1} at wavelength of 205 nm (Dence, 1992).

4.2.2.3 Particle size and particle size distribution

Particle size and distribution were determined in real time from wet process streams by two particle size analyzers using light scattering techniques. Particle sizes were complementary analyzed by microscopy techniques for better accuracy on the diameter size measurement.

The HBKP-CNC and HBKP-CNF isolation was monitored using a laser diffraction particle size analyzer (Mastersizer 3000, Malvern Instruments, UK) with measuring range capacity of 0.01–3500 μm. Measurements were set to minimum of 5 readings carried out with obscuration level of 2 - 3.5%, stir rotation at 3,500 rpm without sonication. The intensity detected was converted to a unique number that refers to the hydrodynamic diameter of an equivalent particle by the software HydroMV (Malvern Instruments, UK) using the Mie algorithm set to non-spherical particle model and a cellulose refractive index of 1.4683 (Sultanova, Kasarova and Nikolov, 2009). Parameters monitored were particle distributions (D10, D50, D90), Span is a weighted average ((D90 – D10) / D50) that quantify the width distribution and it is a polydispersity indication, Uniformity is a measure of the absolute deviation from the median of particle sizes varying 0-1, D [3,2] is the average particle size (Sauter mean diameter, contribution of small particles to the surface area), D [4,3] is the

volume-weighted mean diameter (De Brouckere mean diameter, contribution of bigger particles to the volume), and wet-specific surface area (wet-SSA) of the equivalent particle.

The analysis of fiber morphology and isolation of CNC and CNF were carried out with the image acquisition system MorFi LB-01 fiber analyzer (Techpap, France). Suspensions with 50 mg/L consistency were prepared in deionized water by successive dilutions to a final volume of 1 L in triplicates and pumped into the measuring cell. The suspensions were analyzed using the MorFi software set to fiber / fine limit at 200 μm in length and the total number of analyzed fibers was set to 5,000 counts. According to the manufacturer, the resolution limit is 15 μm, *i.e.*, smaller sizes are not identified by the optical device. All particles with length bigger than 1 mm and smaller than 200 μm and width < 5 μm were counted as fine elements. Fibers were counted within this length range and width of 5 – 75 μm. Parameters monitored were fine content (% in area), average fiber length (μm), fiber length-weighted in length (μm), fines area (μm²), average fiber width (μm), and number of fibers.

Absorbance readings (ABS) were accepted in the range of 0.2 – 0.8 and wavelength screening for turbidity analysis was performed between 300 – 700 nm in quartz cuvette.

4.2.2.4 Optical microscopy

CNC suspensions and CSR were evaluated using optical microscopy (OM). OM images were obtained using an Olympus BX53 X-cite 120 LED microscope (company, country). A drop of sample prepared at solids content of 0.01% (w/w) was stained with 100 μl Congo red 1% on a microscope slide. The images were collected in the monochrome mode using amplification of 10x, 20x, and 40x. At least 100 diameters were measured using the Olympus cellsens Dimension software.

4.2.2.5 Scanning electron microscopy (SEM)

Samples of CNC and CNF suspensions were prepared at different dilutions (0.01 – 0.0001% solids) and dispersed in an ultrasonic bath for 15 min. The preparation of substrates

for Scanning electron microscopy (SEM) followed an adaptation of the negative staining technique by Mattos *et al.* (2019). The samples were placed on a Si chip sputter coated with 4 nm-layer of gold-palladium by Cressington sputter coater model 108auto (Cressington, country) using the Cressington thickness controller. The microstructures were analyzed using the Zeiss NVision 40 Focused Ion Beam Scanning electron microscope (FIB-SEM) (Zeiss, country) at an accelerating voltage of 3 kV at low vacuum. Images were analyzed using the software Image J and at least two images for each sample were analyzed to achieve 100 measurements of the particle's diameters (100 different particles). Images were adjusted for contrast and processed for noise reduction (despeckled).

4.2.2.6 Atomic Force Microscopy (AFM)

Samples of CNC and CNF suspensions were prepared at 0.01% solids and dispersed in an ultrasonic bath. The samples were placed on pre-cleaved high-quality mica support and let dry in a humidity-controlled chamber. The topographies were obtained using an Atomic Force microscope (model MultiMode 8, electronic controlled by NanoScope V, Bruker) using a silicon cantilever with aluminum. The AFM probe was set to capture images in the automatic mode (ScanAsyst-Air, Bruker). The system was operated at PeakForce Tapping Mode (nominal frequency 70 kHz and nominal force of 0.4 $N.m^{-1}$). The captured intensity sign was converted to pixels density to generate topographic images. The images were treated by the software Gwyddion (64 bit) and used for diameter measurements. At least 2 topographic images of each sample were analyzed with at least 100 measurements taken from each image.

4.2.2.7 Viscosity

The shear viscosity was determined using an automatic viscometer (Brookfield DV2TLV Pro digital) with 6.7 mL of a CNF suspension at 0.5% (w/w) and the SCA-18 spindle to according to Berto and Arantes (2019). Torque tests were conducted in triplicates using a torque ramp at 200, 150, 100, 50, and 0 rpm. Viscosity data were collected every 30s before

changing the spindle rotation (total collection time of 5 min) using Brookfield RheocalcT (v 1.2.19). The reported viscosity data was collected at operation conditions of 200 rpm (shear rate 264 s^{-1}), when most of the samples reached a torque of 10% (according to the manufacturer).

4.2.2.8 Zeta Potential

Samples of CNC and CNF suspensions were diluted to 0.03% solids and dispersed in an ultrasonic bath. The zeta potential was analyzed using U-shaped capillary electrophoresis cell by Zetasizer 3000HSa (Malvern Instruments, UK) using He-Ne laser (633nm) at angles of 12^o and 90^o. Measurements were taken on Zeta mode set to automatic temperature and water as dispersant (refractive index 1.33) employing the Dynamic Light Scattering (DLS) technique. Three measurements of each sample were performed using solution turbidity minimum of 1,000 KCps, providing zeta potential distribution and average for each run.

4.2.2.9 Thermogravimetric analysis (TGA)

Lyophilized CNC and CNF samples (2 - 10 mg) had the thermostability analyzed by a TGA Q500 V20.13 (TA Instruments, New Castle, DE, USA) from room temperature to 700°C using a heating ramp method with heating rate of 20°C.min^{-1} under nitrogen gas atmosphere. The TGA data is shown as the variation of the sample mass (TG) and the derivative weight loss (DTG) along with the temperature change to determine respectively the initial temperature of degradation (extrapolated onset, T*onset*) and the maximum mass decomposition rates (temperature of maximum degradation, T*max*) by the software TA Universal analysis 2000 v4.5A.

4.2.2.10 Water Contact Angle analysis

Thin films of CNC (0.1% solids) and CNF (3% solids) were cut to 2 cm square pieces and analyzed for water contact angle using the Mobile surface analyzer (KRÜSS GmbH, MSA, Hamburg, Germany). For each measurement, one 1μL drop of deionized water was applied on

a random area of the film surface. The projection of the water drop on the top of the film surface had the wettability monitored and contact angle (CA) measurements started at 2 s after the drop touched the surface until the drop was fully absorbed. The best fitting method provided by the Kruss Advance software was chosen to fit the shape of the drop projection against a white background. A total of three CA measurements from three different specimens were carried out per sample from the top surface. At least one measurement of the bottom surface from each film. The samples were conditioned in room with controlled humidity (50%) before the analysis.

CHAPTER 5 ENZYME-MEDIATED NANOCELLULOSE PRODUCTION: INDUSTRY PERSPECTIVES AND ANALYSIS OF MASS RATIO[2]

5.1 Introduction

Nanocelluloses can be isolated from plant-based cellulose, algae marine biomass or produced by microbials, fungi, and animals (Klemm *et al.* 2018). The great attractiveness to isolate nanocelluloses from lignocellulosic materials is the wide variety and abundance of plant-cellulose sources at industrial scale (Nechyporchuk *et al.*, 2016). Typical plant-cellulose sources used for nanocelluloses isolation have high content of cellulose. Examples of those are naturally occurring fiber crops, such as cotton (high purity cellulose, average cellulose composition of 98%), or sources industrially prepared, such as microcrystalline cellulose (MCC), microfibrillated cellulose (MFC), and wood-pulp from various pulp and paper processes (*e.g.*, bleached Kraft pulp with cellulose composition of 75 - 80%, sulfite pulp with cellulose composition > 90%, dissolving pulp with cellulose composition > 95%); however, agricultural sources that are not directly linked to human nutrition are considered very attractive from an economic and environmental point of view. Examples of promising agricultural raw material are crop residues (*e.g.*, bagasse and straw obtained from different sources) and bioenergy crops (energy cane, poplar, switchgrass) (Espinosa *et al.*, 2017; Lee *et al.*, 2014; Rajinipriya *et al.*, 2018). Other locally available raw materials were also employed to isolate nanocellulose (Brinchi *et al.*, 2013; Chieng *et al.*, 2017; Corrêa *et al.*, 2010; de Campos *et al.*, 2013; Hideno *et al.*, 2009; Martelli-Tosi *et al.*, 2016; Tibolla *et al.*, 2017).

---

[2] *Part of this chapter was published on the Review paper:*
Arantes, V, Dias, IKR, Berto, GL, Pereira, B, Marotti, BS, Nogueira, CFO. The current status of the enzyme-mediated isolation and functionalization of nanocelluloses: production, properties, technoeconomics, and opportunities. Cellulose (2020) 27:10571–10630. https://doi.org/10.1007/s10570-020-03332-1

Different approaches are proposed to isolate nanocellulose using a biorefinery concept (Leistritz *et al.* 2006; Song *et al.* 2014; Albarelli *et al.* 2016; Nelson and Retsina, 2014; García *et al.* 2017). There are two strategies of using enzymatic treatment to integrate the production of nanocelluloses in a biorefinery. The first alternative employs enzymatic hydrolysis as a pretreatment that promotes cellulose disruption prior to refining or acid hydrolysis, which may or may not recover a considerable sugar amount/concentration. This mild enzymatic treatment generally employs mono-components enzyme cocktail (Hassan *et al.* 2010; De Campos *et al.* 2013; Beltramino *et al.* 2015; Dai *et al.* 2018; Liu *et al.* 2019b; Saelee *et al.* 2016); the second alternative uses a severe treatment that co-produces and recovers high-titer sugars, which may or may not be channelled for biofuel production. The severe enzymatic treatment generally employs an enzyme cocktail for complete saccharification (Zhu *et al.* 2011; Song *et al.* 2014; Camargo *et al.* 2016; Beyene *et al.* 2017; Bondancia *et al.* 2017; Rosales-Calderon *et al.* 2021). Based on the latter, it is proposed an integrated route to co-produce nanocellulose (high-value added) and sugars (low-value added) using a biorefinery concept, aiming to valorize underutilized material to enhance profit.

This chapter aims to discuss perspectives on how pulp and paper and sugarcane industries could benefit by co-producing nanocelluloses using an enzyme-mediate process, comparing the price and availability of the lignocellulosic materials and underutilized subproducts. Moreover, the challenges related to the economic attractiveness of side streams will be discussed. By analyzing the enzyme cost equation, a mathematical adjustment is introduced to propose a feasible mass ratio of coproducts through the breakeven points, revealing trends in the proportions of coproducts and alternatives to integrate sugars and nanocelluloses.

5.2 Integration perspectives of the enzyme-mediated isolation of nanocelluloses within pulp and paper and sugarcane industries

The pulp and paper and the sugarcane industries are the biggest manufacturers of lignocellulose-derived products and important players on the market of commodities. Thus, both segments would benefit from nanocellulose production at industrial scale to enhance their profits in an integrated infrastructure. However, the discussion of producing nanocellulose within those biorefineries require consideration of critical aspects such as the choice of raw material and pretreatments, and market risk.

The choice of raw material influences the technoeconomics of a biorefinery regardless the chosen technology. The price and availability of raw materials, as well as the fluctuations caused by market demands, directly affect the operational expenditure (OPEX) and impact the final price of nanocelluloses. The most common raw materials employed in nanocellulose production are available at the following values, depending on which market they are procured: hardwood bleached Kraft pulp (HBKP) 500 – 1,050 US$/t (ref. Brazil, Jan 2006 – Jul 2019), northern bleached softwood Kraft pulp (NBSKP) 600 – 1,450 US$/t (ref. China, Europe and USA, Sep 2014 - Jul 2019), and dissolving pulp 850 – 1,100 US$/t (ref. China, 2016 - 2017) (Arantes *et al.* 2020). Fibers side streams such as sludge fibers and recycled pulp can be purchased at 20 US$/t and 100 US$/t, respectively (Spence *et al.* 2011).

Notable reviews have discussed the growing importance of agricultural subproducts as potential raw material in nanocellulose isolation (Pereira and Arantes 2018; Rajinipriya *et al.* 2018). However, pulp production from agro-industrial residues is not as popular as woody pulp production (Hurmekoski *et al.*, 2019). China, Colombia, and Brazil are the most known countries to use straw and bagasse to produce non-woody fiber pulp at volume order of 7.5 Bi tons and 188 M tons in 2014, respectively (Faostat, 2020). Sugarcane bagasse pulp has a market price comparable to chemical wood pulp, at approximately 850 US$/t (personal communication

with GCE paper/Propal). Estimations of the price of low-cost agricultural feedstock generally depend on the oil barrel price. The following prices are generally noted for these industrial sub-products: wheat straw 5 – 10 USD/t (Leistritz *et al.* 2006), sugarcane bagasse 15 – 25 US$/t, sugarcane straw 30 – 40 US$/t (ref. Brazil 2019, dollar currency conversion 4.00 R$/US$, communication with industry representative). Table 12 shows a comparison of prices from wood and non-wood raw materials with potential to isolate nanocelluloses. The reported prices do not consider associated costs such as transportation, collection, or soil and nutrient removal.

Table 12. Comparison of prices from wood and non-wood raw materials with potential to produce nanocellulose (Adapted from Arantes *et al.*, 2020).

Raw material	Price (US$/t)	Market and historical price
Hardwood Bleached Kraft pulp (HBKP)	500 – 1,050	Brazil (period Jan 2006 – Jul 2019)
Northern Bleached Softwood Kraft (NBSK) pulp	600 – 1,450	China, Europe and USA (period Sep 2014 - Jul 2019)
Dissolving pulp	850 – 1,100	China (period 2016 – 2017)
Wheat straw	5 – 10*	USA (Leistritz *et al.* 2006)
Corn stover	10 – 15*	USA (Leistritz *et al.* 2006)
Sugarcane bagasse	15 – 25*	Brazil (period 2019)
Sugarcane straw	30 – 40*	Brazil (period 2019)
Sludge fibers	20	(Spence *et al.* 2011)
Recycled pulp	100	(Spence *et al.* 2011)

*The reported prices do not consider the costs of transportation, collection, or soil and nutrient removal

Low-cost agricultural feedstock has been considered more economically attractive as a starting material to isolate nanocelluloses than wood pulp and forestry byproducts due to their price (De Assis *et al.*, 2017b). This can be evidenced by taking into account the Brazilian production and market. The sugarcane biorefinery has much larger scale of production and side-stream availability than the pulp and paper industry (about 10 times). The annual bagasse and straw generation volume is around 172 and 82 million ton and pulp production in Brazil is 20 million ton (UNICA, 2019; FAO, 2021). Adding a high-value product associated with

sugarcane biorefinery is noteworthy, as it may reduce the price of cellulosic ethanol. This has been observed in bioenergy mills considering the 1G ethanol/sugar scenario. When capital is allocated for sugar production, which is a product with higher market price than ethanol, it helps to share operational expenses and hence enhance the profits with 1G ethanol (Dias *et al.*, 2016). Additionally, the reported price for nanocelluloses is quite attractive compared to the prices of traditional products from sugarcane mills (hydrous fuel ethanol 1.46 US$/gallon, raw sugar 0.25 US$/kg, and electricity 150 US$/MWh) (USDA, 2018).

It is known that it is not advantageous to fully convert the cellulose from lignocellulose materials into fermentable sugars for the production of cellulosic ethanol due to reduced gains in sugar conversion levels in longer reaction times, increased demand for heat to maintain the temperature of the bioprocess, in addition to the low solids content and subsequent need for liquor concentration (Arantes and Saddler, 2011; Dias *et al.*, 2013; Modenbach and Nokes, 2013; Newman *et al.*, 2013). Due to the enzymatic model of cellulose depolymerization, Arantes and Saddler (2011) suggested that a level of carbohydrate conversion of 70% could be targeted as an efficient saccharification using the lowest enzyme loading possible regardless of the lignocellulosic source or pretreatment. Dias *et al.* (2013) demonstrated that a higher production of 1G/2G ethanol can be obtained using intermediate conditions of solids content and sugar conversion (15% and 60%, respectively). Although an optimum proportion between sugars and nanocelluloses has not been discussed yet, the residue from enzymatic hydrolysis, also known as cellulosic solid residue (CSR), and the recovered lignin could still be useful for upgrading into products. From a process point of view, the use of the remaining CSR to isolate nanocelluloses will be advantageous because it often contains too much moisture to be burnt. According to Leistritz *et al.* (2006), even a small percentage of CSR such as 1% used to isolate nanocelluloses would improve the biorefinery economics.

On the other hand, the integration of nanocellulose production with the pulp and paper industry is the most promising alternative to reach the market due to technical knowledge in producing pulp and bleached pulp (Hurmekoski *et al.* 2019). Currently, mild enzymatic pretreatment has been considered efficient to reduce clogging and lower the energy input during mechanical treatment (de Assis *et al.*, 2017b; Spence *et al.*, 2011). Conversely, the industry may hesitate to allocate a valuable product such as pulp to a high-risk market using new technology. Challenges related to market demand and competition with the traditional products are some of the hurdles to drive nanocellulose production to a step forward. Hence, new forest products still rely on traditional markets until a permanent shift can occur (Hurmekoski *et al.*, 2019). Some industry representants have indicated the interest of using rejected fibers for nanocellulose isolation (Aguayo *et al.*, 2018), which seems to be competitive as a starting material compared to agricultural subproducts (Table 12). Moon *et al.* (2015) assessed possible alternatives of improving the valorization of side streams from the pulp and paper industry by proposing the use of an additional quantity of logging residues to co-produce CNF and fuels along with the pre-existing products (such as chips, bark, and chip dust). The authors estimated that the ratio of income/expenditure for CNF is as high as the ratio obtained for paper production considering a scenario in the Maniwa region (Japan). Their assessment suggested that the CNF coproduction may double the total plant investiment (TPI) and increase the OPEX but yields 2.5 times higher return on revenue. Moon and collaborators discussed other positive effects of co-producing CNFs beyond improving the pulp valorization, such as the creation of positive social impact in the form of new jobs, expansion of industry value chain to sectors currently non-attended by the pulp and paper industry, and stimulus for the circular economy.

5.3 Mass Ratio Analysis for Co-producing Sugars and Nanocelluloses: Insights from Enzyme Cost Equation

Enzymatic hydrolysis is considered the best economical technology to produce cellulosic ethanol (Kazi *et al.*, 2010; Chen *et al*., 2016). However, the cost of enzymes is one of the largest contributors for the price of cellulosic sugars/ethanol (Newman *et al.,* 2013; Stephen *et al.,* 2012). Therefore, the enzyme cost has been one of the most pursued topics to improve the feasibility of cellulosic ethanol. In the last few years, several approaches were adopted to lower the impact of enzyme cost on the price of cellulosic ethanol. The Eq. 3 was presented by Lynd *et al.* (2017) and Stephen *et al.*, (2012) and leads to the estimation of the cost of cellulases per gallon of ethanol as shown by Eq.3:

$$C = \frac{L.P}{Y} \qquad \text{(Eq. 3)}$$

where C is the cellulase cost ($/gallon of ethanol), L is the cellulase loading (mg protein/g feedstock = kg protein/M ton feedstock), P is the cellulase price ($/kg), Y is the ethanol yield (gallon/Mton feedstock).

Considering process integration for the coproduction of nanocelluloses and cellulosic ethanol as an alternative to lower the impact of the cellulase price, we proposed to adjust the equation Eq. 3 as shown by Eq. 4:

$$C = L.P\left[\frac{1}{(1-x).Y_{EtOH}} - \frac{1}{x}\right] \qquad \text{(Eq. 4)}$$

where C is the cellulase cost ($/gallon of ethanol), L is the cellulase loading (mg protein/g feedstock = kg protein/M ton feedstock), P is the cellulase price ($/kg of protein), Y_{EtOH} is the ethanol yield (gallons/M ton feedstock), x is the mass ratio based on feedstock depolymerization into cellulosic sugars/ethanol.

The mass ratio x can be equal to Y_{Nano}, which is the nanocellulose yield (kg/M ton feedstock), in the case when Y_{Nano} is equal to 1, such as when coproducing CNF.

Figure 8 shows two plots of a range of mass ratio up to 1, that represents 100% of feedstock conversion into cellulosic sugars (Figure 8a) or cellulosic ethanol (Figure 8b). The break-even point obtained for the Eq. 4 was 0.5 for cellulosic sugars (Figure 8c) and 0.6 for cellulosic ethanol (Figure 8d).

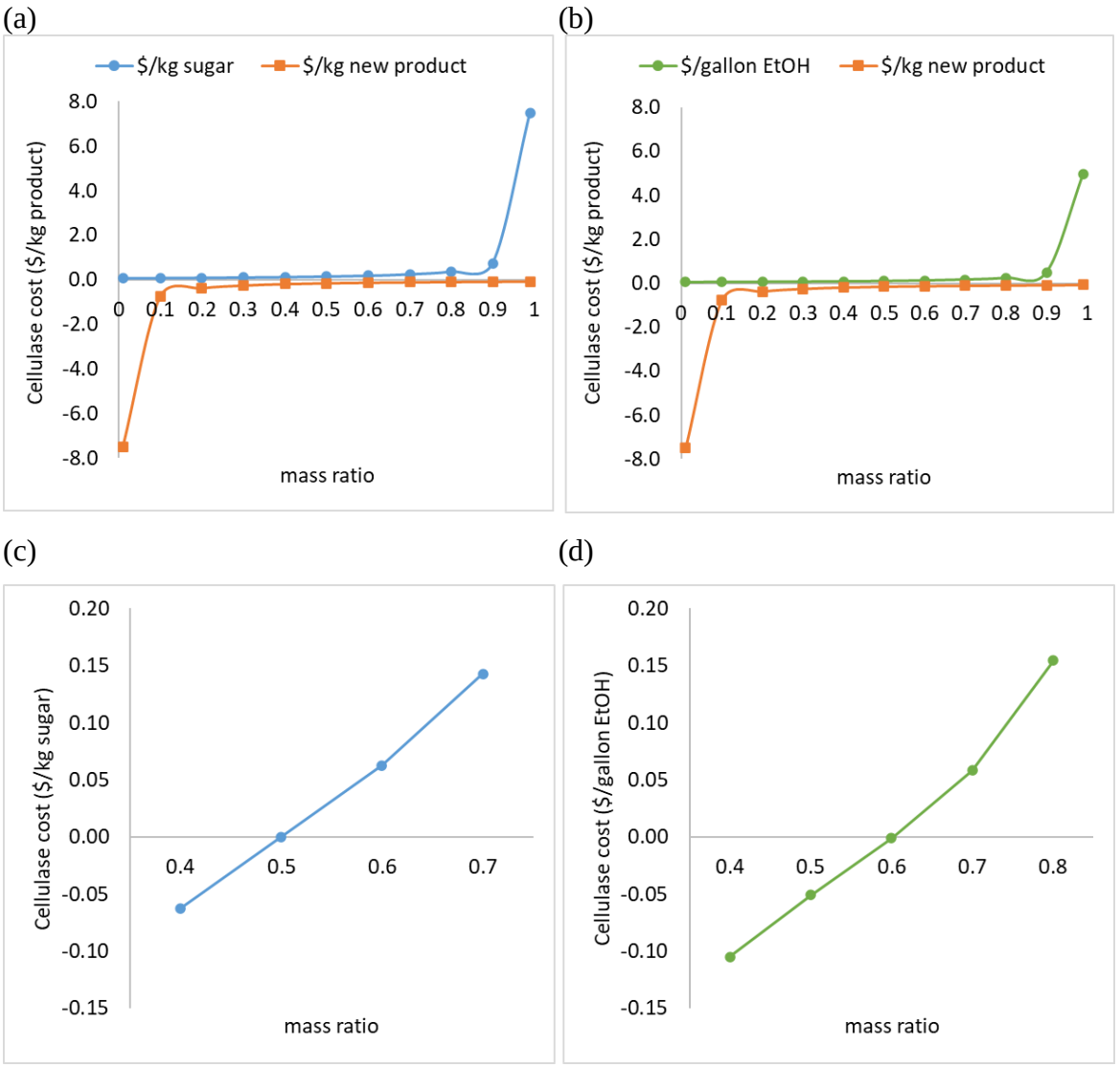

Fig. 8. Simulation of cellulase costs in terms of (a) cellulosic sugar and new products (b) cellulosic ethanol and new products; break-even point for cellulase costs in terms of (c) cellulosic sugars (d) cellulosic ethanol.

The approach proposed here agrees with the current understanding that conducing the cellulose hydrolysis over the rate of 60% for ethanol production is not economically feasible. This result implies that, instead of solely maximizing the yield of cellulosic ethanol by enhancing the feedstock conversion, an improved valorization of the feedstock can be achieved

by utilizing the CSR as a value-added product. When a high-value product is integrated with the cellulosic sugar production, it shares the enzyme costs across the production process. This assessment highlights an intriguing opportunity for cellulosic ethanol facilities reborn through the integration of nanocelluloses as high-value coproducts together with its traditional products.

The integration with a new product is even more beneficial if it has a high yield. Thus, the Eq. 4 shows mass ratio alternatives that may consistute options where nanocellulose could play the role of main product and lead the enzyme costs, hence the production costs. This alternative fosters a possible condition for a versatile process integration.

5.4 Conclusion

The potential of nanocellulose coproduction within the pulp and paper and sugarcane industries was investigated. There is a perspective that pulp and paper industry will be the primary supplier of nanocelluloses in the near future. This was attributed to the production of cellulose-rich pulp, industrial availability of pulp subproducts, and expertise in refining, including trials to isolate CNF using enzymatic pretreatments. As CNF promises a high return on revenue, it may have the potential to offset the decline of traditional markets. In contrast, integrating nanocelluloses within the sugarcane biorefinery holds an enormous potential because of the economic attractiveness and abundance of agricultural subproducts that can be used to isolate nanocelluloses. Sugarcane biorefineries, already proficient in the use of enzymatic treatments to produce cellulosic sugars and ethanol, could benefit from upgrading the cellulosic solid residue (CSR) – a readily available cellulose source – to isolate nanocelluloses and enhance cellulosic ethanol's economic feasibility. Hence, the enzyme-mediated process can provide a platform for nanocelluloses integration that benefits both pulp and paper and sugarcane industries.

The analysis of the enzyme cost equation revealed to be a valuable tool to study mass ratios of cellulosic sugars and nanocelluloses. The introduction of a mathematical adjustment

to the enzyme cost equation may assist in identifying the feasible coproduction proportion. The breakeven point illustrated the mass proportion at which the nanocellulose integration may become viable, confirming the current understanding that exceeding a level of 60% cellulose conversion is not economically feasible. The enzyme cost equation analysis also revealed alternative scenarios where nanocelluloses could play a primary role as coproduct. Although manipulating mass ratios of cellulosic sugars and nanocelluloses may offer new possibilities of introducing a new category of bioproducts in the industries' value chain, more technoeconomic studies are still necessary to discuss the impact of producing different mass ratios.

CHAPTER 6 EXPLORING DIFFERENT CELLULOSE CONVERSION FOR THE COPRODUCTION OF CNC AND HIGH TITER OF SUGARS FROM BLEACHED KRAFT PULP: AN OPTIMIZATION STUDY

6.1 Introduction

The process feasibility is especially governed by the yield of its products. Low yield products require large quantities of raw material to be processed, which enhances the operational costs and hence increases the minimum product selling price (MPSP). These types of processes are highly impacted by the variations of the raw material's cost and availability, which jeopardize the viability of a new product. These aspects need to be evaluated for the production of nanocelluloses via enzyme-mediate processes.

The literature points out that enzyme-mediated processes focusing solely in producing CNC obtain a low CNC yield (< 38%). Other studies that consider the coproduction of CNC and cellulosic sugar also report low CNC yield (< 20%) and only a very few authors report the yield and concentration of sugars as shown on Table 5. Leão *et al.* (2017) indicated that the low CNC yield could impact not only for the process economics but also the sustainability due to higher costs with effluent treatment. Preliminary technical-economic analysis carried out by Rosales-Calderon *et al.* (2021) concluded that it is essential to study alternatives to improve the CNC yield as well as to optimize the separation process between CNC and CSR for enzyme-mediated processes. They suggested that employing filtration to recover sugars would be 7 times more economically effective than using centrifugation and suggested the use of water less pure than osmosis reverse would produce greater CAPEX and OPEX savings. Klemm *et al.* (2018) and Wang *et al.* (2012) also highlighted the need for efficient separation procedures to isolate CNCs and indicated the necessity of a detailed study of the centrifugation and its parameters in the recovery of CNC.

Furthermore, enzyme loading, and time are important variables for the enzymatic kinetics of substrate consumption and product formation, which directly affects the feasibility of a bioprocess. Enzymes are considered a high-cost input and the reaction time is important for defining both the process architecture as well as the scheduling of steps and process flows (*i.e.*, process steps and equipment sizing, and programming reaction times, dead time, unloading and loading times of reactors) (Humbird *et al.*, 2010; Newman *et al.*, 2013; Stephen *et al.*, 2012). The kinetics for cellulosic sugar production have been extensively studied as well as the optimization alternatives for CNC production acid hydrolysis, however the effect of different degrees of cellulose conversion produced by commercial enzyme cocktails is still poorly studied to produce nanocellulose and requires further investigation to assess suitable conditions for the coproduction of nanocelluloses and fermentable sugars at high concentration (Bondancia *et al.*, 2022, 2017; De Aguiar *et al.*, 2020; Pereira *et al.*, 2021; Pereira and Arantes, 2020; J. Wang *et al.*, 2021b).

This chapter has the goal to investigate the isolation of CNC by enzymatic hydrolysis and conduct the recovery of CNC by centrifugation. The separation of CNC from the CSR was investigated by a 12-experiment Plackett Burman (PB) design to screen centrifugation parameters that impact in the CNC yield and energy demand. The parameters for investigations were selected in order to set the centrifugation less energy-demanding and reduce the need for ultra-pure water. Additionally, to investigate the enzyme-mediate isolation of CNC, the enzymatic hydrolysis was conducted to produce different degrees of cellulose conversion from Hardwood Bleached Kraft pulp (HBKP), which was another important parameter in the design of experiments. The expected outcome of this chapter is to provide a correlation between centrifugation parameters and enzymatic hydrolysis conditions to optimize CNC yield using a mathematical model and to investigate possibilities to increase CNC yield while avoiding high-cost processes.

6.2 Reasoning for the selection of centrifugation parameters

When centrifugation by density difference is applied to nanomaterials, the choice of the appropriate rotation is an essential parameter for the separation. Bonaccorso *et al.* (2013) studied different sorting strategies by centrifugation to the selective separation of gold nanoparticles (sizes between 10 – 30 nm). The authors adopted simplifications of particles interactions, such as aggregation and diffusion, and considered that the particles had well-defined and spherical shapes. Using sedimentation-based separation and water medium without any solute, they observed a linear relationship between the applied centrifugal force and the distance that the gold nanoparticles travel within the system. They identified three important regions in which it is possible to distinguish the influence of the rotation speed on the separation of nanoparticles with size equal to 10 and 20 nm: 1) low rotation (< 525×*g*) - no sedimentation of nanoparticles occurred; 2) rotation between 525 – 2,100×*g* - selective sedimentation of nanoparticles occurred for particle size of 20 nm; 3) high rotation (>2,100×*g*) - particles decanted regardless of their size. To investigate the suitable rotation speed to separate CNC from CSR, a similar approach was used although the desired separation would be to recover the maximum of nanoparticles from a mixture with micro-sized particles. Thus, the rotation speed investigated was between 500 - 2,838×*g*.

Other parameters considered for the investigation of centrifugation parameters were the centrifugation scale and water column for separation (represented by tubes with different capacities), the consistency for the separation (represented by the amount of CSR relative to the volume of water for its resuspension), and the water purity (*e.g.*, tap water and reverse osmosis water) which can influence in the coalescence tendency by changing the particle-particle and particle-solvent interactions.

Regarding the centrifugation scale, we understand the limitations of the study using a benchtop equipment (centrifuge with swing-out rotor) and the necessity to repeat the separation

until no turbid layer is not formed after the centrifugation. The water column simulates the maximum distance that the particles can travel and be efficiently separated from micro-sized particles. This parameter was tested using the tube capacity (50 mL and 500 mL) and the volume of water for the CSR resuspension was 20 mL and 50 mL on Falcon tubes and 20 mL and 100 mL on centrifuge tubes.

A second consideration for the study was the consistency for the separation resolution of the particle's mixture. The amount of CSR (o.d.) and resuspended in different volumes of water explores separation conditions, such as concentration, dilution, and aggregation of the particles (particle-particle interactions). These parameters were tested using consistencies of 2.5 – 25% (w/w). The particle-particle interactions could also be affected by the choice of temperature for the separation (4 ºC and 25ºC) and the water purity level. The proposal to use two types of water is based on issues related to minimizing operational costs and literature indeterminations regarding the excess of conductivity, especially referred in studies of CNC produced by acid hydrolysis. Penttilä *et al.* (2013) consider conductivity higher than 20 µS/cm as excessive CNC recovery. Up to date, the study by Hamad and Hu (2010) was the only that mentions the use of tap water to replace deionized water during the dialysis process to remove excess acid and salts after acid hydrolysis. Hamad and Hu (2010) observed that CNC washed with distilled water had lower pH and lower stability in suspension when compared to CNC washed with tap water and De Assis *et al.* (2017a, 2017b) mention the used of tap water in the preliminary technical-economic assessment for CNC and CNF production. However, up to date, there are no studies discussing the impact of using different types of water to isolate and recover CNC.

6.3 CNC recovery by centrifugation and assessment of centrifugation parameters

The 12-experiment PB design was employed to screen the most important centrifugation parameters to study the separation of CNC from CSR. The eight centrifugation

parameters were studied in relation to 15 responses obtained by gravimetry analysis from CNC and CSR recovered after the separation and by light scattering analysis of the 12 CNC suspensions produced. The 15 responses are shown on the Appendix A. Figure 9 shows the visual aspect of the 12 CNC suspensions obtained, which reflect the amount of CNC isolated but also a polydispersity of diameters (Toivonen *et al.*, 2018). Numbers below each vial indicates the experiment identification number (ExpID#).

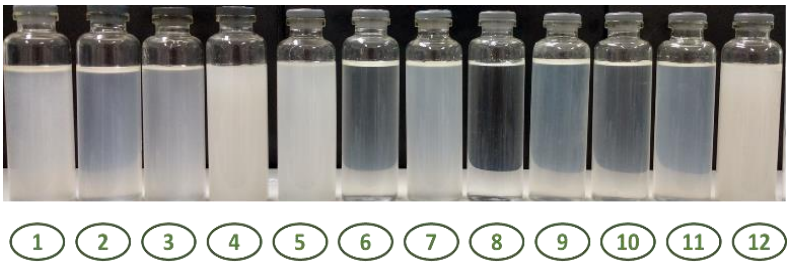

ExpID# 1, 2, 3, 7, 9, 10 – reverse osmosis water
ExpID# 4, 5, 6, 8, 11, 12 – tap water

Fig. 9. Illustration of the 12 suspensions produced with the Placket-Burman Design.

The statistical results indicated that two responses - CNC yield and uniformity – out of the 15 studied were significatively explained by two of the centrifugation parameters – Rotation speed and tube capacity. Table 13 shows the statistical results (main effect, *F-value*, and *p-value*) obtained for the responses CNC yield and uniformity for each centrifugation parameter and a Pareto chart is shown on the Appendix A. The statistical analysis points that CNC yield is explained by two factors Rotation speed (Factor E, main effect - 5.175, *F-value* 6.74, *p-value* 0.081) and Tube capacity (Factor H, main effect - 7.160, *F-value* 12.9, *p-value* 0.037). Because the main effects obtained for Rotation speed and Tube capacity are negative (E -5.175 and H -7.160, respectively), this suggest that performing CNC recovery at low speed (500 ×*g*) and smaller tube capacity (a larger water column for separation) would produce a higher CNC yield response. For the uniformity response, only the Tube capacity (Factor H, main effect -0.1460, *F-value* 8.63, *p-value* 0.099) was considered significant and the main effect is negative (H -0.1460), which indicates that a higher uniformity response would be favored by a smaller tube

capacity (a larger water column for separation). According to the manufacturer, the uniformity value reported by this analysis is a measure of the absolute deviation from the median of the particle sizes, thus a higher value would indicate a higher amplitude of particle size distribution. An example is Exp ID#4 for which and the uniformity value and CNC yield was 0.623, and 24.6%, respectively, which were the highest values obtained for these responses. For this condition, D90 is 2.64 μm, which indicates 90% of the particles present equivalent sphere size smaller than 2.64 μm. However, a fraction of the analyzed particles has equivalent particle size bigger than 2.64 μm, which justifies the visual aspect being opaque white.

Table 13. Statistical results (main effect, *F-value*, and *p-value*) obtained for the responses CNC yield and uniformity by analyzing 8 centrifugation parameters in a 12-experiment PB design.

Factor	Variables	Statistical results (main effects, *F-value, p-value*)	
		CNC yield	Uniformity
A	Cellulose conversion	4.219, F= 4.48, p = 0.125	0.0207, F= 0.17, p = 0.718
B	CSR (g)	-2.830, F= 2.02, p = 0.251	-0.0467, F= 0.88, p = 0.447
C	Water volume (mL)	2.075, F= 1.08, p = 0.374	0.0873, F= 3.09, p = 0.221
D	Water type	2.165, F= 1.18, p = 0.357	0.1153, F= 5.38, p = 0.146
E	**Rotation (×*g*)**	**- 5.175, F= 6.74, p = 0.081***	-0.1117, F= 5.05, p = 0.154
F	Time (min)	2.381, F= 1.43, p = 0.318	0.0873, F= 3.09, p = 0.221
G	Temperature (°C)	- 0.872, F= 0.19, p = 0.691	-0.0550, F= 1.22, p = 0.384
H	**Tube capacity**	**- 7.160, F= 12.9, p = 0.037***	**-0.1460, F= 8.63, p = 0.099***

*Factors in bold are statistically significant considering interval of confidence of 90% ($p < 0.1$) and F critical value at the p = 0.1 level of significance is F (8, 3, 0.01) = 5.25.

The results obtained with the PB design for CNC separation, low rotation and with a higher water column, corroborate with those described by (Bonaccorso *et al.*, 2013), who studied the separation of gold nanoparticles with size range of 10-20 nm and assumed their particles had well-defined and spherical shapes. They observed that at low rotation speed the gold nanoparticles did not decant. For our investigation, similar centrifugation conditions were recommended even though the diversity of morphological structures that can be formed after the enzymatic hydrolysis could turn the separation more complex. These results help to resolve the discrepancies between the data reported in the literature, where different authors have used

different combinations of centrifugation parameter to isolate CNC (Chieng *et al.*, 2017; Pereira and Arantes, 2020; Pirani and Hashaikeh, 2013; Prathapan *et al.*, 2016; Song *et al.*, 2014; Yarbrough *et al.*, 2017; Zhu *et al.*, 2011).

The PB design was useful for an initial screening of the centrifugation parameters. It was determined that six centrifugation parameters were not statistically significant to isolate and recover CNC. This demonstrates the effectiveness of the PB design to reduce the number of process variables based on the main effects. The non-significant factors were A, B, C, D, F, and G, representing cellulose conversion, CSR weight o.d., volume of water for CSR resuspension, type of water, time, and temperature, respectively. Even though the cellulose conversion (Factor A) was not considered statistically significant using level of confidence p=0.1, the magnitude of the *F-value* calculated for cellulose conversion (*F-value* = 4.48) indicates a quadratic sum 4.48 times greater than the quadratic sum of the errors of the system. Moreover, the value of the main effect calculated for cellulose conversion compared to the main effect calculated for other variables points to a greater importance of cellulose conversion for CNC yield response. The literature also shows that different reaction conditions can produce CNC with different CNC yield and morphologies (Arantes et al, 2020). Thus, the lack of statistical significance observed for cellulose conversion in the PB design could be due to the narrow range of cellulose conversion (28 – 38%) rather than the actual unimportance of the parameter for CNC isolation and recovery.

One interesting result from the PB study was regarding the water type parameter and the fact the water type did not significantly influence the CNC recovery even though it is known it affects suspension stability. Although the zeta potential was not analyzed as a response for the PB design, the visual aspect of the CNC suspensions suggests an influence in the overall suspension stability. Since the ionic concentration can alter the surface energy of the nanocelluloses due to the interaction of the hydroxyl groups with the medium, the higher

concentration of ions on the tap water produced suspensions with an opaque aspect than CNC suspensions using reverse osmosis. The tap water used to recover CNC presented conductivity 8.6 times higher than suggested by the literature (172.1 µS/cm against 20 µS/cm). Figure 5 shows vial#1 and vial#4 which present same concentration of CNC (0.005 $g.mL^{-1}$) but different visual aspect. Other consequences for the CNC applicability were not further explored with this study.

To proceed to an experimental design with higher resolution, the centrifuge parameters were set to provide conditions less intensive for high-purity-water and energy. The centrifugation parameters were lower rotation speed, no system cooling (25°C), shorter centrifugation time, and use of tap water for CSR resuspension. The amount of CSR (o.d.) and volume of water for resuspension were set to the lower level, resulting in a solids consistency of 12.5% (w/w). This final combination of parameters has the potential to considerably reduce the operational costs, especially disregarding the necessity of ultra-pure water.

6.4 Exploring different degrees of cellulose conversion

Due to the importance of enzyme loading and time for enzyme-mediate processes, a design of experiments with higher resolution followed by a response surface methodology was carried out using a wider range of cellulose conversion. By increasing the cellulose conversion range used for the Plackett-Burman study, it is possible to investigate the effect of cellulose conversion on CNC yield while exploring enzymatic hydrolysis conditions to obtain high sugar content. Humbird *et al.* (2010) and Newman *et al.* (2013) highlighted that a region of linear correlation between enzyme loading and cellulose conversion leads to a viable region for obtaining sugars at high concentration. According to the literature, the desirable conditions for enzymatic hydrolysis are high solids loading (> 15% solids consistency), enzyme loadings up to 30 $mg.g^{-1}$, and time up to 48h (Humbird *et al.*, 2010; Stephen *et al.*, 2012; Newman *et al.*, 2013; Dias *et al.*, 2013)

Analysis of the carbohydrate conversion from different enzymatic hydrolysis conditions shows a strong linear correlation between the increase of enzyme loading and cellulose and xylan conversion. Figure 10a shows a linear trend between enzyme loading and cellulose conversion for enzyme loading up to 20 $mg.g^{-1}$ with correlation coefficient values of R^2 = 0.9995 and R^2 = 0.996 for 30h and 72h, respectively. By including the condition at enzyme loadings 30 $mg.g^{-1}$, it causes the slope and correlation values to be smaller (slope 1.6 at R^2 = 0.94 and slope 2.3 at R^2 = 0.98 for 30h and 72h , respectively). Figure 10b confirms this observation by showing the glucose concentration did not increase proportionally when the enzyme loading was increased from 20 $mg.g^{-1}$ to 30 $mg.g^{-1}$. The glucose concentration obtained with enzyme loading of 20 $mg.g^{-1}$ was 121 $g.L^{-1}$ and 130 $g.L^{-1}$ for 30h and 72h, respectively, whereas, with enzyme loading of 30 $mg.g^{-1}$, it was 114 $g.L^{-1}$ and 136 $g.L^{-1}$ for 30h and 72h, respectively. The linear region observed represents the fast phase of cellulose conversion (higher cellulose accessibility) whereas the reduction of slope observed, even when enzyme loadings is as high as 30 $mg.g^{-1}$, indicates the reaction is moving to moderate phase of cellulose conversion (less cellulose accessibility) (Arantes and Saddler, 2011). This change in the carbohydrate conversion indicates a stage where the gains in cellulose conversion and glucose production are smaller and hence not advantageous. The linear trend observed for enzyme loading and xylan conversion followed a similar pattern than observed for cellulose conversion. Figure 10d shows a strong linear trend between enzyme loading and xylan conversion with enzyme loading up to 20 $mg.g^{-1}$. By including the condition with enzyme loadings of 30 $mg.g^{-1}$, it also causes the slope and correlation values to be smaller (slope 1.6 at R^2 = 0.994 and slope 2.3 at R^2 = 0.996 for 30h and 72h , respectively).

The enzyme cocktail used in this study was Cellic CTec2, which is an improved enzymatic preparation developed to overcome cellulose recalcitrance and boost cellulose conversion by providing high β-glucosidases activity to prevent inhibition by product and

xylanase activity to enhance the accessibility of cellulases to the cellulose fibers and fiber swelling (Song *et al.*, 2014). Because of the additive/synergistic effect from Cellic CTec2's main components (cellulases, xylanases, and β-glucosidases), this commercial enzyme cocktail can produce high sugar concentration although newer versions of the Cellic's cocktail would reduce the cellulose recalcitrance even further (Teter, 2012). Thus, the observed decrease on the effectiveness of enzymatic hydrolysis and decrease of glucose and xylose production even at high enzyme loading (30 $mg.g^{-1}$) is an indication of reduction in the cellulose accessibility (cellulose recalcitrance) rather than enzymatic inhibition or mass transfer limitation (Arantes and Saddler, 2011).

It is known the combination of hydrolysis time and solid loading play an important role in achieving high carbohydrate conversion and sugar concentration, however it also incurs in the operational cost (Newman *et al.*, 2013). For the same solid consistency of 17.5%, the linear correlations made between cellulose conversion and glucose concentration (Figure 10c) and xylan conversion and xylose concentration (Figure 10f) show that higher gains of sugar concentration are achieved when the cellulose and xylan conversion is increased at reaction time of 30h compared to 72h. This is observed by the trend's slope at reaction time 30h being steeper than at 72h.

Another interesting observation is that, at conditions with low enzyme loadings and longer reaction time, an intermediate level of sugar concentration would be achieved (condition EH-5-72, 5 $mg.g^{-1}$ for 72h, glucose and xylose concentration of 67 ± 6 $g.L^{-1}$ and 17 ± 1 $g.L^{-1}$, respectively) while, at higher enzyme loadings and shorter reaction time, would favor to obtain higher sugar concentrations (condition EH-20-30, 20 $mg.g^{-1}$ for 30h, glucose and xylose concentration of 127 ± 7 $g.L^{-1}$ and 24 ± 3 $g.L^{-1}$, respectively). Using the linearized curves, it appears that the enzyme loading of 12.6 $mg.g^{-1}$ at reaction time of 30h and the enzyme loading of 9.1 $mg.g^{-1}$ at reaction time of 72h would produce same cellulose conversion (33.94%) and

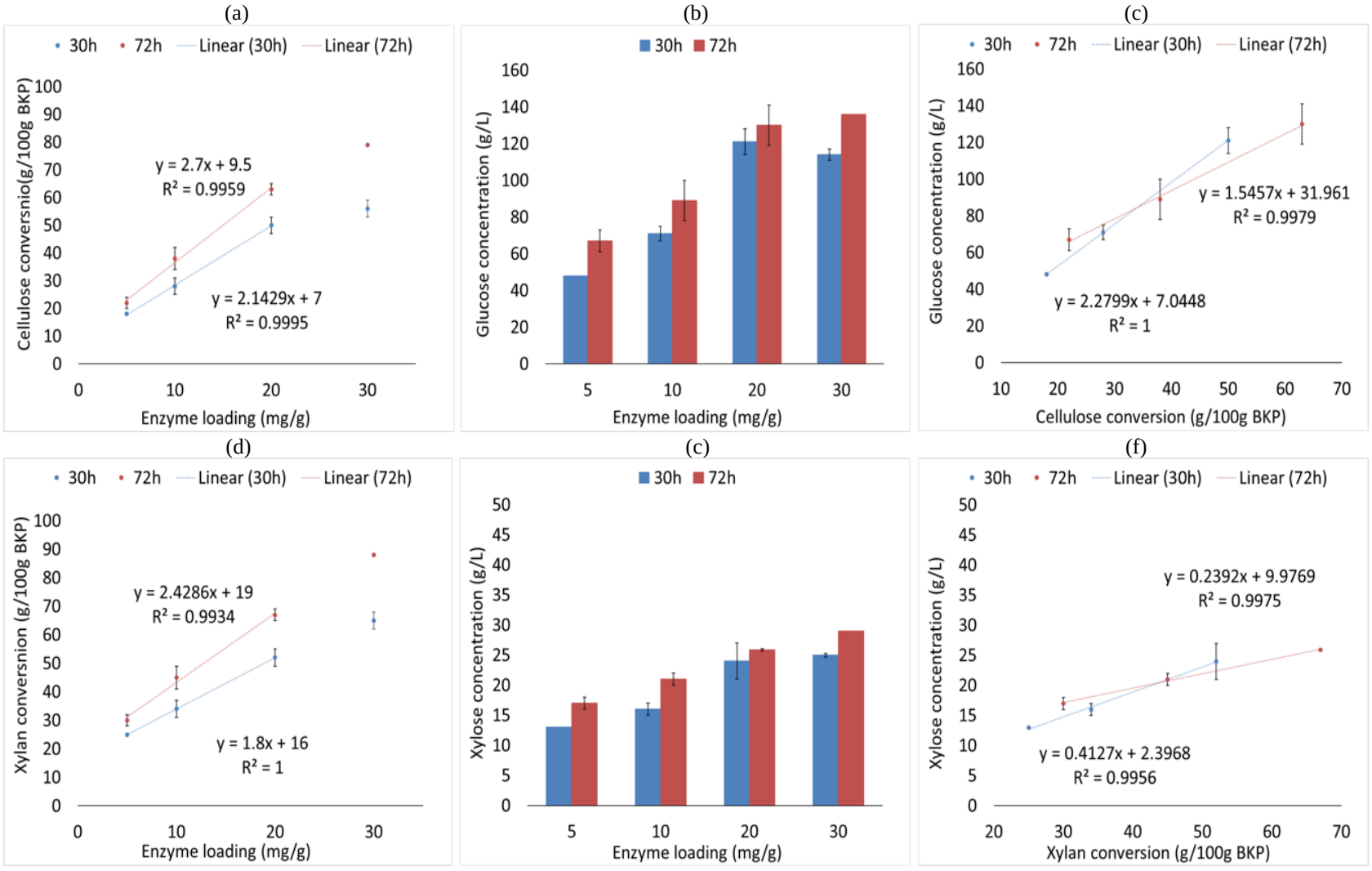

Fig. 10. (a) Cellulose conversion and (b) Glucose concentration obtained for each enzymatic hydrolysis treatment, (c) Correlation between cellulose conversion and glucose concentration, (d) Xylan conversion and (e) Xylose concentration for each enzymatic hydrolysis treatment, (f) Correlation between xylan conversion and xylose concentration.

glucose concentration (84 $g.L^{-1}$). A cost analysis would be necessary to assess the tradeoffs of increasing enzyme loading or time to achieve a higher sugar concentration and reveal best economical condition.

To further understand the effect of cellulose conversion of a commercial enzyme cocktail on CNC yield, the CSR generated within a wider range of cellulose conversions (18 – 79%) was submitted to centrifugation (rotation range of 398 to 1103×g) to recover CNC. The cellulose conversion was used as an indicator of the enzymatic hydrolysis severity to isolate CNC and the rotation speed was a parameter that represents the ability to recover the CNC to build a mathematical model that explains the isolation and recovery of CNC. A second-order quadratic polynomial model (Eq. 5) was obtained using terms considered statistically significant and important for the prediction ability. The regression equation (Eq. 5) shows that the main effect for cellulose conversion is bigger than the main effect of rotation speed for both linear and quadratic terms. The fact that the interactive effect between cellulose conversion and rotation speed (term AB) was not statistically significant indicates that a change on the one parameter level do not produce a differentiate (synergistic) response (CNC yield).

The response surface plot generated from the regression equation (Eq. 5) is shown on Figure 11a and it explains the CNC yield response using the cellulose conversion (non-codified parameter: A), rotation speed (non-codified parameter: B), and their quadratic terms. The response surface shows that higher CNC yield response is obtained for high levels of cellulose conversion and lower levels of rotation speed, which is represented by the dark blue region on the surface. To a practical point of view, the response surface suggests that CNC yield is majorly influenced by the isolation method than the recovery procedure, because a change in the cellulose conversion has greater effect in the CNC yield than a change in the rotation speed. This fact highlights the importance of investigating suitable enzyme cocktails for CNC isolation combined to pre-treatments that can enhance the CNC yield.

(a)

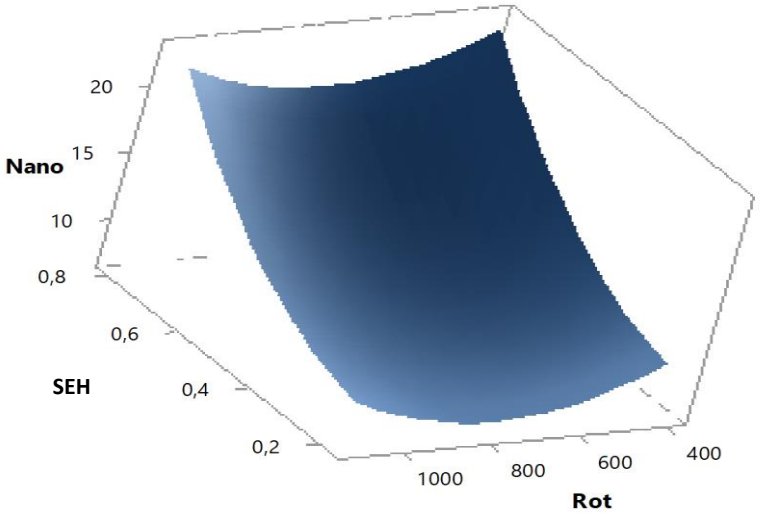

Regression Equation:

CNC yield = 20,39 - 4,5 SEH - 0,0341 Rot + 25,3 SEH^2+ 0,000022 Rot^2 (Eq.5)

where SEH is the Severity of Enzymatic Hydrolysis in terms cellulose conversion (g/g pulp), Rot is the rotation speed (398 – 1103 ×*g*), and Nano is the CNC yield (g/100 CSR)

Summary of the model:

S	R^2	R^2(aj)	R^2(pred)
1,89930	80,64%	75,54%	60,75%

where S, R^2, R^2(adj), R^2(pred) are indicators of the fitting quality and model prediction.

(b)

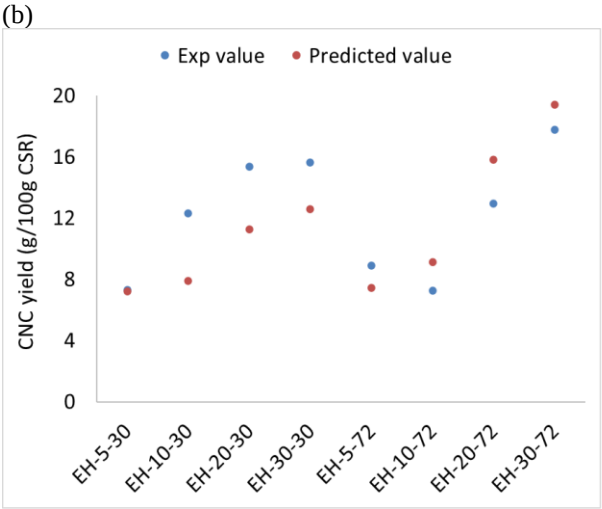

(c)

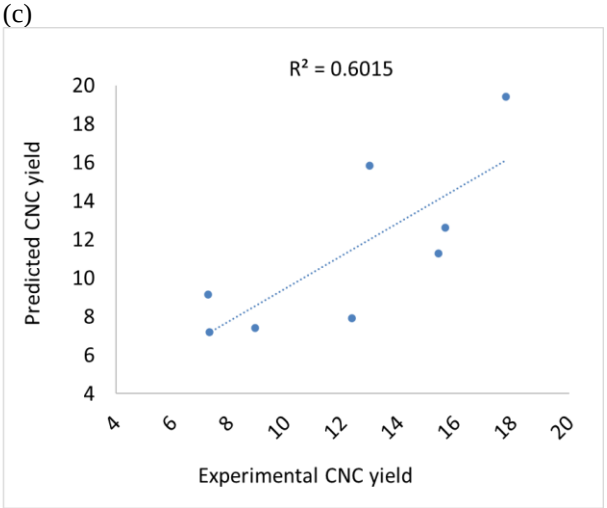

Fig. 11. (a) Response surface for the optimization of the CNC yield (g/100 CSR) for parameter A (cellulose conversion) and parameter B (rotation speed) (b) Real and predicted values for CNC yield (c) Level of adjustment for experimental and predicted CNC yield.

The prediction power of the model was found to be intermediate with R^2 of 80.64% and predicted R^2 of 60.75% (Figure 11b and 11c) and the CNC yield (CSR basis) was in the range of 7.3 - 17.8 g/100g of CSR. A limitation of the centrifugation procedure was noticed by reducing the rotation speed to the lower level (lower than 500×*g*) where it is possible to lose separation resolution and recover large particles than desired (at micrometer scale) (data not shown), which would artificially increase the CNC yield. Thus, especially at low rotation speed, more errors could be incurred to the model's ability of prediction of the CNC yield. Therefore, the rotation speed was set to 750 ×*g* for the validation experiments.

The validation experiments comprehended data produced to build the model and independently of the model. The results shown on Figure 11b suggest that the model is underestimating the CNC yield for conditions with reaction time of 30h and overestimating the CNC yield for conditions with reaction time of 72h. The errors of the model appear to become higher for conditions with cellulose conversion higher than 28% (conditions with enzyme loading of 10 $mg.g^{-1}$). Another potential source of errors for the model possibly comes from the gravimetry analysis for a very dilute CNC suspension (solids content < 0.5%). The solids content of CNC suspensions obtained by gravimetry was conducted with 20-mL samples added to ceramic crucibles and submitted to oven dry at 105^{o}C were compared with the solid content results obtained from IR moisture analyzer, revealing a measurement difference in the range of 1 - 31%.

Enzyme preparations that target the complete saccharification of cellulose-rich substrates, such as the Cellic CTec2 cocktail, produce a slurry-like material with the extent of the reaction, which consists of a mixture of particles at a wider range of sizes and morphologies due to the depolymerization the carbohydrates' fibrillar structure. However, evidence of CNC isolation and recovery was capture by AFM images shown on Figure 12a and 12b for cellulose

conversion of the 28% and 63%, respectively. Measurements of the particle's heigh correlate with the nanocellulose's diameter by AFM (Mattos *et al.*, 2019).

(a)

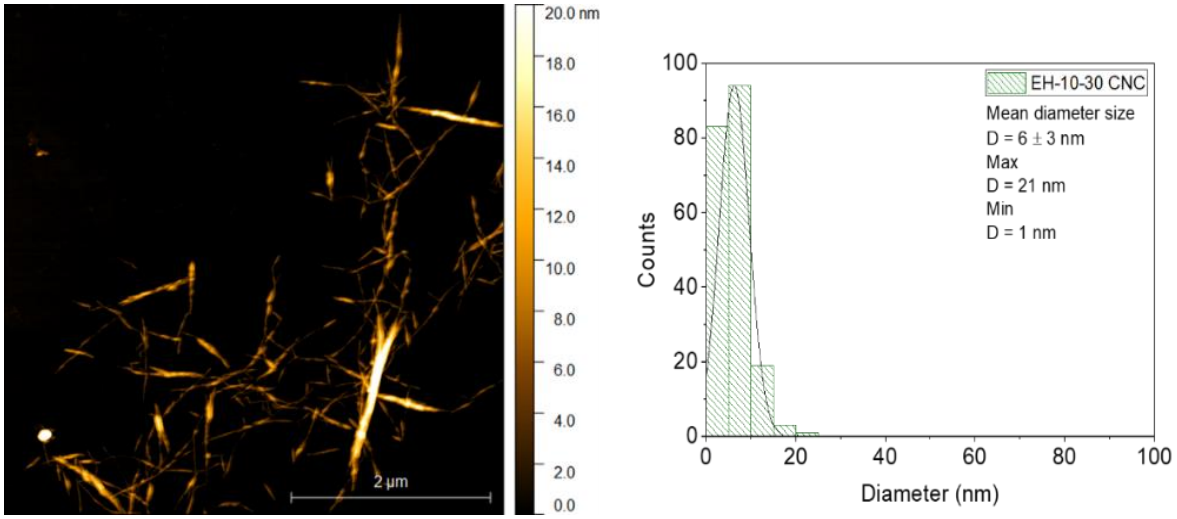

(b)

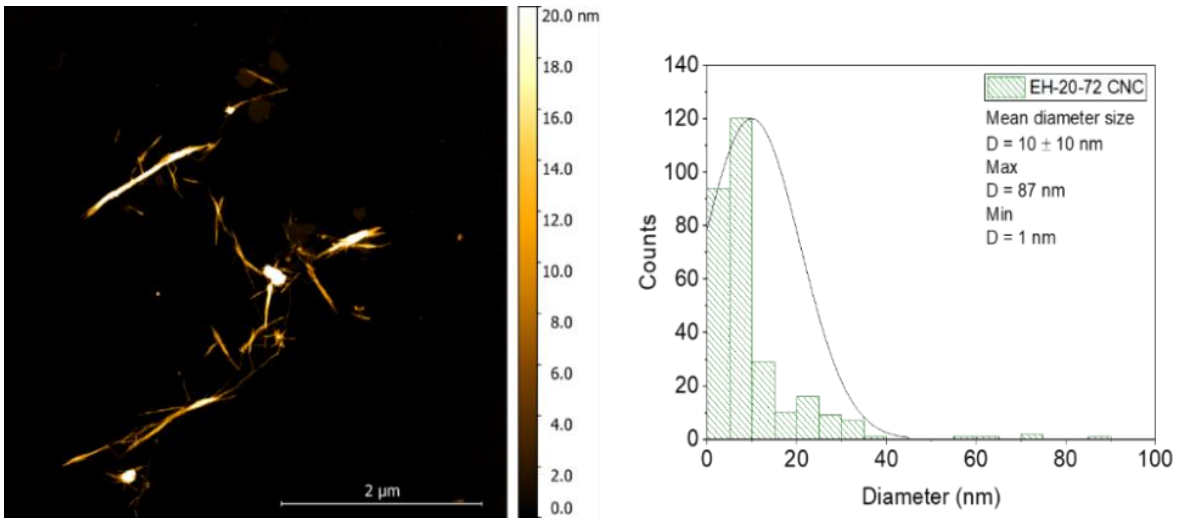

Fig. 12. AFM topographies and diameter distribution of CNC obtained from suspensions recovered at rotation speed 750 ×*g* and isolated after (a) cellulose conversion of 28% (EH-10-30) and (b) cellulose conversion of 63% (EH-20-72). Scale bar shows 2 µm.

The results obtained with the AFM analysis (Figure 12) corroborate to the fact that enzymatic-CNC present high uniformity (Arantes *et al.*, 2020). It was expected that CNC with uniform size would be obtained only at longer reaction times due to a more severe depolymerization and the processivity characteristic of Cellic CTec2 enzymatic cocktail

(Bondancia *et al.*, 2022, 2017). However, the results point to the contrary. Higher uniformity was observed for cellulose conversion of 28% (EH-10-30) and higher polydispersity was observed for cellulose conversion of 63% (EH-20-72), demonstrating that the centrifugation procedure might not have size resolution as selective to CNC compared to golden nanoparticles as pointed by Bonnacorso *et al.* (2013) possibly due to CNC have more diverse morphologies and not spherical as the separation based on density difference assumes. When comparing the diameter distribution, it is observed that both conditions produce similar mean diameter size, however the condition of lower cellulose conversion leads to a more homogeneous diameter size distribution (89% of diameter size up to 10 nm with maximum diameter size of 21 nm) while the condition of higher cellulose conversion leads to a wider diameter size range (87% at diameter size up to 20 nm with maximum diameter size of 87 nm), pointing to greater depolymerization and fiber fragmentation of the material with the extension of enzymatic hydrolysis.

Although the CNC yield (CSR basis) was chosen as an efficiency indicator of CNC recovery to investigate the centrifugation procedure, it is important to consider the overall yield, that is CNC yield (HBKP basis). Figure 13 shows the results for CNC yield (CSR basis) and CNC yield (HBKP basis). The CNC yield (HBKP basis) is in the range of 4.4 - 8.7 g/100g of HBKP and the total sugars concentration is in the range of 61 - 165 $g.L^{-1}$. It was noted that CNC yield obtained present similar range as reported in the literature (approximately 10g/100g of HBKP) (Yang *et al.*, 2023; Yarbrough *et al.*, 2017). Filson *et al.*, (2009) reported higher yields using recycled pulp (20 - 35 g/100g). Therefore, the low CNC yield was already expected. The CNC yield (HBKP basis) does not follow the same pattern as CNC yield (CSR basis) (Figure 13). By enhancing the severity of the enzymatic hydrolysis (higher enzyme loading and reaction time), a higher depolymerization and fragmentation of the cellulose fiber

occur due to the characteristics of enzyme preparation (total saccharification), and sugar is produced as a consequence of higher fragmentation.

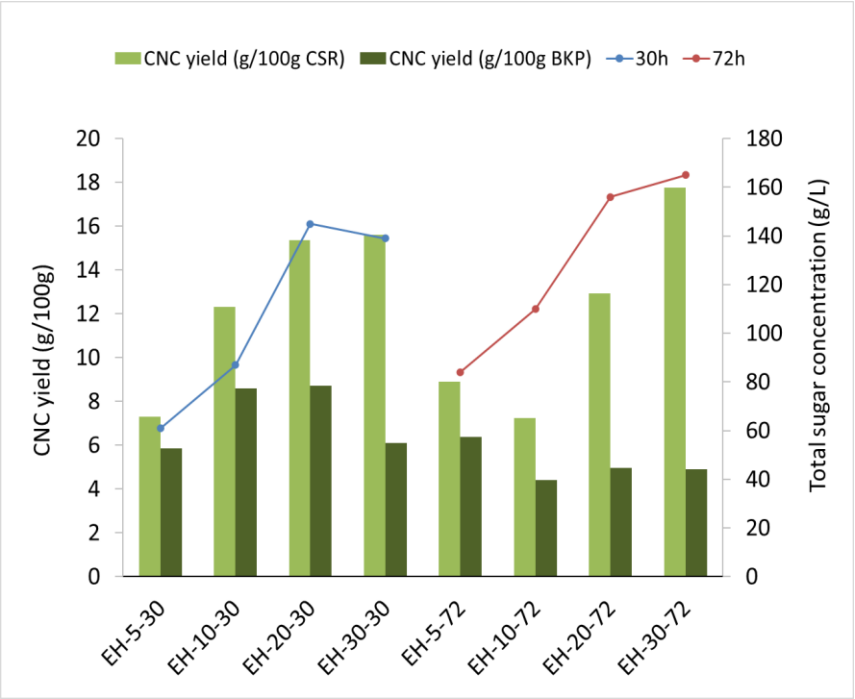

Fig. 13. CNC yield on CSR basis and HBKP basis for each enzyme hydrolysis treatment.

The CNC isolation by the commercial cocktail Cellic CTec2 seems to occur in two patterns:

1) Sugar is produced at a slower rate than CNC is isolated, and hence the fibers fragmentation leads to a higher amount of CNC isolated.

2) Sugar is produced at a higher rate than CNC is isolated, and hence the fibers fragmentation leads to a higher sugar concentration.

Even though there is an initial increase of the CNC yield (CSR basis) with the increase of enzyme loading, the CNC yield does not further increase with higher enzyme loadings or longer reaction time, appearing to be constant with severe enzyme hydrolysis conditions. Thus, it is likely that the CNC precursor fragments isolated during the reaction are degraded to monomeric sugars even though it presents high crystallinity. Zhu *et al.* (2011) employed a low loading of commercial cocktail of cellulases for complete saccharification for hydrolysis of

HBKP and reported that enzyme preparation could not only cause size reduction of long fibers, but also of short fibers and small particles. It is known that 10 – 20% of cellulose is highly recalcitrant and difficult to hydrolyze even with high enzyme loading and long reaction time (Arantes *et al.*, 2014; Arantes and Saddler, 2011; Park *et al.*, 2007).

The comparison of the yields shows that optimizing the CNC yield based only on the centrifugation operation could lead to a misinterpretation of the best condition to obtain higher CNC yield. Based on these results, it can be suggested that the most attractive enzymatic hydrolysis conditions to isolate CNC are the reactions conducted for a shorter reaction time (30 h). The conditions HE-10-30 and HE-20-30 with CNC yield (HBKP basis) of 8.6g/100g and 8.7g/100g, respectively, presented greater CNC yields and produce high total sugar concentrations (87g.L^{-1} and 145 g.L^{-1}, respectively) and while same enzyme loadings at 72h of reaction that produced CNC yield (HBKP basis) in the range of 4 – 5 g/100g and total sugar concentration of 110 - 156 g.L^{-1}.

6.5 Observations regarding the CNC recovery – opportunities for cost reduction

The separation based on density difference assumes that particles of different sizes will stay in an equilibrium position according to the *g*-force applied (Bonaccorso *et al.*, 2013) as illustrated on Figure 14a. Because the CNC suspension contains a range of particles' size and morphologies, multiple centrifugation steps are necessary to recover CNC from CSR. During the recovery of the CNC suspensions, it was observed that there is a maximum absorbance peak at wavelength of 600 nm shown on Figure 14c. Subsequently, the absorbance decreases, and the following fractions of CNC suspension recovered turn to be extremely diluted, contributing to the dilution of the final suspension (solids content < 0.5%), which contains the volume of all each step gathered. Figure 14b and 14d show CNC suspension samples recovered after each centrifugation step for two enzymatic hydrolysis conditions, EH-10-30 and EH-20-72, with cellulose conversion of 28% and 63%, respectively, used for absorbance analysis. It can also

be observed the turbid appearance from condition EH-20-72, pointing to a high CNC initial concentration than for the condition EH-10-30. This suggests that larger particles may carry nano-size particles during the centrifugation, which point that this operation might not be as selective for the solid's consistency employed. From the absorbance profile shown on figure 14c, it can be observed that a reduction of centrifugation steps from #6 steps to #4 steps could recover a considerable amount of the CNC without diluting the final suspension too much. Reducing the number of centrifugation steps as proposed would generate a reduction of about 30% in water volume usage when compared to the total CNC recovery until no turbidity is present (centrifugation step#6 or more).

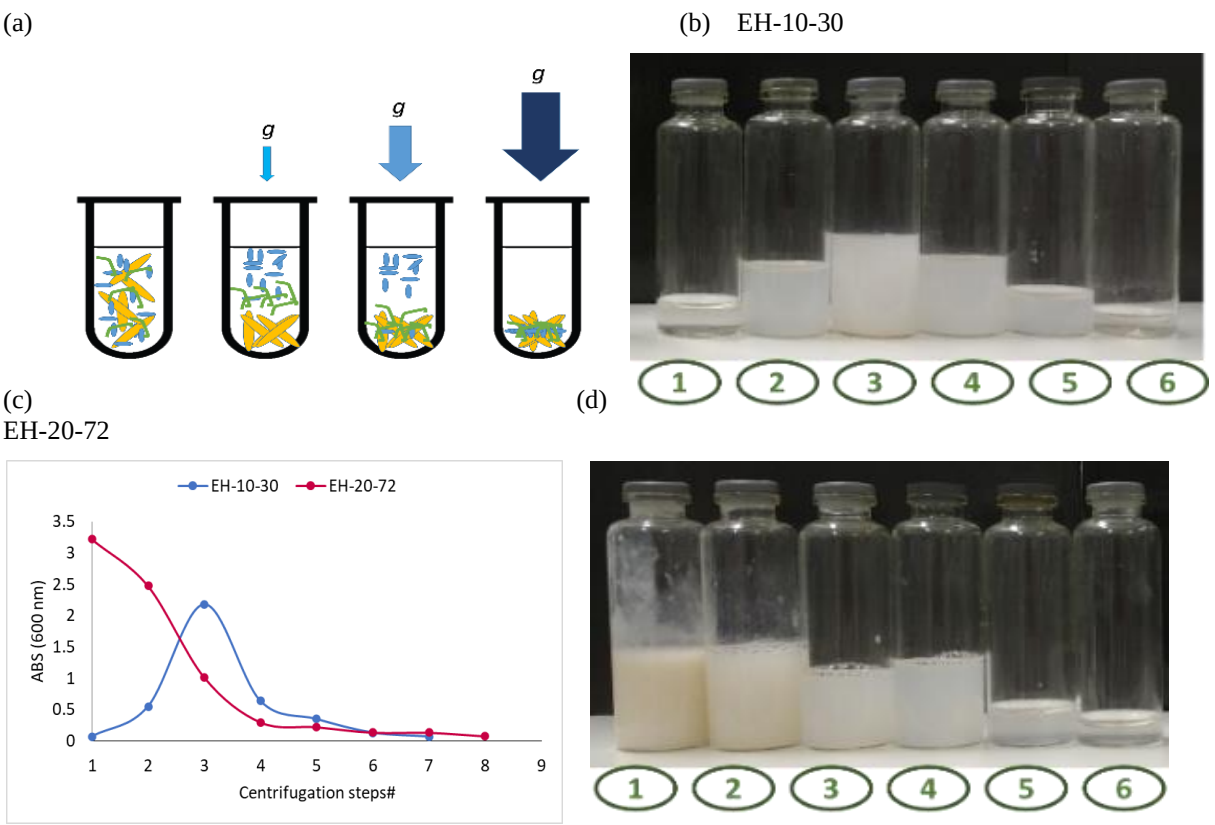

Numbers #1-6 refer to the number of centrifugation steps and the order recovery

Fig. 14. (a) Illustration of *g*-force effect in recovery particles with of different size and morphologies; (b) Illustration of CNC suspensions recovered by centrifugation for enzyme hydrolysis condition EH-10-30; (c) Absorbance profile (600 nm) for CNC suspensions recovered after each centrifugation step; (d) Illustration of CNC suspensions recovered by centrifugation for enzyme hydrolysis condition EH-10-30

6.6 Conclusion

The yield of CNC isolated via enzyme-assisted treatment was investigated and optimized, exploring different degrees of cellulose conversion using the enzymatic cocktail Cellic CTec2. According to our results, the CNC yield is dependent on the mode of action of the enzyme cocktail. For a full saccharification enzymatic cocktail such as Cellic CTec2, depolymerization pattern seems to occur in two main steps: one step in which the fragmentation predominates and a second step in which the production of sugars is prominent. This depolymerization pattern was the reason for CNC yield to be low (4.4 - 8.7 g/100g of HBKP), whereas high titers of sugars were obtained (total sugars concentration in the range of 61 - 165 $g.L^{-1}$).

Although the CNC yield was not significatively improved with the optimization study, alternatives to reduce the operational expenses (OPEX) and capital expenditure (CAPEX) were demonstrated. The use of tap water as a diluent for CNC suspensions did not affect the CNC yield when CNC was isolated by centrifugation. Hence, the substitution of osmose reverse water by tap water could be an economical choice to reduce the OPEX. Once high purity water is not needed, so it is not a water purification system, hence the projected CAPEX may be reduced as well. Moreover, the use of ambient temperature and low-speed centrifugation are options that may reduce the OPEX as well as the reduction of the number of centrifugation steps to recover enzymatic-CNC.

CHAPTER 7 FEASIBILITY ANALYSIS OF THE COPRODUCTION OF CNC, CNF, AND CELLULOSIC SUGARS FROM BLEACHED KRAFT PULP USING AN ENZYMATIC-MECHANICAL APPROACH

7.1 Introduction

Mechanical ultrafibrillation by disc ultra-refiner is a promising alternative to produce CNF with high yield with high potential to achieve large-scale production of CNF (Hu *et al.*, 2015; Wang and Zhu, 2016). However, the setbacks for ultra-refining are the high-energy demand and long refining period (personal communication PDC; Amini *et al* 2020). An alternative to reduce the energy consumption during the CNF isolation is the use of enzymatic pre-treatment, which promotes the amorphogenesis of the fibrillar structure of cellulose and hence facilitates the isolation of CNF in a less energy-intensive manner (Berto *et al.*, 2021; Xiuyu Liu *et al.*, 2019; Zhou *et al.*, 2019; Zhu *et al.*, 2011). Most studies that focus on the enzyme-mediated ultra-refining process employ monocomponent cocktails of endoglucanases or endoxylanases at varied enzyme loadings (0.5 - 3% g/g cellulose). Energy savings can be achieved up to 60% with low or none sugar production (Xiuyu Liu *et al.*, 2019; Wang *et al.*, 2015).

Here, we investigate the feasibility of isolating CNF from CSR recovered after an enzymatic pretreatment, exploring different degrees of cellulose conversion by using an enzyme cocktail that targets complete saccharification of lignocellulosic fibers (Cellic CTec2). We explore a process model that integrates the production of CNF, CNC, and sugars at high titers. Thus, we investigated similar enzyme loadings reported to the literature for single-component enzyme cocktails although we expect higher degree of cellulose conversion and carbohydrates depolymerization due to the characteristics of the enzyme cocktail employed. The commercial cocktail Cellic CTec 2 is a complex cellulolytic preparation able to cause dramatic changes in the fiber promoting complete depolymerization of the ultrastructure of

polysaccharides into monomeric sugars. The macroscopic changes of the fibers promoted by high carbohydrate saccharification cocktails are generally connected to the diversity of families of carbohydrate active enzymes (CAZymes) and their activity. The disruption of less-crystalline regions is a typical effect of endoglucanases, which promotes drastic fiber fragmentation by the cutting effect (Payne *et al.*, 2015). The collapse of the cellulose's crystalline regions is a typical effect of cellobiohydrolases, which forms cellobiose. Moreover, accessory enzymes can act directly or indirectly in the cellulose depolymerization, forming oxidized compounds and making new sites of cellulose available for depolymerization (Dimarogona *et al.*, 2012; Horn *et al.*, 2012). A rich β-glycosidases activity confers cellobiose breakdown into glucose, which prevents cellobiose accumulation and cellobiohydrolases' inhibition (Payne *et al.*, 2015). The enzymatic depolymerization of the fiber's most superficial xylan is an effect of endoxylanases, that, together with xylosidases, promote the exposure of fibers and making new sites of cellulose available for depolymerization (Glass *et al.*, 2013).

The objective of this chapter is to establish the mass balance for an integrated process to produce CNC, CNF, and high-titer of sugars from bleached Kraft pulp and investigate the impact of the severity of enzymatic hydrolysis on the ultra-refining for CNF production.

7.2 The effect of different degrees of cellulose conversion on CSR

The CSR obtained from each enzymatic hydrolysis condition was studied in terms of chemical composition to explore the different degrees of cellulose conversion and wet-SSA, which refers to the specific surface area (SSA) value obtained by an algorithm approximation based on the hydrodynamic particle diameter. CSR materials were obtained with yields varying from 80 % to 28% (HBKP basis) after being treated by the commercial cocktail Cellic CTec2 using with different combination of enzyme loadings (5, 10, 20, and 30 $mg.g^{-1}$) and reaction time (30h and 72h). These enzymatic treatments promoted cellulose conversion ranging from 18% to 79% and xylan conversion ranging from 25% to 88%. Due to carbohydrates

depolymerization, the enzymatic treatments also affected surface area and hence particle size. Figure 15 correlates the polysaccharides conversion and yield with the wet-SSA for each enzymatic treatment. The typical CNF wet-SSA value is equal or greater than 200 m^2/kg (Berto and Arantes, 2019). The wet-SSA ranged from 323.9 $m^2.kg^{-1}$ to 557.2 $m^2.kg^{-1}$ and an exponential trend was obtained between wet-SSA and carbohydrates conversion (cellulose and xylan) (Figure 15a). The increase of the wet-SSA with extend of cellulose conversion was expected due to the highly active cellulases (cellobiohydrolases and endoglucanases) present in the enzyme preparation, which promotes a reduction of the fiber length by "fiber cutting"/fragmentation and a reduction of fiber width by "peeling off" of the fiber layers, leading to an increase of the surface area as consequence of a reduction of the particle size (Arantes *et al.*, 2014; Park *et al.*, 2007; Zhu *et al.*, 2011). The increase of wet-SSA with the xylan removal was expected because it further exposes the fibers by removing portions of xylan that covers the cellulose, which can favor nanocellulose isolation (Long *et al.*, 2017; Penttilä *et al.*, 2013). Figure 15b shows a polynomial trend between wet-SSA and CSR yield. The trend reveals a useful relationship that correlates the overall depolymerization of polysaccharides represented by the reduction of CSR yield and the fiber size reduction described by the increase of the wet-SSA. Berto and Arantes (2019) reported a wet-SSA value of 130 $m^2.kg^{-1}$ (red triangle) for HBKP without treatment using same measurement technique employed here, which can be considered as a reference. A comparison of the reference wet-SSA with the data obtained here shows a gain on surface area ranging from 2.5x to 4.3x when the cellulose conversion varied from 18% to 79%.

Complementary to the wet-SSA results, optical microscopic images were taken of CSR to evaluate the morphologies of the remained fibers after enzymatic treatment (Figure 16). The CSR with lower cellulose conversion presented shortened fibers that became further fragmented in the axial direction with the increase of cellulose conversion, producing fines.

The optical images show both “fiber cutting”/fragmentation as well as “peeling” effect, especially for conditions with cellulose conversion greater than 50%. At enzyme loadings of 5, 10, and 20 $mg.g^{-1}$ (cellulose conversion up to 50%), shorter fibers were clearly visible at 100 µm scale for all reaction times. By increasing reaction time to 72h, the amount shortened fibers further reduced to fines, indicating a predominance of “peeling” effect. The increase of shorter fibers and fine particles with the increase of enzyme loading corroborates with the results obtained for wet-SSA. By increasing the enzyme loading 2x, 4x, and 6x, it leads to a progressive increase in the wet-SSA by 37%, 42%, and 56%, respectively, whereas increasing the reaction time for same each enzyme loading improves the wet-SSA by 20%, 4%, 7%, and 10%, respectively.

The wet-SSA results and macroscopic images fiber resultant after each enzymatic treatment agree with results presented by Arantes *et al.* (2014), who studied the mode of action of Cellic CTec2 for various cellulose-rich pulps prepared by different pretreatments. These authors observed that a rapid shortening of fibers occurs prominently due to fragmentation at the initial stages of enzyme hydrolysis for reaction time up to 6h (cellulose conversion up to 20%). They identified that the “peeling” effect occurs during the entire course of reaction and becomes prominent after the fragmentation effect reaches a “plateau” of macroscopic changes of the fibers. Figure 15c also shows a “plateau” of wet-SSA values observed for cellulose conversion between 30 – 50%. The plateau is illustrated by CSR obtained from conditions EH-20-30 and EH-10-72 shown on Figure 16. Although the CSR materials present similar wet-SSA values and similar morphologies, the cellulose conversion differs (cellulose conversion of 38% and 50%, respectively), which provides evidence of a transition of phases for the macroscopic changes of the fibers. Fiber agglomerations were observed for all conditions investigated. These agglomerations may cause an apparent increase particle width when measured with light diffraction techniques (Arantes *et al.*, 2014; Park *et al.*, 2007).

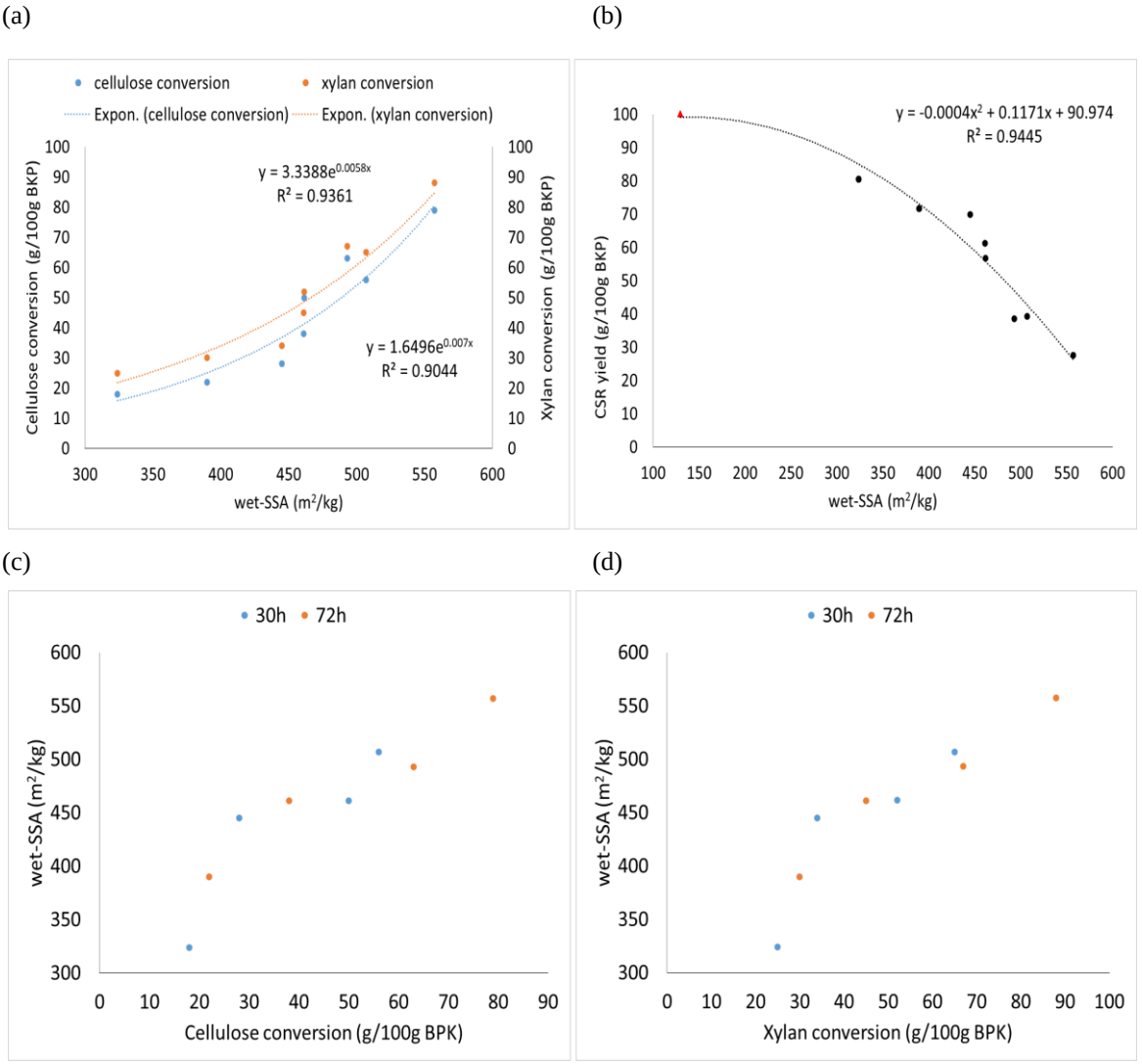

Fig. 15. Relationship between (a) wet specific surface area (wet-SSA) and carbohydrates conversion (b) wet-SSA and CSR yield obtained after each enzyme treatment (c) cellulose conversion and we-SSA (d) xylan conversion and wet-SSA. Red triangle refers to wet-SSA value of 130 $m^2.kg^{-1}$ for HBKP control (Berto and Arantes, 2019)

7.3 The effect of different degrees of cellulose conversion on CNF isolation

The CSR suspensions were prepared with tap water to a consistency of 1.5%(w/v) solids to ultra-refine. Even though the CSR suspensions already had high wet-SSA, the suspensions had the tendency to precipitate. Figure 16 shows the micrographs obtained for each of the CSR suspensions (samples never dried), highlighting the morphology of the particles, the cellulose conversion and the wet-SSA value of each sample. The optical micrographs show aggromerated particles which corroborates with the behavior reported for nanocelluloses obtained from enzymatic treatments (Arantes *et al.*, 2020)

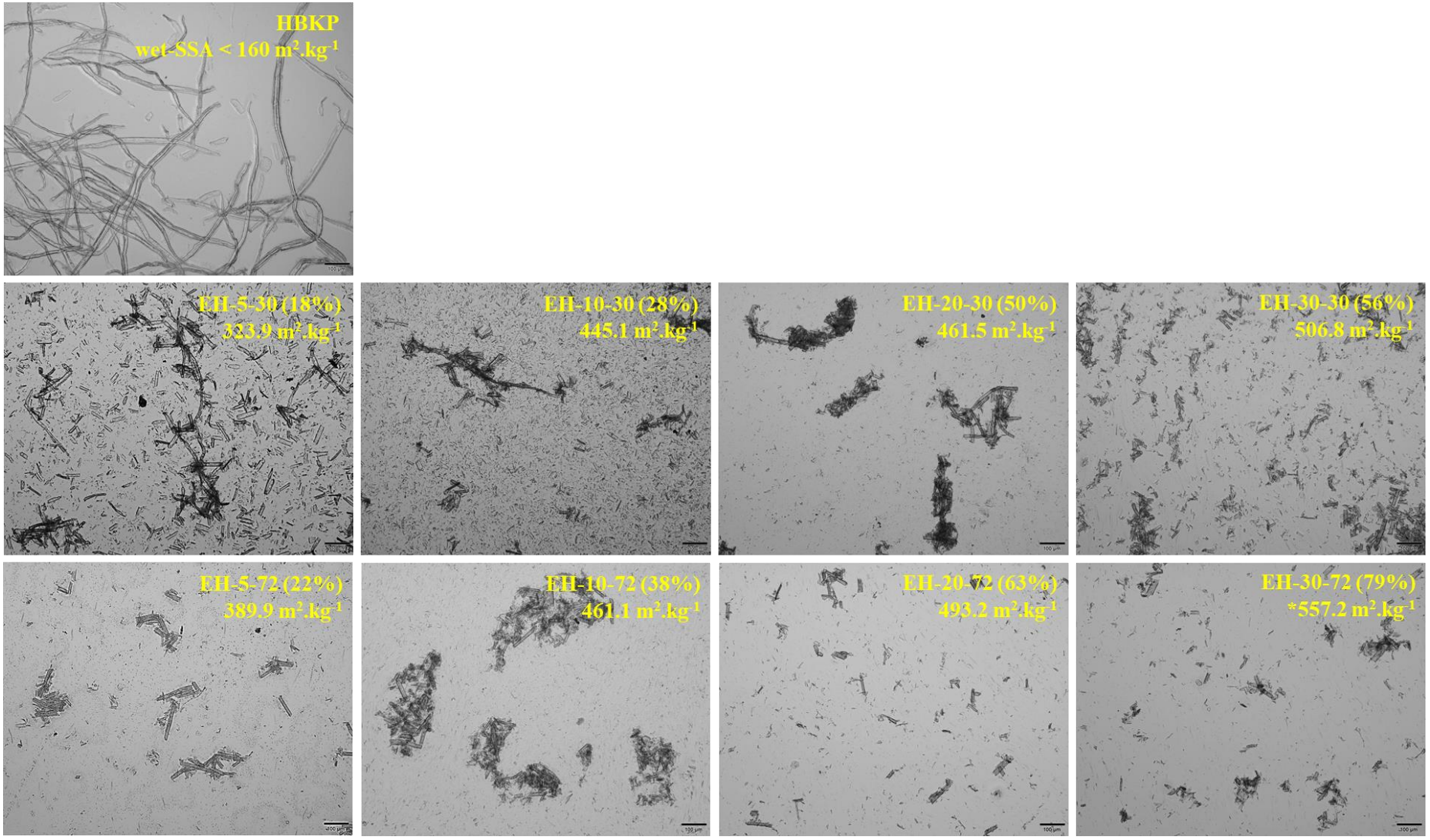

Fig. 16. Microscopic images of CSR after each enzyme treatment, highlighting the enzymatic treatment, cellulose conversion, and the wet-SSA value. Scale bar shows 100 µm. HBKP: Hardwood bleached kraft pulp; *wet-SSA value of 130 $m^2.kg^{-1}$ for HBKP control (Berto and Arantes, 2019); [c] wet-SSA value refers to ultra-refining cycle#1.

The end of ultra-refining process was set by a qualitative aspect of CNF suspensions know as gelation, referred as “gel-like” aspect. The gelation is an indicator of CNF isolation due to the nanocellulose ability of forming thick gels even at low solids concentrations. The formation of gels is explained by the defibrillation process and individualization of the fibers into fibrils, which promotes higher surface area and increase fibril-fibril and fibril-water interactions (Berto and Arantes, 2019; Hu *et al.*, 2015; Malucelli *et al.*, 2018; Pääkko *et al.*, 2007b). The CSR suspensions required a varied number of ultra-refining cycles, summing up 10 to 20 cycles. Table 14 shows a summary of parameters monitored during ultra-refining, such as number of ultra-refining cycles, ultra-refining time, and cumulative energy consumption.

Table 14. Characteristics of CSR suspensions prepared with tap water and parameters monitored during the ultra-refining.

Enzymatic treatment	Cellulose conversion (g/100g HBKP)	CSR wet-SSA ($m^2.kg^{-1}$)	CSR suspension (% solids)	Cycles #	Time (min)	Cumulative energy ($kWh.kg^{-1}$)
EH-5-30	18	323.9	1.5	10	47	16
EH-10-30	28 ± 3	445.1	1.7	15	50	15
EH-20-30	50 ± 3	461.5	1.6	15	65	21
EH-30-30	56 ± 3	506.8	1.4	20	75	23
EH-5-72	22 ± 2	389.9	1.5	10	42	14
EH-10-72	38 ± 4	461.1	1.8	10	55	16
EH-20-72	63 ± 3	493.2	1.7	10	50	16
EH-30-72	79	557.2	1.1	15	68	33

Figure 17 shows the cumulative energy consumption throughout the ultra-refining cycles. It was observed that the cumulative energy consumption for most suspensions occurred at a rate superior to a proportionality line (1 kWh per cycle), except for the conditions EH-10-30 (cellulose conversion of 28%) and EH-30-30 (cellulose conversion of 56%). It is known in that bench-models of the Supermasscolloider ultra-refiner present idle power of 1 kW, which represents the energy consumption necessary to move the disc (Hu *et al.*, 2015; Xiuyu Liu *et al.*, 2019; Wang and Zhu, 2016).

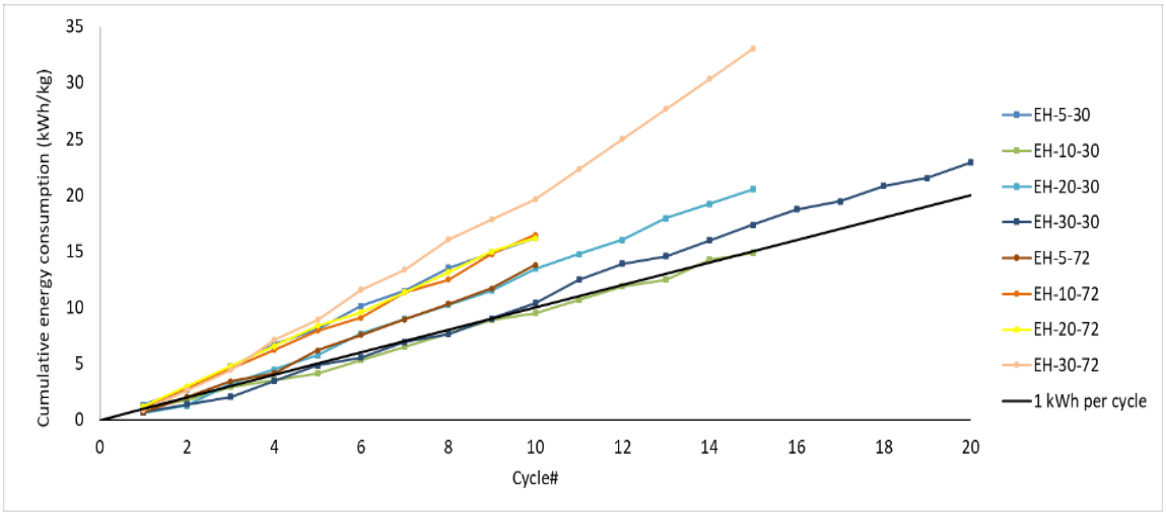

Fig. 17. Energy consumption during ultra-refining of each CSR suspensions (1.5% solids, 1L sample) until the suspensions achieved the "gel-like" aspect.

Figures 18a and 18b show the correlation between cellulosic conversion and the energy consumption required when ultra-refining each CSR suspension prepared. The results show a good fitting for a quadratic trend between the cumulative energy consumption versus cellulose conversion (Figure 18a). The trend suggests that an increase of cellulose conversion produced by the enzymatic treatment with Cellic CTec2 produces cause an increase in the energy demand during the ultra-refining. The trend also suggests that CSR suspensions recovered after cellulose conversion in the range of 20 - 40 % leads to similar energy consumption for CNF isolation. However, when CNF is isolated from CSR with cellulose conversions equal or higher than 50%, it demands higher energy inputs to achieve the desired "gel-like" aspect. The conditions EH-20-30, EH-30-30, and EH-30-72 with cellulose conversion of 50%, 56%, and 79%, respectively, required higher cumulative energy (21 kWh/kg, 23 kWh/kg, and 33 kWh/kg, respectively) as well as higher number of cycles (15, 20, and 15 cycles, respectively). A probable explanation for this is that, at cellulose conversion of 50% or higher, the CSR materials already present high wet-SSA, and, possibly, high crystallinity index (CI) due to the preferential depolymerization of the less crystalline regions of cellulose promoted by the enzymatic treatment. A CSR material with these characteristics would require higher amounts

of energy input to defibrillate the remaining fibers due to higher cellulose recalcitrance represented by the high crystallinity. Bondancia *et al.* (2022) studied the enzymatic hydrolysis of HBKP using the cocktail Cellic CTec2 and showed an increase of CI with the course of reaction, suggesting that a CI of 70% is obtained within 20h when cellulose conversion reaches 50%. Qing *et al* (2013) report that CNF prevenient from extensive enzymatic treatment are CNC-alike, in another words, highly crystalline.

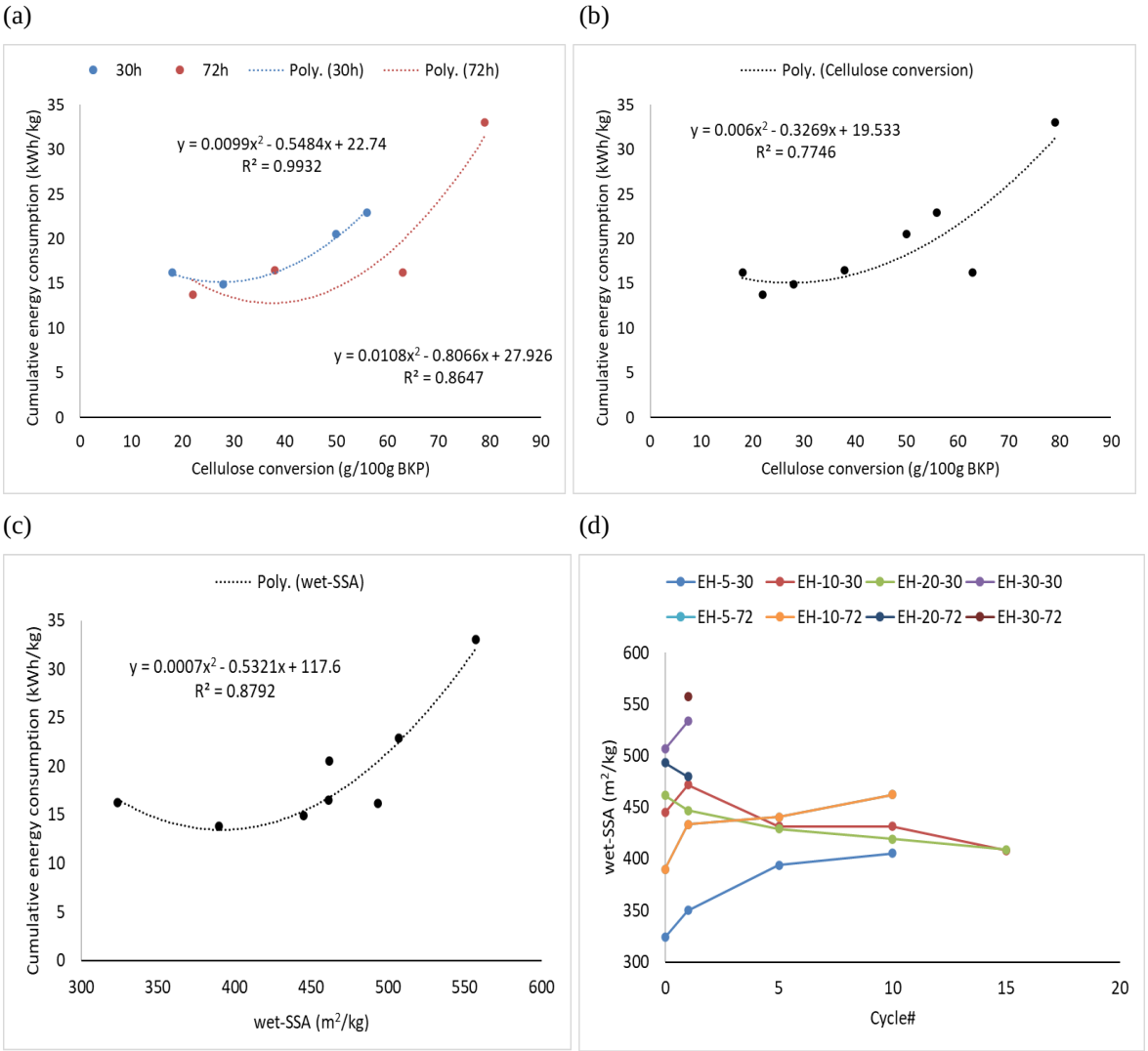

Fig. 18. (a) Relationship between cellulose conversion and cumulative energy consumption highlighting hydrolysis time; (b) Relationship between cellulose conversion and cumulative energy consumption; (c) Relationship between wet-SSA and cumulative energy consumption; (d) Behavior of wet-SSA with sequential cycles of ultra-refining

The trend obtained between wet-SSA and energy input showed a similar pattern to observed for cellulose conversion and energy input. Figure 18c shows the correlation between

wet-SSA and the energy consumption during ultra-refining. The results suggest that a higher energy input is necessary to obtain the "gel-like" aspect when CSR suspensions already had a high wet-SSA value. Thus, the CSR with the highest cellulose conversion (79% cellulose conversion) and highest wet-SSA (557.2 $m^2.kg^{-1}$) was also the suspension that required higher energy input.

Two CNF suspensions were analyzed by AFM (EH-10-30 and EH-20-72 with cellulose conversion of 28% and 63%, respectively) to evaluate the particle size of CNF isolated using the "gel-like" aspect as a reference for the ultra-refining. Figure 19 shows AFM topographic images and diameter distribution.

(a)

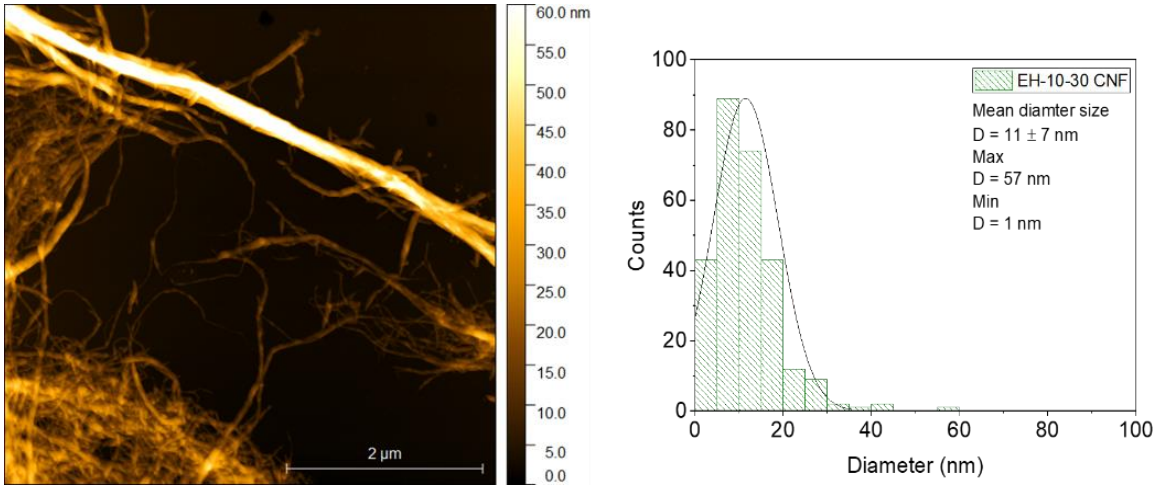

(b)

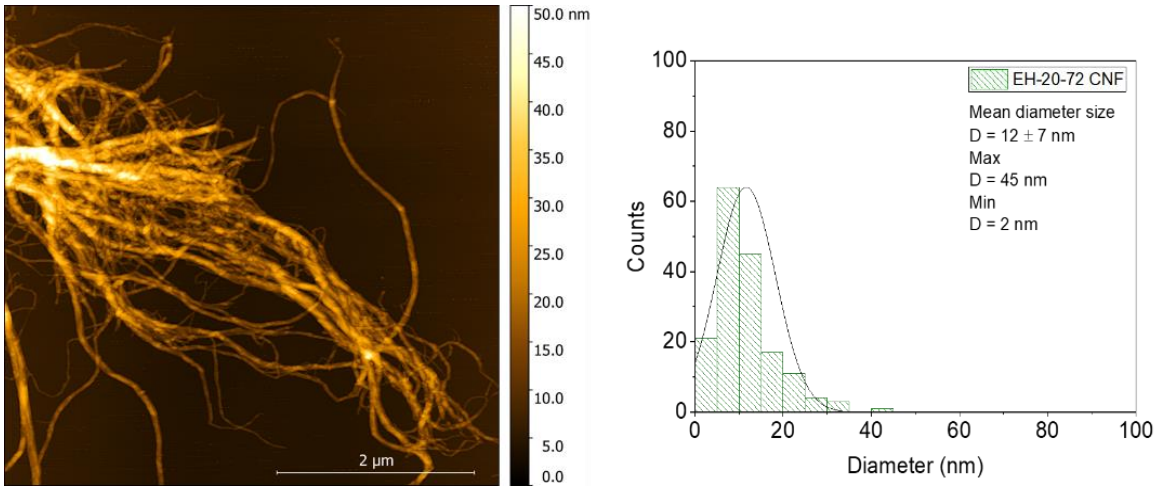

Fig. 19. AFM topographies and diameter distribution of CNF obtained from suspensions isolated by ultra-refining after (a) cellulose conversion of 28% (EH-10-30) and (b) cellulose conversion of 63% (EH-20-72). Scale bar shows 2 µm.

The shear viscosity of the CNF suspensions was investigated along the ultra-refining cycles to study how the gelation behavior occurs during the ultra-refining process preceded by enzymatic treatment. Table 15 shows a summary of the characteristics of the CNF suspensions for each enzymatic treatment (chemical composition and initial wet-SSA), shear viscosity measurements before and after the ultra-refining process (apparent viscosity and torque), and the cumulative energy necessary to achieve the "gel-like" aspect. The shear viscosity of the CNF suspensions varied between 3.4 – 9.7 cP, represented by the cellulose conversion of 28% (EH-10-30) and 18% (EH-5-30) respectively. The shear viscosity measurements showed that the ultra-refining steps promoted an averaged viscosity gain of 4 times the initial viscosity for the CNF suspensions, with exception for the condition with lower cellulose conversion that presented a viscosity gain 7 times higher than the initial viscosity. Although the shear viscosity increased after the ultra-refining steps, most of the CNF suspensions with enzymatic treatment had a viscosity measurement similar to the shear viscosity of HBKP without treatment prior to ultra-grading (3 cP). The CNFs suspensions with enzymatic treatment had viscosity about 5 times lower than BKP after ultra-refining (27 cP).

Table 15. Characteristics of CNF suspension for each enzymatic treatment, shear viscosity measurement before and after the ultra-refining process, and the cumulative energy necessary to achieve the "gel-like" aspect.

Enzymatic treatment	**Cellulose conversion** (g/100g HBKP)	**Xylan conversion** (g/100g HBKP)	**Initial wet-SSA** ($m^2.kg^{-1}$)	**Initial Viscosity** (cP)	**Final Viscosity** (cP)	**Torque** (%)	**Cumulative Energy** ($kWh.kg^{-1}$)
BKP	0	0	130*	3*	27*	-	30*
EH-5-30	18	25	324	1.3	9.7	64.5	16
EH-10-30	28 ± 3	34 ± 4	445	1.1	3.4	22.9	15
EH-20-30	50 ± 3	52 ± 5	462	1.4	4.7	31.2	21
EH-30-30	56 ± 3	65 ± 3	507	1.2	4.4	29.2	23
EH-5-72	22 ± 2	30 ± 3	390	1.2	5.9	39.7	14
EH-10-72	38 ± 4	45 ± 5	461	1.6	7.3	48.4	16
EH-20-72	63 ± 3	67 ± 3	493	1.2	4.6	30.9	16
EH-30-72	79	88	557	1.4[C]	5.3	35.2	33

Viscosity data and torque were collected for spindle rotation at 200 rpm (shear rate 264 s^{-1}).
*Values obtained from Berto and Arantes (2019) and Berto, Mattos, Rojas, and Arantes (2021) for HBKP ultra-grading without treatment.
[c] Value refers to viscosity measurement after one ultra-refining cycle.

By monitoring the shear viscosity gain over the ultra-refining cycles, it was observed that the viscosity gain was not linear neither in relation to the number of cycles, nor in relation to the energy input. The viscosity gain increased more expressively along the cycles especially for materials with lower cellulose conversion. Figure 20 shows that CNF obtained from the hydrolysis conditions EH-5-30 and EH-10-72 presented the highest viscosity gain with the lowest energy input. On the other hand, the materials resulting from high cellulose conversion (hydrolysis conditions EH-30-30 and EH-30-72) presented the smallest viscosity gain with the highest energy demands to achieve the "gel-like" aspect. These results point to the fact that particle-particle interactions and entanglement seems to be occurring easily for the conditions with low cellulose conversion (conditions EH-5-30 and EH-10-72 with cellulose conversion of 18% and 22%, respectively). Conversely, materials with higher polysaccharide depolymerization, containing a more fragmented structure, would require greater energy input to achieve a similar viscous aspect or the complete loss of the property (Henríquez-Gallegos *et al.*, 2021). Because the viscosity gain is an incremental process, visual observation of the suspensions indicated the gelation started approximately at a shear viscosity of 4 cP for most conditions, which can be useful to define quantitatively the "gel-like" aspect (data not shown).

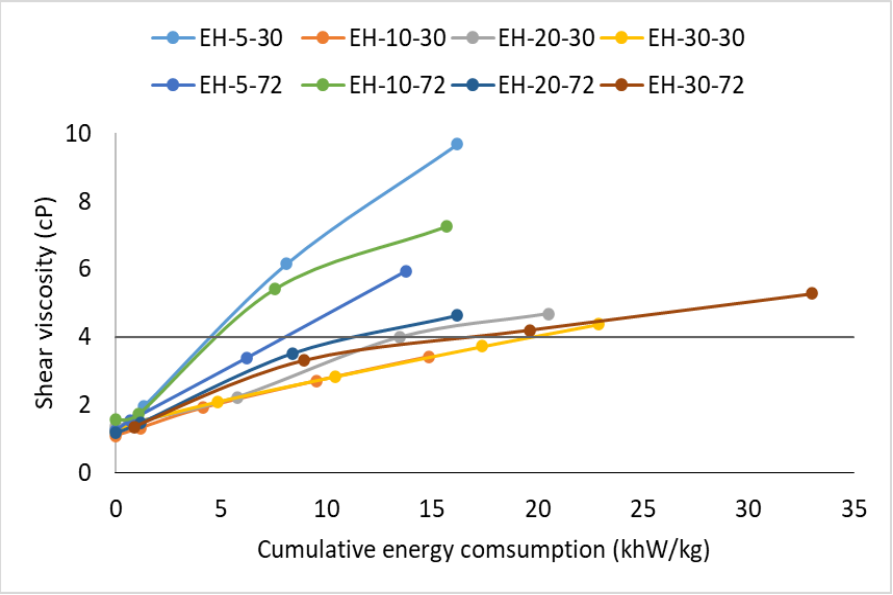

Fig. 20. Shear viscosity versus the cumulative energy during ultra-refining of each CNF suspension. Straight line at shear viscosity of 4 cP refers to beginning of gel-like consistency.

An energy consumption range of 25 – 30 kWh.kg^{-1} is typically reported for CNF isolation from Kraft pulp without pre-treatment (Berto and Arantes, 2019; Hu *et al.*, 2015; Malucelli *et al.*, 2018; Wang and Zhu, 2016). Berto and Arantes (2018) employed the same Supermasscolloider model and suspension volume and obtained CNF diameters in the range of 2 – 64 nm (mean diameter 21 nm) with a cumulative energy consumption of 20 kWh.kg^{-1} although their wet-SSA was approximately 200 m^2.kg^{-1}. By employing 25 kWh.kg^{-1}, they obtain CNF with mean diameter 9.4 nm and wet-SSA values 263 m^2.kg^{-1} and, with 30 kWh.kg^{-1}, a mean diameter 8.6 nm and wet-SSA values 450 m^2.kg^{-1}. Considering an average energy consumption of 25 kWh.kg^{-1} as a reference for ultra-refining HBKP without treatment, Table 16 highlights the potential for reduction of energy expenditure when employing each enzymatic treatment prior to the ultra-refining. The results for energy savings were obtained by comparing the energy consumption required to obtain a viscosity of 4 cP (beginning of gelation) for each condition with the reference.

Table 16. Potential of energy savings during ultra-refining process for the isolation of CNF (shear viscosity 4 cP) based on the highest cumulative energy.

Enzymatic treatment	**Cellulose conversion (g/100g HBKP)**	**Shear Viscosity*** **(cP)**	**Cumulative energy (kWh.kg^{-1})**	**Energy savings (%)**	**Energy savings^R (%)**
EH-5-30	18	4	5	78	80
EH-10-30	28 ± 3	3	15	35	20
EH-20-30	50 ± 3	5	21	9	16
EH-30-30	56 ± 3	4	23	0	8
EH-5-72	22 ± 2	3	6	74	76
EH-10-72	38 ± 4	5	8	65	68
EH-20-72	63 ± 3	4	8	65	68
EH-30-72	79	4	20	13	20

*Data for shear viscosity was collected using the spindle rotation at 200 rpm (shear rate 264 s-1).
^{R}Reference of energy consumption of 25 kWh.kg^{-1} for CNF isolation from HBKP without treatment.

The cumulative energy necessary to isolate CNF for conditions with high cellulose conversion were as high as the reference without treatment. However, for conditions with low cellulose conversion the potential of energy reduction is up to 80% compared to the reference.

This potential reduction is much higher compared to data available in the literature. The Cellic CTec2 cocktail pretreatment used here also achieved superior energy savings when compared to the reported values for enzymatic treatment with monocomponent endoglucanases. Wang *et al.* (2015) obtained a reduction of energy consumption by 30% using a monocomponent endoglucanases (GH5) employing enzyme loads of 1 $mg.g^{-1}$ and 10 $mg.g^{-1}$ using a 48h-reaction and up to 40 passes in the microfluidizer. Liu *et al.* (2019) reported a reduction in energy expenditure of ultra-refiner by 55% and 39% using high loads of endoglucanases (100 $mg.g^{-1}$ 30 $mg.g^{-1}$, respectively, in 2 h of reaction). (Berto *et al.*, 2021) studied mild endoglucanase treatments (0.5 – 25 $EGU.g^{-1}$) of HBKP and reaction times of 1h - 3h followed by ultra-refining and isolated CNF with wet-SSA of approximately 200 $m^2.kg^{-1}$. These authors obtained a reduction in the energy demand up to 50% (10 $kWh.kg^{-1}$ with enzyme loading of 25 $EGU.g^{-1}$) without producing significative amounts of sugar. Conversely, the enzymatic treatments with Cellic CTec2 preparation produce total sugars concentration (glucose and xylose) in the range of 61 - 165 $g.L^{-1}$ (as data shown on Chapter 6), value much higher than any other work proposing a treatment with endoglucanase monocomponent.

It is noteworthy to mention that most studies using endoglucanase monocomponent employ short reaction times (few hours) while studies that investigate rich enzyme cocktails typically employ longer reaction times, such as > 70h (Bondancia *et al.*, 2022, 2017; Pereira and Arantes, 2020; Song *et al.*, 2014). For our study, we explored reaction times desired for production of cellulose sugars, exemplified by treatment at 30h. Figure 21 shows that the pattern for energy savings is different for enzyme treatments at 30 h and 72h of reaction. Thus, there is a strong indication that the enzyme treatments for CNF isolation that promotes lower cellulose conversion 18% (such as condition EH-5-30, enzyme loading of 5 $mg.g^{-1}$ and 30h of reaction) would isolate CNF with lower energy consumption maintaining the “gel-like” aspect typically desired.

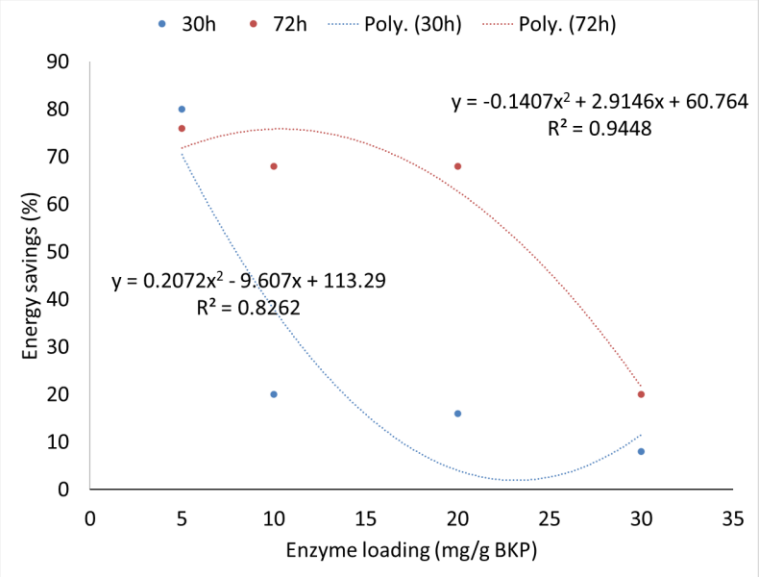

Fig. 21. Potential of energy savings according to the enzyme treatment prior to the ultra-refining.

7.4 Overall mass balance for the coproduction of CNC, CNF, and sugars at high concentration

Two pioneer works that demonstrated the integration of CNF and sugars production reported that after extensive enzymatic hydrolysis the CSR already has a CNF aspect and can be isolated using ultrasonication. Zhu *et al.* (2011) reported to obtain CNF from CSR with 48h of reaction (CSR yield 60%) and (Song *et al.*, 2014) reported to obtain CNF simultaneously with glucose yield of 57.5% - 75.6% (72h of reaction). They demonstrate that CNF can be isolated by ultrasonicating the CSR, however the CNF yield is not discussed. Later, Cebreiros *et al.* (2021) employed a similar strategy using enzyme cocktail for complete saccharification (Cellic CTec3, HTec3, and swollenin) to produce CNF and sugars, isolating CNF from CSR by ultrasonication. They conducted enzymatic hydrolysis of HBKP using solids consistency up to 8%(w/w) for up to 24h obtaining cellulose conversion in the range of 6.3% to 46.3% (glucose up to 45 $g.L^{-1}$), xylan conversion in the range of 25.8% to 84.6% (xylose up to 13 $g.L^{-1}$), and CNF yield in the range of 61% to 97%.

In this chapter, we investigate the ultra-refining process instead of ultrasonicating due to the potential to operate in a continuous-feed and process high amount of raw material. We

studied the simultaneous production of CNC, CNF and high concentration sugars by extracting CNC and CNF from the cellulosic solid residue (CSR). Figure 22 shows the mass balance according to the yield obtained for CNC, CNF and total sugars on HBKP basis for each enzymatic treatment. All conditions investigated resulted in the recovery of the starting material in product equal to 95% or over. The cumulative mass balance for each condition was 99.4%, 98.7%, 107.0%, 96.6%, 94.8%, 100.4%, 102.1%, and 98.8%. Sugar stream concentration varied from 61 - 145 $g.L^{-1}$ at 30h and 84 - 165 $g.L^{-1}$ at 72h. The EH-5-30 condition presented recovered sugars, CNC, and CNF yields of 191 $g.kg^{-1}$ (sugas concentration of 61 $g.L^{-1}$), 59 $g.kg^{-1}$, and 744 $g.kg^{-1}$ on bleached Kraft pulp basis, respectively, which was the only condition to produce total sugars concentration under 80 $g.L^{-1}$. The results showed that the higher the enzymatic hydrolysis severity (combination of enzyme loading and reaction time), the higher is the yield of sugars nevertheless the recovery of CNC and CNF in pulp basis is reduced.

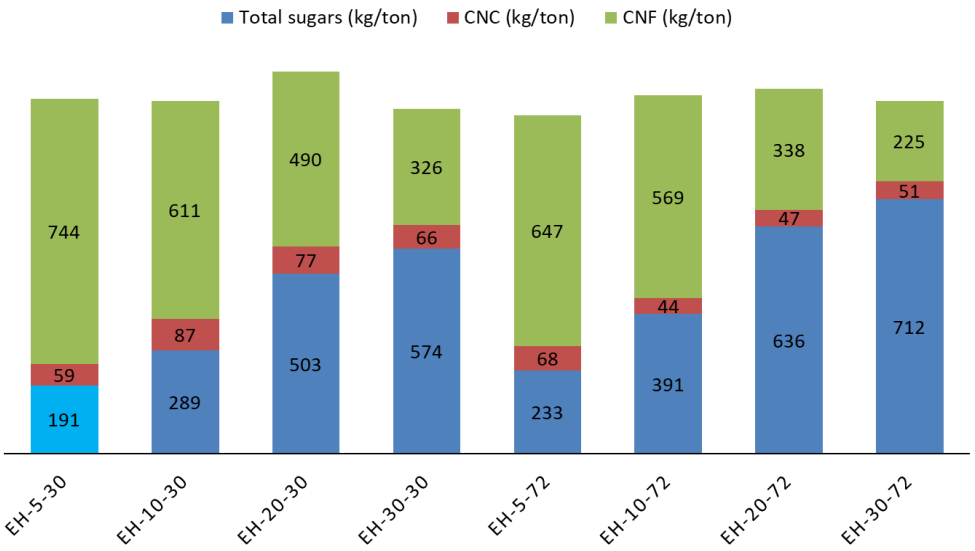

Fig. 22. Mass balance according to the yield obtained for CNC, CNF and total sugars on HBKP basis for each enzymatic treatment. Light blue refers to total sugar concentration < 80 $g.L^{-1}$ and dark blue refers to total sugar concentration > 80 $g.L^{-1}$.

Considering the market price of CNC, CNF, and raw sugars, a projected revenue was plotted for each treatment condition to reveal the economic trade-offs of increasing the sugar production (Figure 23). The price used for CNC was $7.2/kg (De Assis *et al.*, 2017a), CMNF

was \$2.5/kg (De Assis *et al.*, 2017b) and for sugasr was USD 0.25/kg according to raw sugar price (USDA 2018/2019). Figure 23 shows that the conditions with high enzyme loading (20 $mg.g^{-1}$ or greater) that produce greater titers of sugars have a projected revenue value closer to the price of bleached pulps (Table 12). Conversely, a greater projected revenue seems to depend on the CNF yield.

A preliminary estimative of the ratio of income/expenditure, using the projected revenue over raw material price (considering the price of HBKP at 500 US$/ton, the lowest according to Table 12), shows that it could vary from 1.864 to 4.572 times. This suggests that the choice of massic ratio proportion of coproducts would need to justify the high price of bleached Kraft pulp as a raw material. Especially, considering that raw material is the primary operational expense followed by electricity, accounting for 60% and 15% of the total manufacturing cost according to De Assis *et al*., (2017b).

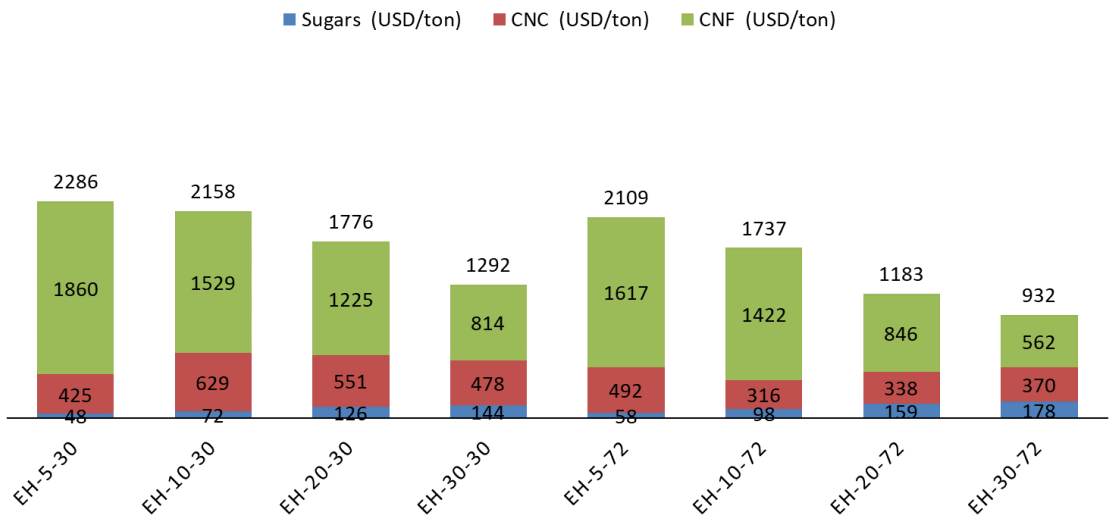

Fig. 23. Projected revenue (\$dollar) for each treatment according to the market price for CNC, CNF, and raw sugar.

7.5 Conclusion

The enzymatic treatment with Cellic CTec2 provided a platform to integrate the CNF production, after the recovery of cellulosic sugars and CNC suspensions. The coproduction of

CNF by ultra-refining the remaining CSR is technically feasible and allowed the full valorization of HBKP. The isolation of CNF was successfully conducted with tap water, which suggests a potential to reduce operational costs.

The mass balance of CNC, CNF, and cellulosic sugars was evaluated for eight enzymatic conditions with different proportions of coproducts obtained due to different degrees of cellulose conversion. The cumulative energy measurement from ultra-refining each CSR suspension revealed the potential to save energy input up to 80%, depending on the enzymatic treatment conditions. This reduction in energy consumption was far superior to those found in the literature. However, the properties of the CNF suspensions need to be further investigated if viscosity is desired. That is because the enzymatic-CNF had a lower viscosity than CNF suspensions without pretreatment.

The analysis of mass balance combined with cumulative energy measurements during ultra-refining showed that the reaction condition EH-5-30 produced the lowest glucan conversion (18 g/100g HBKP) and isolated CNF with the smallest energy input (5 $kWh.kg^{-1}$). However, the same reaction condition produced the lowest sugars titer (61 $g.L^{-1}$). Hence, the trade-off of producing high titers of sugars is the reduction of CNF yield and increase of energy input.

The ratio of income/expenditure calculated using the projected revenue over raw material price showed that there will be a revenue variation of about 1.9 to 4.6 times the value of HBKP by varying the massic proportions of CNC, CNF, and sugars recovered, which seems to be especially dependent on the CNF yield. Within the pulp and paper industry, the production of nanocelluloses is, in fact, more interesting than the production of cellulosic sugars when taking into consideration their traditional products. Thus, the reaction conditions that recover a higher yield of CNF could be more economically adequate.

CHAPTER 8 A NEW PROCESS FOR THE COPRODUCTION OF SODIUM ACETATE, NANOCELLULOSES, AND CELLULOSIC SUGARS FROM SUGARCANE BAGASSE AND STRAW

8.1 Introduction

Several processes have been developed aiming to obtain cellulosic sugars, followed by fermentation and production of bioethanol as a sole product. The Deacetylation and Mechanical Refining (DMR) process is currently the most promising method to produce bioethanol with great economic feasibility (MPSP US$2.24 - 2.54/gal of ethanol or US$2.49/gallon of gasoline equivalent according to Davis *et al.* (2021), Davis *et al.* (2018), and Chen *et al.* (2016). We are proposing here a modified DMR approach that focusses on producing high lignin-containing nanocelluloses (LCNC and LCNF) together with sodium acetate and cellulosic sugars. The goal of our process is to employ mild alkaline conditions as pretreatment to allow sodium acetate recovery and prevent significant xylan depolymerization and lignin solubilization. The expectation is to promote the valorization of sugarcane bagasse (SCB) and sugarcane straw (SCS) by minimizing the loss of biomass fractions in streams that may impose i) difficulties in separating and recovering the biomass components as value-added products, ii) difficulties with the chemical recovery. Additionally, the production of nanocelluloses associated with the DMR process has not been investigated yet.

In order to evaluate the feasibility of the proposed process to obtain sodium acetate, cellulosic sugars, and lignin-containing nanocelluloses, the mass balance and characterization of SCB and SCS main fractions is discussed in the present chapter (Chapter 8), while the properties of the lignin-containing nanocelluloses is addressed in the Chapter 9.

8.2 Preparation of SCB and SCS and ash removal

The preparation of lignocellulosic materials generally includes particle size reduction and decreasing the content of inorganics, which respectively reduces mass transfer resistance

during chemical and enzymatic reactions and avoids accumulation of inorganics in the recovered fractions, leading to unwanted side reactions. The reduction of feedstock inorganic content also reduces equipment corrosion.

To homogenize the particle size and ash content, SCB and SCS were subjected to air drying, milling, and sieving, which is referred as biomass preparation. The mass and ash content balances are shown on Table 17. The particle size of the air dried SCB was much smaller than the SCS. Therefore, the SCB was screened using a 100-mesh screen while a 30-mesh screen was used for SCB. It can be seen that only 49% of the SCS was retained on the 30-mesh screen with an ash content of 6% compared to 20% in the original SCS. This means that about 85% of the ash was removed by sieving, and thus sieving is important for SCS, albeit at an overall mass loss of 51%. Conversely, the reduction in ash content for SCB was insignificant at the small amount of rejected material of 5.4%, calling into question whether to apply sieving in practice for SCB, also because it was received with a low ash content (3%). The difference of inorganics contect from two feedstocks is explained due to the common handling procedure in the field. Sugarcane bagasse (SCB) typically has a reduced inorganic content due to extensive mechanical and hot water treatments during sugarcane juice extraction (with efficiencies up to 98%) (Negrão *et al.* 2021). On the other hand, sugarcane straw (SCS) is collected during harvest without further treatment, hence it could be returned to the field due to its high inorganic content with fertilizing properties (Negrão *et al.* 2021).

Table 17. Mass balance and ash composition of SCB and SCS before and after biomass preparation.

Milled biomass	**Sieve mesh size (opening)**	**Retained (g/100g starting material)**	**Rejected (g/100g starting material)**	**Ash composition (%)**		
				as received	**after sieving**	**rejected portion**
SCB	100-mesh (150 μm)	94.6 ± 0.5	5.4 ± 0.5	3 ± 1	3.0 ± 0.9	18.5 ± 0.7
SCS	30-mesh (595 μm)	49 ± 3	51 ± 3	20 ± 5	6 ± 1	24 ± 5

8.3 Effects of deacetylation on pulp yield and the removal of main components

The effects of dilute alkaline pretreatment conditions (NaOH loading on biomass (40-80 mg.g^{-1}), temperature (50 and 80ºC), solid to liquid ratio (1:4, 1:6, and 1:8)) were studied to determine the deacetylated pulp yield, referred as DEAC SCB yield and DEAC SCB yield. The deacetylation reactions produced solids solubilization even at the lowest NaOH loading on biomass and temperature. Figure 24 shows a linear correlation between NaOH loading on biomass and solid solubilization. The yield of DEAC SCB was in the range of 84.4 – 97.1% (SCB basis) and 82 – 94.2% (SCB basis) at 50ºC and 80ºC, respectively, and the yield of DEAC SCS was in the range of 74.5 – 90% (SCS basis) and 66 – 82% (SCS basis) at 50ºC and 80ºC, respectively.

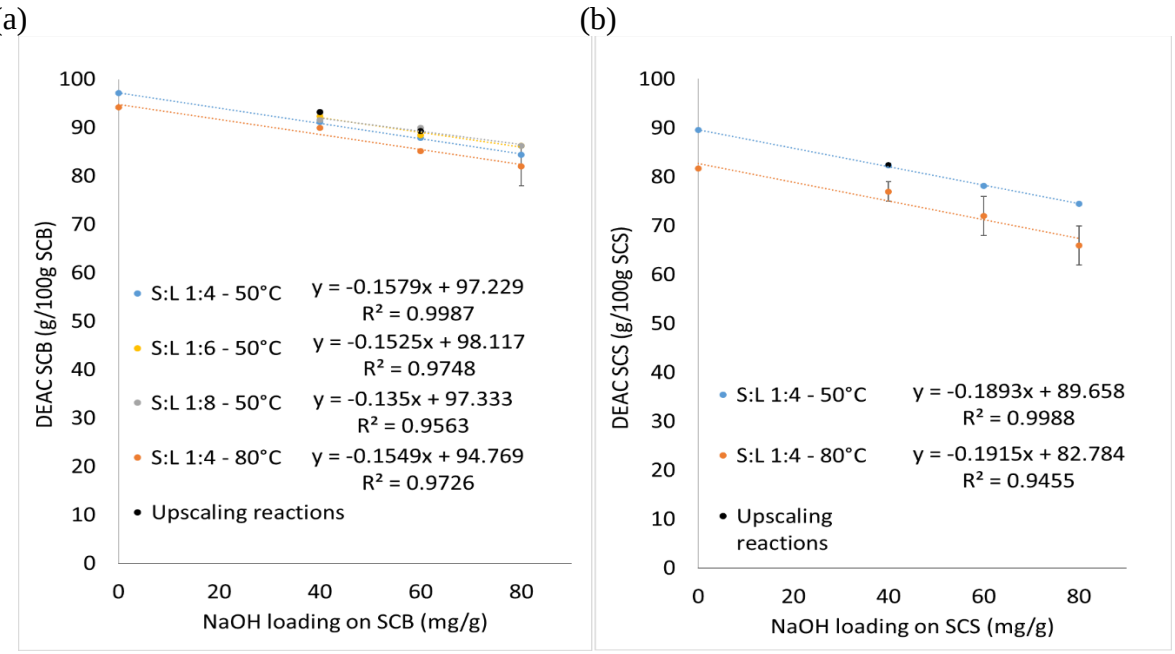

Fig. 24. (a) DEAC SCB and (b) DEAC SCS yield in relationship to the NaOH loading on biomass for different temperatures (50ºC and 80ºC) and solid to liquid ratios (1:4, 1:6, and 1:8).

The difference in solid solubilization obtained for SCB and SCS can be attributed to two factors - previous pretreatment that SCB underwent, while SCS was just removed from the field as such, and differences in cell wall recalcitrance. The difference in recalcitrance is evidenced by the fact that the two materials respond differently to the alkaline pretreatment

conditions. Figure 24a shows that the slope of the yield loss is relatively unchanged when the temperature is increased from 50 ^{o}C to 80^{o}C and the increase of NaOH loading on SCB from 0 to 80 mg.g^{-1} results in similar DEAC SCB with up to 18 g/100g yield loss. The two-factor ANOVA indicated that NaOH loading on SCB (p = 0.012) was statistically significant whereas temperature was not significant (p = 0.17) at the interval of confidence of 95%. The effect of solid to liquid ratio on the DEAC pulp yield was investigated with SCB, by keeping the temperature constant at 50^{o}C (Figure 24a). A two-factor ANOVA indicated that the solid to liquid ratio (p = 0.00027) and NaOH loading on SCB (p = 3.4.10^{-9}) parameters significantly affects the DEAC SCB as well as their interaction (p = 0.019) at the interval of confidence of 95% although the yield loss is very small for the range tested. This result suggests that the kneading technique employed was suitable to guarantee caustic impregnation and good mass transfer at the small-scale level of 12g o.d. biomass. However, when the scale of the reaction was increased about 4.2 times (up to 50g o.d. biomass), the yield loss of DEAC SCB was slightly smaller than that at the 12 g level (Table 18). Consequently, the liquors recovered after at the larger scale alkaline treatment for SCB show having a higher pH than those obtained at the smaller scale because less caustic was consumed in the deacetylation reactions as is evidenced by the higher acetyl group content for the larger scale samples (Table 18). These results suggest a mass transfer challenge for SCB when increasing the dry matter content of the suspension, which may reduce the efficacy of the alkaline reaction for SCB (Inalbon *et al.*, 2013).

Figure 24b shows that the slope of the DEAC SCS yield is significantly larger than that of the DEAC SCB, while the yield loss with water alone (0 mg.g^{-1} NaOH charge) is much larger at both 50 and 80^{o}C. Statistical analysis indicated that NaOH loading on SCS (p = 0.016) and temperature (p = 0.012) were statistically significant at the interval of confidence of 95%, but

an interaction between these parameters was not significant (p = 0.78). The yield of DEAC SCS at the larger scale remained similar that obtained at the smaller scale (Table 19).

The effect of the deacetylation reaction was investigated in terms of the removal of the main components of lignocellulosic material, with the objective to recover sodium acetate and achieve low solubilization of lignin. The data are summarized in Tables 18 and 19 for untreated, extractives-free, and SCB and SCS after the selected alkaline pretreatments at 50^{o}C for 1.5h and solid to liquid ratio of 1:4. The chemical composition of SCB and SCS (milled and sieved) shows that SCS has a higher content of soluble components, referred to as extractives. The extractives content for SCS was 17.1 ± 0.6 g/100g SCS, which was superior to the SCB extractives content of 5.0 ± 0.3 g/100g SCB for water-ethanol extraction (Table 18 and 19). The extractives content overestimates the content of non-soluble lignin and sugars (*i.e.*, glucan) in the whole biomass composition (Carvalho *et al.* 2015).

The percentile removal of components from SCB and SCS according to the different pretreatment conditions (NaOH loading on biomass and temperature) with solid to liquid ratio of 1:4 is shown on Figure 25. As expected for alkaline reactions, the components removed in major proportions were acetyl groups and lignin. The acetyl groups are removed as sodium acetate in a saponification reaction and lignin is solubilized by the cleavage of ester and ether links (Chen *et al.* 2014). A mild alkaline treatment (NaOH loading on biomass of 40 mg.g^{-1}) with temperature up to 80^{o}C removed about 70 – 80% of the acetyl groups for both SCB and SCS. Interestingly, the range of acetyl removal of 70 – 80% is obtained at a DEAC pulp yield that coincides with the threshold of solids solubilization that increases SCB and SCS nanopores. According to Lima *et al.* 2018), a solubilization of 10% and 20% for SCB and SCS, respectively, would be enough to produce larger nanopores and increase accessibility to the carbohydrates. A removal of 100% in the acetyl groups is obtained by increasing the NaOH loading on biomass to 60 mg.g^{-1} regardless of the pretreatment temperature 50^{o}C or 80^{o}C

Table 18. Chemical composition of sugarcane bagasse (SCB) main components before and after selected alkaline treatment, pulp yield, and pH of the recovered liquor.

Material	Yield (g/100g SCB)	Lignin (g/100g pulp)	Glucan (g/100g pulp)	Xylan (g/100g pulp)	Arabinosyl (g/100g pulp)	Acetyl (g/100g pulp)	Liquor pH
SCB milled and sieved	94.6 ± 0.5	24.8 ± 0.3	45.8 ± 0.3	20.28 ± 0.08	4.02 ± 0.06	4.708 ± 0.002	-
SCB milled and sieved (extractives-free)	95 ± 0.3	20.2 ± 0.7	43 ± 1	19.5 ± 0.4	3.82 ± 0.05	4.0 ± 0.3	-
DEAC Control 50 °C	97.1*	22.3 ± 0.3	45.6 ± 0.4	20.5 ± 0.1	3.97 ± 0.03	4.05 ± 0.07	5.14
DEAC SCB4 (12 g o.d.)	91.1 ± 0.3	20 ± 1	45 ± 1	19.5 ± 0.4	3.84 ± 0.06	1.36 ± 0.08	10.0 ± 0.07
DEAC SCB4 (50 g o.d.)	93.2 ± 0.1	20.1 ± 0.5	46.7 ± 0.5	19.8 ± 0.1	4.1 ± 0.2	2.3 ± 0.5	10.8 ± 0.2
DEAC SCB6 (12 g o.d.)	87.9 ± 0.2	18 ± 1	44 ± 3	19 ± 1	3.7 ± 0.1	0.0 ± 0.0	10.840 ± 0.005
DEAC SCB6 (50 g o.d.)	89.3 ± 0.1	18.2 ± 0.9	46 ± 1	19.4 ± 0.6	4.03 ± 0.09	0.8 ± 0.4	11.86 ± 0.02

*: Replicate not available; -: data not available; DEAC SCB4: deacetylated sugacarcane bagasse treated at NaOH loading on biomass of 40 $mg.g^{-1}$; DEAC SCB6: deacetylated sugacarcane bagasse treated at NaOH loading on biomass of 60 $mg.g^{-1}$

Table 19. Chemical composition of sugarcane straw (SCS) main components before and after selected alkaline treatment, pulp yield, and pH of the recovered liquor.

Material	Yield (g/100g SCS)	Lignin (g/100g pulp)	Glucan (g/100g pulp)	Xylan (g/100g pulp)	Arabinosyl (g/100g pulp)	Acetyl (g/100g pulp)	Liquor pH
SCS milled and sieved	49 ± 3	26.0 ± 0.7	41.8 ± 0.6	18.5 ± 0.1	5.01 ± 0.06	3.2 ± 0.2	-
SCS milled and sieved (extractives-free)	82.9 ± 0.6	22 ± 2	37.0 ± 0.9	16.6 ± 0.4	4.3 ± 0.1	2.5 ± 0.2	-
DEAC Control 50 °C	89.5*	24 ± 1	39.5 ± 0.4	18.0 ± 0.2	4.57 ± 0.06	2.43 ± 0.04	4.98
DEAC SCS4 (12 g o.d.)	82.4 ± 0.4	19.7 ± 0.4	37 ± 2	16.4 ± 0.7	4.3 ± 0.3	1.1 ± 0.4	-
DEAC SCS4 (50 g o.d.)	82.4 ± 0.3	19.5 ± 0.8	38.3 ± 0.9	16.6 ± 0.7	4.4 ± 0.1	1.6 ± 0.2	10.4 ± 0.1

*: Replicate not available; -: data not available; DEAC SCS4: deacetylated sugacarcane straw treated at NaOH loading on biomass of 40 $mg.g^{-1}$

(a)

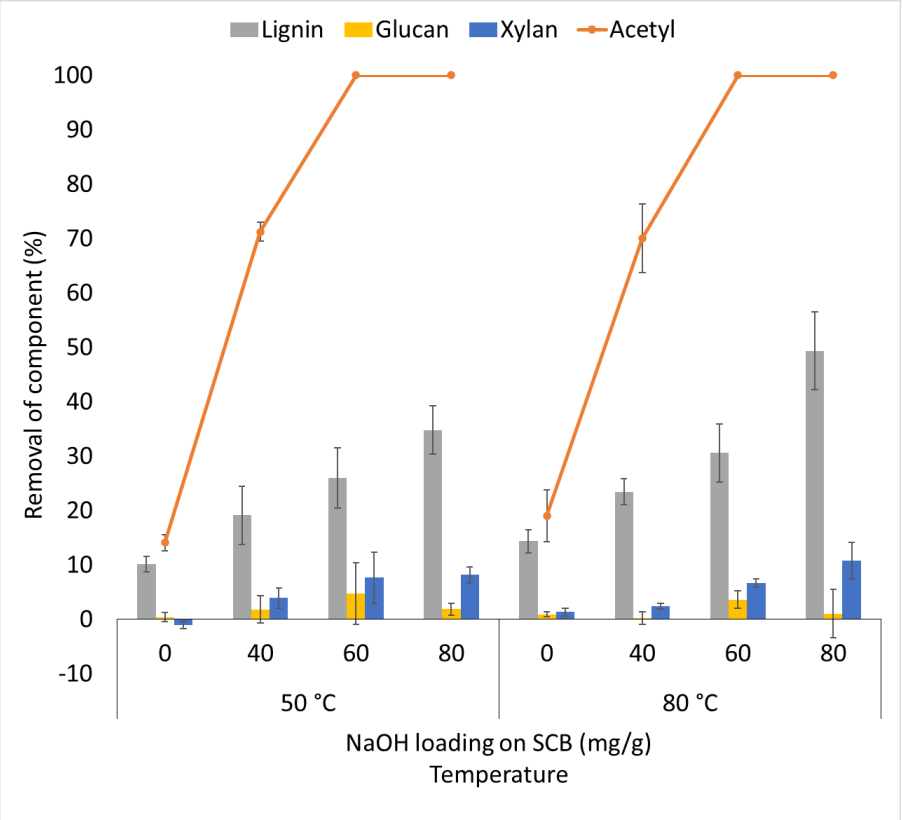

(b)

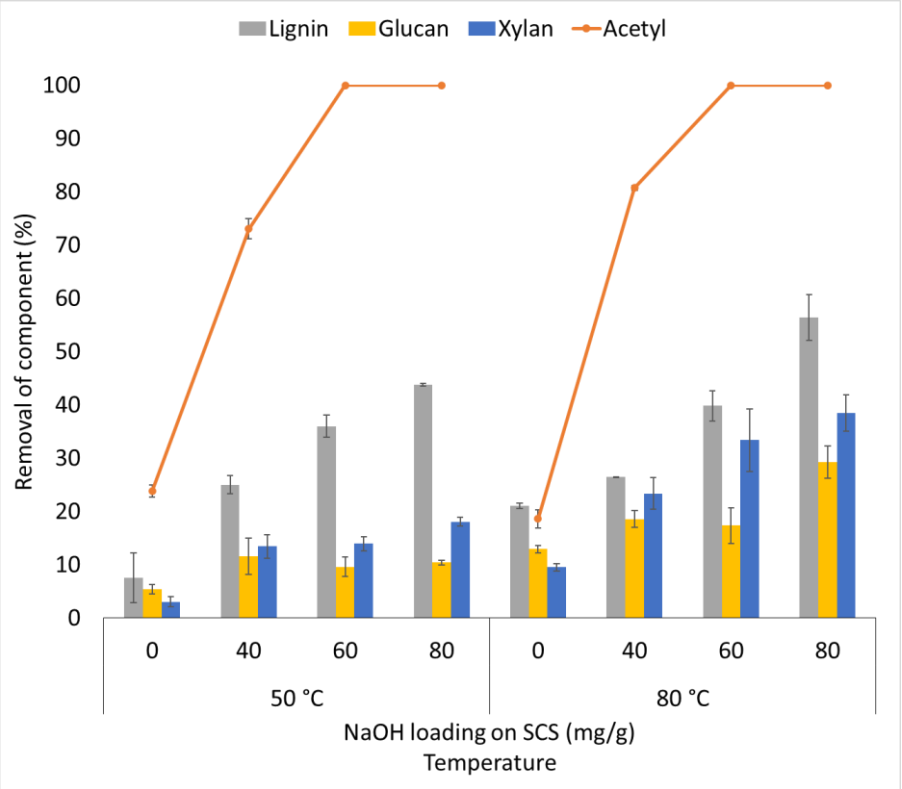

Fig. 25. Percentile removal of main components (lignin, glucan, xylan, and acetyl) with deacetylation treatment according to NaOH loading on biomass (0, 40, 60, and 80 $mg.g^{-1}$) at different temperatures (50°C and 80°C) for (a) SCB and (b) SCS.

Moreover, figure 25 shows that the DEAC pulp yield is governed by the solubilization of lignin. Lignin is removed in the range of 19 – 34.8% and 23.5 – 49.3% based on SCB at 50ºC and 80ºC, respectively, and 25 – 44% and 26 – 56% based on SCS at 50ºC and 80ºC, respectively. The removal of lignin increases linearly by increasing the NaOH loading on biomass at pretreatment temperature of 50ºC, and it increases exponentially when the temperature is set at 80ºC for both SCB (Figure 26) and SCS (Figure 27). These ranges of acetyl and lignin removal are similar to those obtained using corn stover treated by DMR, that is a removal of about 30% of lignin and 80% of acetyl groups (Chen *et al.* 2014).

The conditions tested for deacetylation reaction did not cause a great loss of carbohydrates although xylan was more affected than glucan for both SCB and SCS. Xylan and lignin are linked by the lignin-carbohydrate complex (LCC) and hence the solubilization of lignin and hydrolysis of ferulate ester link that causes the co-removal of xylan, which stands as the xylan easy to extract (Buranov and Mazza, 2008b; Carvalho *et al.*, 2016; Murciano Martínez *et al.*, 2016; Tarasov *et al.*, 2018). The results show that the removal of xylan increased linearly by increasing the NaOH loading on biomass for both SCB (Figure 26) and SCS (Figure 27). For SCB, the removal of xylan was similar at 50ºC and 80ºC even with NaOH loading on SCB up to 80 $mg.g^{-1}$ (maximum removal up to 11%). However, the removal of SCS xylan increased with a combined effect of NaOH loading on SCS and temperature, being more expressive at 80ºC (up to 38%) than at 50ºC (up to 18%). The removal of glucan from SCB was small (up to 5%) whereas the removal of SCS glucan was more expressive at 80ºC (up to 29%) then at 50ºC (up to 12%) (Figure 26 and Figure 27).

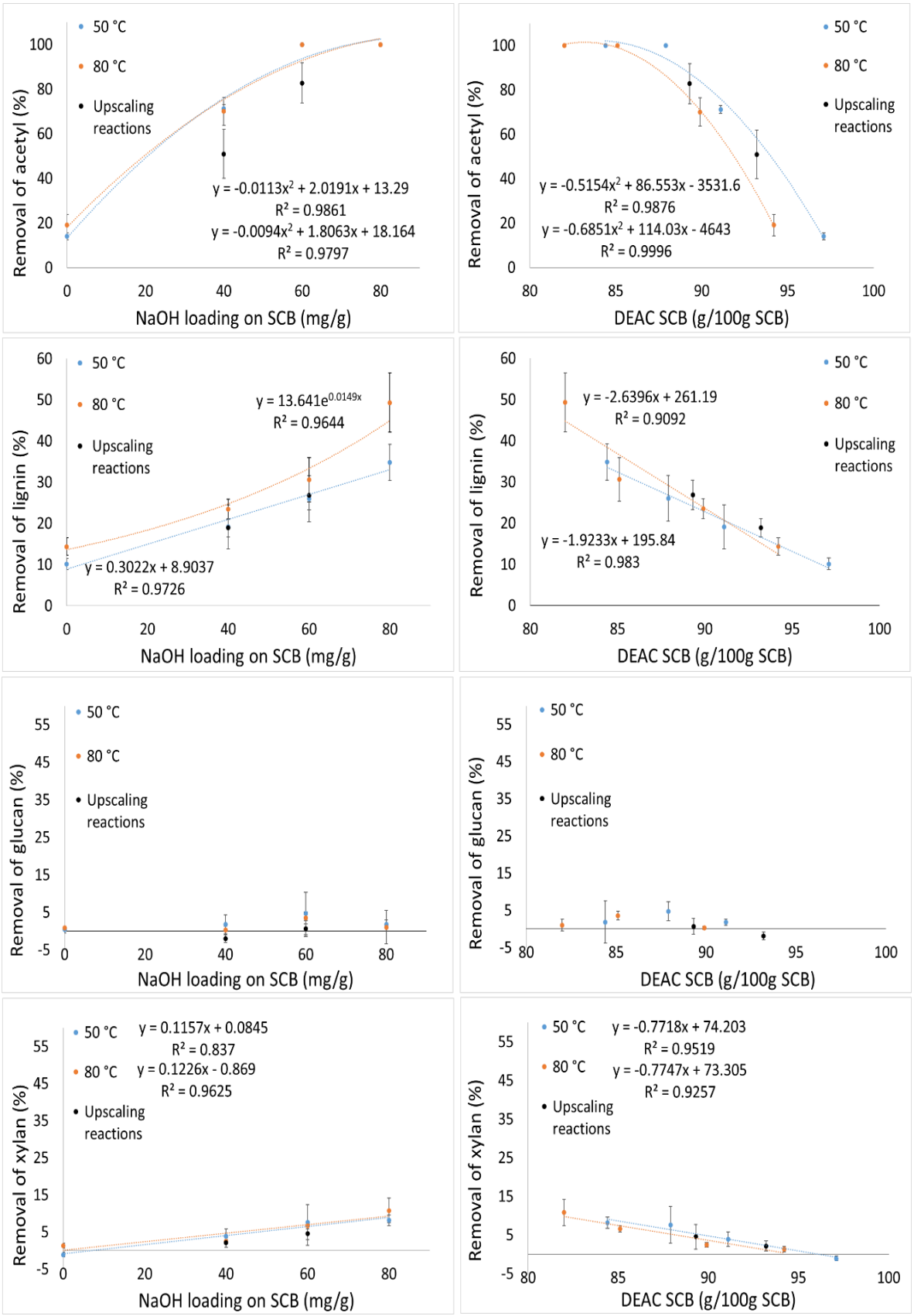

Fig. 26. Removal of lignocellulosic main components (acetyl, lignin, glucan, and xylan) in relation to the NaOH loading on SCB (*left column*) and DEAC SCB yield (*right column*) for reactions conducted at 50°C and 80°C with solid to liquid ratio of 1:4, and two different dry matter (12g o.d. and 50g o.d.).

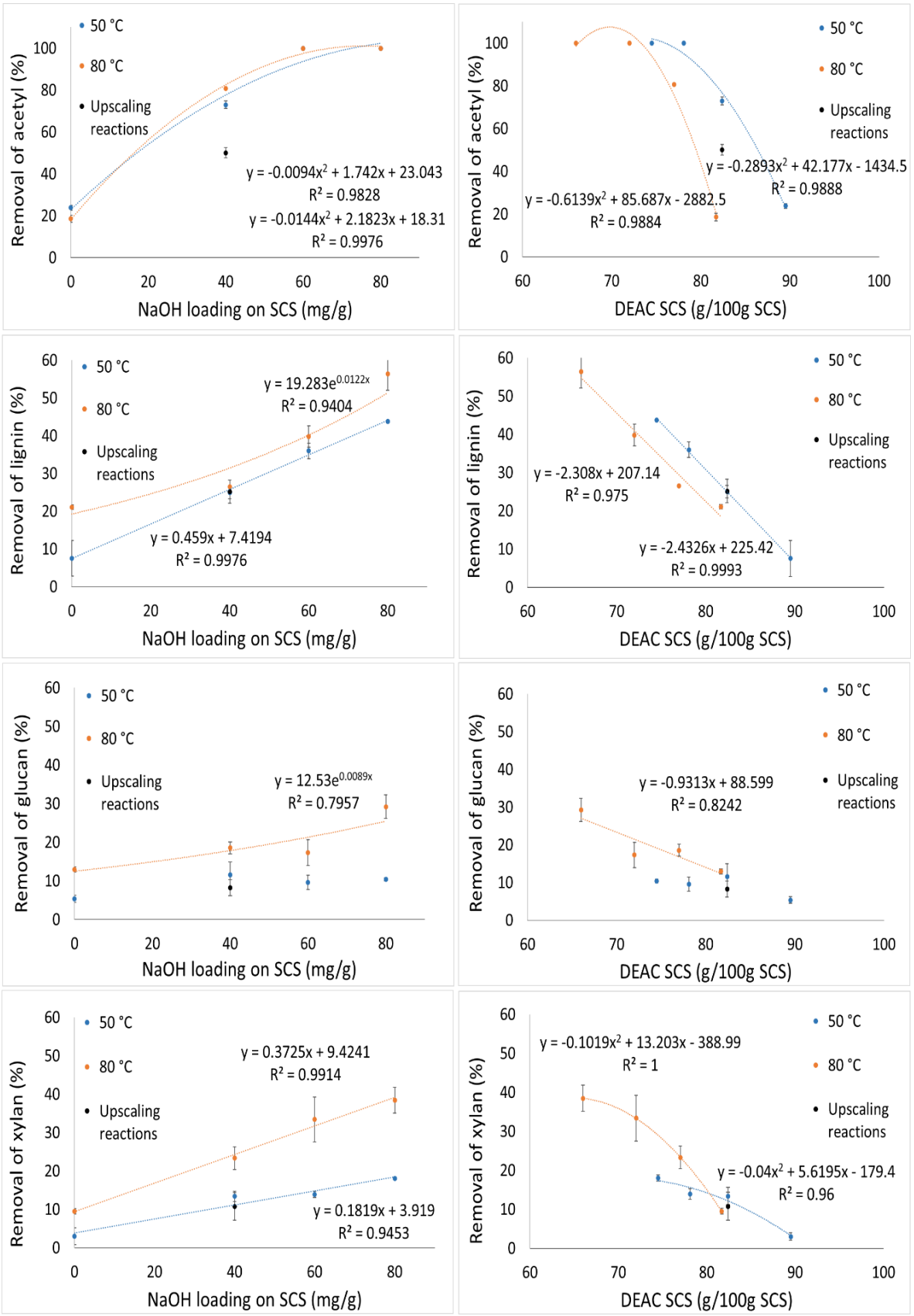

Fig. 27. Removal of lignocellulosic main components (acetyl, lignin, glucan, and xylan) in relation to the NaOH loading on SCS (*left column*) and DEAC SCS yield (*right column*) for reactions conducted at 50°C and 80°C with solid to liquid ratio of 1:4, and two different dry matter (12g o.d. and 50g o.d.)

The removal of lignin is required in order to facilitate subsequent enzymatic hydrolysis, since lignin presents a physical barrier for the enzymes to reach the cellulose polymers (Siqueira *et al.* 2013; Siqueira *et al.* 2017). However, the opening-up of the lignocellulosic matrix by the deacetylation as shown by Inalbon *et al.* (2013) allows one to choose milder conditions with less lignin solubilization, and thus to achieve good enzymatic hydrolysis with minimum biomass solubilization. To upscale the deacetylation reaction and proceed to PFI refining, milder alkaline conditions (40-60 $mg.g^{-1}$ NaOH loading on biomass and a lower temperature of 50 ^{o}C) were chosen to preserve the carbohydrates and enhance their recovery as nanocelluloses.

8.4 Macroscopic changes of SCB and SCS fibers and fines

The mild deacetylation conditions employed produced pretreated materials with a considerably higher lignin content, which may impose a recalcitrance to enzymatic treatments and sugars production. In the DMR process, deacetylation is followed by refining, which improves carbohydrate accessibility and reduces the particle size, hence reducing the enzyme loading necessary to produce sugars (Chen *et al.*, 2015). Hence, the expectation was that PFI refining would improve the cell wall breakdown. Thus, fibers and fines were monitored with a MorFi fiber analyzer to evaluate the macroscopic changes of deacetylated SCB and SCS after refining. Table 20 summarizes the monitored parameters obtained in terms of fiber and fines and Figure 28 highlights the trends of morphology change for untreated, deacetylated, and deacetylated plus refined SCB and SCS.

Both surface area and particle size are important to improve carbohydrate accessibility and enhance enzymatic hydrolysis (Leu and Zhu, 2013). The main effect observed with deacetylation and PFI refining was the increase in fines area, which represents an increase in the surface area, and reduction of fiber width for SCB, which represents a reduction of the particle size (Figure 28).

Table 20. Parameters monitored for fines and fibers by Morfi of untreated, deacetylated, deacetylated and refined, and LCNF isolated serial pretreatments.

Material	Fines (%)	Average fines length (µm)	Fiber length -weighted in length (µm)	Fines area (µm²)	Average fiber width (µm)	Number of fibers	Fiberconcentration (million/g)
DI water (control)	100 ± 0	23.7 ± 0.9	185 ± 135	369 ± 71	25 ± 20	2 ± 2	-
SCS milled and sieved	100 ± 0	24.7 ± 0.5	404 ± 47	469 ± 9	35 ± 2	64 ± 28	0.014 ± 0.008
DEAC SCS4	98 ± 4	29 ± 2	415 ± 29	644 ± 48	38 ± 2	308 ± 86	0.07 ± 0.03
Refined DEAC SCS4	88.8 ± 0.8	41.7 ± 0.5	402 ± 7	1,362 ± 23	39.9 ± 0.4	5,005 ± 2	1.6 ± 0.2
SCS4 LCNF cycle#0	88.0 ± 0.5	38 ± 0	384 ± 7	1,100 ± 11	43.7 ± 0.2	5,009 ± 2	1.43 ± 0.05
SCS4 LCNF cycle#5	99.6 ± 0.4	31.4 ± 0.5	360 ± 7	641 ± 9	43.0 ± 0.6	2,340 ± 234	0.48 ± 0.05
SCS4 LCNF cycle#10	100 ± 0	29 ± 0	356 ± 10	520 ± 2	40.4 ± 0.3	539 ± 15	0.115 ± 0.006
SCB milled and sieved	100 ± 2	27 ± 2	383.7 ± 0.9	604 ± 83	56 ± 2	224 ± 47	0.06 ± 0.01
DEAC SCB4	100 ± 0	28 ± 0.9	424 ± 26	678 ± 34	45 ± 2	422 ± 44	0.10 ± 0.02
Refined DEAC SCB4	86.1 ± 0.3	39 ± 0	415 ± 5	1,245 ± 4	35.4 ± 0.4	5,006 ± 2	1.36 ± 0.03
SCB4 LCNF cycle#0	87.5 ± 0.5	40 ± 0	392 ± 9	1,329 ± 9	39.4 ± 0.4	3,741 ± 42	0.75 ± 0.02
SCB4 LCNF cycle#5	98.8 ± 0.1	33 ± 0	353 ± 3	689 ± 5	46 ± 0.3	4,270 ± 167	0.85 ± 0.03
SCB4 LCNF cycle#10	100.0 ± 0.1	30 ± 0	344 ± 9	564 ± 3	46.2 ± 0.6	1,265 ± 48	0.250 ± 0.005
DEAC SCB6	99 ± 2	28.7 ± 0.5	397 ± 14	745 ± 31	52 ± 2	438 ± 7	0.094 ± 0.001
Refined DEAC SCB6	80.3 ± 0.4	43 ± 0	443 ± 3	1,440 ± 3	36.6 ± 0.2	5,006 ± 4	1.89 ± 0.02
SCB6 LCNF cycle#0	83.6 ± 0.5	38 ± 0	407 ± 4	1,081 ± 9	35.8 ± 0.4	5,006 ± 3	1.26 ± 0.03
SCB6 LCNF cycle#5	88.8 ± 0.3	38.7 ± 0.5	359 ± 2	969 ± 7	37.9 ± 0.2	5,011 ± 4	2.95 ± 0.05
SCB6 LCNF cycle#10	90.1 ± 0.2	39.7 ± 0.5	348 ± 3	1,013 ± 14	38.1 ± 0.1	5,016 ± 7	3.60 ± 0.03

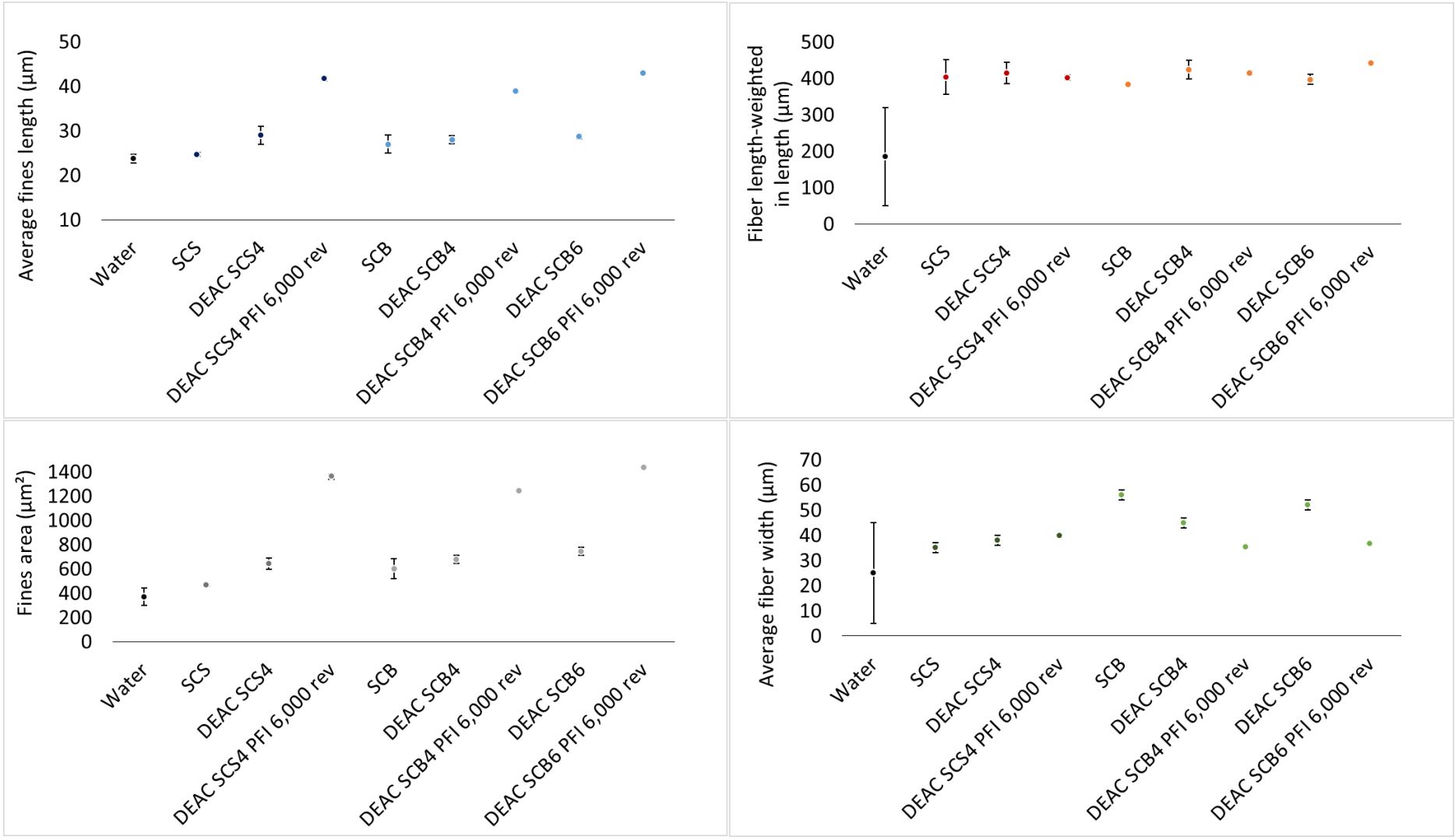

Fig. 28. Macroscopic changes of morphology of SCB and SCS untreated, deacetylated, and deacetylated and refined using parameters obtained by MorFi fiber analyzer (Average fines length, fiber length-weighted length, fines area, and average fiber width)

After PFI refining, the fiber concentration reached its maximum for SCB and SCS treated at NaOH loading on biomass of 40 $mg.g^{-1}$ (DEAC SCB4 and DEAC SCS4) and an even higher fiber concentration was obtained for SCB treated at NaOH loading on biomass of 60 $mg.g^{-1}$ (DEAC SCB6). This result corroborates with the literature that a higher removal of lignin favors the liberation of fibers by removing the physical barrier of lignin. With the refining step, a dramatic increase in the fines area was obtained for all the pretreated materials, being 1,245 μm^2, 1,440 μm^2, and 1,362 μm^2 respectively for refined DEAC SCB4, DEAC SCB6, and DEAC SCS4 (Table 20 and Figure 28).

Figure 28 also shows that the fiber length-weighted in length was 415 µm, 443 µm, and 402 µm, respectively for refined DEAC SCB4, DEAC SCB6, and DEAC SCS4, which is in accordance with De Assis *et al.* (2018) who subjected hydrothermally-treated sugarcane bagasse to PFI refining at 2,000 – 4,000 rev and 6,000 – 8,000 rev and obtained fiber length-weighted in length of 475 and 300 µm, respectively, using same measurement technique.

The parameters fines area, average fines length, fiber concentration, and number of fibers did not present a linear behavior along the serial pretreatments employed until obtaining nanocelluloses. This could be explained due to the reading limitation from the equipment (size range) and the preparation of samples being based on their concentration (50 $mg.L^{-1}$). According to the manufactures' manual, Morfi's limit of detection for fibers' length and width is 200-2000 µm and 5-75 µm, respectively, and the limit of detection for fines' length and width is 1-200 µm and < 5 µm, respectively. Hence, the subsequent treatments altered the particle distribution. That is, more fibers and fines entered the Morfi's limit of detection causing a change in the particle distribution. The PFI refining significatively modified the particle size distribution by producing shorter fibers and fines and the ultra-refining modified the particle size distribution by producing particles smaller than fines.

The fibers and fines analysis were evaluated prior to and along the isolation of LCNF by ultra-refining (Table 20). The materials referred to LCNF cycle#0 refers to the remainder solids recovered after enzymatic treatment that have also been fractionated by low centrifugation to recover LCNC. This explains why the fine area values reduced when it would be expected to increase. It is noteworthy to mention that the enzymatic treatment does promotes morphology changes due to the carbohydrates depolymerization into smaller fibers are fines, which is one of the effects that facilities the fibrillation and saves energy during mechanical treatments (X. Liu *et al.* 2019). This effect can be referred to as biorefining.

By proceeding with 10 cycles of ultra-refining, the number of fibers and fiber concentration reduced even further, while the percentage of fines content increased up to 100% at cycle #10 for all the pretreated materials. The LCNFs at cycle #10 had the smallest fiber length-weighted in length recorded, which was 344, 348 µm, and 356 µm, respectively for SCB4 LCNF, SCB6 LCNF, and SCS4 LCNF. Interestingly, the fiber length-weighted in length became the smallest when fines content was approximately 90% for all materials. Fines content have been defined as the fraction of fibril bundles smaller than 200 µm measured by MorFi, which stands as a good online operational correlation to the production of a mixture of cellulose micro- and nano-fibrils (CMNF).

8.5 Enzymatic digestibility of unrefined and refined DEAC SCB and DEAC SCS

The digestibility of unrefined and refined DEAC SCB and DEAC SCS was compared using enzymatic microassays conducted at 2% solids consistency. High-solids enzymatic hydrolysis was conducted at 15% solids consistency to evaluate the sugars concentration at high-dry matter using only the refined deacetylated materials. Figure 29a shows the carbohydrate conversion in terms of glucan, xylan, and arabinan and Figure 29b shows the sugars titer obtained by enzymatically treating unrefined and refined DEAC SCB4, DEAC SCB6, and DEAC SCS4. The results suggest that the enzymatic digestibility was facilitated by

an increased removal of lignin, which corroborates with the literature (Siqueira *et al.* 2013; Siqueira *et al.* 2017). When the alkaline charge was increased, causing lignin removal to increase from 19% to 27%, the total carbohydrate conversion improved from 28 g/100g DEAC SCB4 to 43 g/100g DEAC SCB6. This improvement means an increase of 54% in carbohydrate conversion, and total sugar titer increased from 4.78 $g.L^{-1}$ to 7.4 $g.L^{-1}$ for unrefined pretreated materials DEAC SCB4 and DEAC SCB6, respectively. The improvement in the digestibility for unrefined DEAC SCB6 (27% of lignin removed) was especially led by an increased xylan depolymerization, which changed the pattern of carbohydrate conversion comparatively to unrefined DEAC SCB4 (Figure 29a). Glucose conversion improved by 44% (from 30.5 to 44 g/100g DEAC SCB6) and xylan conversion improved by 75% (from 25.2 to 44 g/100g DEAC SCB6). Contrarily to expected, further improvement in the digestibility was not observed for refined deacetylated sugarcane bagasse (DEAC SCB4 and SCB6) although the particle size analysis suggests an increase in the fiber concentration and fines area for refined comparatively to unrefined DEAC SCB4 and 6 (Table 20). The digestibility of refined DEAC SCB remained similar to that of the unrefined DEAC SCB for both alkaline charges tested. Total carbohydrate conversion had only a small increase of 6% and 5% for refined pretreated materials DEAC SCB4 and DEAC SCB6, respectively. On the other hand, the DEAC SCS4, which had a similar amount of lignin removed (25%) compared to DEAC SCB6, showed a higher enzymatic digestibility when refined. The total carbohydrate conversion improved from 28.9 and 34.9 g/100g DEAC SCS, which means an increase of 21% in carbohydrate conversion. When DEAC SCS4 was refined, the glucan and xylan conversions were 41.4 g/100g and 26.4 g/100 DEAC SCS, respectively, and the total sugar titer increased from 4.64 $g.L^{-1}$ to 5.5 $g.L^{-1}$. These results suggest that the pretreated solids of sugarcane bagasse (DEAC SCB4 and SCB6) remained more recalcitrant than DEAC SCS4 even when a similar level of lignin removal was obtained.

The relationship between lignin removal and cellulose digestibility (Siqueira *et al.* 2013; Siqueira *et al.* 2017) as well as cellulose digestibility and methods and severity of refining (Chen *et al.*, 2013; X. Chen *et al.*, 2015; De Assis *et al.*, 2018) have been previously reported in the literature. They show that the digestibility of deacetylated materials could be improved by removing a greater amount of lignin (40 to 60%) or by employing a more intensive refining step. However, a technoeconomic assessment would be required to define whether these operational changes would be economically beneficial, considering the biorefinery goal of co-producing cellulose nanomaterials. Higher enzyme loadings and different proportions of CTec3:HTec3 were tested, however it did not result into significatively higher enzymatic conversion or or improvement in the production of glucose in terms of g of glucose per g of enzyme (Data not shown).

Figure 30a shows that high-solids enzymatic hydrolysis produced total sugars concentration of 40 ± 3 $g.L^{-1}$, 43 ± 5 $g.L^{-1}$, and 31.3 ± 0.5 $g.L^{-1}$ for DEAC SCB4, DEAC SCB6, and DEAC SCS4, respectively. From that, glucose concentration was 24 ± 1 $g.L^{-1}$, 27 ± 4 $g.L^{-1}$, and 21.6 ± 0.4 $g.L^{-1}$ and xylose concentration was 13 ± 2 $g.L^{-1}$, 14.2 ± 0.7 $g.L^{-1}$, and 7.58 ± 0.06 $g.L^{-1}$ DEAC SCB4, DEAC SCB6, and DEAC SCS4, respectively. Additionally, the acetic acid was obtained in the concentrations of 4.0 ± 0.3 $g.L^{-1}$, 3.31 ± 0.09 $g.L^{-1}$, and 2.8 ± 0.2 $g.L^{-1}$ for DEAC SCB4, DEAC SCB6, and DEAC SCS4, respectively, which is below the threshold for fermentation inhibition for baker yeasts. The acetic acid concentration is resultant from lower removal of acetyl groups (50 – 83 % and 50% removal for SCB and SCS, respectively) when upscaling the deacetylation reactions.

Figure 30b shows that the glucose concentration did not increase as expected for DEAC SCB6 and DEAC SCS4 using 15% solids consistency whereas, for DEAC SCB4, glucose concentration increased proportionally with the solids content, following the proportion obtained with the microassays at 2% solids consistency. This difference can be attributed to the

(a)

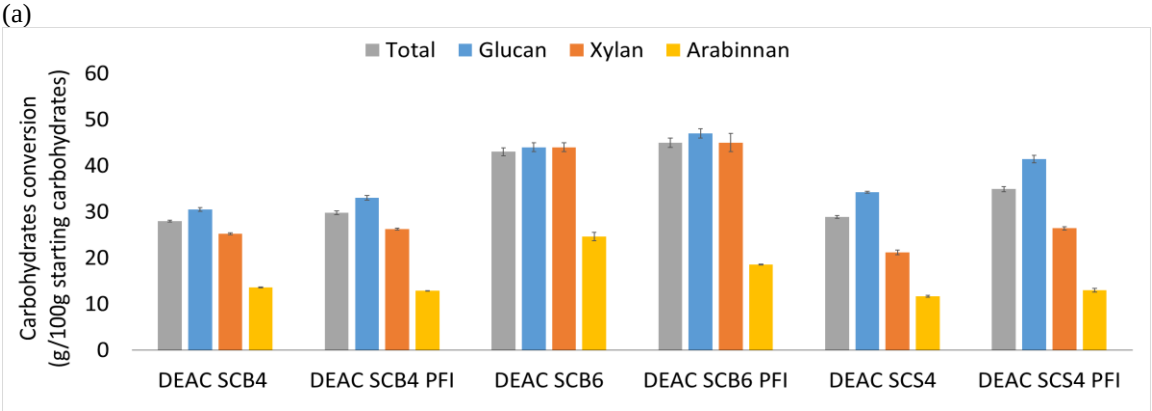

(b)

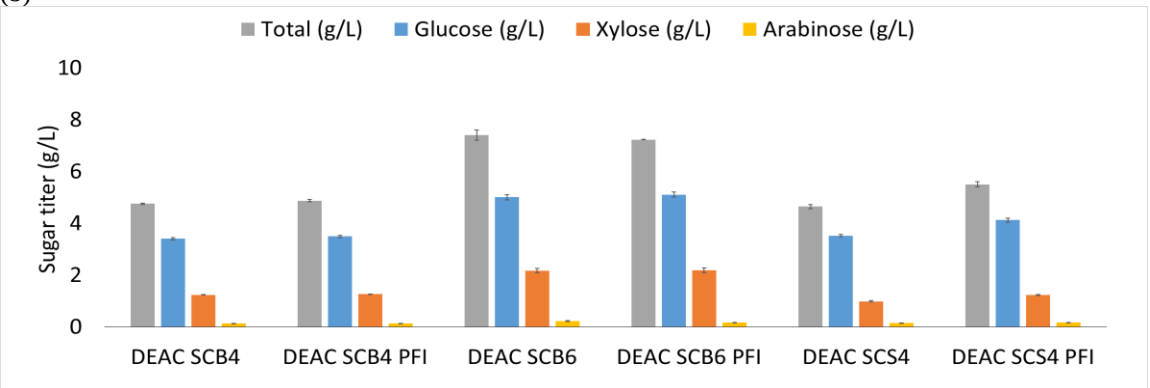

Fig. 29. (a) Carbohydrates conversion and (b) Sugar titer obtained from enzymatic treatment of unrefined and refined pretreated materials.

(a)

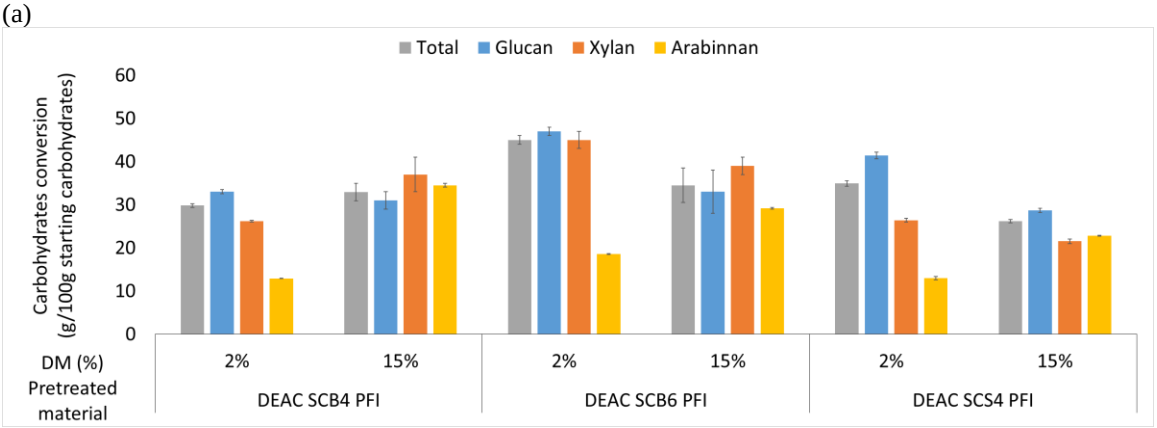

(b)

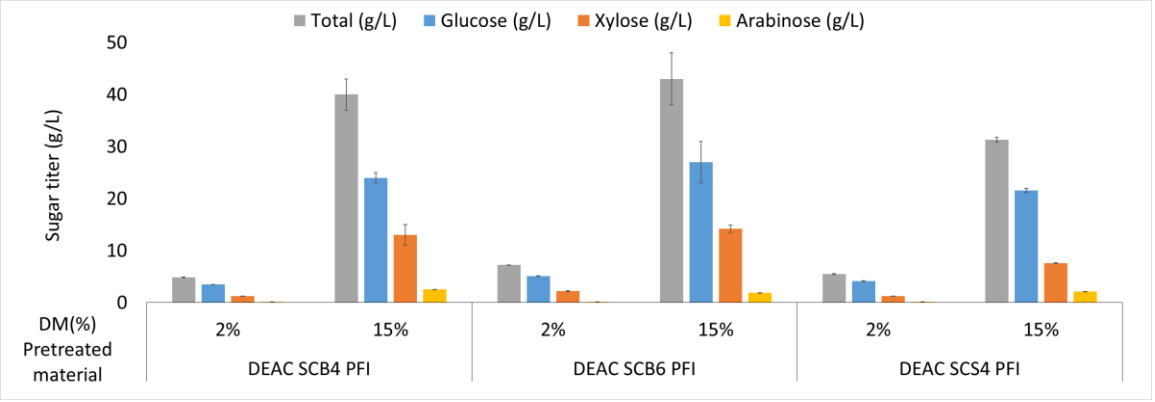

Fig. 30. (a) Carbohydrates conversion and (b) Sugar titer obtained from enzymatic treatment of refined pretreated materials using low and high consistencies (dry matter (DM) of 2% and 15%).

method of incubation and the recalcitrance of the materials rather than relative to the performance of the enzymatic cocktail.

The deacetylated materials remained highly recalcitrant even after refining. Thus, the sugar concentrations obtained were lower than the typical sugar concentration required to make cellulosic ethanol industrially feasible (100 g/L). However, the sugar stream recovered after enzymatic hydrolysis liquor is still valuable stream and it could be directed to other applications, such as sugars supply for in-house production of enzymes, mixed with sucrose in case of a co-located biorefinery, or used as food syrup. Other upgrading options for sugar streams have been thoroughly reviewed by Rosales-Calderon and Arantes (2019).

Alternative conditions to recover sugars at higher concentrations would require NaOH loading to be set at 60 or 80 $mg.g^{-1}$ on SCB at 80^{o}C and NaOH loading of 40 $mg.g^{-1}$ on SCS at 80^{o}C. That is because the deacetylated SCB was shown to be more recalcitrant than deacetylated SCS. Another option that could be considered is to employ a higher refining intensity during the PFI refining steps.

8.6 Isolation of LCNC and LCNF

In order to investigate the feasibility of isolating LCNC and LCNF from the pretreated solids, the cellulose solid residue (CSR) recovered after enzymatic treatment was submitted to centrifugation to isolate LCNC and the remainder solids was ultra-refined to isolate LCNF. The energy consumption for mechanical fibrillation was evaluated as well as the morphology and the chemical composition of the recovered nanocelluloses.

8.6.1 Energy consumption to isolate LCNF by ultra-refining

The intensive-energy consumption for CNF isolation via mechanical fibrillation is a hurdle for industrialization and commercialization of this bionanomaterial. However, enzyme pretreatments are an alternative to lower the energy requirement due to their mechanism of carbohydrate depolymerization, also referred as biorefining (Henríquez-Gallegos *et al.*, 2021;

Nagl *et al.*, 2021). Thus, the cumulative energy consumption of ultra-refining was monitored as an important parameter for the viability of isolating LCNF. The isolation of CNF from northern bleached softwood kraft (NBSK) pulp and LCNF from unbleached softwood kraft (UBK) pulp were used as a reference for fibrillation in terms of energy required to achieve a typical fines content (90% fines).

Figure 31 shows the relationship between the cumulative energy consumption during ultra-refining and the gain of fines content for each suspension up to cycle #10. The reference materials had very low fines content prior to ultra-refining, being 26% and 27.9% for NBSK pulp and UBK pulp, respectively. The literature shows similar relationship between fines content and energy input with the evolution of fibrillation for the reference materials (Copenhaver *et al.*, 2021; Diop *et al.*, 2017; He *et al.*, 2018). Conversely, the enzymatic solid residue (or cellulosic solid residue - CSR) suspensions had a significantly higher fines content prior to ultra-refining, being 87.4%, 83.6%, 87.9% for DEAC SCB4 PFI-EH, DEAC SCB6 PFI-EH, and DEAC SCS4 PFI-EH, respectively. Although the gain of fines content with energy input is higher for UBK and NBSK pulps, the CSR suspensions prepared from pretreated SCB and SCS clearly required less energy to reach a fines content of 90%. Using the quadratic curves, it was estimated that an energy consumption of 11.2 kW, 8.4 kW, 1.2 kW, 6.1 kW, 0.9 kW respectively for NBSK pulp, UBK pulp, DEAC SCB4 PFI-EH, DEAC SCB6 PFI-EH, and DEAC SCS4 PFI-EH would be necessary to reach 90% fines when ultra-refining each suspension. This result represents a reduction in energy consumption of 89%, 45%, and 92% when ultra-refining DEAC SCB4 PFI-EH, DEAC SCB6 PFI-EH, and DEAC SCS4 PFI-EH compared to the energy required to isolate CNF (at 90% fines) from NBSK pulp and 86%, 27%, and 90% compared to the energy required to isolate LCNF (at 90% fines) from UBK pulp. These results suggest that the enzymatic solid residue has potential as a source to obtain

nanocelluloses and provide excellent savings of energy consumption using the ultra-refining method, since savings greater than 50-60% are generally not found.

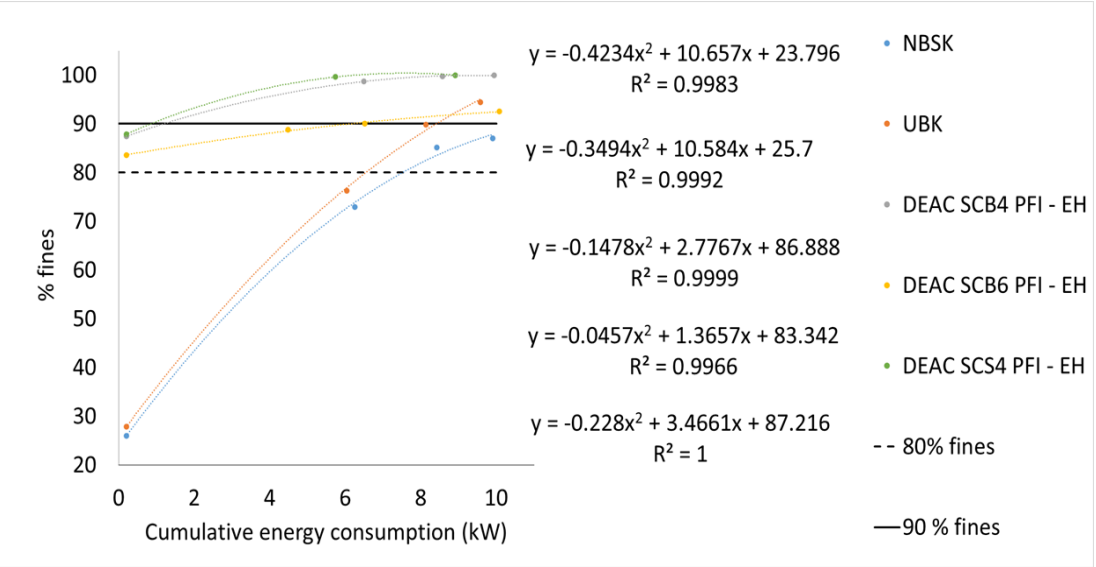

NBSK: Northern bleached softwood kraft pulp; UBK: unbleached softwood kraft pulp, DEAC SCB4 PFI-EH: enzymatic hydrolysis residue from refined DEAC SCB4: enzymatic hydrolysis residue from refined DEAC SCB4; DEAC SCB6 PFI-EH: enzymatic hydrolysis residue from refined DEAC SCB6; DEAC SCS4 PFI-EH: enzymatic hydrolysis residue from refined DEAC SCS4.

Fig. 31. Cumulative energy consumption for ultra-refining different suspensions (1.5%(w/v) solids, 1.5L sample) and their percentual of fines at cycle# 0, 5, 8, and 10.

The literature often refers to the impact of different biomass sources and prior pretreatments on the mechanical fibrillation, with emphasis on the energy consumption and its impact on the final morphology of the nanocelluloses (He *et al.*, 2018; Spence *et al.*, 2011). Monitoring the energy consumption was important not only to investigate the energy required to achieve a reference particle size (set as 90% fines) but to observe how two parameters - initial fines content and the chemical composition of the material - interferes in the evolution of the fibrillation of each suspension and its energy consumption during ultra-griding. Figure 31 also highlights that a pulp with higher lignin content requires a smaller energy input to liberate its fibrils. This can be verified by comparing the refining behavior of the NBSK and UBK pulps in Figure 31 which shows that UBK always requires a lower energy input to achieve same fine content as NBSK. A similar behavior is seen for DEAC SCB4 PFI-EH with higher

lignin content (DEAC SCB4 PFI-EH) compared to DEAC SCB6 PFI-EH with a lower lignin content. This behavior corroborates with the literature, that describes that lignin facilitates the fibrillation of cellulose due to the formation of mechanoradicals (Hon, 1979; Solala *et al.*, 2012).

8.6.2 Chemical composition of LCNC and LCNF

The cellulose solid residue (CSR) obtained from pretreated SCB and SCS still contained significant amounts of lignin and xylan after the enzymatic treatment. The chemical composition of LCNC and LCNF was determined to investigate the nanocelllluloses' composition. Table 21 and Table 22 shows the main lignocellulose components of LCNC and LCNF, respectively, in terms of the contents of lignin, cellulose, and hemicelluloses (xylan, arabinan, and acetyl groups). The nanocelluloses' chemical composition was used to calculate the composition ratio of lignin to glucan (L/G) and xylan to glucan (X/G) shown in Table 23.

The chemical composition of SCB4 LCNC, SCB6 LCNC, and SCS4 LCNC indicated that lignin was the major component with a content in the range of 39.2 – 43.5g/100g of LCNC (Table 21) and a composition ratio of lignin to glucan (L/G) ranging between 1.59 – 2.42 (Table 23). Hence, they can be referred to as high lignin-containing cellulose nanocrystals (LCNC). On the other hand, the chemical composition of SCB4 LCNF, SCB6 LCNF, and SCS4 LCNF showed a lower content of lignin in the range of 26.1 – 31.1g/100g of LCNF (Table 21). Hence, they can be referred to as lignin-containing cellulose nanofibrils (LCNF). LCNF samples had glucan as their major component with a content in the range of 39.3 – 41.9 g/100g of LCNF, thus leading to a much lower L/G ratio in the range 0.65 – 0.74. The xylan to glucan (X/L) ratio in the LCNF samples is 0.52 – 0.61 (Table 23).

It was interesting to note that the centrifugation step may have affected the chemical composition of LCNC and LCNF. This may have happened because LCNC was isolated from CSR by low-speed centrifugation and the remained material was employed to isolate CNF.

Table 21. Chemical composition of LCNC isolated from cellulosic solid residue (CSR) by centrifugation.

Pretreated material	Lignin (g/100g)	Glucan (g/100g)	Xylan (g/100g)	Arabinosyl (g/100g)	Acetyl (g/100g)	Ash (g/100g)	Total (g/100g)
SCB4 LCNC	43 ± 2	22.2 ± 0.4	14.427 ± 0.001	3.0 ± 0.2	1.26 ± 0.02	0.81 ± 0.02	84 ± 2
SCB6 LCNC	39.3 ± 0.3	24.74 ± 0.08	15.15 ± 0.07	2.68 ± 0.01	0.8217 ± 0.0004	0.41 ± 0.04	83.1 ± 0.2
SCS4 LCNC	43.5 ± 0.4	18.0 ± 0.7	12.44 ± 0.08	3.2 ± 0.5	1.5 ± 0.3	2.1 ± 0.2	80.7 ± 0.8

Table 22. Chemical composition of LCNF isolated from cellulosic solid residue (CSR) by ultra-refining.

Pretreated material	Lignin (g/100g)	Glucan (g/100g)	Xylan (g/100g)	Arabinosyl (g/100g)	Acetyl (g/100g)	Ash (g/100g)	Total (g/100g)
SCB4 LCNF	27.19 ± 0.06	41.9 ± 0.4	24.33 ± 0.08	1.80 ± 0.01	1.74 ± 0.03	3.5 ± 0.2	100.4 ± 0.7
SCB6 LCNF	31.1 ± 0.4	42.0 ± 0.4	21.7 ± 0.2	1.77 ± 0.02	0.74 ± 0.01	6.66 ± 0.09	104 ± 0.7
SCS4 LCNF	26.1 ± 0.6	39.3 ± 0.1	23.9 ± 0.2	2.84 ± 0.02	1.30 ± 0.02	1.7 ± 0.5	96 ± 2

Table 23. Composition ratio of lignin to glucan (L/G) and xylan to glucan (X/G) relative to each sample chemical composition.

Material	L/G	X/G
SCB4 LCNC	1.94	0.65
SCB6 LCNC	1.59	0.61
SCS4 LCNC	2.42	0.69
SCB4 LCNF	0.65	0.58
SCB6 LCNF	0.74	0.52
SCS4 LCNF	0.66	0.61
NBSK pulp[1,3]	-	0.23
UBK pulp[2,3]	0.1 - 0.2	0.1 - 0.2

[1]Copenhaver *et al.* (2021);[2]Imani *et al.* (2019); [3]He *et al.* (2018)

It was observed that SCB4 LCNC and SCS4 LCNC had higher lignin content whereas SCB6 LCNC had a lower lignin content. For the latter, the major fraction of lignin remained in the CSR after the centrifugation. SCB6 LCNF had the highest lignin content among all LCNFs.

Imani *et al.* (2019) fractionated TEMPO-LCNF by centrifugation to study the influence of particle size and lignin content on film properties. They suggested that low molecular weight lignin bonds to fibrils more strongly and high molecular weight lignin tends to collapse more and hence interact less with fibrils. This may be an explanation of how the lignocellulose fractions were distributed during centrifugation and recovery of cellulosic residues. Moreover, Xuran Liu *et al.* (2019) studied the coproduction of lignin and LCNF, using alkaline treatment. They combined alkaline pretreatment (NaOH loading of 1 - 7%(w/w) on biomass) with ball milling and isolated LCNF by homogenization. They observed that only a trace amount of cellulose was isolated with lignin and up to 39% of xylan was isolated together with lignin. Tricin was the only substance observed to precipitate in the aqueous medium. They recovered lignin by centrifugation 13,000×*g* and observed that the chemistry of the lignin obtained was native-like with minimal condensation even for higher alkali loadings.

8.6.3 Particle size of LCNC and LCNF

Centrifugation can selectively fractionate nanocelluloses according to particle size by adjusting the rotation speed (Bonaccorso *et al.*, 2013; Imani *et al.*, 2019; Toivonen *et al.*, 2018). We presented in Chapter 6 that enzymatic-CNC with diameters under 100 nm and high uniformity can be successfully isolate by centrifugation at 750×*g*. Thus, similar procedure was used to recover LCNC from CSR. Scanning Electron Microscopy (SEM) images were evaluated to investigate the distribution of diameters from LCNC recovered by low-speed centrifugation (Figure 32) and the final diameter of LCNF isolated after 10 cycles of ultra-refining (Figure 33).

(a)

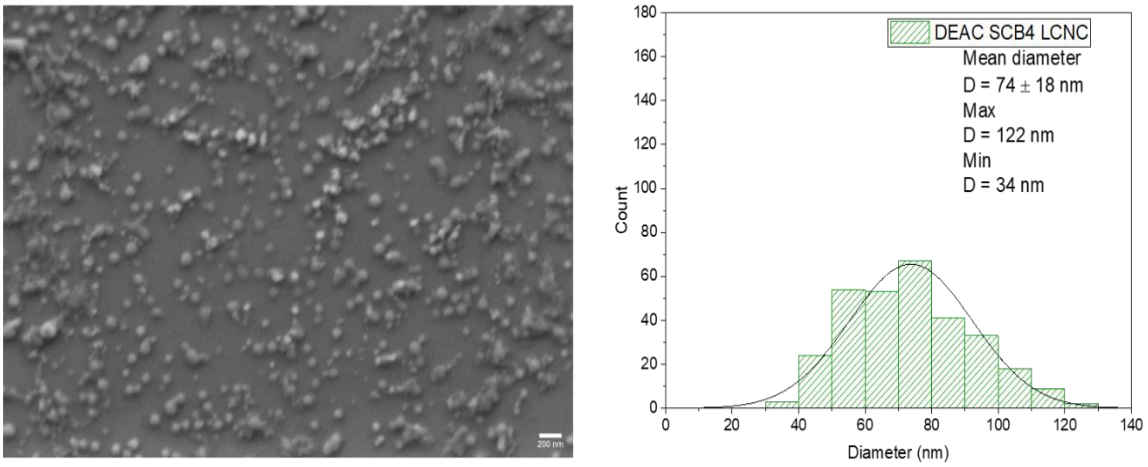

(b)

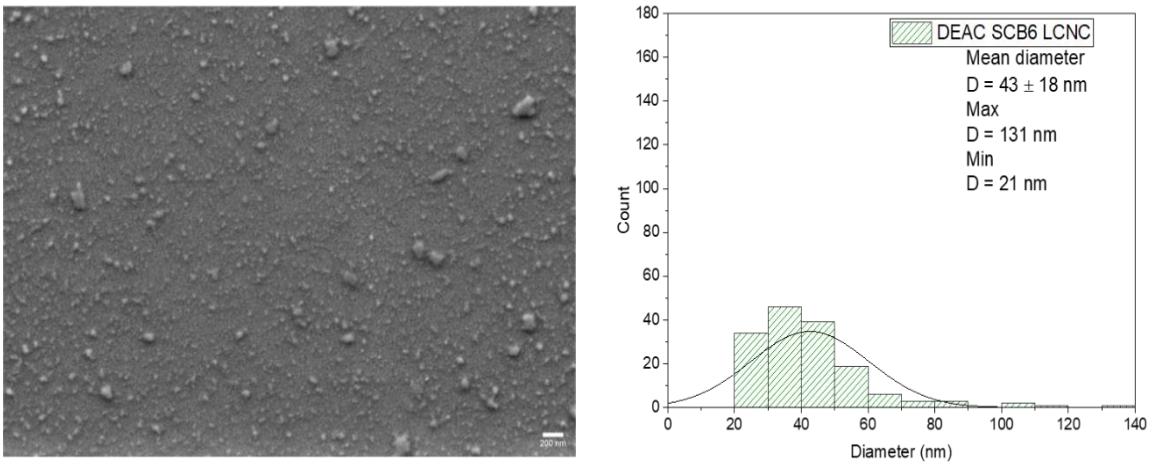

(c)

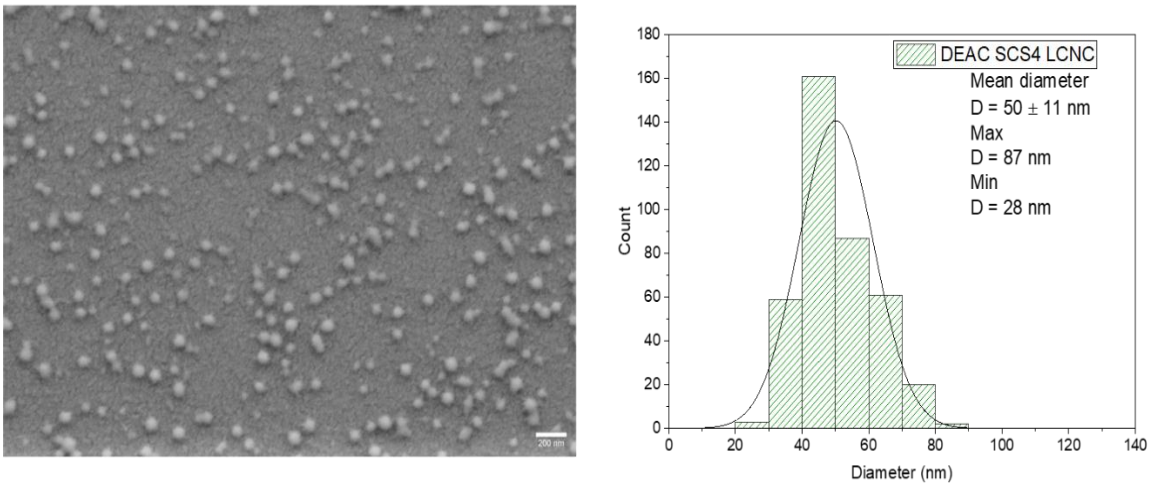

Fig. 32. SEM images and distribution of diameters obtained from (a) DEAC SCB4 LCNC, (b) DEAC SCB6 LCNC, and (c) DEAC SCS4 LCNC. Scale bar shows 200 nm.

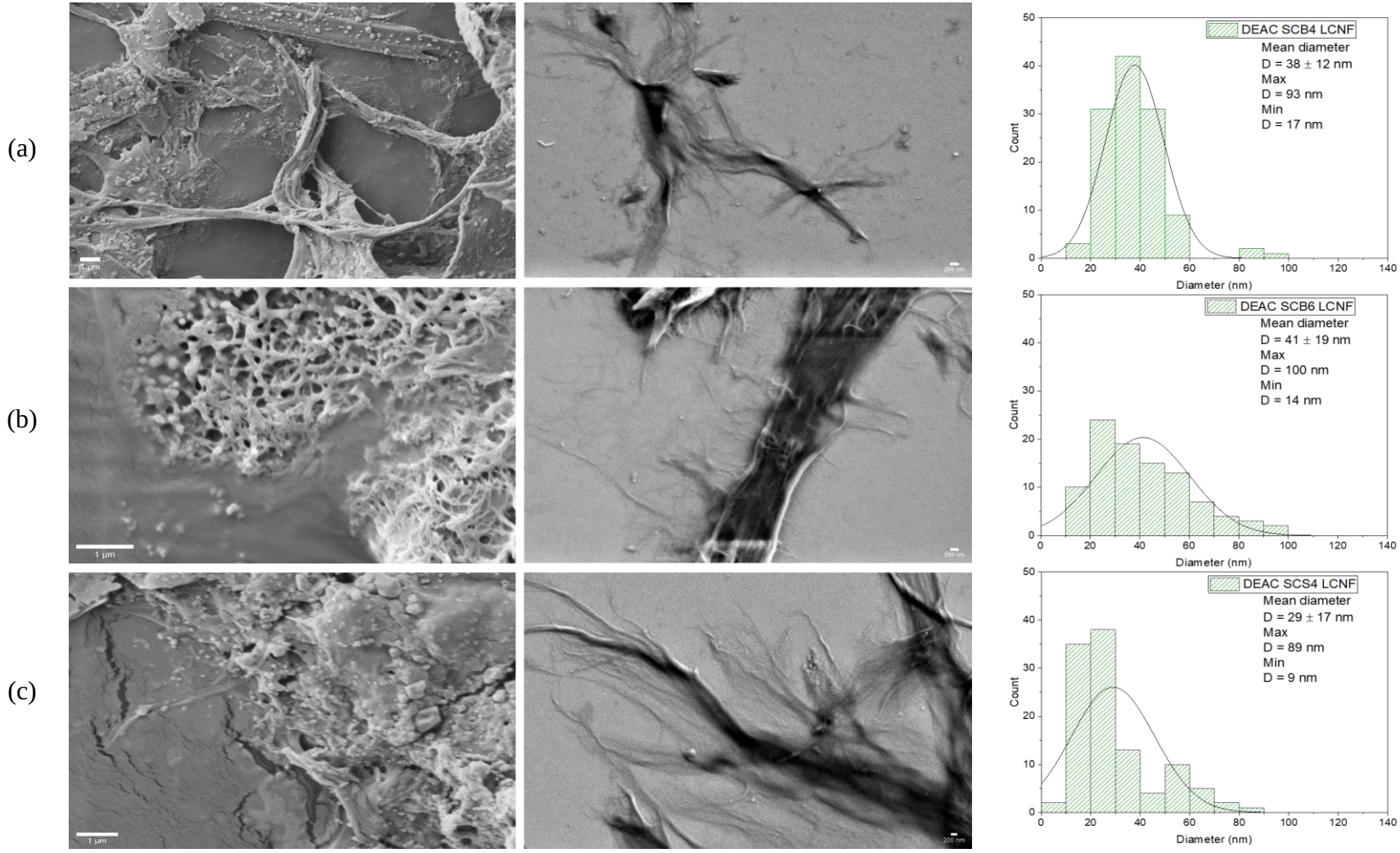

Fig. 33. SEM images and diameter distribution of LCNF cycle#10 obtained from pretreated materials (a) DEAC SCB4-EH, (b) DEAC SCB6-EH, and (c) DEAC SCS4-EH. (images on the left taken using traditional sample preparation, images on the right taken using negative contrast and ultrasonicated samples). Scale bar shows 1µm (*left*) and 200 nm (*right*)

Figure 32 shows the SEM images and diameter distribution obtained from DEAC SCB4 LCNC, DEAC SCB6 LCNC, and DEAC SCS4 LCNC. The measurements of the particle or fibril's width correlate with the nanocellulose's diameter (Mattos *et al.*, 2019). The analysis of the distribution of diameters shows that a mean diameter under 100nm was obtained for all three LCNC samples with values of 74 nm, 43nm, and 50 nm respectively for DEAC SCB4 LCNC, DEAC SCB6 LCNC, and DEAC SCS4 LCNC. However, a few particles in the range of 100 – 131 nm were also collected for DEAC SCB4 LCNC and DEAC SCB6 LCNC. This may indicate that the optimized condition of centrifugation was not sufficiently selective to isolate LCNC under 100 nm due to the myriad of particles from different lignocellulose fractions (lignin, hemicellulose, and cellulose). Indeed, Imani *et al.* (2019) employed a higher rotation speed to isolate different grades of uniform nanoparticles from LCNF suspensions, considering that a higher centrifuge force is necessary to fractionate a smaller distribution of sizes. Additionally, the morphology observed for most of the particles was spherical. Ribbon-like morphologies were not observed. Since lignin particles are also found to be spherical, it was not possible to correlate morphology with composition (Jiang *et al.*, 2020; Xuran Liu *et al.*, 2019; Marotti and Arantes, 2022; Nair *et al.*, 2018; Wei *et al.*, 2018), thereby constituting a limitation of the technique.

Figure 33 shows the distribution of diameters obtained for the three LCNF samples ultra-refined for ten cycles, when all samples had fines content over 90%. All three samples had a range of diameters smaller than 100 nm, which indicates a successful isolation of LCNFs. The mean diameter obtained for DEAC SCB4 LCNF, DEAC SCB6 LCNF, and DEAC SCS4 LCNF was 38 nm, 41nm, and 29 nm, respectively, which can be considered highly uniform even when different materials (SCB and SCS) were processed. This may be an interesting advantage of using the proposed sequential pretreatment to isolate LCNF with similar diameter from different feedstock sources.

Regarding the LCNF and lignin morphologies, because the LCNF contains a considerable portion of lignin, it was possible to identify the spherical from fibril-like particles. Appendix C shows a SEM image obtained from DEAC SCS4 LCNF and diameter distribution obtained from measurements taken from the spherical particles. The globular particles are likely to be lignin, although it had a diameter larger than expected within the range of 212 – 396 nm (APPENDIX C).

8.7 Mass balance

In order to evaluate the technical feasibility of isolating the bionanomaterials (LCNC and LCNF) together with sugars and sodium acetate, a mass balance of the final products from deacetylated, refined, and enzymatically hydrolyzed materials was made. The distribution between the coproducts based on the deacetylated material is shown in Figure 34, and the overall mass balance is shown in Figure 35.

Figure 34 shows that the multistep process generates a similar portfolio of products for the three pretreated materials. It was observed that the condition DEAC SCB6 produced slightly higher amount of LCNC and sugars than DEAC SCB4 and DEAC SCS4. Whether or not the increase in alkali loading on biomass for DEAC SCB6 compared DEAC SCB4 is justified needs to be evaluated based on a technoeconomic analysis and evaluation of the LCNC properties. Because almost 100% of mass was recovered for the three conditions tested, the process fulfills the requirement of full valorization of the biomass into products.

Figure 35 shows the mass balance analysis based in the starting materials (SCB and SCS) and highlights a great mass loss of SCS due to the necessity of reducing the high inorganics content. This amount of material rejected also needs to be evaluated together with a technoeconomic analysis and investigation of the properties of DEAC SCS4 LCNC and DEAC SCS4 LCNF. It is anticipated that a biorefinery using this process for SCS would need to be two times bigger than the one processing SCB.

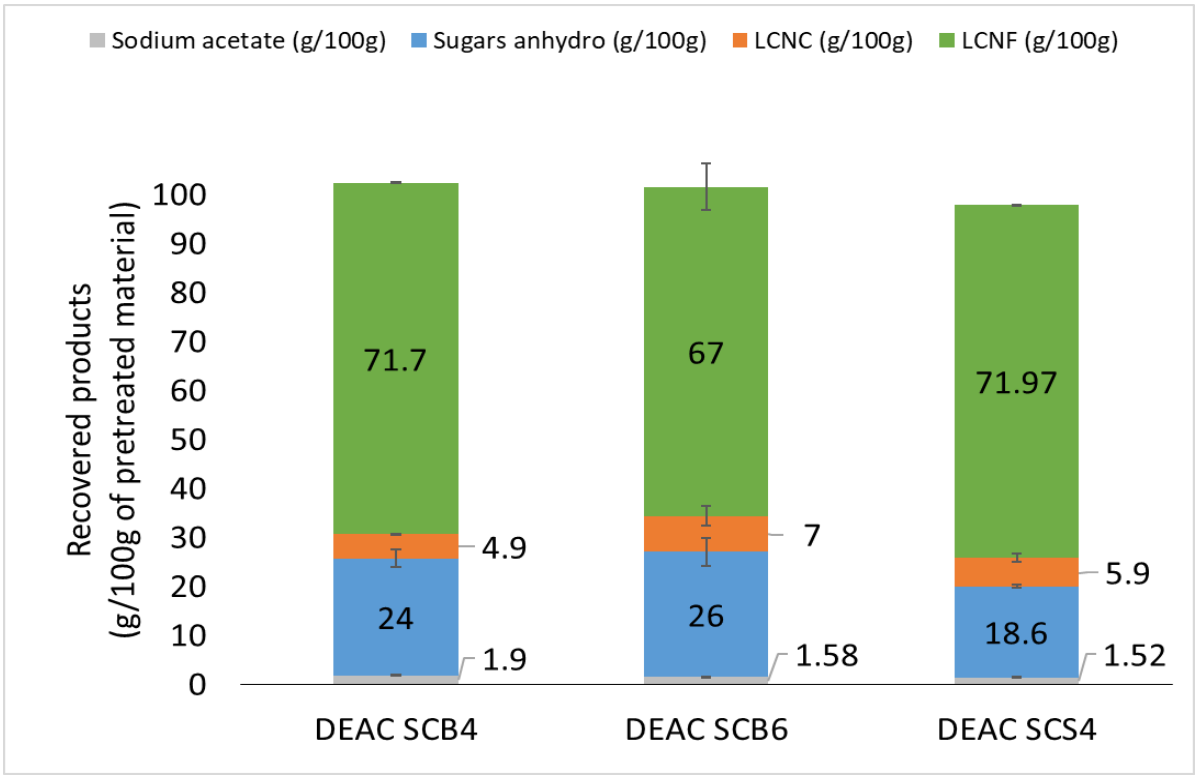

Fig. 34. Mass balance according to the yield obtained for sodium acetate, LCNC, LCNF, and total sugars based on deacetylated material.

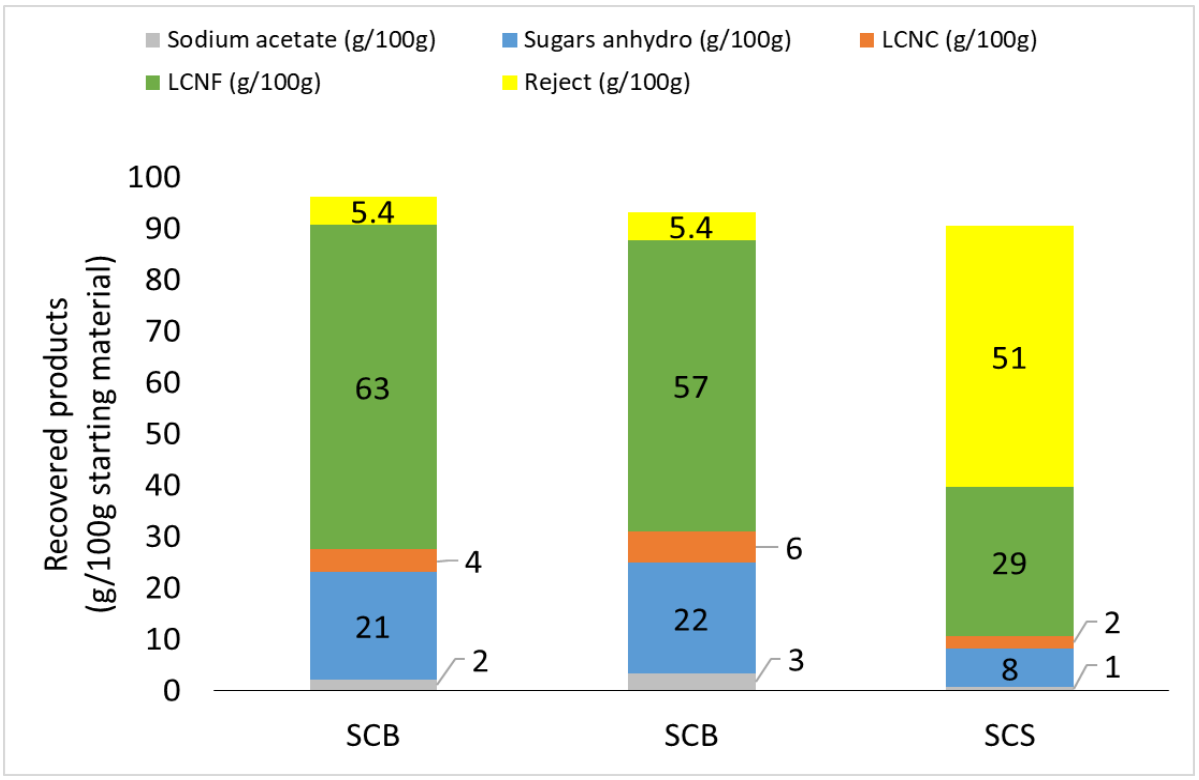

Fig. 35. Mass balance according to the yield obtained for sodium acetate, LCNC, LCNF, and total sugars based on starting material.

8.8 Conclusion

A multistep process was investigated to fractionate SCB and SCS and promote their integral valorization, with emphasis in isolating lignin containing nanocelluloses (LCNC and LCNF).

The method consisted of applying mild deacetylation, PFI refining, high-solids enzymatic hydrolysis followed by low-speed centrifugation of the CSR to recover LCNC, and ultra-refining the remaining CSR for the isolation of LCNF. The full valorization of the lignified biomasses was achieved because the pretreatment conditions were chosen to minimize the loss of biomass main fractions, hence streams could be upgraded into products. Thus, about 50 – 80% of acetyl groups were removed from SCB and SCS and recovered in the deacetylation liquor as sodium acetate. During the deacetylation step, there was limited lignin solubilization (up to 27% and 25% from SCB and SCS, respectively) and reduced sugar loss (xylan removal up to 4.6% and 11% from SCB and SCS, respectively, minimal glucan removal from SCB and up to 8% from SCS). The choice of deacetylation conditions was unconventional due to not targeting greater lignin solubilization that would favor sugar production (lignin removal of about 40 – 60%). However, the deacetylation conditions could be adjusted according to the biomass type to further improve the selectivity of the fractionation to produce nanocelluloses or higher amount of sugar, if desired. This versatilitiy of process conditions is important for a biorefinery, especially in the sugarcane industry sector to handle market changes. Additionally, this multi-step process has a competitive advantage of requiring low energy input to isolate LCNF compared to isolating LCNF and CNF from unbleached and bleached pulp, respectively. The remaining CSR after enzymatic hydrolysis had high fines (about 83.6 - 87.9%) that require ultra-refining steps only to uniformize the LCNF (mean diameter obtained in the range of 29 – 41 nm).

The multistep process stands as an approach for efficient utilisation of lignocellulosic materials and conversion into bioproducts rather than biofuels. The overall mass balance indicated that sodium acetate yielded 2 – 3 g/100g SCB and 1 g/100g SCB as a recoverable product. The sugars yielded 21 – 22 g/100g SCB and 8 g/100g SCS. The sugars stream recovered after high-solids enzymatic hydrolysis had total carbohydrates concentration of 40 – 43 $g.L^{-1}$ and 31.3 $g.L^{-1}$ obtained from SCB and SCS, respectively, and acetic acid concentration up to 4.0 $g.L^{-1}$ and 2.8 $g.L^{-1}$ for SCB and SCS, respectively, which facilitates fermentation of the sugar stream if desired. The LCNF yielded 57 – 53 g/100g SCB and 29 g/100g SCS and LCNC yielded 4 – 6 g/100g SCB and 2 g/100g SCS.

It is worth mentioning that there is not a standard for lignin containing nanocelluloses up to date and the lignin content required to classify a lignin containing nanocelluloses as high lignin containing has not been stabilished in the literature. Thus, we suggested the use of the L/G ratio as a reference. The recovered LCNCs and LCNFs had high lignin content of up to 43% and 31%, respectively. The LCNCs had the L/G ratio up to 2.4, which indicates a had higher lignin content than glucan content in its chemical composition (up to 2.4 times more). Thus, the recovered LCNCs were classified as high lignin-containing cellulose nanocrystals. The LCNFs had the L/G ratio up to 0.7 and were classified as lignin-containing cellulose nanofibrils.

CHAPTER 9 CHARACTERIZATION OF LCNC AND LCNF PRODUCED FROM SUGARCANE BAGASSE AND SUGARCANE STRAW

9.1 Introduction

The surface chemistry of nanocelluloses directly influences various properties and determines the compatibility with other polymers when producing nanocomposites. In Chapter 8, it was observed that sequential pretreatment steps can be tailored to selectively remove the desired fractions from the biomass feedstock. As a result, it was possible to obtain LCNC and LCNF using the enzymatic hydrolysis residue instead of converting cellulose to sugars at a greater yield. Moreover, a considerable amount of of lignin and residual fractions of xylan was retained in the nanocelluloses. According to Xuran Liu *et al.* (2019) who investigated similar mild alkaline pretreatment, the resultant lignin is native-like, and it may be connected to fractions of xylan. Lignin-containing nanocellulose combines the strength and biocompatibility of cellulose with the rigidity and hydrophobic nature of lignin, which may result in a versatile material with improved hydrophobicity and higher thermostability. Additionally, the considerable amount of xylan may confer an improved stability in aqueous solution. We hypothesize that native relationships between xylan and cellulose, and xylan and lignin may enhance the potential of LCNC and LCNF to have different properties due to the presence of various groups that may impart an amphiphilic type of surface interaction.

9.2 Zeta potential

Colloidal stability is determined by the presence of surface charges in a liquid medium. A stable suspension has enough surface charges leading to repulsive forces between the particles so that they do not coalesce. A larger overall intensity of the charged layer around a nanocellulose particle will prevent it to precipitate. The reference value is ±25 mV (Prathapan *et al.*, 2016).

Figure 36a shows that all three LCNC suspensions may be considered stable. The zeta potential value for DEAC SCB4 LCNC, DEAC SCB6 LCNC, and DEAC SCS4 LCNC was -34±5 mV, -39±7 mV, and -30±2 mV, respectively. This result can be considered an improvement comparatively to other enzymatic-CNCs, which generally tend to aggregate due to the preservation of the hydroxyl groups after the enzymes' action (Arantes *et al.* 2020). Figure 36b shows that the zeta potential changed only slightly with increasing ultra-refining cycles. The zeta potential value for DEAC SCB4 LCNF, DEAC SCB6 LCNF, and DEAC SCS4 LCNF was -28.1±0.3 mV, -38±2 mV, and -24±2 mV, respectively. This result may suggest that the extent of fibrillation is not contributing to a significant increase in the overall intensity of the charges.

Interestingly, the zeta potential results seem to be connected to the pretreament condition. Both LCNC and LCNF obtained from the deacetylation condition of 60 $mg.g^{-1}$ NaOH loading on biomass (DEAC SCB6) had the higher zeta potential, whereas LCNC and LCNC obtained by the deacetylation conditions of 40 $mg.g^{-1}$ NaOH loading on biomass (DEAC SCB4 and SCS4) had lower values. The suggested explanation for this behavior seems to go beyond solely the nanocelluloses' chemical composition (Table 23) and may be associated with the interactions between the remaining fractions of xylan and lignin and the nanocelluloses as well as its interaction in aqueous medium. That is because the xylan to glucan (X/G) ratio ranged between 0.61 – 0.69 and 0.52 – 0.61 for LCNCs and LCNFs, respectively, and the lignin to glucan (L/G) ration ranged between 1.59 – 2.42 and 0.65 – 0.74 for LCNCs and LCNFs, respectively. A possible explanation would be that the displacement of lignin fractions from the surface seem to be affecting the zeta potential results.

(a)

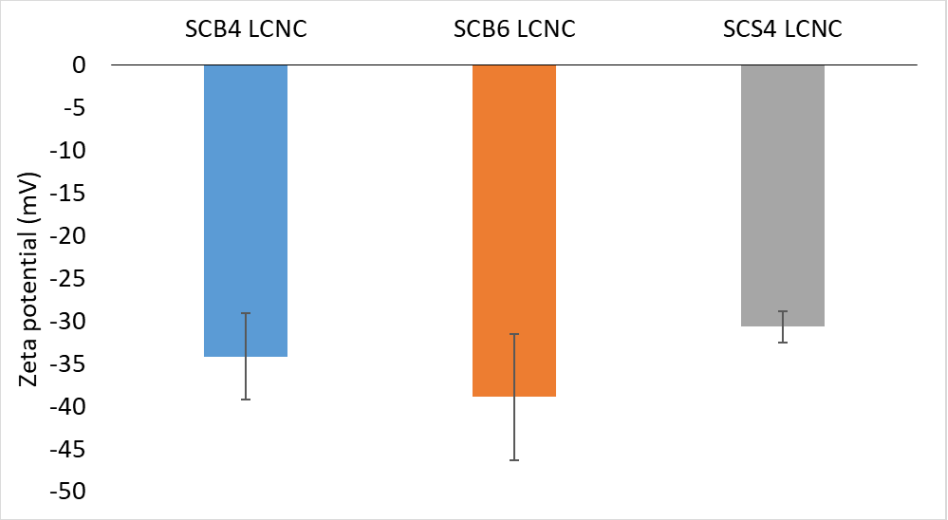

(b)

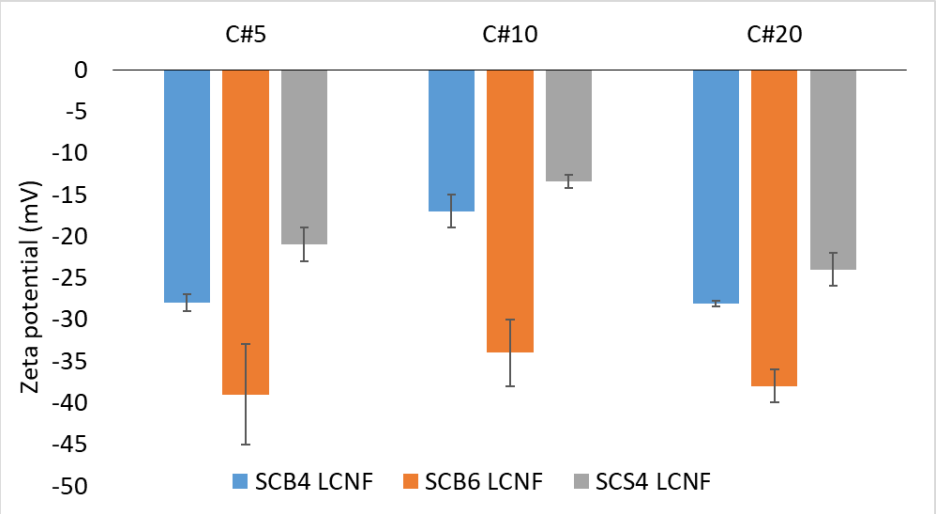

Fig. 36. Zeta potential estimated for nanocelluloses suspensions in deionized water at 0.03% solids constituted of (a) SCB4 LCNC, SCB6 LCNC, and SCS4 LCNC (b) SCB4 LCNF, SCB6 LCNF, and SCS4 LCNF during ultra-refining cycles #5, 10, and 20.

9.3 Water contact angle

The water contact angle indicates the surface wettability of CNF films. The film wettability can provide important information regarding its hydrophobicity, which can be evaluated by the initial contact angle (Figure 37) and the water adsorption over time (Figure 38).

Figure 37 shows that the initial contact angle varied between the samples of LCNCs, with higher value observed for DEAC SCS4 LCNC (CA of 81±13º) (Figure 37). On the other hand, the initial contact angle was somehow similar between the different samples of LCNF, being around 101±5º, 102±7º, 94±6º for DEAC SCB4 LCNF, DEAC SCB6 LCNF, and DEAC SCS4 LCNF, respectively.

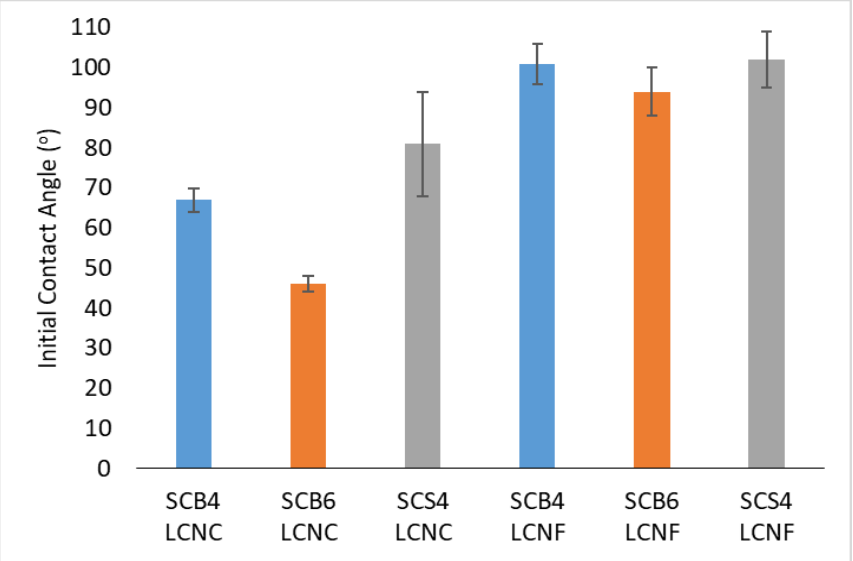

Fig. 37. Initial contact angle estimated for a drop of deionized water placed on the surface of SCB4 LCNC, SCB6 LCNC, SCS4 LCNC, SCB4 LCNF, SCB6 LCNF, and SCS4 LCNF.

Figure 38a shows that the LCNCs had a good barrier against water and had water drop adsorption after 300s, 512s, and 810s for DEAC SCB4 LCNC, DEAC SCB6 LCNC, and DEAC SCS4 LCNC, respectively. Conversely, the wettability of the three LCNF samples differed greatly (Figure 38b). The water drop was adsorbed within 14s, 210s, and 660s for DEAC SCB4 LCNF, DEAC SCB6 LCNF, and DEAC SCS4 LCNF, respectively.

These results suggest a correlation between the nanocelluloses' content of lignin and the wettability. That is, the DEAC SCS4 LCNF had the highest lignin content between the three samples analyzed and it exhibited the highest initial contact angles. Similarly, the DEAC SCS4 LCNC, which had the highest lignin content, also had the longest time for water adsorption. Moreover, the LCNCs analyzed here had higher hydrophobicity and lower wettability than a

LCNC with similar lignin composition reported in literature (48.6% Klason lignin, CA average 10s of 68.7º) (Wei *et al.*, 2018).

(a)

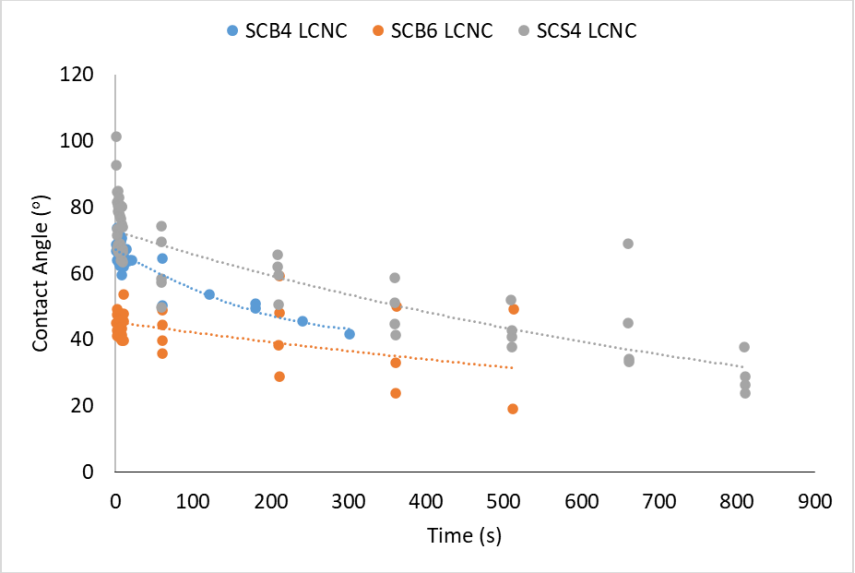

(b)

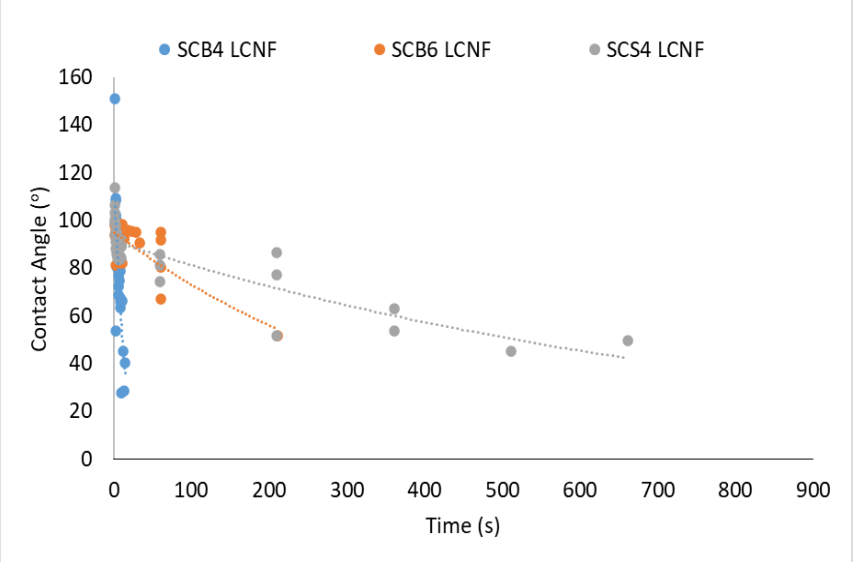

Fig. 38. Dynamic contact angle evaluated by water adsorption kinetics and measured until the water drop disappearance for (a) SCB4 LCNC, SCB6 LCNC, and SCS4 LCNC (b) SCB4 LCNF, SCB6 LCNF, and SCS4 LCNF.

9.4 Thermogravimetric Analysis (TGA)

The thermostability of the nanocellulose films was evaluated by thermogravimetric analysis (TGA) under a nitrogen atmosphere up to 700°C. A higher stability is generally

attributed to the presence of a higher lignin content due to the various aromatic groups and chemical bonds that usually decompose at a higher temperature range than carbohydrates (xylan and cellulose). The thermal degradation stages and mass loss data are shown on Table 24. It was observed that the LCNFs had higher initial temperature of degradation (T*onset*) and higher temperature of maximum degradation (T*max*) than LCNCs samples. Since the LCNCs had a higher lignin content and higher lignin to glucan (L/G) ratio, a parameter other than chemical composition seems to be playing a role. On the other hand, when comparing LCNF samples obtained from different sources, it was observed that the T*max* for SCB4 LCNF, SCB6 LCNF, and SCS4 LCNF were slightly superior to UBK LCNF, indicating that these materials are stable at higher temperatures although they initiate the degradation earlier.

Table 24. Thermal degradation stages and mass loss for LCNC and LCNF from different sources.

Nanocellulose	T*onset* (ºC)	T*max* (ºC)	T (ºC) at 10% weight loss	T (ºC) at 50% weight loss	Residue (%)
SCB4 LCNC	217 ± 1	292 ± 2	206 ± 17	306 ± 5	25 ± 1
SCB6 LCNC	220 ± 10	288 ± 5	197 ± 27	303 ± 7	4 ± 0.1
SCS4 LCNC	241 ± 1	293 ± 3	229 ± 19	322 ± 6	17 ± 10
SCB4 LCNF	280.2 ± 0.7	336.84 ± 0.03	246 ± 2	325.33 ± 0.01	14.7 ± 0.5
SCB6 LCNF	284 ± 4	334 ± 3	240 ± 23	327 ± 5	17 ± 4
SCS4 LCNF	284 ± 1	335.4 ± 0.4	255.9 ± 0.3	326.8 ± 0.2	13.3 ± 1
UBK LCNF	297 ± 2	330 ± 1	264 ± 13	332 ± 2	15 ± 7
NBSK CNF	289 ± 2	318 ± 2	263 ± 9	323.2 ± 0.7	14 ± 8

T*onset*: initial temperature of degradation; T*max*: temperature of maximum degradation; Residue: residual weight at 700°C.

9.5 Conclusion

The properties of lignin-containing nanocelluloses, LCNC and LCNF, were studied based on the surface chemistry of the particles in suspension or as films.

The zeta potential results indicate that the LCNC and LCNF suspensions were stable, which may prevent common aggregation problems of enzyme-CNC and -CNF.

The contact angle results showed promising hydrophobicity. LCNCs stood out for their low wettability, varying 300s to 810s, although the initial contact agle varied from 46º to 81º.

On the other hand, LCNFs films had high initial contact angle, varying 96º to 102º, but the wettability varied according to the sample source (14s to 660s). Overall, the LCNC and LCNF obtained from SCB DEAC4 had the highest wettability, and LCNC and LCNF obtained from SCB DEAC6 had the lowest initial contact angle. Lignin containing nanocelluloses obtained from SCS DEAC4 seems to be the most promising sample, with the highest initial contact angle (81º and 101º for LCNC and LCNF, respectively) and lower wettability (660s and 810s for LCNC and LCNF, respectively), showing a promising potential to be used in applications that require hydrophobicity such as compatibilization with commercial polymers to formulate nanocomposites.

The LCNCs and LCNFs also exhibited good thermostability. However, the increase in thermalstability was not proportional to the lignin content as expected. In terms of temperature of maximum degradation (T_{max}), LCNCs had T_{max} of 288 – 293 ºC and LCNFs had of T_{max} 334 – 337 ºC.

Although the LCNC and LCNF isolated in the multistep process from SCB and SCS presented remarkable characteristics, the correlation between chemical composition and properties was not obvious. Further studies are necessary to investigate how the remaining biomass main fractions as well as the types of bonds may affect the hydrophobicity and thermostability properties and even enhance it.

CHAPTER 10 FINAL REMARKS

We investigated the coproduction of cellulosic sugars and cellulose nanomaterials produced from three different feedstocks (one non-lignified and wood-derived, and two being lignified and non-wood-derived). A combined enzymatic-mechanical approach served as a platform to integrate the nanocelluloses isolation (CNC and CNF, or LCNC and LCNF) and production of cellulose sugars. This approach was thoroughly investigated using efficient saccharification enzyme cocktails (Cellic CTec2 and Cellic CTec3/HTec3) that defined the carbohydrates conversion and yield of each coproduct. Ultimately, the mass balance of each condition investigated was used to demonstrate the valorization of the starting raw material. Ultimately, we have developed an approach for biorefineries based on cellulosic ethanol to shift to bionanoproducts.

Chapter 5 established a perspective that the pulp and paper industry could be the primary supplier of nanocelluloses in the future, given its cellulose-rich pulp production, availability of subproducts, and refining expertise with CNF trials and use of enzymes. Conversely, sugarcane biorefineries were identified as having enormous potential for nanocellulose production from agricultural subproducts. The enzyme cost equation analysis was introduced as a valuable tool, suggesting a breakeven point for viable nanocellulose integration. This chapter stabilished the mass ratio of 50:50 as an important parameter for the integration of nanocelluloses.

Chapter 6 delved into optimizing the yield of cellulose nanocrystals (CNC) through enzyme-assisted treatments with Cellic CTec2, exploring different degress of cellulose conversion. Despite challenges in improving CNC yield, that remained low, the study discussed the mode of action of a complete saccharification enzyme cocktail to understand the CNC isolation. It also presented alternatives to reduce operational and capital expenses, such as using

tap water and ambient temperature during CNC isolation by centrifugation. These findings contribute to understanding the technical feasibility of CNC production, emphasizing cost-effective approaches.

Chapter 7 extended the investigation of **Chapter 6** with the coproduction of cellulose nanofibrils (CNF) from cellulosic solid residue (CSR). We have demonstrated that the coproduction of CNF by ultra-refining the remaining CSR is technically feasible and allowed the full valorization of HBKP with a potential cost reduction by using tap water. The mass balance and cumulative energy measurements suggested the energy-saving potential of up to 80%, with an emphasis on the trade-off between CNF yield, energy input, and sugars titer. The analysis of a preliminary projected revenue based on the mass balance obtained, using a simplified ratio of income/expenditure, suggested that higher CNF yields could be more economically viable than higher cellulosic sugars yield when starting from wood-pulp such as hardwood bleached kraft pulp (HBKP). This adds a question of the use of mass ratio of 50:50 there is a focus on nanocelluloses production, and the starting raw material has a price, which may be the case for pulp and paper industry.

Chapter 8 introduced a multistep process for the integral valorization of sugarcane bagasse (SCB) and straw (SCS) to isolate lignin-containing nanocelluloses (LCNC and LCNF), cellulosic sugars, and sodium acetate. The method, involving deacetylation, enzymatic hydrolysis, and ultra-refining, achieved full valorization of the materials by minimizing biomass fraction loss during the pretreatment steps. The process required a low energy input to isolate nanocelluloses, which may present a competitive advantage over other methods. Additionally, we suggested use of the L/G ratio as a reference for high lignin-containing nanocelluloses contributes as an alterinative to classify to lignin-containing nanocelluloses.

Chapter 9 focused on studying the properties of LCNC and LCNF, emphasizing properties such as suspension stability, hydrophobicity, and thermostability. The promising

results of LCNC and LCNF both as suspension and films, especially for the nanocelluloses obtained from SCS DEAC4, suggest a potential for applications in which hydrophobicity is needed. We also highlighted the need for further investigations into how biomass main fractions (chemical composition) and bond types influence these three properties that are essential to produce nanocomposites.

REFERENCES

Abd El-Sayed, E.S., El-Sakhawy, M., El-Sakhawy, M.A.M., 2020. Non-wood fibers as raw material for pulp and paper industry. Nord Pulp Paper Res J 35, 215–230. https://doi.org/10.1515/NPPRJ-2019-0064/MACHINEREADABLECITATION/RIS

Aguayo, M.G., Pérez, A.F., Reyes, G., Oviedo, C., Gacitúa, W., Gonzalez, R., Uyarte, O., 2018. Isolation and characterization of cellulose nanocrystals from rejected fibers originated in the Kraft Pulping process. Polymers (Basel) 10. https://doi.org/10.3390/polym10101145

Ålander, E., Östlund, I., Lindgren, K., Johansson, M., Gimåker, M., 2017. Towards a more-cost-efficient paper and board making using microfibrillated cellulose, in: 7th Nordic Wood Biorefinery Conference (NWBC). RISE Bioeconomy, Stockholm.

Albarelli, J., Paidosh, A., Santos, D.T., Maréchal, F., Meireles, M.A.A., 2016. Environmental , energetic and economic evaluation of implementing a supercritical fluid-based nanocellulose production process in a sugarcane biorefinery. Chem Eng Trans 47, 49–54. https://doi.org/10.3303/CET1647009

Alonso-Lerma, B., Barandiaran, L., Ugarte, L., Larraza, I., Reifs, A., Olmos-Juste, R., Barruetabeña, N., Amenabar, I., Hillenbrand, R., Eceiza, A., Perez-Jimenez, R., 2020. High performance crystalline nanocellulose using an ancestral endoglucanase. Commun Mater 1. https://doi.org/10.1038/s43246-020-00055-5

Alwani, M.S., Khalil, H.P.S.A., Asniza, M., Suhaily, S.S., Amiranajwa, A.S.N., Jawaid, M., 2014. Agricultural Biomass Raw Materials: The Current State and Future Potentialities, in: Hakeem, K.R., Jawaid, Mohammad, Rashid, U. (Eds.), Biomass and Bioenergy. Springer International Publishing, Cham, pp. 77–100. https://doi.org/10.1007/978-3-319-07641-6_5

Anderson, S.R., Esposito, D., Gillette, W., Zhu, J.Y., Baxa, U., Mcneil, S.E., 2014. Enzymatic preparation of nanocrystalline and microcrystalline cellulose. Tappi J 13, 35–42. https://doi.org/10.1021/ic50013a030

Ankerfors, M., Lindström, T., Henriksson, G., 2009. Method for the manufacture of microfibrillated cellulose. US 2009/0221812 A1.

Arantes, V., Dias, I.K.R., Berto, G.L., Pereira, B., Marotti, B.S., Nogueira, C.F.O., 2020. The current status of the enzyme-mediated isolation and functionalization of nanocelluloses: production, properties, techno-economics, and opportunities. Cellulose 2020 27:18 27, 10571–10630. https://doi.org/10.1007/S10570-020-03332-1

Arantes, V., Gourlay, K., Saddler, J.N., 2014. The enzymatic hydrolysis of pretreated pulp fibers predominantly involves “peeling/erosion” modes of action. Biotechnol Biofuels 7. https://doi.org/10.1186/1754-6834-7-87

Arantes, V., Saddler, J.N., 2011. Cellulose accessibility limits the effectiveness of minimum cellulase loading on the efficient hydrolysis of pretreated lignocellulosic substrates. Biotechnol Biofuels 4, 1–17. https://doi.org/10.1186/1754-6834-4-3/FIGURES/7

Arantes, V., Saddler, J.N., 2010. Access to cellulose limits the efficiency of enzymatic hydrolysis: The role of amorphogenesis. Biotechnol Biofuels 3, 1–11. https://doi.org/10.1186/1754-6834-3-4/FIGURES/2

Beltramino, F., Roncero, M.B., Vidal, T., Torres, A.L., Valls, C., 2015. Increasing yield of nanocrystalline cellulose preparation process by a cellulase pretreatment. Bioresour Technol 192, 574–581. https://doi.org/10.1016/j.biortech.2015.06.007

Berto, G.L., Arantes, V., 2019. Kinetic changes in cellulose properties during defibrillation into microfibrillated cellulose and cellulose nanofibrils by ultra-refining. Int J Biol Macromol 127, 637–648. https://doi.org/10.1016/j.ijbiomac.2019.01.169

Berto, G.L., Mattos, B.D., Rojas, O.J., Arantes, V., 2021. Single-Step Fiber Pretreatment with Monocomponent Endoglucanase: Defibrillation Energy and Cellulose Nanofibril Quality. ACS Sustain Chem Eng 9, 2260–2270. https://doi.org/10.1021/acssuschemeng.0c08162

Beyene, D., Chae, M., Dai, J., Danumah, C., Tosto, F., Demesa, A.G., Bressler, D.C., 2017. Enzymatically-Mediated Coproduction of Cellulose Nanocrystals and Fermentable Sugars. Catalysts 7, 322. https://doi.org/10.3390/catal7110322

Bian, H., Dong, M., Chen, L., Zhou, X., Ni, S., Fang, G., Dai, H., 2019. Comparison of mixed enzymatic pretreatment and post-treatment for enhancing the cellulose nanofibrillation efficiency. Bioresour Technol 293, 122171. https://doi.org/10.1016/J.BIORTECH.2019.122171

Bissaro, B., Rohr, A.K., Skaugen, M., Forsberg, Z., Horn, S.J., Vaaje-Kolstad, G., Eijsink, V., 2016. Fenton-type chemistry by a copper enzyme: molecular mechanism of polysaccharide oxidative cleavage. bioRxiv 1–14. https://doi.org/10.1101/097022

Bonaccorso, F., Zerbetto, M., Ferrari, A.C., Amendola, V., 2013. Sorting nanoparticles by centrifugal fields in clean media. Journal of Physical Chemistry C 117, 13217–13229. https://doi.org/10.1021/jp400599g

Bondancia, T.J., Florencio, C., Baccarin, G.S., Farinas, C.S., 2022. Cellulose nanostructures obtained using enzymatic cocktails with different compositions. Int J Biol Macromol 207, 299–307. https://doi.org/10.1016/j.ijbiomac.2022.03.007

Bondancia, T.J., Mattoso, L.H.C., Marconcini, J.M., Farinas, C.S., 2017. A new approach to obtain cellulose nanocrystals and ethanol from eucalyptus cellulose pulp via the biochemical pathway. Biotechnol Prog 33, 1085–1095. https://doi.org/10.1002/btpr.2486

Brinchi, L., Cotana, F., Fortunati, E., Kenny, J.M., 2013. Production of nanocrystalline cellulose from lignocellulosic biomass: Technology and applications. Carbohydr Polym 94, 154–169. https://doi.org/10.1016/j.carbpol.2013.01.033

Buranov, A.U., Mazza, G., 2008a. Lignin in straw of herbaceous crops. Ind Crops Prod 28, 237–259. https://doi.org/10.1016/J.INDCROP.2008.03.008

Buranov, A.U., Mazza, G., 2008b. Lignin in straw of herbaceous crops. Ind Crops Prod. https://doi.org/10.1016/j.indcrop.2008.03.008

Camargo, L.A., Pereira, S.C., Correa, A.C., Farinas, C.S., Marconcini, J.M., Mattoso, L.H.C., 2016. Feasibility of Manufacturing Cellulose Nanocrystals from the Solid Residues of Second-Generation Ethanol Production from Sugarcane Bagasse. Bioenergy Res 9, 894–906. https://doi.org/10.1007/s12155-016-9744-0

Carpio, L.G.T., Souza, F.S. de, 2019. Competition between Second-Generation Ethanol and Bioelectricity using the Residual Biomass of Sugarcane: Effects of Uncertainty on the Production Mix. Molecules 24, 1–15. https://doi.org/10.3390/molecules24020369

Carpita, N.C., 1996. Structure and biogenesis of the cell walls of grasses, Annu. Rev. Plant Physiol. Plant Mol. Biol.

Carpita, N.C., Gibeaut, D.M., 1993. Structural models of primary cell walls in flowering plants: Consistency of molecular structure with the physical properties of the walls during growth. Plant Journal 3, 1–30. https://doi.org/10.1111/J.1365-313X.1993.TB00007.X

Carvalho, D.M. de, Queiroz, J.H. de, Colodette, J.L., 2016. Assessment of alkaline pretreatment for the production of bioethanol from eucalyptus, sugarcane bagasse and sugarcane straw. Ind Crops Prod 94, 932–941. https://doi.org/10.1016/j.indcrop.2016.09.069

Carvalho, D.M. de, Sevastyanova, O., Penna, L.S., Silva, B.P. da, Lindström, M.E., Colodette, J.L., 2015. Assessment of chemical transformations in eucalyptus, sugarcane bagasse and straw during hydrothermal, dilute acid, and alkaline pretreatments. Ind Crops Prod 73, 118–126. https://doi.org/10.1016/j.indcrop.2015.04.021

Castro, R.C. de A., Fonseca, B.G., dos Santos, H.T.L., Ferreira, I.S., Mussatto, S.I., Roberto, I.C., 2017. Alkaline deacetylation as a strategy to improve sugars recovery and ethanol production from rice straw hemicellulose and cellulose. Ind Crops Prod 106, 65–73. https://doi.org/10.1016/j.indcrop.2016.08.053

Cebreiros, F., Seiler, S., Dalli, S.S., Lareo, C., Saddler, J., 2021. Enhancing cellulose nanofibrillation of eucalyptus Kraft pulp by combining enzymatic and mechanical pretreatments. Cellulose 28, 189–206. https://doi.org/10.1007/s10570-020-03531-w

Chauve, G., Bras, J., 2014. Industrial Point of View of Nanocellulose Materials and Their Possible Applications, in: Handbook of Green Materials. pp. 233–252. https://doi.org/10.1142/9789814566469_0014

Chen, L., Wang, Q., Hirth, K., Baez, C., Agarwal, U.P., Zhu, J.Y., 2015. Tailoring the yield and characteristics of wood cellulose nanocrystals (CNC) using concentrated acid hydrolysis. Cellulose 22, 1753–1762. https://doi.org/10.1007/s10570-015-0615-1

Chen, Xiaoquan, Deng, X., Shen, W., Jiang, L., 2012. Enzymolysis preparation of NCC, BioResources.

Chen, X., Kuhn, E., Nagle, N., Nelson, R., Tao, L., Crawford, N., Tucker, M., 2018. Recycling of dilute deacetylation black liquor to enable efficient recovery and reuse of spent chemicals and biomass pretreatment waste. Front Energy Res 6, 384126. https://doi.org/10.3389/FENRG.2018.00051/BIBTEX

Chen, X., Kuhn, E., Wang, W., Park, S., Flanegan, K., Trass, O., Tenlep, L., Tao, L., Tucker, M., 2013. Comparison of different mechanical refining technologies on the enzymatic

digestibility of low severity acid pretreated corn stover. Bioresour Technol 147, 401–408. https://doi.org/10.1016/J.BIORTECH.2013.07.109

Chen, X., Shekiro, J., Elander, R., Tucker, M., 2011. Improved xylan hydrolysis of corn stover by deacetylation with high solids dilute acid pretreatment. Ind Eng Chem Res 51, 70–76. https://doi.org/10.1021/IE201493G

Chen, Xiaowen, Shekiro, J., Franden, M.A., Wang, W., Zhang, M., Kuhn, E., Johnson, D.K., Tucker, M.P., 2012a. The impacts of deacetylation prior to dilute acid pretreatment on the bioethanol process. Biotechnol Biofuels 5. https://doi.org/10.1186/1754-6834-5-8

Chen, X., Shekiro, J., Pschorn, T., Sabourin, M., Tao, L., Elander, R., Park, S., Jennings, E., Nelson, R., Trass, O., Flanegan, K., Wang, W., Himmel, M.E., Johnson, D., Tucker, M.P., 2014. A highly efficient dilute alkali deacetylation and mechanical (disc) refining process for the conversion of renewable biomass to lower cost sugars. Biotechnol Biofuels 7, 1–12. https://doi.org/10.1186/1754-6834-7-98/TABLES/5

Chen, X., Shekiro, J., Pschorn, T., Sabourin, M., Tucker, M.P., Tao, L., 2015. Techno-economic analysis of the deacetylation and disk refining process: Characterizing the effect of refining energy and enzyme usage on minimum sugar selling price and minimum ethanol selling price. Biotechnol Biofuels 8, 1–13. https://doi.org/10.1186/S13068-015-0358-0/FIGURES/5

Chen, Xiaowen, Tao, L., Shekiro, J., Mohaghaghi, A., Decker, S., Wang, W., Smith, H., Park, S., Himmel, M.E., Tucker, M., 2012b. Improved ethanol yield and reduced minimum ethanol selling price (MESP) by modifying low severity dilute acid pretreatment with deacetylation and mechanical refining: 1 Experimental. Biotechnol Biofuels 5, 1–10. https://doi.org/10.1186/1754-6834-5-60/TABLES/3

Chen, X., Wang, W., Ciesielski, P., Trass, O., Park, S., Tao, L., Tucker, M.P., 2016. Improving Sugar Yields and Reducing Enzyme Loadings in the Deacetylation and Mechanical Refining (DMR) Process through Multistage Disk and Szego Refining and Corresponding Techno-Economic Analysis. ACS Sustain Chem Eng 4, 324–333. https://doi.org/10.1021/acssuschemeng.5b01242

Chen, X.-Q., Deng, X.-Y., Shen, W.-H., Jia, M.-Y., 2018. Preparation and characterization of the spherical nanosized cellulose by the enzymatic hydrolysis of pulp fibers. Carbohydr Polym 181, 879–884. https://doi.org/10.1016/J.CARBPOL.2017.11.064

Chen, X.Q., Deng, X.Y., Shen, W.H., Jia, M.Y., 2018. Preparation and characterization of the spherical nanosized cellulose by the enzymatic hydrolysis of pulp fibers. Carbohydr Polym 181, 879–884. https://doi.org/10.1016/j.carbpol.2017.11.064

Chen, X.Q., Pang, G.X., Shen, W.H., Tong, X., Jia, M.Y., 2019. Preparation and characterization of the ribbon-like cellulose nanocrystals by the cellulase enzymolysis of cotton pulp fibers. Carbohydr Polym 207, 713–719. https://doi.org/10.1016/J.CARBPOL.2018.12.042

Chen, X.-Q., Pang, G.-X., Shen, W.-H., Tong, X., Jia, M.-Y., 2019. Preparation and characterization of the ribbon-like cellulose nanocrystals by the cellulase enzymolysis of

cotton pulp fibers. Carbohydr Polym 207, 713–719. https://doi.org/10.1016/J.CARBPOL.2018.12.042

Chieng, B.W., Lee, S.H., Ibrahim, N.A., Then, Y.Y., Loo, Y.Y., 2017. Isolation and characterization of cellulose nanocrystals from oil palm mesocarp fiber. Polymers (Basel) 9, 1–11. https://doi.org/10.3390/polym9080355

Coelho, S.T., Goldemberg, J., Lucon, O., Guardabassi, P., 2006. Brazilian sugarcane ethanol: lessons learned. Energy for Sustainable Development 10, 26–39. https://doi.org/10.1016/S0973-0826(08)60529-3

Copenhaver, K., Li, K., Lamm, M.E., Walker, C., Johnson, D., Han, Y., Wang, L., Zhao, X., Pu, Y., Hinton, H., Tekinalp, H., Bhagia, S., Ragauskas, A.J., Gardner, D.J., Ozcan, S., 2021. Recycled cardboard containers as a low energy source for cellulose nanofibrils and their use in poly(l -lactide) nanocomposites. ACS Sustain Chem Eng 9, 13460–13470. https://doi.org/10.1021/acssuschemeng.1c03890

Corrêa, A.C., de Teixeira, E.M., Pessan, L.A., Mattoso, L.H.C., 2010. Cellulose nanofibers from curaua fibers. Cellulose 17, 1183–1192. https://doi.org/10.1007/s10570-010-9453-3

Cosgrove, D.J., 2014. Re-constructing our models of cellulose and primary cell wall assembly. Curr Opin Plant Biol 22, 122–131. https://doi.org/10.1016/J.PBI.2014.11.001

Cui, S., Zhang, S., Ge, S., Xiong, L., Sun, Q., 2016. Green preparation and characterization of size-controlled nanocrystalline cellulose via ultrasonic-assisted enzymatic hydrolysis. Ind Crops Prod 83, 346–352. https://doi.org/10.1016/j.indcrop.2016.01.019

Dai, J., Chae, M., Beyene, D., Danumah, C., Tosto, F., Bressler, D.C., 2018. Coproduction of cellulose nanocrystals and fermentable sugars assisted by endoglucanase treatment of wood pulp. Materials 11. https://doi.org/10.3390/ma11091645

Davis, R., Bartling, A., Tao, L., 2021. Biochemical conversion of lignocellulosic biomass to hydrocarbon fuels and products: 2020 state of technology and future research, National Renewable Energy Lab. (NREL). Golden, CO (United States). https://doi.org/10.2172/1784889

Davis, R., Grundl, N., Tao, L., Biddy, M.J., Tan, E.C.D., Beckham, G.T., Humbird, D., Thompson, D.N., Roni, M.S., 2018. Process Design and Economics for the Conversion of Lignocellulosic Biomass to Hydrocarbon Fuels and Coproducts: 2018 Biochemical Design Case Update: Biochemical Deconstruction and Conversion of Biomass to Fuels and Products via Integrated Biorefinery Pathways.

de Aguiar, J., Bondancia, T.J., Claro, P.I.C., Mattoso, L.H.C., Farinas, C.S., Marconcini, J.M., 2020. Enzymatic Deconstruction of Sugarcane Bagasse and Straw to Obtain Cellulose Nanomaterials. ACS Sustain Chem Eng 8, 2287–2299. https://doi.org/10.1021/acssuschemeng.9b06806

de Amorim dos Santos, A., Silva, M.J.F. e, Scatolino, M.V., Durães, A.F.S., Dias, M.C., Damásio, R.A.P., Tonoli, G.H.D., 2023. Comparison of pre-treatments mediated by endoglucanase and TEMPO oxidation for eco-friendly low-cost energy production of

cellulose nanofibrils. Environmental Science and Pollution Research 30, 4934–4948. https://doi.org/10.1007/s11356-022-22575-y

de Assis, C.A., Houtman, C., Phillips, R., Bilek, E.M.T., Rojas, O.J., Pal, L., Peresin, M.S., Jameel, H., Gonzalez, R., 2017a. Conversion Economics of Forest Biomaterials: Risk and Financial Analysis of CNC Manufacturing. Biofuels, Bioproducts and Biorefining 11, 682–700. https://doi.org/10.1002/bbb.1782

de Assis, C.A., Iglesias, M.C., Bilodeau, M., Johnson, D., Phillips, R., Peresin, M.S., Bilek, E.M.T., Rojas, O.J., Venditti, R., Gonzalez, R., 2017b. Cellulose micro- and nanofibrils (CMNF) manufacturing - financial and risk assessment. Biofuels, Bioproducts and Biorefining 12, 251–264. https://doi.org/10.1002/bbb.1835

de Assis, T., Huang, S., Driemeier, C.E., Donohoe, B.S., Kim, C., Kim, S.H., Gonzalez, R., Jameel, H., Park, S., 2018. Toward an understanding of the increase in enzymatic hydrolysis by mechanical refining. Biotechnol Biofuels 11, 1–11. https://doi.org/10.1186/S13068-018-1289-3/FIGURES/6

de Campos, A., Correa, A.C., Cannella, D., de M Teixeira, E., Marconcini, J.M., Dufresne, A., Mattoso, L.H.C., Cassland, P., Sanadi, A.R., 2013. Obtaining nanofibers from curauá and sugarcane bagasse fibers using enzymatic hydrolysis followed by sonication. Cellulose 20, 1491–1500. https://doi.org/10.1007/s10570-013-9909-3

de Oliveira Júnior, S.D., Asevedo, E.A., de Araújo, J.S., Brito, P.B., dos Santos Cruz Costa, C.L., de Macedo, G.R., dos Santos, E.S., 2022. Enzymatic extract of Aspergillus fumigatus CCT 7873 for hydrolysis of sugarcane bagasse and generation of cellulose nanocrystals (CNC). Biomass Convers Biorefin 12, 5515–5526. https://doi.org/10.1007/s13399-020-01020-5

del Río, J.C., Lino, A.G., Colodette, J.L., Lima, C.F., Gutiérrez, A., Martínez, Á.T., Lu, F., Ralph, J., Rencoret, J., 2015. Differences in the chemical structure of the lignins from sugarcane bagasse and straw. Biomass Bioenergy 81, 322–338. https://doi.org/10.1016/J.BIOMBIOE.2015.07.006

Delepierre, G., Vanderfleet, O.M., Niinivaara, E., Zakani, B., Cranston, E.D., 2021. Benchmarking Cellulose Nanocrystals Part II: New Industrially Produced Materials. Langmuir 37, 8393–8409. https://doi.org/10.1021/acs.langmuir.1c00550

Delgado-Aguilar, M., Tarrés, Q., Puig, J., Boufi, S., Blanco, Á., Mutjé, P., 2015. Enzymatic Refining and Cellulose Nanofiber Addition in Papermaking Processes from Recycled and Deinked Slurries, Biorefining & CNF.

Dence, Carlton W., 1992. The Determination of Lignin, in: Lin, S.Y., Dence, C.W. (Eds.), Springer Series in Wood Science; Methods in Lignin Chemistry. Berlin, pp. 33–58. https://doi.org/10.1007/978-3-662-03898-7

Dias, M.O. de S., 2011. Desenvolvimento e otimização de processos de produção de etanol de primeira e segunda geração e eletricidade a partir da cana-de-açúcar. Universidade Estadual de Campinas.

Dias, M.O.S., Junqueira, T.L., Rossell, C.E. V., MacIel Filho, R., Bonomi, A., 2013. Evaluation of process configurations for second generation integrated with first generation bioethanol production from sugarcane. Fuel Processing Technology 109, 84–89. https://doi.org/10.1016/j.fuproc.2012.09.041

Dias, M.O.S., Junqueira, T.L., Sampaio, I.L.M., Chagas, M.F., Watanabe, M.D.B., Morais, E.R., Gouveia, V.L.R., Klein, B.C., Rezende, M.C.A.F., Cardoso, T.F., Souza, A., Jesus, C.D.F., Pereira, L.G., Rivera, E.C., Filho, R.M., Bonomi, A., 2016. Use of the VSB to Assess Biorefinery Strategies, in: Bonomi, A., Cavalett, O., Pereira da Cunha, M., Lima, M.A.P. (Eds.), Virtual Biorefinery - An Optimization Strategy for Renewable Carbon Valorization, Green Energy and Technology. Springer International Publishing, Campinas - SP, Brazil, pp. 189–256. https://doi.org/10.1007/978-3-319-26045-7

Dimarogona, M., Topakas, E., Christakopoulos, P., 2012. Cellulose degradation by oxidative enzymes. Comput Struct Biotechnol J 2, 1–8. https://doi.org/10.5936/csbj.201209015

Diop, C.I.K., Tajvidi, M., Bilodeau, M.A., Bousfield, D.W., Hunt, J.F., 2017. Isolation of lignocellulose nanofibrils (LCNF) and application as adhesive replacement in wood composites: example of fiberboard. Cellulose 24, 3037–3050. https://doi.org/10.1007/s10570-017-1320-z

Espinosa, E., Sánchez, R., Otero, R., Domínguez-Robles, J., Rodríguez, A., 2017. A comparative study of the suitability of different cereal straws for lignocellulose nanofibers isolation. Int J Biol Macromol 103, 990–999. https://doi.org/10.1016/j.ijbiomac.2017.05.156

Espinosa, E., Tarrés, Q., Delgado-Aguilar, M., González, I., Mutjé, P., Rodríguez, A., 2016. Suitability of wheat straw semichemical pulp for the fabrication of lignocellulosic nanofibres and their application to papermaking slurries. Cellulose 23, 837–852. https://doi.org/10.1007/s10570-015-0807-8

European Technology and Innovation Platform (ETIP) Bioenergy, 2020. Current status of advanced biofuels demonstrations in Europe - Production Facilities https://www.etipbioenergy.eu/databases/production-facilities (accessed 6.5.21).

Faostat, 2020. World Food and Agriculture: Statistical Yearbook 2020. https://www.fao.org/faostat/en/%3F%23data/FBS (accessed 9.7.21).

Food and Agriculture Organization (FAO), 2021. Pulp and paper capacities, survey 2020-2025. Rome, Italy. p. 218. https://doi.org/10.4060/cb7300t (accessed 9.7.21).

Feng, Y.H., Cheng, T.Y., Yang, W.G., Ma, P.T., He, H.Z., Yin, X.C., Yu, X.X., 2018. Characteristics and environmentally friendly extraction of cellulose nanofibrils from sugarcane bagasse. Ind Crops Prod 111, 285–291. https://doi.org/10.1016/j.indcrop.2017.10.041

Fengel, D., 1970. The ultrastructure of cellulose from wood - Part 2: Problems of the isolation of cellulose. Wood Sci Technol 4, 15–35. https://doi.org/10.1007/BF00356234/METRICS

Fengel, D., 1969. The ultrastructure of cellulose from wood - Part 1: Wood as the basic material for the isolation of cellulose. Wood Sci Technol 3, 203–217. https://doi.org/10.1007/BF00367212/METRICS

Fengel, D., Wegener, G., 1983. Wood: Chemistry, ultrastructure, reactions, Wood: Chemistry, Ultrastructure, Reactions. DE GRUYTER, Berlin, New York. https://doi.org/10.1515/9783110839654

Ferdous, T., Ni, Y., Quaiyyum, M.A., Uddin, M.N., Jahan, M.S., 2021. Non-wood fibers: relationships of fiber properties with pulp properties. ACS Omega 6, 21613–21622. https://doi.org/10.1021/ACSOMEGA.1C02933/ASSET/IMAGES/MEDIUM/AO1C02933_M014.GIF

Filson, P.B., Dawson-Andoh, B.E., Schwegler-Berry, D., 2009. Enzymatic-mediated production of cellulose nanocrystals from recycled pulp. Green Chemistry 11, 1808–1814. https://doi.org/10.1039/b915746h

Galbe, M., Wallberg, O., 2019. Pretreatment for biorefineries: A review of common methods for efficient utilisation of lignocellulosic materials. Biotechnol Biofuels. https://doi.org/10.1186/s13068-019-1634-1

García, A., Labidi, J., Belgacem, M.N., Bras, J., 2017. The nanocellulose biorefinery: woody versus herbaceous agricultural wastes for NCC production. Cellulose 24, 693–704. https://doi.org/10.1007/s10570-016-1144-2

Ghose, T.K., 1987. Measurement of cellulase activities. Pure and Applied Chemistry 59, 257–268. https://doi.org/10.1351/PAC198759020257/MACHINEREADABLECITATION/RIS

Glass, N.L., Schmoll, M., Cate, J.H.D., Coradetti, S., 2013. Plant cell wall deconstruction by ascomycete fungi. Annu Rev Microbiol 67, 477–98. https://doi.org/10.1146/annurev-micro-092611-150044

Global Market Insights GMI, 2023. Nanocellulose Market Share 2023-2032-Global Analysis Report 0–416.

Grabber, J.H., 2005. How do lignin composition, structure, and cross-linking affect degradability? A review of cell wall model studies, in: Crop Science. pp. 820–831. https://doi.org/10.2135/cropsci2004.0191

Halappanavar, S., Ede, J.D., Mahapatra, I., Krug, H.F., Kuempel, E.D., Lynch, I., Vandebriel, R.J., Shatkin, J.A., 2021. A methodology for developing key events to advance nanomaterial-relevant adverse outcome pathways to inform risk assessment. Nanotoxicology 15, 289–310. https://doi.org/10.1080/17435390.2020.1851419

Hartman, R.R., 1985. Mechanical treatment of pulp fibers for paper property development. Papermaking Raw Materials 413–442. https://doi.org/10.15376/frc.1985.1.413

Hatfield, R., Vermerris, W., 2001. Update on Lignification Lignin Formation in Plants. The Dilemma of Linkage Specificity.

He, M., Yang, G., Chen, J., Ji, X., Wang, Q., 2018. Production and Characterization of Cellulose Nanofibrils from Different Chemical and Mechanical Pulps. https://doi.org/10.1080/02773813.2017.1411368 38, 149–158. https://doi.org/10.1080/02773813.2017.1411368

Heiskanen, I., Backfolk, K., Vehvilainen, M., Kamppuri, T., Nousianen, P., 2012. Process for the production of microfibrillated cellulose and produced microfibrillated cellulose. US 2012/0136146A1.

Henriksson, M., Henriksson, G., Berglund, L.A., Lindström, T., 2007. An environmentally friendly method for enzyme-assisted preparation of microfibrillated cellulose (MFC) nanofibers. Eur Polym J 43, 3434–3441. https://doi.org/10.1016/j.eurpolymj.2007.05.038

Henríquez-Gallegos, S., Albornoz-Palma, G., Andrade, A., Soto, C., Pereira, M., 2021. Impact of the enzyme charge on the production and morphological features of cellulose nanofibrils. Polymers (Basel) 13. https://doi.org/10.3390/polym13193238

Henrissat, B., 1991. A classification of glycosyl hydrolases based on amino acid sequence similarities. Biochem J 280 (Pt 2, 309–16. https://doi.org/10.1007/s007920050009

Henrissat, B., Davies, G., 1997. Structural and sequence-based classification of glycoside hydrolases. Curr Opin Struct Biol 7, 637–44. https://doi.org/10.1016/S0959-440X(97)80072-3

Hideno, A., Inoue, H., Tsukahara, K., Fujimoto, S., Minowa, T., Inoue, S., Endo, T., Sawayama, S., 2009. Wet disk milling pretreatment without sulfuric acid for enzymatic hydrolysis of rice straw. Bioresour Technol 100, 2706–2711. https://doi.org/10.1016/j.biortech.2008.12.057

Hiltunen, J., Katariina, K., Pere, J., 2015. Process for producing fibrillated cellulose material. WO 2015/092146 Al.

Hoeger, I.C., Nair, S.S., Ragauskas, A.J., Deng, Y., Rojas, O.J., Zhu, J.Y., 2013. Mechanical deconstruction of lignocellulose cell walls and their enzymatic saccharification. Cellulose 20, 807–818. https://doi.org/10.1007/s10570-013-9867-9

Hon, D.N. -S, 1979. Formation and behavior of mechanoradicals in pulp cellulose. J Appl Polym Sci 23, 1487–1499. https://doi.org/10.1002/app.1979.070230519

Horn, S.J., Vaaje-Kolstad, G., Westereng, B., Eijsink, V.G., 2012. Novel enzymes for the degradation of cellulose. Biotechnol Biofuels 5, 45. https://doi.org/10.1186/1754-6834-5-45

Hu, C., Zhao, Y., Li, K., Zhu, J.Y., Gleisner, R., 2015. Optimizing cellulose fibrillation for the production of cellulose nanofibrils by a disk grinder. Holzforschung 69, 993–1000. https://doi.org/10.1515/hf-2014-0219

Hubbe, M.A., Rojas, O.J., Lucia, L.A., Sain, M., 2008. Cellulosic nanocomposites: A review. Bioresources 3, 929–980.

Humbird, D., Davis, R., Tao, L., Kinchin, C., Hsu, D., Aden, A., Shoen, P., Lukas, J., Olthof, B., Worley, M., Sexton, D., Dudgeon, D., 2011. Process Design and Economics for Biochemical Conversion of Lignocellulosic Biomass to Ethanol. Golden, CO.

Humbird, D., Mohagheghi, A., Dowe, N., Schell, D.J., 2010. Economic impact of total solids loading on enzymatic hydrolysis of dilute acid pretreated corn stover. Biotechnol Prog 26, 1245–1251. https://doi.org/10.1002/btpr.441

Hurmekoski, E., Lovrić, M., Lovrić, N., Hetemäki, L., Winkel, G., 2019. Frontiers of the forest-based bioeconomy – A European Delphi study. For Policy Econ 102, 86–99. https://doi.org/10.1016/J.FORPOL.2019.03.008

Imani, M., Ghasemian, A., Dehghani-Firouzabadi, M.R., Afra, E., Borghei, M., Johansson, L.S., Gane, P.A.C., Rojas, O.J., 2019. Coupling nanofibril lateral size and residual lignin to tailor the properties of lignocellulose films. Adv Mater Interfaces 6. https://doi.org/10.1002/admi.201900770

Inalbon, M.C., Montagna, P.N., Galván, M.V., Demonte, L., Zanuttini, M.A., 2013. Wood capillarity and deacetylation during Eucalyptus alkaline impregnation. Sulphidity effects and comparison between transverse directions. Holzforschung 67, 41–46. https://doi.org/10.1515/HF-2012-0030/HTML

Independent Commodity Intelligence Services (ICIS), 2018. Americas Chemicals Outlook 109.

International Energy Agency (IEA) Task 39, 2020. Commercializing liquid biofuels - Database [WWW Document]. URL https://demoplants.best-research.eu/ (accessed 6.5.21).

International Organization for Standardization, 2005. ISO/TC 229 - Nanotechnologies [WWW Document]. URL https://www.iso.org/committee/381983.html (accessed 9.21.21).

Isogai, A., Saito, T., Fukuzumi, H., 2011. TEMPO-oxidized cellulose nanofibers. Nanoscale. https://doi.org/10.1039/c0nr00583e

Iwamoto, S., Nakagaito, A.N., Yano, H., 2007. Nano-fibrillation of pulp fibers for the processing of transparent nanocomposites. Appl Phys A Mater Sci Process 89, 461–466. https://doi.org/10.1007/s00339-007-4175-6

Jakes, J.E., Zelinka, S.L., Hunt, C.G., Ciesielski, P., Frihart, C.R., Yelle, D., Passarini, L., Gleber, S.C., Vine, D., Vogt, S., 2020. Measurement of moisture-dependent ion diffusion constants in wood cell wall layers using time-lapse micro X-ray fluorescence microscopy. Scientific Reports 2020 10:1 10, 1–11. https://doi.org/10.1038/s41598-020-66916-8

Ji, H., Xiang, Z., Qi, H., Han, T., Pranovich, A., Song, T., 2019. Strategy towards one-step preparation of carboxylic cellulose nanocrystals and nanofibrils with high yield, carboxylation and highly stable dispersibility using innocuous citric acid. Green Chemistry 21, 1956–1964. https://doi.org/10.1039/C8GC03493A

Jiang, J., Carrillo-Enríquez, N.C., Oguzlu, H., Han, X., Bi, R., Saddler, J.N., Sun, R.C., Jiang, F., 2020. Acidic deep eutectic solvent assisted isolation of lignin containing nanocellulose from thermomechanical pulp. Carbohydr Polym 247, 116727. https://doi.org/10.1016/J.CARBPOL.2020.116727

Jiang, J., Chen, Xi, Chen, Xiaowen, Ren, Z.J., 2022. Energy-efficient microbial electrochemical lignin and alkaline hydroxide recovery from DMR black liquor. Resour Conserv Recycl 186, 106529. https://doi.org/10.1016/J.RESCONREC.2022.106529

Junyuan, Y., 2017. Manufacturing of nanocrystalline cellulose (Master' thesis). Aalto University, Espoo.

Kafle, K., Shin, H., Lee, C.M., Park, S., Kim, S.H., 2015. Progressive structural changes of Avicel, bleached softwood and bacterial cellulose during enzymatic hydrolysis. Scientific Reports 2015 5:1 5, 1–10. https://doi.org/10.1038/srep15102

Kangas, H., Pere, J., 2016. High-consistency enzymatic fibrillation (HefCel) - a cost-efficient way to produce cellulose nanofibrils (CNF). Advanced Materials: TechConnect Briefs 2016 1, 181–183.

Karp, E.M., Resch, M.G., Donohoe, B.S., Ciesielski, P.N., O'Brien, M.H., Nill, J.E., Mittal, A., Biddy, M.J., Beckham, G.T., 2015. Alkaline Pretreatment of Switchgrass. ACS Sustain Chem Eng 3, 1479–1491. https://doi.org/10.1021/acssuschemeng.5b00201

Kazi, F.K., Fortman, J.A., Anex, R.P., Hsu, D.D., Aden, A., Dutta, A., Kothandaraman, G., 2010. Techno-economic comparison of process technologies for biochemical ethanol production from corn stover. Fuel 89, S20–S28. https://doi.org/10.1016/j.fuel.2010.01.001

Kelly, P. V., Gardner, D.J., Gramlich, W.M., 2021. Optimizing lignocellulosic nanofibril dimensions and morphology by mechanical refining for enhanced adhesion. Carbohydr Polym 273, 118566. https://doi.org/10.1016/J.CARBPOL.2021.118566

Khatiwada, D., Leduc, S., Silveira, S., McCallum, I., 2016. Optimizing ethanol and bioelectricity production in sugarcane biorefineries in Brazil. Renew Energy 85, 371–386. https://doi.org/10.1016/J.RENENE.2015.06.009

Klemm, D., Cranston, E.D., Fischer, D., Gama, M., Kedzior, S.A., Kralisch, D., Kramer, F., Kondo, T., Lindström, T., Nietzsche, S., Petzold-welcke, K., Rauchfuß, F., Association, P.J., 2018. Nanocellulose as a natural source for groundbreaking applications in materials science : Today ' s state. Materials Today 21, 720–748. https://doi.org/10.1016/j.mattod.2018.02.001

Kortschot, M., 1997. The role of the fibre in the structural hierarchy of paper. The Fundametals of Papermaking Materials 351–399. https://doi.org/10.15376/frc.1997.1.351

Lam, N.T., Chollakup, R., Smitthipong, W., Nimchua, T., Sukyai, P., 2017. Characterization of Cellulose Nanocrystals Extracted from Sugarcane Bagasse for Potential Biomedical Materials. Sugar Tech 19, 539–552. https://doi.org/10.1007/s12355-016-0507-1

Leão, R.M., Miléo, P.C., Maia, J.M.L.L., Luz, S.M., 2017. Environmental and technical feasibility of cellulose nanocrystal manufacturing from sugarcane bagasse. Carbohydr Polym 175, 518–529. https://doi.org/10.1016/j.carbpol.2017.07.087

Lee, H. V., Hamid, S.B.A., Zain, S.K., 2014. Conversion of lignocellulosic biomass to nanocellulose: Structure and chemical process. Scientific World Journal 2014. https://doi.org/10.1155/2014/631013

Leistritz, F.L., Senechal, D.M., Stowers, M.D., McDonald, W.F., Saffron, C.M., Hodur, N.M., 2006. Preliminary feasibility analysis for an integrated biomaterials and ethanol biorefinery using wheat straw feedstock. Agribusiness Applied Economics Report 48.

Leu, S.Y., Zhu, J.Y., 2013. Substrate-Related factors affecting enzymatic saccharification of lignocelluloses: our recent understanding. Bioenergy Res 6, 405–415. https://doi.org/10.1007/S12155-012-9276-1/METRICS

Li, M., Pu, Y., Ragauskas, A.J., 2016. Current understanding of the correlation of lignin structure with biomass recalcitrance. Front Chem. https://doi.org/10.3389/fchem.2016.00045

Lima, C.S., Rabelo, S.C., Ciesielski, P.N., Roberto, I.C., Rocha, G.J.M., Driemeier, C., 2018. Multiscale Alterations in Sugar Cane Bagasse and Straw Submitted to Alkaline Deacetylation. ACS Sustain Chem Eng 6, 3796–3804. https://doi.org/10.1021/acssuschemeng.7b04158

Lindström, T., 2017. Aspects on nanofibrillated cellulose (NFC) processing, rheology and NFC-film properties. Curr Opin Colloid Interface Sci 29, 68–75. https://doi.org/10.1016/j.cocis.2017.02.005

Liu, X., Jiang, Y., Qin, C., Yang, S., Song, X., Wang, S., Li, K., 2018. Enzyme-assisted mechanical grinding for cellulose nanofibers from bagasse: energy consumption and nanofiber characteristics. Cellulose 25, 7065–7078. https://doi.org/10.1007/s10570-018-2071-1

Liu, Xiuyu, Jiang, Y., Song, X., Qin, C., Wang, S., Li, K., 2019. A bio-mechanical process for cellulose nanofiber production – Towards a greener and energy conservation solution. Carbohydr Polym 208, 191–199. https://doi.org/10.1016/j.carbpol.2018.12.071

Liu, Xuran, Li, Y., Ewulonu, C.M., Ralph, J., Xu, F., Zhang, Q., Wu, M., Huang, Y., 2019. Mild Alkaline Pretreatment for Isolation of Native-Like Lignin and Lignin-Containing Cellulose Nanofibers (LCNF) from Crop Waste. ACS Sustain Chem Eng 7, 14135–14142. https://doi.org/10.1021/ACSSUSCHEMENG.9B02800/ASSET/IMAGES/MEDIUM/SC9B02800_M003.GIF

Liu, Yuxin, Liu, Yanxue, Wang, Z., Peng, J., 2014. Bagasse pentosans hydrolysis, BioResources.

Long, L., Tian, D., Hu, J., Wang, F., Saddler, J., 2017. A xylanase-aided enzymatic pretreatment facilitates cellulose nanofibrillation. Bioresour Technol 243, 898–904. https://doi.org/10.1016/j.biortech.2017.07.037

Lynd, L.R., Liang, X., Biddy, M.J., Allee, A., Cai, H., Foust, T., Himmel, M.E., Laser, M.S., Wang, M., Wyman, C.E., 2017. Cellulosic ethanol: status and innovation. Curr Opin Biotechnol 45, 202–211. https://doi.org/10.1016/j.copbio.2017.03.008

Macrelli, S., Mogensen, J., Zacchi, G., 2012. Techno-economic evaluation of 2nd generation bioethanol production from sugar cane bagasse and leaves integrated with the sugar-based ethanol process. Biotechnol Biofuels 5, 22. https://doi.org/10.1186/1754-6834-5-22

Malucelli, L.C., Matos, M., Jordão, C., Lacerda, L.G., Carvalho Filho, M.A.S., Magalhães, W.L.E., 2018. Grinding severity influences the viscosity of cellulose nanofiber (CNF) suspensions and mechanical properties of nanopaper. Cellulose 25, 6581–6589. https://doi.org/10.1007/s10570-018-2031-9

Mansfield, S.D., Mooney, C., Saddler, J.N., 1999. Substrate and enzyme characteristics that limit cellulose hydrolysis. Biotechnol Prog 15, 804–816. https://doi.org/10.1021/BP9900864

Marotti, B.D.S., Arantes, V., 2022. Ultra-refining for the production of long-term highly pH-stable lignin nanoparticles in high yield with high uniformity. Green Chemistry 24, 1238–1258. https://doi.org/10.1039/D1GC03525H

Martelli-Tosi, M., Torricillas, M. da S., Martins, M.A., Assis, O.B.G. de, Tapia-Blácido, D.R., 2016. Using Commercial Enzymes to Produce Cellulose Nanofibers from Soybean Straw. J Nanomater 2016, 1–10. https://doi.org/10.1155/2016/8106814

Mattos, B.D., Tardy, B.L., Rojas, O.J., 2019. Accounting for Substrate Interactions in the Measurement of the Dimensions of Cellulose Nanofibrils. Biomacromolecules 20, 2657–2665. https://doi.org/10.1021/ACS.BIOMAC.9B00432/ASSET/IMAGES/LARGE/BM-2019-004329_0006.JPEG

Meier, H., 1962. Chemical and morphological aspects of the fine structure of wood. Pure and Applied Chemistry 5, 37–52. https://doi.org/10.1351/PAC196205010037/MACHINEREADABLECITATION/RIS

Meyabadi, T.F., Dadashian, F., 2012. Optimization of enzymatic hydrolysis of waste cotton fibers for nanoparticles production using response surface methodology. Fibers and Polymers 13, 313–321. https://doi.org/10.1007/S12221-012-0313-7/METRICS

Miller, G.L., 1959. Use of dinitrosalicylic acid reagent for determination of reducing sugar. Anal Chem 31, 426–428. https://doi.org/10.1021/AC60147A030/ASSET/AC60147A030.FP.PNG_V03

Miller, J., 2019. Nanocellulose: packaging applications and commercial development, in: 2019 International Conference on Nanotechnology for Renewable Materials. TAPPI NANO Division, Chiba, Japan.

Ministério de Minas e Energia do Brasil (MME), 2016. Setor sucroenergético no brasil - uma visão para 2030. São Paulo.

Modenbach, A.A., Nokes, S.E., 2013. Enzymatic hydrolysis of biomass at high-solids loadings – A review. Biomass Bioenergy 56, 526–544. https://doi.org/10.1016/j.biombioe.2013.05.031

Mok, Y.K., Arantes, V., Saddler, J.N., 2015. A NaBH4 Coupled Ninhydrin-Based Assay for the Quantification of Protein/Enzymes During the Enzymatic Hydrolysis of Pretreated Lignocellulosic Biomass. Appl Biochem Biotechnol 176, 1564–1580. https://doi.org/10.1007/S12010-015-1662-7/FIGURES/8

Moon, D., Kitagawa, N., Sagisaka, M., Genchi, Y., 2015. Economic Impact of Utilizing Woody Biomass to Manufacture High Value-Added Material Products: a Study of Cellulose

Nanofiber and High Standard Chip-Dust Production in Maniwa, Japan. Journal of the Japan Institute of Energy 94, 582–587. https://doi.org/10.3775/JIE.94.582

Moon, R., Hensdal, C.L., Beck, S., Fall, A., Costa, J., Kojima, E., Abitbol, T., Raghuwanshi, V., Walker, C., 2023. Setting priorities in CNF particle size measurement: What is needed vs. what is feasible. Tappi J 22, 116–137.

Murciano Martínez, P., Punt, A.M., Kabel, M.A., Gruppen, H., 2016. Deconstruction of lignin linked p-coumarates, ferulates and xylan by NaOH enhances the enzymatic conversion of glucan. Bioresour Technol 216, 44–51. https://doi.org/10.1016/j.biortech.2016.05.040

Nagl, M., Haske-Cornelius, O., Skopek, L., Pellis, A., Bauer, W., Nyanhongo, G.S., Guebitz, G., 2021. Biorefining: the role of endoglucanases in refining of cellulose fibers. Cellulose 28, 7633–7650. https://doi.org/10.1007/s10570-021-04022-2

Nair, S.S., Chen, H., Peng, Y., Huang, Y., Yan, N., 2018. Polylactic Acid Biocomposites Reinforced with Nanocellulose Fibrils with High Lignin Content for Improved Mechanical, Thermal, and Barrier Properties. ACS Sustain Chem Eng 6, 10058–10068. https://doi.org/10.1021/ACSSUSCHEMENG.8B01405/SUPPL_FILE/SC8B01405_SI_001.PDF

Nakagaito, A.N., Yano, H., 2004. The effect of morphological changes from pulp fiber towards nano-scale fibrillated cellulose on the mechanical properties of high-strength plant fiber based composites. Appl Phys A Mater Sci Process 78, 547–552. https://doi.org/10.1007/s00339-003-2453-5

Nechyporchuk, O., Belgacem, M.N., Bras, J., 2016. Production of cellulose nanofibrils: A review of recent advances. Ind Crops Prod 93, 2–25. https://doi.org/10.1016/j.indcrop.2016.02.016

Nechyporchuk, O., Pignon, F., Belgacem, M.N., 2014. Morphological properties of nanofibrillated cellulose produced using wet grinding as an ultimate fibrillation process. J Mater Sci 50, 531–541. https://doi.org/10.1007/s10853-014-8609-1

Negrão, D.R., Grandis, A., Buckeridge, M.S., Rocha, G.J.M., Leal, M.R.L.V., Driemeier, C., 2021. Inorganics in sugarcane bagasse and straw and their impacts for bioenergy and biorefining: A review. Renewable and Sustainable Energy Reviews. https://doi.org/10.1016/j.rser.2021.111268

Nelson, K., Retsina, R., 2014. Innovative nanocellulose process breaks the cost barrier. Tappi J 13, 19–23.

Nelson, K.., Retsina, T., 2014. Innovative nanocellulose process breaks the cost barrier. Tappi J 13, 19–23.

Newman, R.H., Vaidya, A.A., Imroz Sohel, M., Jack, M.W., 2013. Optimizing the enzyme loading and incubation time in enzymatic hydrolysis of lignocellulosic substrates. Bioresour Technol 129, 33–38. https://doi.org/10.1016/j.biortech.2012.11.028

Nguyen, Q.A., Dickow, J.H., Duff, B.W., Farmer, J.D., Glassner, D.A., Ibsen, K.N., Ruth, M.F., Schell, D.J., Thompson, I.B., Tucker, M.P., 1996. NREL/DOE ethanol pilot-plant:

Current status and capabilities. Bioresour Technol 58, 189–196. https://doi.org/10.1016/S0960-8524(96)00098-3

N.J. Heyn, A., 1969. The elementary fibril and supermolecular structure of cellulose in soft wood fiber. J Ultrastruct Res 26, 52–68. https://doi.org/10.1016/S0022-5320(69)90035-5

Nova Cana, 2014. Disponibilidade de bagaço e palha para os processos de hidrólise 4–7.

Paajanen, A., Ceccherini, S., Maloney, T., Ketoja, J.A., 2019. Chirality and bound water in the hierarchical cellulose structure. Cellulose 26, 5877–5892. https://doi.org/10.1007/S10570-019-02525-7/TABLES/3

Pääkko, M., Ankerfors, M., Kosonen, H., Nykänen, A., Ahola, S., Österberg, M., Ruokolainen, J., Laine, J., Larsson, P.T., Ikkala, O., Lindström, T., 2007a. Enzymatic hydrolysis combined with mechanical shearing and high-pressure homogenization for nanoscale cellulose fibrils and strong gels. Biomacromolecules 8, 1934–1941. https://doi.org/10.1021/bm061215p

Pääkko, M., Ankerfors, M., Kosonen, H., Nykänen, A., Ahola, S., Österberg, M., Ruokolainen, J., Laine, J., Larsson, P.T., Ikkala, O., Lindström, T., 2007b. Enzymatic hydrolysis combined with mechanical shearing and high-pressure homogenization for nanoscale cellulose fibrils and strong gels. Biomacromolecules 8, 1934–1941. https://doi.org/10.1021/BM061215P/ASSET/IMAGES/MEDIUM/BM061215PN00001.GIF

Padella, M., O'Connell, A., Prussi, M., 2019. What is still Limiting the Deployment of Cellulosic Ethanol? Analysis of the Current Status of the Sector. Applied Sciences 2019, Vol. 9, Page 4523 9, 4523. https://doi.org/10.3390/APP9214523

Park, S., Venditti, R.A., Abrecht, D.G., Jameel, H., Pawlak, J.J., Lee, J.M., 2007. Surface and pore structure modification of cellulose fibers through cellulase treatment. J Appl Polym Sci 103, 3833–3839. https://doi.org/10.1002/APP.25457

Patil, R., Genco, J., Pendse, H., van Heiningen, A., 2017. Process for producing acetic acid in hardwood kraft pulp mills. Tappi J 16, 287–300.

Patil, R., Hermant, P., Genco, J., van Heininguen, A., 2015. Treating kraft mill extract using bipolar membrane electrodialysis for the production of acetic acid. Tappi J 15, 215–226.

Payne, C.M., Knott, B.C., Mayes, H.B., Hansson, H., Himmel, M.E., Sandgren, M., Ståhlberg, J., Beckham, G.T., 2015. Fungal cellulases. Chem Rev 115, 1308–448. https://doi.org/10.1021/cr500351c

Penttilä, P.A., Várnai, A., Pere, J., Tammelin, T., Salmén, L., Siika-aho, M., Viikari, L., Serimaa, R., 2013. Xylan as limiting factor in enzymatic hydrolysis of nanocellulose. Bioresour Technol 129, 135–141. https://doi.org/10.1016/J.BIORTECH.2012.11.017

Pere, J., Tammelin, T., Niemi, P., Lille, M., Virtanen, T., Penttilä, P.A., Ahvenainen, P., Grönqvist, S., 2020. Production of High Solid Nanocellulose by Enzyme-Aided Fibrillation Coupled with Mild Mechanical Treatment. ACS Sustain Chem Eng 8, 18853–18863. https://doi.org/10.1021/acssuschemeng.0c05202

Pereira, B., Arantes, V., 2020. Production of cellulose nanocrystals integrated into a biochemical sugar platform process via enzymatic hydrolysis at high solid loading. Ind Crops Prod 152. https://doi.org/10.1016/j.indcrop.2020.112377

Pereira, B., Marcondes, W.F., Carvalho, W., Arantes, V., 2021. High yield biorefinery products from sugarcane bagasse: Prebiotic xylooligosaccharides, cellulosic ethanol, cellulose nanofibrils and lignin nanoparticles. Bioresour Technol 342. https://doi.org/10.1016/j.biortech.2021.125970

Pirani, S., Hashaikeh, R., 2013. Nanocrystalline cellulose extraction process and utilization of the byproduct for biofuels production. Carbohydr Polym 93, 357–363. https://doi.org/10.1016/j.carbpol.2012.06.063

Prathapan, R., Thapa, R., Garnier, G., Tabor, R.F., 2016. Modulating the zeta potential of cellulose nanocrystals using salts and surfactants. Colloids Surf A Physicochem Eng Asp 509, 11–18. https://doi.org/10.1016/j.colsurfa.2016.08.075

Qing, Y., Sabo, R., Zhu, J.Y., Agarwal, U., Cai, Z., Wu, Y., 2013. A comparative study of cellulose nanofibrils disintegrated via multiple processing approaches. Carbohydr Polym 97, 226–234. https://doi.org/10.1016/j.carbpol.2013.04.086

Raizen, 2019. Etanol [WWW Document]. Nossos negocios. URL https://www.raizen.com.br/nossos-negocios/etanol (accessed 9.22.19).

Rajinipriya, M., Nagalakshmaiah, M., Robert, M., Elkoun, S., 2018. Importance of Agricultural and Industrial Waste in the Field of Nanocellulose and Recent Industrial Developments of Wood Based Nanocellulose: A Review. ACS Sustain Chem Eng 6, 2807–2828. https://doi.org/10.1021/acssuschemeng.7b03437

Reid, M.S., Villalobos, M., Cranston, E.D., 2017. Benchmarking Cellulose Nanocrystals: From the Laboratory to Industrial Production. Langmuir 33, 1583–1598. https://doi.org/10.1021/acs.langmuir.6b03765

Reis, D., Vian, B., 2004. Helicoidal pattern in secondary cell walls and possible role of xylans in their construction. C R Biol 327, 785–790. https://doi.org/10.1016/J.CRVI.2004.04.008

Rosales-Calderon, O., Arantes, V., 2019. A review on commercial-scale high-value products that can be produced alongside cellulosic ethanol. Biotechnol Biofuels 12, 1–58. https://doi.org/10.1186/S13068-019-1529-1/FIGURES/6

Rosales-Calderon, O., Pereira, B., Arantes, V., 2021. Economic assessment of the conversion of bleached eucalyptus Kraft pulp into cellulose nanocrystals in a stand-alone facility via acid and enzymatic hydrolysis. Biofuels, Bioproducts and Biorefining 15, 1775–1788. https://doi.org/10.1002/bbb.2277

Roux, J.C., Mayade, T.L., 1999. Modeling of the particle breakage kinetics in the wet mills for the paper industry, Powder Technology.

Saelee, K., Yingkamhaeng, N., Nimchua, T., Sukyai, P., 2016. An environmentally friendly xylanase-assisted pretreatment for cellulose nanofibrils isolation from sugarcane bagasse by high-pressure homogenization. Ind Crops Prod 82, 149–160. https://doi.org/10.1016/j.indcrop.2015.11.064

Satyamurthy, P., Jain, P., Balasubramanya, R.H., Vigneshwaran, N., 2011. Preparation and characterization of cellulose nanowhiskers from cotton fibres by controlled microbial hydrolysis. Carbohydr Polym 83, 122–129. https://doi.org/10.1016/j.carbpol.2010.07.029

Savignon, L.T., Gonçalves, V. de L., 2016. Estudo de viabilidade técnica e econômica da produção de nanocelulose. Universidade Federal Fluminense.

Scheller, H.V., Ulvskov, P., 2010. Hemicelluloses. Annu Rev Plant Biol 61, 263–289. https://doi.org/10.1146/annurev-arplant-042809-112315

Serra, A., González, I., Oliver-Ortega, H., Tarrès, Q., Delgado-Aguilar, M., Mutjé, P., 2017. Reducing the amount of catalyst in TEMPO-oxidized cellulose nanofibers: Effect on properties and cost. Polymers (Basel) 9. https://doi.org/10.3390/polym9110557

Siddiqui, N., Mills, R.H., Gardner, D.J., Bousfield, D., 2010. Production and characterization of cellulose nanofibers from wood pulp. J Adhes Sci Technol 25, 709–721. https://doi.org/10.1163/016942410X525975

Siqueira, G., Tapin-Lingua, S., Bras, J., da Silva Perez, D., Dufresne, A., 2010. Morphological investigation of nanoparticles obtained from combined mechanical shearing, and enzymatic and acid hydrolysis of sisal fibers. Cellulose 17, 1147–1158. https://doi.org/10.1007/s10570-010-9449-z

Siqueira, G., Várnai, A., Ferraz, A., Milagres, A.M.F., 2013. Enhancement of cellulose hydrolysis in sugarcane bagasse by the selective removal of lignin with sodium chlorite. Applied Energy 102, 399-402. https://doi.org/10.1016/j.apenergy.2012.07.029.

Siqueira, G., Arantes, V., Saddler, J.N., Ferraz, A., Milagre, A.M.F., 2017. Limitation of cellulose accessibility and unproductive binding of cellulases by pretreated sugarcane bagasse lignin. Biotechnol Biofuels 10 (176). https://doi.org/10.1186/s13068-017-0860-7

Siqueira, G.A., Dias, I.K.R., Arantes, V., 2019. Exploring the action of endoglucanases on bleached eucalyptus kraft pulp as potential catalyst for isolation of cellulose nanocrystals. Int J Biol Macromol 133, 1249–1259. https://doi.org/10.1016/j.ijbiomac.2019.04.162

Sluiter, A., Hames, B., Ruiz, R., Scarlata, C., Sluiter, J., Templeton, D., 2008a. Determination of Ash in Biomass - Technical Report NREL/TP-510-42622, National Renewable Energy Laboratory (NREL).

Sluiter, A., Hames, B., Ruiz, R., Scarlata, C., Sluiter, J., Templeton, D., 2008b. Determination of sugars, byproducts, and degradation products in liquid fraction process samples - Technical Report NREL/TP-510-42623, National Renewable Energy Laboratory (NREL).

Sluiter, A., Hames, B., Ruiz, R., Scarlata, C., Sluiter, J., Templeton, D., Crocker, D., 2012. Determination of structural carbohydrates and lignin in biomass - NREL/TP-510-42618 analytical procedure, National Renewable Energy Laboratory (NREL). https://doi.org/10.1007/s11947-014-1349-z

Sluiter, A, Ruiz, R., Scarlata, C., Sluiter, J., Templeton, D., 2008. Determination of Extractives in Biomass: Laboratory Analytical Procedure (LAP); Issue Date 7/17/2005.

Smith, B.G., Harris, P.J., 1999. The polysaccharide composition of Poales cell walls: Poaceae cell walls are not unique. Biochem Syst Ecol 27, 33–53. https://doi.org/10.1016/S0305-1978(98)00068-4

Solala, I., Volperts, A., Andersone, A., Dizhbite, T., Mironova-Ulmane, N., Vehniäinen, A., Pere, J., Vuorinen, T., 2012. Mechanoradical formation and its effects on birch kraft pulp during the preparation of nanofibrillated cellulose with Masuko refining. Holzforschung 66, 477–483. https://doi.org/10.1515/HF.2011.183

Song, Q., Winter, W.T., Bujanovic, B.M., Amidon, T.E., 2014. Nanofibrillated cellulose (NFC): A high-value coproduct that improves the economics of cellulosic ethanol production. Energies (Basel) 7, 607–618. https://doi.org/10.3390/en7020607

Souza, A., Jair, A., Pontes, A., Soares, C., Garcia, C., Trez, C., Carvalho, D., Forchezatto, D., Castioni, G., Sampaio, I., Carvalho, J., Neves, J., Bressiani, J., Menandro, L., Leal, M., Watanabe, M., Souza, N., Guizelini Júnior, P., Mantelatto, P., Bordonal, R., Castro, S., Junqueira, T., Cardoso, T., Hernandes, T., Celente, V., Bononi, W., Souza, Z., 2020. Sugarcane Renewable Electricity (SUCRE) - Project BRA/10/G31. Campinas.

Spence, K.L., Venditti, R.A., Rojas, O.J., Habibi, Y., Pawlak, J.J., 2011. A comparative study of energy consumption and physical properties of microfibrillated cellulose produced by different processing methods. Cellulose 18, 1097–1111. https://doi.org/10.1007/s10570-011-9533-z

Stephen, J.D., Mabee, W.E., Saddler, J.N., 2012. Will second-generation ethanol be able to compete with first-generation ethanol? Opportunities for cost reduction. Biofuels, Bioproducts and Biorefining 6, 159–176. https://doi.org/10.1002/bbb.331

Taherzadeh, M.J., Karimi, K., 2008. Pretreatment of lignocellulosic wastes to improve ethanol and biogas production: A review, International Journal of Molecular Sciences. https://doi.org/10.3390/ijms9091621

Tang, Y., Shen, X., Zhang, J., Guo, D., Kong, F., Zhang, N., 2015. Extraction of cellulose nano-crystals from old corrugated container fiber using phosphoric acid and enzymatic hydrolysis followed by sonication. Carbohydr Polym 125, 360–366. https://doi.org/10.1016/j.carbpol.2015.02.063

Taniguchi, T., Okamura, K., 1998. New films produced from microfibrillated natural fibres. Polym Int 47, 291–294. https://doi.org/10.1002/(SICI)1097-0126(199811)47:3<291::AID-PI11>3.0.CO;2-1

Tao, L., Aden, A., Elander, R.T., Pallapolu, V.R., Lee, Y.Y., Garlock, R.J., Balan, V., Dale, B.E., Kim, Y., Mosier, N.S., Ladisch, M.R., Falls, M., Holtzapple, M.T., Sierra, R., Shi, J., Ebrik, M.A., Redmond, T., Yang, B., Wyman, C.E., Hames, B., Thomas, S., Warner, R.E., 2011. Process and technoeconomic analysis of leading pretreatment technologies for lignocellulosic ethanol production using switchgrass. Bioresour Technol 102, 11105–11114. https://doi.org/10.1016/j.biortech.2011.07.051

TAPPI/ANSI, 2021. Laboratory beating of pulp (PFI mill method) - Test Method TAPPI/ANSI T 248 sp-21, TAPPI Journal.

Tarasov, D., Leitch, M., Fatehi, P., 2018. Lignin–carbohydrate complexes: properties, applications, analyses, and methods of extraction: a review. Biotechnology for Biofuels 2018 11:1 11, 1–28. https://doi.org/10.1186/S13068-018-1262-1

Tayeb, A.H., Tajvidi, M., Bousfield, D., 2020. Paper-based oil barrier packaging using lignin-containing cellulose nanofibrils. Molecules 25. https://doi.org/10.3390/molecules25061344

Teixeira, R.S.S., Da Silva, A.S.A., Jang, J.H., Kim, H.W., Ishikawa, K., Endo, T., Lee, S.H., Bon, E.P.S., 2015. Combining biomass wet disk milling and endoglucanase/β-glucosidase hydrolysis for the production of cellulose nanocrystals. Carbohydr Polym 128, 75–81. https://doi.org/10.1016/j.carbpol.2015.03.087

Tejado, A., Alam, M.N., Antal, M., Yang, H., van de Ven, T.G.M., 2012. Energy requirements for the disintegration of cellulose fibers into cellulose nanofibers. Cellulose 19, 831–842. https://doi.org/10.1007/S10570-012-9694-4/METRICS

Teter, S.A., 2012. DECREASE Final Technical Report: Development of a Commercial Ready Enzyme Application System for Ethanol. United States. https://doi.org/10.2172/1039767

The Engineering ToolBox, 2003. Fuels - Higher and Lower Calorific Values [WWW Document]. URL https://www.engineeringtoolbox.com/fuels-higher-calorific-values-d_169.html (accessed 7.21.23).

The Process Development Center (PDC), 2022. Order Nanocellulose - The Process Development Center (PDC) University of Maine [WWW Document]. URL https://umaine.edu/pdc/nanocellulose/nanocellulose-products/order-nanocellulose/ (accessed 1.27.23).

Tibolla, H., Pelissari, F.M., Rodrigues, M.I., Menegalli, F.C., 2017. Cellulose nanofibers produced from banana peel by enzymatic treatment: Study of process conditions. Ind Crops Prod 95, 664–674. https://doi.org/10.1016/j.indcrop.2016.11.035

Toivonen, M.S., Onelli, O.D., Jacucci, G., Lovikka, V., Rojas, O.J., Ikkala, O., Vignolini, S., 2018. Anomalous-Diffusion-Assisted Brightness in White Cellulose Nanofibril Membranes. Advanced Materials 30. https://doi.org/10.1002/adma.201704050

Tong, X., Shen, W., Chen, X., Jia, M., Roux, J.C., 2020. Preparation and mechanism analysis of morphology-controlled cellulose nanocrystals via compound enzymatic hydrolysis of eucalyptus pulp. J Appl Polym Sci 137, 48407. https://doi.org/10.1002/APP.48407

Travália, B.M., Soares Forte, M.B., 2020. New Proposal in a Biorefinery Context: Recovery of Acetic and Formic Acids by Adsorption on Hydrotalcites. J Chem Eng Data 65, 4503–4511. https://doi.org/10.1021/ACS.JCED.0C00340/ASSET/IMAGES/LARGE/JE0C00340_0006.JPEG

Trifol, J., Marin Quintero, D.C., Moriana, R., 2021. Pine Cone Biorefinery: Integral Valorization of Residual Biomass into Lignocellulose Nanofibrils (LCNF)-Reinforced Composites for Packaging. ACS Sustain Chem Eng 9, 2180–2190. https://doi.org/10.1021/acssuschemeng.0c07687

United States Department of Agriculture (USDA), 2018. Data Products. https://www.ers.usda.gov/data-products/ (accessed 07.31.2018)

União da Indústria de cana-de-açúcar (ÚNICA), 2019. http://www.unicadata.com.br/ (acessed 12.6.2019).

Vanmarcke, G., Demeke, M.M., Foulquié-Moreno, M.R., Thevelein, J.M., 2021. Identification of the major fermentation inhibitors of recombinant 2G yeasts in diverse lignocellulose hydrolysates. Biotechnol Biofuels 14, 1–15. https://doi.org/10.1186/S13068-021-01935-9/TABLES/3

Vogel, J., 2008. Unique aspects of the grass cell wall. Curr Opin Plant Biol 11, 301–307. https://doi.org/10.1016/J.PBI.2008.03.002

Walter, A., Galdos, M.V., Scarpare, F.V., Verde Leal, M.R.L., Abel Seabra, J.E., da Cunha, M.P., Araujo Picoli, M.C., de Oliveira, C.O.F., 2015. Brazilian Sugarcane Ethanol: Developments so far and Challenges for the Future, in: Advances in Bioenergy. John Wiley & Sons, Ltd, Oxford, UK, pp. 373–394. https://doi.org/10.1002/9781118957844.ch24

Wang, C., Qi, W., Liang, C., Wang, Q., Wang, W., Wang, Z., Yuan, Z., 2021. Impact of Alkaline Pretreatment Condition on Enzymatic Hydrolysis of Sugarcane Bagasse and Pretreatment Cost. Appl Biochem Biotechnol 193, 2087–2097. https://doi.org/10.1007/s12010-021-03530-y

Wang, J., Chae, M., Beyene, D., Sauvageau, D., Bressler, D.C., 2021a. Coproduction of ethanol and cellulose nanocrystals through self-cycling fermentation of wood pulp hydrolysate. Bioresour Technol 330. https://doi.org/10.1016/j.biortech.2021.124969

Wang, J., Chae, M., Beyene, D., Sauvageau, D., Bressler, D.C., 2021b. Coproduction of ethanol and cellulose nanocrystals through self-cycling fermentation of wood pulp hydrolysate. Bioresour Technol 330, 124969. https://doi.org/10.1016/J.BIORTECH.2021.124969

Wang, Q., Wang, W., Tan, X., Zahoor, Chen, X., Guo, Y., Yu, Q., Yuan, Z., Zhuang, X., 2019. Low-temperature sodium hydroxide pretreatment for ethanol production from sugarcane bagasse without washing process. Bioresour Technol 291. https://doi.org/10.1016/j.biortech.2019.121844

Wang, Q.Q., Zhu, J.Y., 2016. Effects of mechanical fibrillation time by disk grinding on the properties of cellulose nanofibrils. Tappi J 15, 419–423.

Wang, Q.Q., Zhu, J.Y., Gleisner, R., Kuster, T.A., Baxa, U., McNeil, S.E., 2012. Morphological development of cellulose fibrils of a bleached eucalyptus pulp by mechanical fibrillation. Cellulose 19, 1631–1643. https://doi.org/10.1007/s10570-012-9745-x

Wang, W., Mozuch, M.D., Sabo, R.C., Kersten, P., Zhu, J.Y., Jin, Y., 2015. Production of cellulose nanofibrils from bleached eucalyptus fibers by hyperthermostable endoglucanase treatment and subsequent microfluidization. Cellulose 22, 351–361. https://doi.org/10.1007/s10570-014-0465-2

Wei, L., Agarwal, U.P., Matuana, L., Sabo, R.C., Stark, N.M., 2018. Performance of high lignin content cellulose nanocrystals in poly(lactic acid). Polymer (Guildf) 135, 305–313. https://doi.org/10.1016/J.POLYMER.2017.12.039

Xie, H., Du, H., Yang, X., Si, C., 2018. Recent Strategies in Preparation of Cellulose Nanocrystals and Cellulose Nanofibrils Derived from Raw Cellulose Materials. Int J Polym Sci 2018, 1–25. https://doi.org/10.1155/2018/7923068

Xu, H., Sanchez-Salvador, J.L., Balea, A., Blanco, A., Negro, C., 2022. Optimization of reagent consumption in TEMPO-mediated oxidation of Eucalyptus cellulose to obtain cellulose nanofibers. Cellulose 29, 6611–6627. https://doi.org/10.1007/s10570-022-04672-w

Xu, R., Du, H., Wang, H., Zhang, M., Wu, M., Liu, C., Yu, G., Zhang, X., Si, C., Choi, S.E., Li, B., 2021. Valorization of Enzymatic Hydrolysis Residues from Corncob into Lignin-Containing Cellulose Nanofibrils and Lignin Nanoparticles. Front Bioeng Biotechnol 9. https://doi.org/10.3389/fbioe.2021.677963

Xu, Y., Salmi, J., Kloser, E., Perrin, F., Grosse, S., Denault, J., Lau, P.C.K., 2013. Feasibility of nanocrystalline cellulose production by endoglucanase treatment of natural bast fibers. Ind Crops Prod 51, 381–384. https://doi.org/10.1016/j.indcrop.2013.09.029

Yang, T., Li, X., Guo, Y., Zhao, J., Qu, Y., 2023. Preparation of nanocellulose crystal from bleached pulp with an engineering cellulase and coproduction of ethanol. Carbohydr Polym 301. https://doi.org/10.1016/j.carbpol.2022.120291

Yarbrough, J.M., Zhang, R., Mittal, A., Vander Wall, T., Bomble, Y.J., Decker, S.R., Himmel, M.E., Ciesielski, P.N., 2017. Multifunctional Cellulolytic Enzymes Outperform Processive Fungal Cellulases for Coproduction of Nanocellulose and Biofuels. ACS Nano 11, 3101–3109. https://doi.org/10.1021/acsnano.7b00086

Zhang, Y., Lu, X. Bin, Gao, C., Lv, W.J., Yao, J.M., 2012. Preparation and characterization of nano crystalline cellulose from Bamboo fibers by controlled cellulase hydrolysis. Journal of Fiber Bioengineering and Informatics 5, 263–271. https://doi.org/10.3993/jfbi09201204

Zhou, H., St. John, F., Zhu, J.Y., 2019. Xylanase pretreatment of wood fibers for producing cellulose nanofibrils: a comparison of different enzyme preparations. Cellulose 26, 543–555. https://doi.org/10.1007/s10570-019-02250-1

Zhu, J.Y., Sabo, R., Luo, X., 2011. Integrated production of nano-fibrillated cellulose and cellulosic biofuel (ethanol) by enzymatic fractionation of wood fibers. Green Chemistry 13, 1339–1344. https://doi.org/10.1039/c1gc15103g

APPENDICES

APPENDIX A. PLACKETT-BURMAN DESIGN OF EXPERIMENT

Table A. 1. Matrix produced by Minitab to conduct the design of experiments of Plackett-Burman and responses based on gravimetry analysis

Exp ID#	Exp Order#	FACTORS											RESPONSE						
		A	B	C	D	E	F	G	H	I	J	K	C #	Suspension volume (mL)	CNC (g)	CNC yield (%)	Remaining CSR (g)	CSR (%)	Ratio W/C (g/#C)
1	4	1	1	-1	1	1	1	-1	-1	-1	1	-1	8	120	0.544	10.9	4.397	87.7	0.622
2	3	1	-1	1	1	1	-1	-1	-1	1	-1	1	4	100	0.154	6.1	2.360	93.2	0.342
3	2	-1	1	1	1	-1	-1	-1	1	-1	1	1	6	500	0.357	7.1	4.680	93.1	2.378
4	8	1	1	1	-1	-1	-1	1	-1	1	1	-1	12	250	1.237	24.6	4.000	79.7	1.874
5	5	1	1	-1	-1	-1	1	-1	1	1	-1	1	14	280	0.545	10.9	4.433	88.4	0.783
6	9	1	-1	-1	-1	1	-1	1	1	-1	1	1	7	120	0.088	3.5	2.424	97.2	0.117
7	7	-1	-1	-1	1	-1	1	1	-1	1	1	1	7	120	0.306	12.2	2.192	87.3	0.407
8	11	-1	-1	1	-1	1	1	-1	1	1	1	-1	2	200	0.037	1.5	2.499	99.5	0.498
9	10	-1	1	-1	1	1	-1	1	1	1	-1	-1	8	140	0.243	4.8	4.752	94.0	0.324
10	6	1	-1	1	1	-1	1	1	1	-1	-1	-1	7	600	0.256	10.2	2.380	95.2	1.707
11	12	-1	1	1	-1	1	1	1	-1	-1	-1	1	7	200	0.268	5.3	4.715	93.4	0.596
12	1	-1	-1	-1	-1	-1	-1	-1	-1	-1	-1	-1	6	100	0.253	10.0	2.256	89.5	0.337

Order: experiment collection order; Exp ID: experiment identification; Factors A, B, C, D, E, F, G e H: 8 “real” factors studied using codified variables (level low -1 and level high +1); Factor I, J e K: additional factors without a parameter (dummy factors) using codified variables (level low -1 and level high +1); C#: number of centrifugation steps, Volume: total volume recovered, CNC: cellulose nanocrystals o.d. weight, CNC yield: yield based on CSR o.d. weight, Remaining CSR: Weight of CSR after CNC isolation o.d. weight, Ratio W/C: Ratio obtained by CNC weight by number of centrifugations.

Table A. 2. Matrix produced by Minitab to conduct design of experiments of Plackett-Burman and responses obtained by light scattering analysis using the Mastersizer 3000

Exp ID#	Exp Order#	FACTORS											RESPONSE							
		A	B	C	D	E	F	G	H	I	J	K	**Span**	**Uniformity**	**wet-SSA (m^2/kg)**	**D [3,2] (µm)**	**D [4,3] (µm)**	**D10 (µm)**	**D50 (µm)**	**D90 (µm)**
1	4	1	1	-1	1	1	1	-1	-1	-1	1	-1	0.431	0.179	2876	2.09	2.09	0.524	0.630	0.795
2	3	1	-1	1	1	1	-1	-1	-1	1	-1	1	0.483	0.170	4310	1.39	150	0.467	0.576	0.745
3	2	-1	1	1	1	-1	-1	-1	1	-1	1	1	0.422	0.196	2666	2.25	14.1	0.555	0.662	0.834
4	8	1	1	1	-1	-1	-1	1	-1	1	1	-1	2.832	0.623	868.9	6.9	16	0.618	0.712	2.64
5	5	1	1	-1	-1	-1	1	-1	1	1	-1	1	0.348	0.240	1196	3.23	9.69	0.612	0.709	0.859
6	9	1	-1	-1	-1	1	-1	1	1	-1	1	1	0.322	0.168	581	10.3	668	0.553	0.647	0.761
7	7	-1	-1	-1	1	-1	1	1	-1	1	1	1	0.345	0.420	1025	5.85	77.6	0.614	0.700	0.855
8	11	-1	-1	1	-1	1	1	-1	1	1	1	-1	ND	ND	ND	ND	ND	ND	ND	ND
9	10	-1	1	-1	1	1	-1	1	1	1	-1	-1	0.302	0.217	467.6	12.8	267	0.621	0.716	0.836
10	6	1	-1	1	1	-1	1	1	1	-1	-1	-1	0.408	0.168	3154	1.9	23.6	0.525	0.628	0.781
11	12	-1	1	1	-1	1	1	1	-1	-1	-1	1	0.396	0.152	742.1	8.09	1220	0.561	0.669	0.826
12	1	-1	-1	-1	-1	-1	-1	-1	-1	-1	-1	-1	0.350	0.277	1575	3.81	9.74	0.596	0.686	0.835

Order: experiment collection order; Exp ID: experiment identification; Factors A, B, C, D, E, F, G e H: 8 “real” factors studied using codified variables (level low -1 and level high +1); Factor I, J e K: additional factors without a parameter (dummy factors) using codified variables (level low -1 and level high +1); ND: not detected.

Table A. 3. Analysis of Variance (ANOVA) for Plackett-Burman with CNC yield response in relationship to factors A, B, C, D, E, F, G, and H

Source	**Df**	**SS (Adj.)**	**MS (Adj.)**	***F-value***	***p-value***
Model	8	357.841	44.730	3.75	0.152
Linear	8	357.841	44.730	3.75	0.152
A	1	53.388	53.388	4.48	0.125
B	1	24.028	24.028	2.02	0.251
C	1	12.916	12.916	1.08	0.374
D	1	14.062	14.062	1.18	0.357
E	1	80.348	80.348	6.74	0.081
F	1	17.002	17.002	1.43	0.318
G	1	2.282	2.282	0.19	0.691
H	1	153.814	153.814	12.90	0.037
Error	3	35.770	11.923		
Total	11	393.611			

df: degree of freedom; SS (Adj.): Sum of Squares adjusted; MS (Adj.): Mean Squares adjusted

Regression Model Summary

S	R^2	R^2(adj)	R^2(pred)
3.45303	90.91%	66.68%	0.00%

S, R^2, R^2(adj), R^2(pred) are indicators of the fitting quality and model prediction.

Table A. 4. Effect-coded coeficients for Plackett-Burman with CNC yield response in relationship to factors A, B, C, D, E, F, G, and H

Term	**Effects**	**Coef**	**EP de Coef**	**t-value**	***p-value***	**VIF**
Constant		8.924	0.997	8.95	0.003	
A	4.219	2.109	0.997	2.12	0.125	1.00
B	-2.830	-1.415	0.997	-1.42	0.251	1.00
C	2.075	1.037	0.997	1.04	0.374	1.00
D	2.165	1.083	0.997	1.09	0.357	1.00
E	-5.175	-2.588	0.997	-2.60	0.081	1.00
F	2.381	1.190	0.997	1.19	0.318	1.00
G	-0.872	-0.436	0.997	-0.44	0.691	1.00
H	-7.160	-3.580	0.997	-3.59	0.037	1.00

Regression equation with effect-non-coded coefficients (Eq. 6)

$$\text{CNC yield} = 8.924 + 2.109\,A - 1.415\,B + 1.037\,C + 1.083\,D - 2.588\,E + 1.190\,F - 0.436\,G - 3.580\,H$$

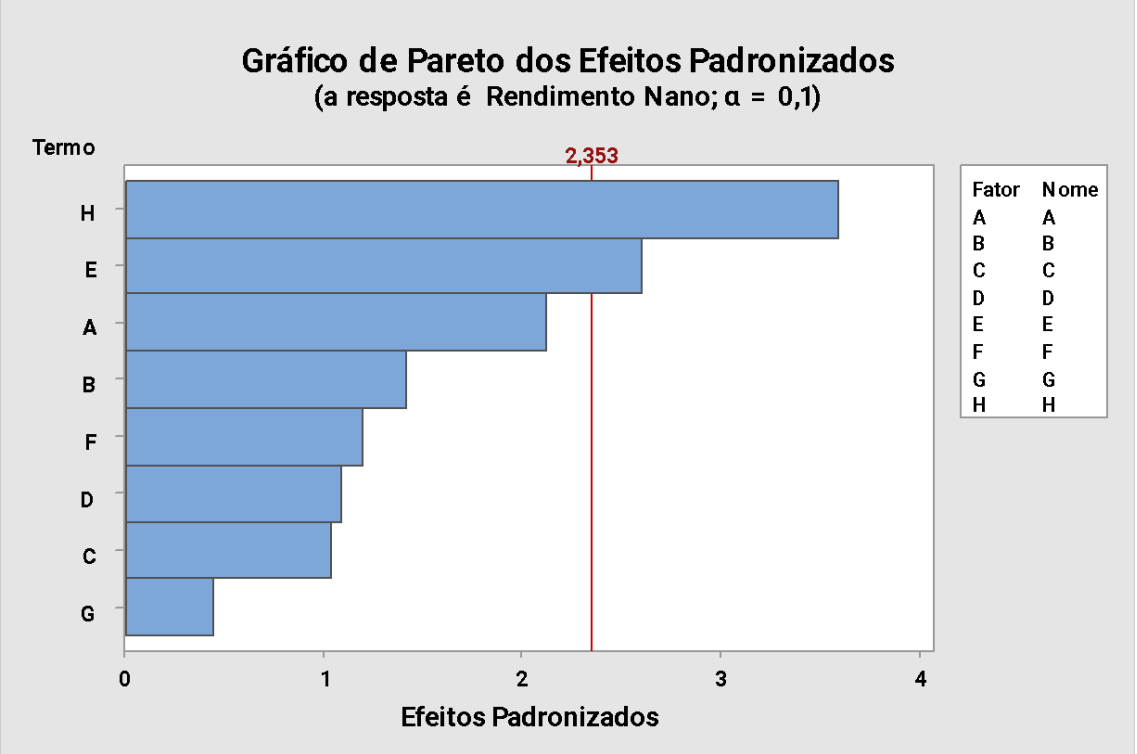

Fig. A. 1. Pareto chart for Plackett-Burman with CNC yield response in relationship to factors A, B, C, D, E, F, G, and H, using α = 0.1

Table A. 5. Factorial Regression: Uniformity versus A; B; C; D; E; F; G; H

Source	**df**	**SS (Adj.)**	**MS (Adj.)**	***F-value***	***p-value***
Model	8	0.195908	0.024489	4.40	0.198
Linear	8	0.195908	0.024489	4.40	0.198
A	1	0.000961	0.000961	0.17	0.718
B	1	0.004900	0.004900	0.88	0.447
C	1	0.017161	0.017161	3.09	0.221
D	1	0.029929	0.029929	5.38	0.146
E	1	0.028056	0.028056	5.05	0.154
F	1	0.017161	0.017161	3.09	0.221
G	1	0.006806	0.006806	1.22	0.384
H	1	0.047961	0.047961	8.63	0.099
Error	2	0.011121	0.005560		
Total	10	0.207029			

df: degree of freedom; SS (Adj.): Sum of Squares adjusted; MS (Adj.): Mean Squares adjusted

Regression Model Summary

S	R^2	R^2(aj)	R^2(pred)
0.0745676	94.63%	73.14%	*

S, R^2, R^2(adj), R^2(pred) are indicators of the fitting quality and model prediction.

Table A. 6. Effect-coded coeficients for Factorial Regression: Uniformity versus A; B; C; D; E; F; G; H

Term	Effect	Coef	EP de Coef	t-value	*p-value*	VIF
Constant		0.2477	0.0249	9.96	0.010	
A	0.0207	0.0103	0.0249	0.42	0.718	1.21
B	-0.0467	-0.0233	0.0249	-0.94	0.447	1.21
C	0.0873	0.0437	0.0249	1.76	0.221	1.21
D	0.1153	0.0577	0.0249	2.32	0.146	1.21
E	-0.1117	-0.0558	0.0249	-2.25	0.154	1.21
F	0.0873	0.0437	0.0249	1.76	0.221	1.21
G	-0.0550	-0.0275	0.0249	-1.11	0.384	1.21
H	-0.1460	-0.0730	0.0249	-2.94	0.099	1.21

Regression equation with effect-non-coded coefficients (Eq. 7)

Uniformity = 0.2477 + 0.0103 A – 0.0233 B + 0.0437 C + 0.0577 D – 0.0558 E + 0.0437 F – 0.0275 G – 0.0730 H

Atypical observations

Obs.	Uniformity	Adj	Resd	Std Resd	
1	0.1790	0.1790	0.0000	*	X
9	0.2170	0.2170	0.0000	*	X

X Atypical X

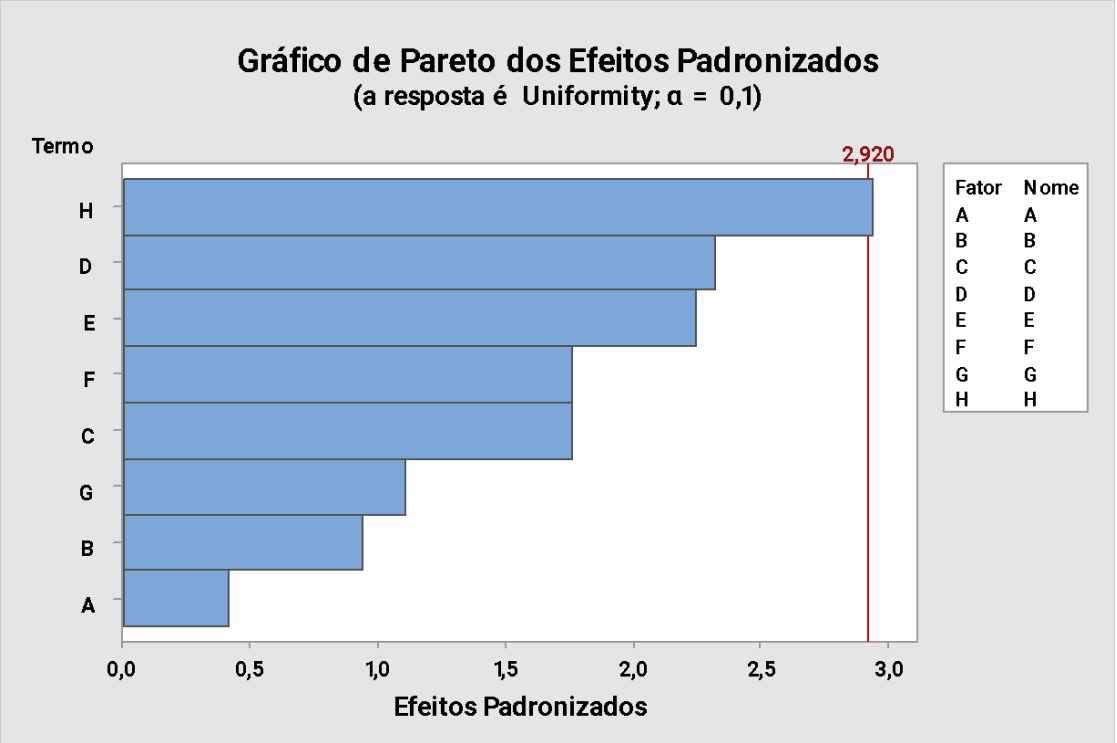

Fig. A. 2. Pareto chart for Plackett-Burman with Uniformity response in relationship to factors A, B, C, D, E, F, G, and H, using α = 0.1.

APPENDIX B. FULL FACTORIAL DESIGN OF EXPERIMENT

Table B. 1. Matrix produced by Minitab to conduct the Full factorial design of experiments using two variables cellulose conversion (A) and rotation (B) to obtain the response CNC yield.

Experiment#	FACTOR		RESPONSE
	SEH (A)	Rot (B)	CNC Yield (Nano)
1	0.28	500	9.8
2	0.68	500	17.0
3	0.28	1,000	9.9
4	0.68	1,000	20.0
5	0.28	500	10.9
6	0.68	500	19.0
7	0.28	1,000	10.1
8	0.68	1,000	17.1
9	0.28	500	10.4
10	0.68	500	18.0
11	0.28	1,000	13.0
12	0.68	1,000	16.5
13	0.50	750	10.2
14	0.50	750	9.8
15	0.50	750	10.9
16	0.50	750	10.2
17	0.50	750	14.9
18	0.50	750	12.7
19	0.50	750	11.8
20	0.50	750	15.8
21	0.50	750	14.7
22	0.79	750	19.8
23	0.18	750	5.0
24	0.50	1,103	11.4
25	0.50	398	14.9

SEH: Severity of Enzymatic Hydrolysis in terms cellulose conversion (g/g pulp)
Rot: Rotation speed (398 – 1103 ×*g*)
Nano: CNC yield (g/100 CSR)

Table B. 2. Analysis of Variance (ANOVA) for Full factorial design using two variables cellulose conversion (SEH) and rotation (Rot) to obtain the response CNC yield

Source	**Df**	**SS (Adj.)**	**MS (Adj.)**	***F-value***	***p-value***
Model	5	285.463	57.093	15.83	0.000
Blocks	1	10.896	10.896	3.02	0.098
Linear	2	266.041	133.020	36.88	0.000
SEH	1	265.327	265.327	73.55	0.000
Rot	1	0.710	0.710	0.20	0.662
Interaction of 2 factors	2	29.411	14.705	4.08	0.034
SEH * SEH	1	10.653	10.653	2.95	0.102
Rot*Rot	1	17.353	17.353	4.81	0.041
Error	19	68.539	3.607		
Curvature	3	10.706	3.569	0.99	0.424
Pure error	16	57.833	3.615	*	*
Total	24	354.002			

df: degree of freedom; SS (Adj.): Sum of Squares adjusted; MS (Adj.): Mean Squares adjusted

Regression Model Summary

S	R^2	R^2(aj)	R^2(pred)
1.89930	80.64%	75.54%	60.75%

S, R^2, R^2(adj), R^2(pred) are indicators of the fitting quality and model prediction.

Table B. 3. Effect-coded coeficients for regression model

Term	**Coef**	**EP de Coef**	***t*-value**	***p*-value**	**VIF**
Constant	11.043	0.867	12.73	0.000	
Blocks					
1	0.975	0.561	1.74	0.098	1.17
SEH	6.108	0.712	8.58	0.000	1.01
Rot	-0.297	0.670	-0.44	0.662	1.00
SEH * SHE	2.36	1.37	1.72	0.102	1.13
Rot*Rot	2.75	1.25	2.19	0.041	1.07

Regression model using non-coded parameters (Eq. 5)

$$\text{Nano} = 20.39 - 4.5\ \text{SEH} - 0.0341\ \text{Rot} + 25.3\ \text{SEH} * \text{SEH} + 0.000022\ \text{Rot}*\text{Rot}$$

Regression Model Summary

S	R^2	R^2(aj)	R^2(pred)
1.89930	80.64%	75.54%	60.75%

S, R^2, R^2(adj), R^2(pred) are indicators of the fitting quality and model prediction.

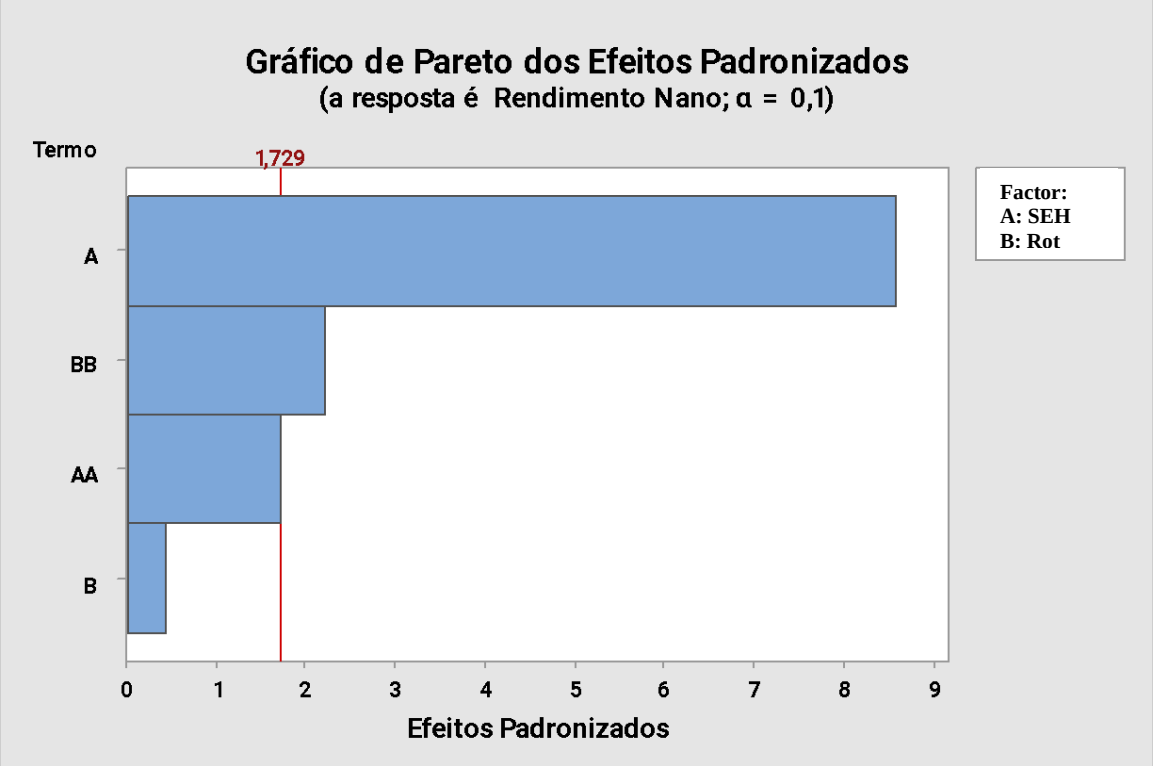

Fig. B. 1. Pareto chart for response surface with CNC yield response in relationship to factors SEH (A) and Rot (B) and their 2 factor interactions, using α = 0.1.

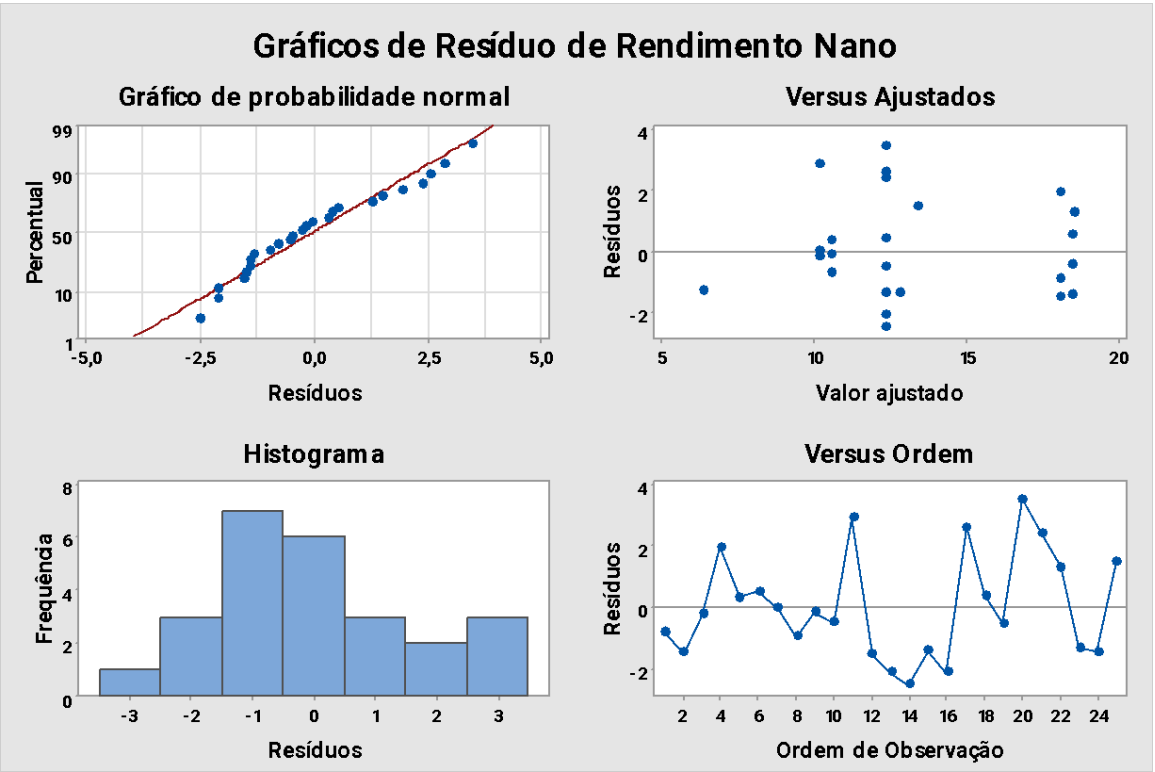

Fig. B. 2. Analysis of residuals from data collected for response: CNC yield

APPENDIX C. HIGHLIGHT OF LIGNIN-CONTAINING NANOCELLULOSE

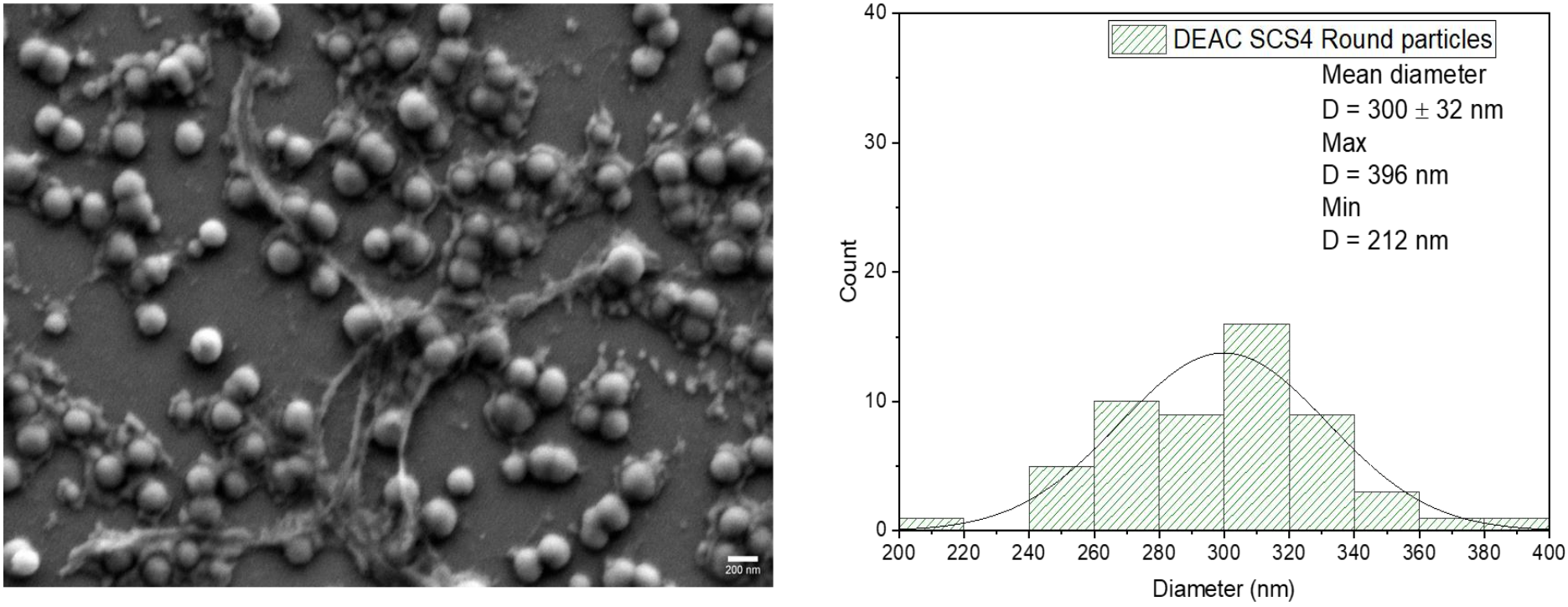

Fig. C.1. SEM image obtained for DEAC SCS4 LCNF and diameter distribution obtained for the spherical particles. Scale bar 200 nm

BIOGRAPHY OF THE AUTHOR

Carlaile Fernanda de Oliveira Nogueira was born in Tupã, São Paulo, Brazil and raised in Umuarama, Paraná, Brazil. She attended Lorena School of Engineering (EEL) located in Lorena, São Paulo, Brazil, which is one of the campuses of University of São Paulo (USP). She graduated in 2014 with a Bachelor's degree in Biochemical Engineering and a Master of Science degree in Industrial Biotechnology (Applied Microbiology concentration) in 2017.

She started her Doctorade in Industrial Biotechnology graduate program at EEL/USP in August 2017. After defending her doctorade candidacy in Brazil, she came to Maine as a visiting PhD student in the Fall 2019 for a one-year project funded by the Brazilian government agency CAPES Foundation. Carlaile started her PhD in Chemical Engineering graduate program at the University of Maine in the Spring of 2021. She had a cotutelle agreement signed to pursue a joint doctorade degree, being Doctor of Philosophy degree in Chemical Engineering from the University of Maine and Doctor in Science degree in Industrial Biotechnology (Biomass conversion concentration) from University of São Paulo.

Carlaile is a candidate for Doctor of Philosophy degree in Chemical Engineering from the University of Maine in December 2023.